



INSTITUTE OF
CHEMICAL TECHNOLOGY
PRAGUE

Proceedings
of
4th Scientific Colloquium

In honor of Prof. Alois Klíč and Prof. Milan Kubíček



June 24 - 26, 2014

Institute of Chemical Technology, Prague
Czech Republic

ISBN 978-80-7080-890-0



Department of Mathematics,
in cooperation with
Department of Chemical Engineering,
Institute of Chemical Technology, Prague
and with
Center for Discrete Mathematics (DIMATIA),
Charles University, Prague

Proceedings
of
4th Scientific Colloquium

In honor of Prof. Alois Klíč and Prof. Milan Kubíček

June 24 - 26, 2014

Institute of Chemical Technology, Prague
Czech Republic

Published by the Institute of Chemical Technology, Prague
Technická 5
166 28 Praha 6
Czech Republic

All contributions have been reviewed by experts in the relevant fields.
The publication has not passed the language correction.

Copyright © 2014 by the Institute of Chemical Technology, Prague

ISBN 978-80-7080-890-0

Printed in the Czech Republic by KANAG - TISK, s.r.o.,
Technická 1905/5, 160 00 Praha 6.

Preface

The 4th Scientific Colloquium is dedicated to two of our colleagues, Prof. A. Klíč and Prof. M. Kubíček, who have built the Department of Mathematics at Institute of Chemical Technology, Prague over the past 30 years. Under their guidance the department lived its mathematical life, unified in stimulating discussions and fruitful cooperation. Such an environment naturally motivated students to study mathematics with deeper interest which resulted in acquiring new skills to solve difficult technical problems.

Professor Alois Klíč started to work at our institute already in 1969. He is an expert in the field of Complex Analysis, Differential Geometry and Dynamical Systems.

Professor Milan Kubíček has been working at the Department of Chemical Engineering since 1964 and at the Department of Mathematics since 1985. His favorite subjects are Numerical Methods, Algorithms and Dynamical Systems. He was one of the members of the research group that invented, nowadays the world-wide used, method of continuation in dynamical systems. During the Colloquium, there will be two talks devoted to our honored colleagues. Professor Miloš Marek from the Chemical Engineering Department ICT, Prague, and Professor Ivo Marek from the Civil Engineering Faculty of the Technical University, Prague, will remember the time spent with them, shared experiences and stories.

Mathematics is the science of pattern, order and relationships. It is the language and logic of our technological world. Mathematical power is the ability to explore and to use a variety of mathematical methods to solve engineering problems effectively. The main purpose of the Colloquium is to exchange ideas, discuss issues of common concern, establish contacts, and gather information in the same field of research. Many of the contributions are closely related to the need for mathematical modeling and simulation of physical and engineering phenomena.

We have the pleasure to welcome several outstanding researchers from various countries, namely from Germany, Italy, Japan, Slovakia, and Great Britain, as well as distinguished Czech professors. We would like to thank all colleagues and friends who helped us to organize this Colloquium.

June 2014, Prague

Daniel Turzík
Head of the Department of Mathematics

Drahoslava Janovská
On behalf of the Organizing Committee

Program committee

Prof. RNDr. Alois Klíč, CSc. Institute of Chemical Technology Prague Faculty of Chemical Engineering Department of Mathematics	kolokvium@vscht.cz
Prof. RNDr. Milan Kubíček, CSc. Institute of Chemical Technology Prague Faculty of Chemical Engineering Department of Mathematics	Milan.Kubicek@vscht.cz
Prof. RNDr. Jaroslav Nešetřil, DrSc. Charles University in Prague Faculty of Mathematics and Physics Department of Applied Mathematics	nesetril@karlin.mff.cuni.cz
Prof. RNDr. Vladimír Janovský, DrSc. Charles University in Prague Faculty of Mathematics and Physics Department of Numerical Mathematics	janovsky@karlin.mff.cuni.cz
Prof. Ing. Igor Schreiber, CSc. Institute of Chemical Technology Prague Faculty of Chemical Engineering Department of Chemical Engineering	Igor.Schreiber@vscht.cz
Doc. RNDr. Daniel Turzík, CSc. Institute of Chemical Technology Prague Faculty of Chemical Engineering Department of Mathematics	Daniel.Turzík@vscht.cz
Prof. RNDr. Drahoslava Janovská, CSc. Institute of Chemical Technology Prague Faculty of Chemical Engineering Department of Mathematics	Drahoslava.Janovska@vscht.cz

Organization

4rd Scientific Colloquium on Mathematics in honor of Prof. Alois Klíč and Prof. Milan Kubíček is organized by the Department of Mathematics of the Institute of Chemical Technology, Prague in cooperation with Center for Nonlinear Dynamics, Faculty of Chemical Engineering of the Institute of Chemical technology, Prague and with Center For Discrete Mathematics (DIMATIA), Charles University.

The main objective of the Colloquium is to provide the possibility to exchange ideas and experience in different areas of mathematics and applications. Main topics include mathematical formulation, modelling and simulations of current problems in chemical engineering and biology.

Organizing Committee

Organizing Chair: **Prof. RNDr. Drahoslava Janovská, CSc.**
ICT Prague
Faculty of Chemical Engineering
Department of Mathematics
Drahoslava.Janovska@vscht.cz

Committee Members: **Doc. RNDr. Daniel Turzík, CSc.**
Daniel.Turzik@vscht.cz
RNDr. Miroslava Dubcová, PhD.
Miroslava.Dubcova@vscht.cz
Mgr. Jana Šnupárková, PhD.
Jana.Snuparkova@vscht.cz
Mgr. Marketa Zikmundová
Marketa.Zikmundova@vscht.cz
RNDr. František Jaroš
jarosf@vscht.cz

Contents

Analysis and applications of the space-time discontinuous Galerkin method <i>Miloslav Feistauer</i>	9
Exponential stability of solutions of nonlinear differential equations with Riemann-Liouville fractional integrals in the nonlinearities <i>Milan Medved'</i>	10
The algebraic Riccati equation with matrix entries from noncommutative algebras <i>Gerhard Opfer</i>	21
Reaction network analysis of oscillatory instabilities in a model of noxious components removal in the three-way catalytic converter <i>Otto Hadač and Igor Schreiber</i>	22
The detection of Hopf bifurcations in large scale problems arising in computational fluid dynamics <i>Alastair Spence</i>	42
Cancer Diagnosis with PESI-Mass Spectrometry Data: A learning machine approach alternative to the morphology-based pathological method <i>Kunio Tanabe</i>	43
Ecoepidemics with a nonlinear disease incidence <i>Ezio Venturino</i>	46
Microscopic traffic model on the infinite line with bottleneck: standing and traveling waves <i>Bodo Werner</i>	57
Some developments on the global conditional regularity of the Navier-Stokes equations concerning one velocity component <i>Šimon Axmann^{1,2}</i>	61
Spiders on the vineyard with the ballooning effect <i>Martin Biák and Drahoslava Janovská</i>	72
Maximization of schedule reliability under uncertain job processing times <i>Martin Branda¹</i>	80
Numerical study of cooperating thermosolutal convection in a cylindrical annular geometry - Effect of thermal Rayleigh number <i>Bouchra Cheddadi¹ and Abdelkhalek Cheddadi²</i>	88

Solution of Advanced Model of Membrane Diffusion Processes	96
<i>Miroslava Dubcová, Miroslav Zgažar</i>	
Simplified model for a rivulet spreading down an inclined wetted plate	102
<i>Martin Isoz</i>	
On a Toeplitz structure of the characteristic polynomials	119
<i>Drahoslava Janovská¹ and Gerhard Opfer²</i>	
Lumped parameter friction models	132
<i>Vladimír Janovský</i>	
On cover-incomparability graphs	150
<i>Jana Maxová and Daniel Turzík</i>	
Study on Bi-Substrate Enzymatic Reactions through Variational Iteration Method	157
<i>F A Basir[†] S Nandi[‡] Priti Kumar Roy[†] R Bhattacharyya[‡] M K Ghosh[†]</i>	
Homomorphisms, Structural Ramsey Theory and Limits	168
<i>Jaroslav Nešetřil</i>	
Seven Conjectures On Lucky Numbers	169
<i>Pavla Pavlíková</i>	
Fourier Invariants	175
<i>Pavel Pokorný</i>	
Enhancement of Biodiesel Production from Jatropha Curcas oil: A Math- ematical Study through Control on Backward Reaction Process	178
<i>Priti Kumar Roy and Fahad Al Basir</i>	
Theory of multipoint boundary value problem and some of its applications	190
<i>Carmen Šimerská</i>	
One example of correspondence between deterministic and stochastic dif- ferential equations	204
<i>Jana Šnupárková</i>	
The number of symmetric colorings of the dihedral group D_4	211
<i>Iryna Kashuba¹ and Yuliya Zelenyuk²</i>	
Segment Point Processes	219
<i>Markéta Zikmundová</i>	

Analysis and applications of the space-time discontinuous Galerkin method

Miloslav Feistauer

Charles University Prague, Faculty of Mathematics and Physics

Abstract

The subject of the lecture is the analysis of the space-time discontinuous Galerkin method for the solution of nonstationary, nonlinear, convection - diffusion problems and dynamic elasticity. In the formulation of the numerical scheme, the nonsymmetric, symmetric and incomplete versions of the discretization of diffusion terms and interior and boundary penalty are used. Error estimates are characterized and then the attention is paid to the investigation of unconditional stability of the method. Theoretical results are accompanied by numerical experiments. In the second part the application to the solution of dynamic elasticity problem and fluid-structure interaction will be mentioned.

The results were obtained in cooperation with Monika Balázsová, Martin Hadrava, Adam Kosík and Jaromír Horáček.

Exponential stability of solutions of nonlinear differential equations with Riemann-Liouville fractional integrals in the nonlinearities

Milan Medved[†]

Department of Mathematical Analysis and Numerical Mathematics,
Faculty of Mathematics, Physics and Informatics,
Comenius University
Mlynská dolina, 842 48 Bratislava, Slovakia
e-mail: Milan.Medved@fmph.uniba.sk

Keywords: Riemann-Liouville integral, Caputo's derivative, exponential stability, fractionally damped pendulum.

Abstract We study a nonlinear fractional differential equations with power nonlinearities containing Riemann-Liouville fractional integrals of different fractional orders in the nonlinearities. Equations of this type can be obtained e.g. from fractionally damped second order differential equations with a fractional damping terms, depending on the Caputo's fractional derivatives. An example of such type of equations is the fractionally damped pendulum or fractionally damped oscillator. Using a desingularization method a sufficient condition for the exponential stability of the zero solution of this type of equations is proved.

1 INTRODUCTION

Fractional Calculus and the theory of fractional differential equations have become very useful in many applications in applied sciences. Fundamentals of this calculus and the theory of fractional differential equations can be found in the book by K. Miller and B. Ross [22]. The book by I. Podlubny [28] contains a very good introduction to the theory of fractional differential equations. Fundamentals of this theory can be found also in the books [13] and [10].

Fractional differential equations of the Caputo's type in an explicit general form can be defined as equations of the form

$${}^c D^\alpha x(t) = \tag{1}$$

$$F(x(t), x'(t), \dots, x^{(k)}(t), {}^c D^{\beta_1} x(t), \dots, {}^c D^{\beta_m} x(t), I^{\alpha_1} x(t), \dots, I^{\alpha_l} x(t)),$$

where ${}^c D^\alpha x(t)$, ${}^c D_i^\beta x(t)$, $i = 1, 2, \dots, m$ are the Caputo's fractional derivatives and $I_j^\alpha x(t)$, $j = 1, 2, \dots, l$ are the Riemann-Liouville fractional integrals of $x(t)$ defined below.

The fractional differential equations are recently very intensively studied. However even linear fractional differential equations are very complicated. There

are many differences between the theory of ordinary differential and the theory of fractional differential equations. The most close to the dynamical system defined by the autonomous differential equation

$$\dot{x}(t) = f(x), \quad x \in R^n$$

is the fractional differential equation

$${}^c D^\alpha x(t) = f(x(t)), \quad x \in R^n.$$

Real solutions of the equation $f(x) = 0$ are constant solutions, or equilibrium points, respectively, for the both equations. Generic results for the autonomous differential equations and vector fields on manifolds and generic results on bifurcations of one-parameter families of vector fields, locally defined as equations of the form

$$\dot{x}(t) = g(x, \mu), \quad x \in R^n, \mu \in R, \quad (2)$$

are proved in details in the monograph [20]. The books [9] and [1] contain many results and information on dynamical systems, bifurcation theory, on chaotic properties of different mathematical models of mechanical systems, electronic systems, chemical and biological systems and hydrodynamical systems.

From the generic results (see [20]) it follows that the set of $K(g) := \{(x, \mu) \in R^n \times R : g(x, \mu) = 0\}$, where $g : R^n \times R \rightarrow R^n, f \in C^r, r \geq 3$ is generically a one-dimensional C^r -submanifold of $R^n \times R$ and the set of all bifurcation points, where the saddle node or the Hopf bifurcations appear, consists of isolated points. The set $K(g)$ is also the set of equilibrium points of the one-parameter family of fractional differential equation

$${}^c D^\alpha x(t) = g(x(t), \mu), \quad x \in R^n, \mu \in R^n.$$

However the generic bifurcations of these fractional differential equations have not been studied yet. There are no results about an existence of a "center manifold" which plays an important role in the theory of generic bifurcations for dynamical systems. The stability results for equilibrium points of fractional differential equations are much more complicated than those for the dynamical systems (see e. g. [13], [15] and [27]). Many problems concerning generic properties and bifurcations of fractional differential equations, their numerical analysis and their applications remain open.

In this paper we study equations of the type (1), where α is a natural number and the right-hand side is independent of the Caputo's derivatives.

An example of equation of this type is the well known Bargley-Torvik equation

$$u''(t) + A {}^c D^{\frac{3}{2}} u(t) = au(t) + \phi(t), \quad (3)$$

(see [31]) modelling the motion of a rigid plate immersing in a viscous liquid with the fractional damping term $A {}^c D^{\frac{3}{2}} u(t)$.

Solutions of the linear fractionally damped oscillator equation with the Caputo's derivative are analyzed in the paper [23]. Interesting results concerning

boundary value problems for the following generalized Bagely-Torvik equation

$$u''(t) + A {}^c D^\alpha u(t) = f(t, u(t), {}^c D^\beta u(t), u'(t)) \quad (4)$$

and for some further fractional differential equations are published in the papers [1], [2], [24] and [30]. We were motivated by the paper [29], where an existence and uniqueness result for the initial value problem

$$Au'' + \sum_{k=1}^N B_k {}^c D^{\alpha_k} u(t) = f(t, u), \quad u(0) = u_0, \quad u'(0) = c_1, \quad (5)$$

$$0 < \alpha_k < 2, \quad k = 1, 2, \dots, N$$

is proved. The Caputo's fractional derivatives in the equation (5) play there the role of damping terms. This type of equations can be written as a system of differential equations with the Riemann-Liouville integrals on their right-hand sides (see Section 2). Abstract evolution equations with fractional derivatives in the nonlinearities are studied in the paper [11].

This paper is concerned with the following initial value problem

$$\dot{x}(t) = Ax(t) + f\left(t, x(t), (I^{\alpha_1}[g_1x])(t), \dots, (I^{\alpha_m}[g_mx])(t)\right), \quad x(t) \in R^n, \quad (6)$$

$$x(0) = x_0, \quad (7)$$

where A is a constant matrix, $0 < \alpha < 1$, $f : R \times R^n \times R^n \rightarrow R^n$ is a continuous map, $g_i : R \times R^n \rightarrow R^n$, $(t, x) \mapsto g_i(t, x)$, $i = 1, 2, \dots, m$ are continuous maps,

$$(I^{\alpha_i}[g_ix])(t) := \frac{1}{\Gamma(\alpha_i)} \int_0^t (t-s)^{\alpha_i-1} g_i(s, x(s)) ds, \quad 0 < \alpha_i < 1 \quad (8)$$

- the Riemann-Liouville fractional integrals of the function $[g_ix](t) := g_i(t, x(t))$ of order α_i .

In the paper [21] a theorem on the nonexistence of blowing-up solutions for a delay fractional differential equation of the type (6) is proved. In the paper [12] a similar theorem is proved for the delay equation of the type (6) with $m = 1$. In this paper we study the stability problem for the equation (6).

Fractionally damped pendulums or oscillators are studied e. g. in the papers [23], [29], where also some further papers devoted to this type of equations can be found in the list of references.

The following equation is a fractionally ordinary damped pendulum with the damping term $\lambda x'(t)$:

$$x''(t) + \lambda_1 {}^c D^{\beta_1} x(t) + \dots + \lambda_m {}^c D^{\beta_m} x(t) + \lambda x'(t) + \omega^2 x(t) = g(t, x(t), x'(t)), \quad t > 0,$$

where

$${}^c D^{\beta_i} x(t) = \frac{1}{\Gamma(1-\beta_i)} \int_0^t (t-s)^{-\beta_i} x'(s) ds$$

is the Caputo's derivative of the function $x(t)$ of order $\beta_i \in (0, 1)$. The fractional damping terms are

$$\lambda_1 {}^c D^{\beta_1} x(t), \dots, \lambda_m {}^c D^{\beta_m} x(t).$$

If we denote $z_1(t) = x(t), y_2(t) = x'(t), z(t) = (z_1(t), z_2(t))^T$ then we can write this equation as a system of the form (4).

In the paper [23] the equation

$$x'' + \lambda_0 {}^c D^\alpha x + \omega^2 x = 0, \quad x(0) = x_0, x'(0) = x_1, \lambda > 0.$$

is analyzed by using the fractional version of the Laplace transformation.

The Laplace image of $x(t)$ is

$$X(s) = \frac{sx_0 + x_1 + \lambda s^{\alpha-1} x_0}{s^2 + \lambda s^\alpha + \omega^2}$$

and equation

$$s^2 + \lambda s^\alpha + \omega^2 = 0.$$

is the characteristic equation for the fractional differential equation.

If $\alpha = \frac{p}{q}$, then the characteristic equation is

$$s^2 + \lambda s^{\frac{p}{q}} + \omega = 0.$$

This type of equations is analyzed e. g. in [26], [27] and [23].

It is clear that the exact analysis of linear fractional systems is extraordinary difficult. Some analysis and simulations of fractional-order systems can be found in the book [26] and in the paper [27].

The form of the equation (4) enables us to avoid these difficulties in the study of the stability problem by using a desingularization method developed in the papers [17], [18], [19].

2 BIHARI INTEGRAL INEQUALITY AND ITS FRACTIONAL VERSION

In this section we recall the well-known Bihari inequality (see e. g. [3], [4], [5], [7] and [25]) and its generalizations to integral inequalities with weakly singular kernels which are recently frequently used in the theory of fractional differential equations.

Theorem 1. . Let $F(t)$ be a continuous, nonnegative function on $[a, \infty)$, c is a nonnegative constant, $\omega(u)$ is a continuous, nonnegative and nondecreasing function on $[0, \infty)$, positive for $u > 0$ and let $u(t)$ be a continuous, nonnegative function satisfying the integral inequality

$$u(t) \leq c + \int_a^t F(s)\omega(u(s))ds, \quad t \geq a.$$

Then

$$u(t) \leq \Omega^{-1} \left(\Omega(c) + \int_a^t F(s) ds \right), t \geq a.$$

$$\Omega(v) = \int_{v_0}^v \frac{d\sigma}{\omega(\sigma)}, v \geq v_0 > 0.$$

Corollary 1. . If $\omega(u) = u$, then

$$u(t) \leq ce^{\int_a^t F(s) ds}, t \geq a$$

- the Gronwall inequality.

Corollary 2. If $\omega(u) = u^m$, $m > 1$ and

$$\int_a^\infty F(s) ds < \frac{1}{(m-1)c^{m-1}}$$

then

$$u(t) \leq \frac{c}{\left(1 - (m-1)c^{m-1} \int_a^t F(s) ds\right)^{\frac{1}{m-1}}}, t \geq a.$$

Corollary 3. . If $\omega(u) = u^m$, $0 < m < 1$, then

$$u(t) \leq \left(c^{1-m} + (1-m) \int_a^t F(s) ds \right)^{\frac{1}{1-m}}, t \geq a.$$

Singular version of the Bihari inequality, studied in the papers [17] - [19], is an inequality of the form

$$u(t) \leq c + \int_0^t (t-s)^{\alpha-1} F(s) \omega(u(s)) ds, t \geq 0,$$

where $u(t), F(t), c$ are as in Theorem 1 and $0 < \alpha < 1$.

If $\omega(u) = u, F(t) \equiv b$, where $b > 0$ is a constant, then by [8] this inequality yields

$$u(t) \leq c + b\Theta \int_0^t E'_\alpha(\Theta(t-s)) ds,$$

where

$$\Theta = (b\Gamma(\alpha))^{\frac{1}{\alpha}}, E_\alpha(z) = \sum_{n=0}^{\infty} \frac{z^{n\alpha}}{\Gamma(n\alpha + 1)}, E'_\alpha(z) = \frac{d}{dz} E_\alpha(z).$$

The proof of this result is obtained by an iteration argument. However it is clear that this method is not applicable to the nonlinear case. We have developed a method of desingularization of the nonlinear singular integral inequality in the papers [17]- [19] which enables to reduce this inequality to the Bihari case. We will use this method also in the next section in the proof of a stability theorem.

3 EXPONENTIAL STABILITY OF FRACTIONALLY PERTURBED DIFFERENTIAL EQUATIONS

In the stability theory of ordinary differential equations, Lyapunov's direct method, called also the second Lyapunov's method, is frequently used. It is also used in the theory of partial and integral equations. This method has been successfully applied also for fractional differential equations (see e. g. the papers [14] and [15]). The stability of integral and fractional differential equations by an application of the second Lyapunov's method is studied in the monograph by T. A. Burton [6]. However this method is not applicable to a wide class of systems not having the Lyapunov's function. One of the most effective method applicable to this class of systems is the method of integral inequalities. We present a result on the exponential stability of a class of fractional differential equations with its proof, where the method of integral inequalities with weakly singular kernels is applied.

Theorem 2. *Let the following conditions be satisfied:*

(H1)

$$\|e^{At}x\| \leq Ke^{-at}\|x\|$$

for all $t \geq 0, x \in R^n$, i.e. all eigenvalues of the matrix A have negative real parts;

(H2)

Let $f : R \times R^n \times R^{nm} \rightarrow R^n$ be a continuous mapping with

$$\|f(t, u, w_1, \dots, w_m)\| \leq$$

$$P(t)e^{-\gamma t}\|u\|^k + S_1e^{-\omega_1 t}\|w_1\|^k + \dots + S_me^{-\omega_m t}\|w_m\|^k$$

for all $(t, u, \dots, w_m) \in R_+ \times R^n \times R^{nm}$, where $P(t)$ is a continuous, nonnegative function on $[0, \infty)$, $S_j, j = 1, 2, \dots, m$ are nonnegative constants, $\gamma > 0, \omega_j > 0, j = 1, 2, \dots, m, k > 0$ are constants;

(H3)

Let $g_j : R \times R^n \rightarrow R^n, j = 1, 2, \dots, m$ are continuous mappings with

$$\|g_j(t, w)\| \leq R_j(t)\|w\|^k$$

for all $(t, w) \in R \times R^n$, where $R_j(t)$ are nonnegative, continuous functions;

(H4)

There exist numbers $p_j > 1, j = 1, 2, \dots, m$ such that $p_j(\alpha_j - 1) + 1 > 0$ and

$$\int_0^\infty P(s)^q ds < \infty, \int_0^\infty R_j(s)^{q_j} ds < \infty, j = 1, 2, \dots, m,$$

where $q_j = \frac{p_j}{p_j - 1}, q = q_1 q_2 \dots q_m$;

(H5)

$$\gamma > a(1+k), \omega_j > 1+a, j = 1, 2, \dots, m,$$

Then the following assertions hold:

(A1) If $0 < k \leq 1$, then the trivial solution of the initial value problem (4), (5) is exponentially stable for any initial value x_0 .

(A2) If $k > 1$, then the trivial solution of the initial value problem (4), (5) is exponentially stable for $\|x_0\|$ small enough.

We shall need the following lemma in the proof of this theorem.

Lemma 1. Let $p_j, \alpha_j, j = 1, 2, \dots, m$ satisfy the condition (H4). Then

$$\int_0^t (t-s)^{p_j(\alpha_j-1)} e^{p_j s} ds \leq Q_j e^{p_j t}, \quad t \geq 0, \quad j = 1, 2, \dots, m,$$

where

$$Q_j = \frac{\Gamma(1+p_j(\alpha_j-1))}{p^{1+p_j(\alpha_j-1)}},$$

$\Gamma(u)$ is the Gamma function.

For the proof of this lemma see [17].

Proof :

Let $x(t)$ be a solution of the initial value problem (4), (5) defined on $[0, \infty)$ and $u(t) = \|x(t)\|e^{at}$, $C = K\|x_0\|$, $S = \max\{S_j : j = 1, 2, \dots, m\}$. Then (H1) – (H4) yields

$$\begin{aligned} u(t) &\leq C + K \int_0^t e^{-[\gamma-(1+k)]as} P(s) u(s)^k ds + \\ &KS \sum_{j=1}^m \int_0^t e^{-(\omega_j-a)s} \int_0^s (s-\tau)^{\alpha_j-1} R_j(\tau) e^{-ak\tau} u(\tau)^k d\tau ds, \end{aligned}$$

Using the Hölder inequality and Lemma 1 we can estimate

$$\begin{aligned} &\int_0^s (s-\tau)^{\alpha_j-1} R_j(\tau) e^{-ak\tau} u(\tau)^k d\tau \leq \\ &\left(\int_0^s (s-\tau)^{p_j(\alpha_j-1)} e^{p_j\tau} d\tau \right)^{\frac{1}{p_j}} \left(\int_0^s e^{-(1+ak)q_j\tau} R_j(\tau)^{q_j} u(\tau)^{kq_j} d\tau \right)^{\frac{1}{q_j}} \leq \\ &Qe^s \left(\int_0^s e^{-(1+ak)q_j\tau} R_j(\tau)^{q_j} u(\tau)^{kq_j} d\tau \right)^{\frac{1}{q_j}}, \end{aligned}$$

where $Q = \max\{Q_j : j = 1, 2, \dots, m\}$ and

$$\int_0^s e^{-[\gamma-(1+k)a]\tau} P(\tau) u(\tau)^k d\tau \leq \int_0^s \left(e^{-[\gamma-(1+k)a]p\tau} d\tau \right)^{\frac{1}{p}} \left(\int_0^s P(\tau)^q u(\tau)^{kq} d\tau \right)^{\frac{1}{q}},$$

where $q = q_1 q_2 \dots q_m, p = \frac{q}{q-1}$. These two inequalities yield the following estimate for $u(t)$:

$$\begin{aligned} u(t) &\leq C + \frac{1}{\gamma - (1+k)a} \left(\int_0^t P(s)^q u(s)^q ds \right)^{\frac{1}{q}} + \\ KSQ \sum_{j=1}^m \int_0^t e^{-[\omega_j - (1+a)]s} &\left(\int_0^s e^{-(1+ak)q_j \tau} R_j(\tau)^{kq_j} u(\tau)^{kq_j} d\tau \right)^{\frac{1}{q_j}} \leq \\ C + \frac{1}{\gamma - (1+k)a} &\left(\int_0^t P(s)^q u(s)^q ds \right)^{\frac{1}{q}} + \\ KSQ \sum_{j=1}^m \frac{1}{\omega_j - (1+a)} &\left(\int_0^t e^{-(1+ak)q_j \tau} R_j(\tau)^{kq_j} u(\tau)^{kq_j} d\tau \right)^{\frac{1}{q_j}}. \end{aligned}$$

Therefore there are positive constants D_1, D_2 such that

$$u(t) \leq C + D_1 \left(\int_0^t P(s)^q u(s)^q ds \right)^{\frac{1}{q}} + D_2 \sum_{j=1}^m \left(\int_0^t e^{-(1+ak)q_j \tau} R_j(\tau)^{kq_j} u(\tau)^{kq_j} d\tau \right)^{\frac{1}{q_j}}.$$

Using the elementary inequality

$$\left(\sum_{i=1}^{m+2} a_i \right)^q \leq (m+2)^{q-1} \sum_{i=1}^{m+2} a_i^q$$

for any nonnegative numbers a_1, a_2, \dots, a_m we obtain

$$\begin{aligned} u(t)^q &\leq (m+2)^{q-1} [C^q + D_1^q \int_0^t P(s)^q u(s)^q ds + \\ D_2^q \sum_{j=1}^m &\left(\int_0^t e^{-(1+ak)q_j \tau} R_j(\tau)^{kq_j} u(\tau)^{kq_j} d\tau \right)^{\hat{q}_j}, \end{aligned}$$

where $\hat{q}_j = q_1 q_2 \dots q_{j-1} q_{j+1} \dots q_m$. The Hölder inequality yields

$$\begin{aligned} \int_0^t e^{-(1+ak)q_j \tau} R_j(\tau)^{kq_j} u(\tau)^{kq_j} d\tau &\leq \\ \left(\int_0^t e^{-(1+ak)q_j \hat{p}_j \tau} d\tau \right)^{\frac{1}{\hat{p}_j}} &\left(\int_0^t R_j(\tau)^q u(\tau)^{kq} d\tau \right)^{\frac{1}{q_j}} \leq \frac{1}{(1+ak)q_j} \left(\int_0^t R_j(\tau)^q u(\tau)^{kq} d\tau \right)^{\frac{1}{q_j}}, \end{aligned}$$

where $\hat{p}_j = \frac{q_j}{q_j-1}$. Therefore we have the inequality

$$u(t)^q \leq (m+2)^{q-1} K^q \|x_0\|^q + H_1 \int_0^t P(s)^q u(s)^{kq} ds + H_2 \sum_{j=1}^m \int_0^t R_j(s)^q u(s)^{kq} ds$$

form some constants H_1, H_2 . Thus we have the inequality for $v(t) = u(t)^q$:

$$v(t) \leq (m+2)^{q-1} K^q \|x_0\|^q + \int_0^t F(s) v(s)^k ds,$$

where

$$F(t) = H_1 P(t)^q + H_2 \sum_{j=1}^m \int_0^t R_j(s) ds$$

From the condition (H4) it follows that $\int_0^\infty F(s) ds < \infty$ and therefore we have:

If $k = 1$, then the Gronwall inequality yields

$$v(t) \leq G_1 = (m+2)^{q-1} K^q \|x_0\|^q \int_0^\infty F(s) ds < \infty$$

and thus $u(t) = v(t)^{\frac{1}{q}} \leq G_1^{\frac{1}{q}}$ for all $t \geq 0$

or

$$\|x(t)\| \leq (m+2)^{\frac{q-1}{q}} K \|x_0\| e^{-at}, \quad t \geq 0$$

If $0 < k < 1$, then by the Corollary 3

$$v(t) \leq G_1 = \left([(m+2)^{q-1} K^q \|x_0\|^q]^{1-k} + (1-k) \int_0^\infty F(s) ds \right)^{\frac{1}{1-k}}, \quad t \geq 0 < \infty$$

and thus

$$\|x(t)\| \leq G_2^{\frac{1}{q}} e^{-at} \quad t \geq 0.$$

If $k > 1$, then by the Corollary 2

$$v(t) \leq G_3 = \frac{(m+2)^{q-1} K^q \|x_0\|^q}{\left(1 + (k-1) [(m+2)^{q-1} K^q \|x_0\|^q]^{k-1} \int_0^\infty F(s) ds \right)^{\frac{1}{k-1}}}, \quad t \geq 0.$$

Obviously $G_3 < \infty$ for $\|x_0\|$ sufficiently small,

$$\|x(t)\| \leq G_3^{\frac{1}{q}} e^{-at}, \quad t \geq 0$$

and the proof is complete. ■

Acknowledgments: This work was supported by the Slovak Grant Agency VEGA No. 1/0071/14.

References

1. R. P. AGARWAL, D. O'REGAN AND S. STANĚK: *Positive solutions for Dirichlet problems of singular fractional differential equations*, J. Math. Anal. Appl. , Vol. 371 (2010), pp.57-68.

2. R. P. AGARWAL, D. O'REGAN AND S. STANĚK: *Positive solutions for mixed problems of singular fractional differential equations*, *Mathematische Nachrichten*, Vol. 11 (2011), pp. 329-341. pp.57-68.
3. D. BAINOV: *Integral inequalities and Applications*, Kluwer Academic Publisher, Dordrecht, Boston, London 1992.
4. E. F. BECKENBACH AND R. BELLMAN: *Inequalities*, Springer-Verlag, New York 1961.
5. I. BIHARI: *A generalization of a lemma of Bellman and its application to uniqueness problems of differential equations*, *Acta Math. Acad. Sci. Hungar.*, Vol. 7 (1956), 71-94.
6. T. A. BURTON: *Liapunov Theory for Integral Equations with Singular Kernels and Fractional Differential Equations*, Northwest Research Institute, Port Angeles 2012.
7. B. P. DEMIDOVICH: *Lectures on Mathematical Theory of Stability*, Nauka, Moscow 1967 (in Russian).
8. D. HENRY: *Geometric Theory of Semilinear Parabolic Equations*, LNM 840, Springer-Verlag, Berlin 1981.
9. M. HOLODNIOK, A. KLÍČ, M. KUBÍČEK AND M. MAREK: *Matematická Analýza Nelineárních Dynamických Modelu*, *Academia*, Praha 1986 (in Czech).
10. A. A. KILBAS, H. M. SRIVASTAVA AND J. J. TRUJILLO: *Theory and Applications of Fractional Differential Equations*, North-Holland Mathematics Studies 2014, Elsevier, Amsterdam 2006.
11. M. KIRANE, M. MEDVEĎ AND N. E. TATAR: *Semilinear Volterra integrodifferential problems with fractional derivatives in the nonlinearities*, *Abstract and Applied Analysis*, Vol. 2011 (2011), Article ID 510314.
12. M. KIRANE, M. MEDVEĎ AND N. E. TATAR: *On the nonexistence of blowing-up solutions to a fractional functional-differential equations*, *Georgia J. Math.* 19 (2012), 127-144.
13. V. LAKSHMIKANTHAM, S. LEELA AND J. VASUNDHARA DEVI: *Theory of Fractional Dynamic Systems*, Cambridge Scientific Publishers 2009.
14. Y. LI, Y. Q. CHEN AND I. PODLUBNÝ: *Mittag-Leffler stability of fractional order nonlinear dynamic systems*, *Automatica* 45 (2009), 1965-1969.
15. C. P. LI AND F. R. ZHANG: *A survey on the stability of fractional differential equations*, *Eur. Phys. J. Special Topics* 193 (2011), 27-47.
16. M. MAREK AND I. SCHREIBER: *Chaotic Behaviour of Deterministic Dissipative Systems*, *Academia*, Prague 1991.
17. M. MEDVEĎ: *A new approach to an analysis of Henry type integral inequalities and their Bihari type versions*, *J. Math. Anal. Appl.*, Vol. 214 (1997), pp. 349-366.
18. M. MEDVEĎ: *Integral inequalities and global solutions of semilinear evolution equations*, *J. Math. Anal. Appl.*, Vol. 267 (2002), pp. 643-650.
19. M. MEDVEĎ: *Singular integral inequalities with several nonlinearities and integral equations with singular kernels*, *Nonlinear Oscillations*, Vol. 11 (2008), pp. 71-80.
20. M. MEDVEĎ: *Fundamentals of Dynamical Systems and Bifurcation Theory*, Adam Hilger, Bristol, Philadelphia and New York 1992.
21. M. MEDVEĎ: *Functional-differential equations with Riemann-Liouville integrals in the nonlinearities*, accepted to *Mathematica Bohemica*, *Proceedings of Equadiff 13*, Prague 2013.
22. K. MILLER AND B. ROSS: *An Introduction to the Fractional Calculus and Fractional Differential Equations*, John Wiley and Sons, Inc. New York 1993.
23. M. NABER: *Linear fractionally damped oscillator*, *International J. Diff. Eqs.*, Vol. 2010 (2010), ID 197020.

24. D. O'REGAN AND S. STANĚK: *Fractional boundary value problems with singularities in space variables*, Nonlinear Dyn., Vol. 71 (2013), pp. 641-652.
25. B. G. PACHPATTE: *Integral and Finite Difference Inequalities and Applications*, North-Holland Mathematical Studies 205, Elsevier, Amsterdam 2006.
26. I. PETRÁŠ: *Stability of fractional-order systems with rational orders: Survey*, Fractional Calculus and Applied Analysis, Vol. 12 (2009), 272-298.
27. I. PETRÁŠ: *Fractional-order Nonlinear Systems. Modeling, Analysis and Simulation*, Higher Education Press, Springer 2011.
28. I. PODLUBNÝ: *Fractional Differential Equations*, Academic Press, New York 1999.
29. M. SEREDYNSKA AND A. HANYGA: *Nonlinear differential equations with fractional damping with applicatios to the 1dof and 2dof pendulum*, Acta Mechanica, Vol. 176 (2005), pp. 169-183.
30. S. STANĚK: *Two-point boundary value problems for the generalized Bagley-Torvik fractional differential equations*, Nonlinear Dyn., Vol. 71 (2013), 574-592.
31. P. J. TORVIK AND R. L. BAGLEY: *On the appearance of the fractional derivatives in the behavior of real materials*, Trans. ASME J. Appl. Mech., Vol. 51 (1984), pp. 294-298.

The algebraic Riccati equation with matrix entries from noncommutative algebras

Gerhard Opfer

University of Hamburg

Keywords: Algebraic Riccati equation, quaternions, noncommutative algebras in \mathbb{R}^4 , Newton method

Abstract

The equation mentioned in the title is the simplest nonlinear matrix equation

$$(*) \quad \mathbf{R}(\mathbf{X}) := \mathbf{XDX} + \mathbf{CX} + \mathbf{XB} + \mathbf{A} = \mathbf{0}, \quad \text{where}$$

$$\mathbf{X} \in \mathbb{C}^{m \times n}, \mathbf{D} \in \mathbb{C}^{n \times m}, \mathbf{C} \in \mathbb{C}^{m \times m}, \mathbf{B} \in \mathbb{C}^{n \times n}, \mathbf{A} \in \mathbb{C}^{m \times n}.$$

See e. g. Abou-Kandil, Freiling, Ionescu, Jank, 2003. The equation (*) mimics the stationary solutions of the Riccati differential equation

$$\dot{x}(t) = d(t)x^2(t) + b(t)x(t) + a(t) \quad (\text{see e. g. Reid, 1972}).$$

The one dimensional equation (*) with $\mathbf{X}, \mathbf{D}, \mathbf{C}, \mathbf{B}, \mathbf{A} \in \mathbb{H}$ where \mathbb{H} stands for the space of quaternions was recently solved by Janovská & O., 2013. In this talk we want to discuss the case where the above \mathbb{C} , the field of complex numbers, is replaced with an algebra \mathcal{A} in \mathbb{R}^4 . The set of these algebras contains coquaternions tessarines, cotessarines (Cockle, 1849) and others (Schmeikal, 2014). Thus we consider (*) where the matrix entries are from \mathcal{A} . Since explicit solutions of (*) can in general not be expected, we show that the linearized version of (*) is easy to derive by results from Lauterbach & O., 2014, and we will also show by presenting numerical examples, that the corresponding Newton method works very well and produces solutions of (*) for various algebras in \mathbb{R}^4 .

The talk is based on joint research with Drahoslava Janovská, Institute of Chemical Technology, Prague.

Acknowledgments: The research was supported by DFG, GZ OP 33/19-1.

Reaction network analysis of oscillatory instabilities in a model of noxious components removal in the three-way catalytic converter

Otto Hadač and Igor Schreiber

Institute of Chemical Technology, Prague

Keywords: stoichiometric network, extreme currents, oscillatory subnetwork, role of species, classification of chemical oscillators

Abstract This paper presents stability analysis of the reaction network corresponding to the mechanism of simultaneous oxidation of carbon monoxide CO, unburned hydrocarbons represented by acetylene C₂H₂ and reduction of nitrogen oxides NO_x, taking place in the three-way catalytic converter used in cars to remove noxious components from exhaust gases. We use stoichiometric network analysis as a methodology for decomposing the entire mechanism into irreducible subnetworks (extreme currents) and examining stability of corresponding steady states. This method allows for indication of those subnetworks, which may within a range of kinetic parameters display instabilities leading to oscillations. Within those subnetworks the major positive and negative feedbacks are used to explain the oscillatory dynamics in chemical terms, i.e., the role of chemical species and classification of the oscillatory modes are proposed.

1 Introduction

Although oscillatory dynamics in heterogeneous chemical reaction systems were already discovered in the 19th century [1], the research on oscillations in the course of catalytic CO oxidation over Pt has not begun before the 1970s [2, 3]. Since then oscillatory surface reactions became a field of very active research where some 65 oscillatory heterogeneous catalytic systems have been discovered [4]. Most of these catalytic systems represent catalytic oxidation of organic compounds on noble metal catalysts followed by catalytic hydrogenation or catalytic decomposition of various compounds.

Heterogeneous catalytic reactions represent nonlinear multilevel dynamical systems, operated far from thermodynamic equilibrium, which are capable of generating a broad variety of complex temporal and spatiotemporal patterns

that can originate at various levels of a heterogeneous catalytic system. These levels range from an element on a single crystal surface up to a catalyst bed or a monolith. From a spatially extended single crystal surface up, a heterogeneous catalytic system can be modeled as a set of local oscillators where more or less synchronized behavior not only depends upon the properties of local oscillators but also on the strength and the nature of the coupling between them [5]. If periodic oscillatory behavior of the global reaction rate is observed, then there is complete synchronization of the local oscillators at each level of the system. Coupling between the local oscillators may occur through surface diffusion, diffusion through the gas phase, and by heat transfer. The dominant mechanism of synchronization depends upon the nature of the local oscillators and the experimental conditions used [6, 7].

Dynamic behavior taking place on extended single crystal surfaces can be visualized by the photoemission electron microscopy (PEEM) [8]. Then a broad variety of spatiotemporal patterns was observed, including target patterns, rotating spiral waves, standing waves and cellular structures [7]. It was shown that two mechanisms of coupling via surface diffusion and diffusion via the gas phase operated over single crystal surfaces under ultra high vacuum (UHV) conditions. However, in contrast to the very fine metal tips used in the group of Nieuwenhuys (see for example ref. [9]), synchronization under these conditions takes place via gas phase coupling.

Since most surface science methods are limited to the study of reactions over single crystal surfaces under UHV conditions, the study of oscillatory behavior at the macro-level (cm-scale), i.e., extended polycrystalline surfaces under atmospheric pressure conditions, is complicated by several factors. These include gradients of concentration and temperature which can originate both in the reactor and within the catalyst particles. However, the study of the oscillatory behavior of heterogeneous catalytic reactions under atmospheric pressure conditions can produce important information about the reaction mechanism. The information about the reaction mechanism can be obtained from the waveforms of reaction rate oscillations, from the phase shifts between oscillations of different product concentrations, and from visual observations of surface spatiotemporal behavior [5].

2 Chemical processes in the three-way converter

The three-way catalytic converter (TWC) [10] is a catalytic reactor used for simultaneous degradation of carbon monoxide, unburned hydrocarbons and oxides of nitrogen. The device is operated mostly under transient conditions close to a stoichiometric composition. The stoichiometric composition is the ratio of air and fuel injected into gasoline engine such that the mixture has just enough air

to completely burn the available fuel. In practice this is never quite achieved, due to the very short time for each combustion cycle.

Table 1. The detailed reaction mechanism of the TWC; * represents a noble metal (Pt) catalytic site and s indicates an oxygen storing (Ce) site), \square denotes an external source (input) or a sink (output).

No.	Reaction step	Kinetic expression
R ₁	$\text{CO} + * \rightarrow \text{CO}^*$	$v_1 = k_1[\text{CO}][*]$
R ₂	$\text{CO}^* \rightarrow \text{CO} + *$	$v_2 = k_2[\text{CO}^*]$
R ₃	$\text{O}_2 + 2* \rightarrow 2\text{O}^*$	$v_3 = k_3[\text{O}_2][*]$
R ₄	$\text{CO}^* + \text{O}^* \rightarrow \text{CO}_2 + 2*$	$v_4 = k_4[\text{CO}^*][\text{O}^*]$
R ₅	$\text{CO} + \text{O}^* \rightarrow \text{OCO}^*$	$v_5 = k_5[\text{CO}][\text{O}^*]$
R ₆	$\text{OCO}^* \rightarrow \text{CO} + \text{O}^*$	$v_6 = k_6[\text{OCO}^*]$
R ₇	$\text{OCO}^* \rightarrow \text{CO}_2 + *$	$v_7 = k_7[\text{OCO}^*]$
R ₈	$\text{O}_2 + 2s \rightarrow 2\text{O}^s$	$v_8 = k_8[\text{O}_2][s]$
R ₉	$\text{CO}^* + \text{O}^s \rightarrow \text{CO}_2 + * + s$	$v_9 = k_9[\text{CO}^*][\text{O}^s]$
R ₁₀	$\text{C}_2\text{H}_2 + * \rightarrow \text{C}_2\text{H}_2^*$	$v_{10} = k_{10}[\text{C}_2\text{H}_2][*]$
R ₁₁	$\text{C}_2\text{H}_2^* \rightarrow \text{C}_2\text{H}_2 + *$	$v_{11} = k_{11}[\text{C}_2\text{H}_2^*]$
R ₁₂	$\text{C}_2\text{H}_2^* + 2* \rightarrow \text{C}_2\text{H}_2^{**}$	$v_{12} = k_{12}[\text{C}_2\text{H}_2^*][*]^2$
R ₁₃	$\text{C}_2\text{H}_2^{**} \rightarrow \text{C}_2\text{H}_2^* + 2*$	$v_{12} = k_{13}[\text{C}_2\text{H}_2^{**}]$
R ₁₄	$\text{C}_2\text{H}_2^* + 3\text{O}^* \rightarrow 2\text{CO}^* + \text{H}_2\text{O} + 2*$	$v_{14} = k_{14}[\text{C}_2\text{H}_2^*][\text{O}^*]$
R ₁₅	$\text{C}_2\text{H}_2^{**} + 3\text{O}^* \rightarrow 2\text{CO}^* + \text{H}_2\text{O} + 4*$	$v_{15} = k_{15}[\text{C}_2\text{H}_2^{**}][\text{O}^*]$
R ₁₆	$\text{C}_2\text{H}_2 + \text{O}^* \rightarrow \text{C}_2\text{H}_2\text{O}^*$	$v_{16} = k_{16}[\text{C}_2\text{H}_2][\text{O}^*]$
R ₁₇	$\text{C}_2\text{H}_2\text{O}^* \rightarrow \text{C}_2\text{H}_2 + \text{O}^*$	$v_{17} = k_{17}[\text{C}_2\text{H}_2\text{O}^*]$
R ₁₈	$\text{C}_2\text{H}_2^* + 3\text{O}^s + * \rightarrow 2\text{CO}^* + \text{H}_2\text{O} + 3s$	$v_{18} = k_{18}[\text{C}_2\text{H}_2^*][\text{O}^s]$
R ₁₉	$\text{C}_2\text{H}_2\text{O}^* + 2\text{O}^* \rightarrow 2\text{CO}^* + \text{H}_2\text{O} + *$	$v_{19} = k_{19}[\text{C}_2\text{H}_2\text{O}^*][\text{O}^*]$
R ₂₀	$\text{NO} + * \rightarrow \text{NO}^*$	$v_{20} = k_{20}[\text{NO}][*]$
R ₂₁	$\text{NO}^* \rightarrow \text{NO} + *$	$v_{21} = k_{21}[\text{NO}^*]$
R ₂₂	$\text{NO}^* + * \rightarrow \text{N}^* + \text{O}^*$	$v_{22} = k_{22}[\text{NO}^*][*]$
R ₂₃	$\text{NO}^* + \text{N}^* \rightarrow \text{N}_2\text{O}^* + *$	$v_{23} = k_{23}[\text{NO}^*][\text{N}^*]$
R ₂₄	$\text{N}_2\text{O}^* \rightarrow \text{N}_2\text{O} + *$	$v_{24} = k_{24}[\text{N}_2\text{O}^*]$
R ₂₅	$\text{N}_2\text{O}^* \rightarrow \text{N}_2 + \text{O}^*$	$v_{25} = k_{25}[\text{N}_2\text{O}^*]$
R ₂₆	$\text{N}^* + \text{N}^* \rightarrow \text{N}_2 + 2*$	$v_{26} = k_{26}[\text{N}^*]^2$
R ₂₇	$\text{NO} + \text{O}^* \rightarrow \text{NO}_2^*$	$v_{27} = k_{27}[\text{NO}][\text{O}^*]$
R ₂₈	$\text{NO}_2^* \rightarrow \text{NO} + \text{O}^*$	$v_{28} = k_{28}[\text{NO}_2^*]$
R ₂₉	$\text{NO}_2^* \rightarrow \text{NO}_2 + *$	$v_{29} = k_{29}[\text{NO}_2^*]$
R ₃₀	$\text{NO}_2 + * \rightarrow \text{NO}_2^*$	$v_{30} = k_{30}[\text{NO}_2][*]$
R ₃₁	$\square \rightarrow \text{CO}$	$v_{31} = k_{31}[\text{CO}]_{\text{in}}$
R ₃₂	$\text{CO} \rightarrow \square$	$v_{32} = k_{32}[\text{CO}]$
R ₃₃	$\square \rightarrow \text{O}_2$	$v_{33} = k_{33}[\text{O}_2]_{\text{in}}$
R ₃₄	$\text{O}_2 \rightarrow \square$	$v_{34} = k_{34}[\text{O}_2]$
R ₃₅	$\text{CO}_2 \rightarrow \square$	$v_{36} = k_{36}[\text{CO}_2]$
R ₃₆	$\square \rightarrow \text{C}_2\text{H}_2$	$v_{37} = k_{37}[\text{C}_2\text{H}_2]_{\text{in}}$
R ₃₇	$\text{C}_2\text{H}_2 \rightarrow \square$	$v_{38} = k_{38}[\text{C}_2\text{H}_2]$
R ₃₈	$\square \rightarrow \text{NO}$	$v_{39} = k_{39}[\text{NO}]_{\text{in}}$
R ₃₉	$\text{NO} \rightarrow \square$	$v_{40} = k_{40}[\text{NO}]$
R ₄₀	$\square \rightarrow \text{NO}_2$	$v_{41} = k_{41}[\text{NO}_2]_{\text{in}}$
R ₄₁	$\text{NO}_2 \rightarrow \square$	$v_{42} = k_{42}[\text{NO}_2]$

The catalytic oxidation of CO is the most frequently studied oscillatory heterogeneous catalytic system. Under the UHV conditions, CO oxidation on platinum single-crystal surfaces proceeds via a Langmuir-Hinshelwood mechanism [11]. Mechanism of oscillatory CO oxidation under these conditions is connected with a periodic change in surface structure: hex \rightleftharpoons (1 \times 1) phase transition of Pt(100), and (1 \times 1) \rightleftharpoons (1 \times 2) phase transition of Pt(110) [7]. Temporal oscillations of the reaction rate are possible due to an adsorbate-driven phase transition in the top substrate layer [12,13]. Under atmospheric conditions, both periodic and chaotic regimes in the course of CO oxidation on Pt/ γ -Al₂O₃ pellets were found in a fixed-bed reactor containing a large number of catalytic particles [14, 15]. Kapička and Marek [15] observed experimentally transition to chaos via period-doubling bifurcations during a slow, continuous change of the catalyst activity. They found that under gradient as well as nongradient conditions both periodic and aperiodic oscillations have the same mechanistic causes and do not result from transport limitations in the bed or from a different course of the reaction on individual particles. They also found that synchronization/desynchronization of oscillations takes place via the gas phase.

Based on experiments with the commercial Pt/Rh/CeO₂/ γ -Al₂O₃ TWC catalyst, Eindhoven group [16-19] proposed and evaluated detailed kinetics of the TWC. Dynamics of this detailed reaction mechanism was thoroughly studied and compared with experimental results [20,21]. In the following we analyze the mechanism of the TWC taking into account CO, C₂H₂ (a typical hydrocarbon) and NO_x (NO and NO₂) as reactants, see Table 1. In addition to the 30 chemical reactions in the Table, there are also 11 pseudoreactions corresponding to an external source (input) and sink (output) to each of the reactants CO, O₂, C₂H₂, NO, NO₂ and output of CO₂.

3 Stoichiometric network analysis

The stoichiometric network analysis (SNA) [22] begins with the definition of the stoichiometric network involving $n = 19$ chemical species and $r = 41$ (pseudo)reactions. The corresponding rate expressions essentially follow mass action kinetics except where more than two molecules/active sites interact. The first 30 steps are true chemical reactions, the rest are inlets and outlets treated here as pseudoreactions. We assume that the converter behaves as an isothermal ideally mixed system, which is a simplification that does not take into account mass/heat transport phenomena and the spatial extension of the converter but is adequate for examining instabilities caused by nonlinear chemistry of this complex mechanism.

The dynamics of the network is given by the mass balance equations for all species:

$$\begin{aligned}
\frac{d[\text{CO}]}{dt} &= -v_1 + v_2 - v_5 + v_6 + v_{31} - v_{32}, \\
\frac{d[\text{CO}^*]}{dt} &= v_1 - v_2 - v_4 - v_9 + 2v_{14} + 2v_{15} + 2v_{18} + 2v_{19}, \\
\frac{d[\text{OCO}^*]}{dt} &= v_5 - v_6 - v_7, \\
\frac{d[\text{CO}_2]}{dt} &= v_4 + v_7 + v_9 - v_{35}, \\
\frac{d[\text{O}_2]}{dt} &= -v_3 - v_8 + v_{33} - v_{34}, \\
\frac{d[\text{O}^*]}{dt} &= 2v_3 - v_4 - v_5 + v_6 - 3v_{14} - 3v_{15} - v_{16} + v_{17} - 2v_{19} + v_{22} \\
&\quad + v_{25} - v_{27} + v_{28}, \\
\frac{d[\text{O}^s]}{dt} &= 2v_8 - v_9 - 3v_{18}, \\
\frac{d[*]}{dt} &= -v_1 + v_2 - 2v_3 + 2v_4 + v_7 + v_9 - v_{10} + v_{11} - 2v_{12} + 2v_{13} \\
&\quad + 2v_{14} + 4v_{15} - v_{18} + v_{19} - v_{20} + v_{21} - v_{22} + v_{23} + v_{24} \\
&\quad + 2v_{26} + v_{29} - v_{30}, \\
\frac{d[\text{s}]}{dt} &= -2v_8 + v_9 + 3v_{18}, \tag{1} \\
\frac{d[\text{C}_2\text{H}_2]}{dt} &= -v_{10} + v_{11} - v_{16} + v_{17} + v_{36} - v_{37}, \\
\frac{d[\text{C}_2\text{H}_2^*]}{dt} &= v_{10} - v_{11} - v_{12} + v_{13} - v_{14} - v_{18}, \\
\frac{d[\text{C}_2\text{H}_2^{**}]}{dt} &= v_{12} - v_{13} - v_{15}, \\
\frac{d[\text{C}_2\text{H}_2\text{O}^*]}{dt} &= v_{16} - v_{17} - v_{19}, \\
\frac{d[\text{NO}]}{dt} &= -v_{20} + v_{21} - v_{27} + v_{28} + v_{38} - v_{39}, \\
\frac{d[\text{NO}^*]}{dt} &= v_{20} - v_{21} - v_{22} - v_{23}, \\
\frac{d[\text{NO}_2]}{dt} &= v_{29} - v_{30} + v_{40} - v_{41}, \\
\frac{d[\text{NO}_2^*]}{dt} &= v_{27} - v_{28} - v_{29} + v_{30}, \\
\frac{d[\text{N}^*]}{dt} &= v_{22} - v_{23} - 2v_{26}, \\
\frac{d[\text{N}_2\text{O}^*]}{dt} &= v_{23} - v_{24} - v_{25}.
\end{aligned}$$

The rate coefficients in Table 1 are either taken to be Arrhenius temperature-dependent (see [16-19] for relevant expressions) when directly solving Eqs. (1) or considered to be freely adjustable non-negative parameters when applying the SNA. In the former case the control parameters are chosen to be the temperature T (assumed equal at the inlet and inside of the reactor) and the inlet concentration/inflow of reactants (oxygen in particular). Other parameters, such as flow rate, loading capacities of the catalyst and oxygen stores are set so as to maintain consistence with our previous work [23]. Our aim is to systematically compare oscillatory characteristics found by constructing a bifurcation diagram for Eqs. (1) in the temperature—oxygen inflow parameter plane with generic oscillatory characteristics obtained by the SNA approach. From this comparison we draw conclusions on the mechanistic causes of the observed oscillatory dynamics.

Eqs. (1) can be rewritten in a compact matrix form,

$$\frac{d\mathbf{x}}{dt} = \mathbf{S} \mathbf{v}(\mathbf{x}, \mathbf{k}), \quad (2)$$

where $\mathbf{x} \in \mathbb{R}_+^n$ is the concentration vector, $\mathbf{S} \in \mathbb{R}^{n \times r}$ is the stoichiometric matrix whose elements are differences of the right and left stoichiometric coefficients of species i in reaction j , $\nu_{ij} = \nu_{ij}^R - \nu_{ij}^L$, $\mathbf{v} \in \mathbb{R}_+^r$ is the reaction rate vector, and $\mathbf{k} \in \mathbb{R}_+^f$ is the vector of the rate coefficients. The rank of \mathbf{S} is $d = 17$ and determines both the maximum number of linearly independent species and the maximum number of linearly independent reactions. This also implies that there are $n - d = 2$ conservation constraints, which correspond to chemical species bound to platinum ($*$) or cerium (s) catalytic sites.

In general, reaction rates obey the physical constraint $v_i(\mathbf{x}, \mathbf{k}) \geq 0$, for $i = 1, \dots, 41$. Since any steady state \mathbf{x}^0 solves the equation $\mathbf{S} \mathbf{v} = \mathbf{0}$, the corresponding steady-state rate vector $\mathbf{v}^0 = \mathbf{v}^0(\mathbf{x}^0, \mathbf{k})$ lies in the intersection of the null space of \mathbf{S} and the positive orthant $\bar{\mathbb{R}}_+^r$, i.e. $\mathbf{v}^0 \in \text{Ker}(\mathbf{S}) \cap \bar{\mathbb{R}}_+^r$. Thus the set of all \mathbf{v}^0 s form an unbounded convex cone $\mathcal{C}_v \equiv \{\mathbf{v}^0 \in \bar{\mathbb{R}}_+^r \mid \mathbf{S} \mathbf{v}^0 = \mathbf{0}\}$ of dimension $\dim \mathcal{C}_v = \dim \text{Ker}(\mathbf{S}) = r - d = 24$. The cone \mathcal{C}_v can be expressed as a convex combination of column vectors \mathbf{E}_i of a matrix $\mathbf{E} \in \mathbb{R}^{r \times f}$,

$$\mathcal{C}_v = \{\mathbf{E} \mathbf{j} \mid \mathbf{j} \in \bar{\mathbb{R}}_+^f\}, \quad (3)$$

The vectors \mathbf{E}_i point along the edges of the cone \mathcal{C}_v so that they form the cone's frame. The edges of the cone \mathcal{C}_v represent a set of steady states having a minimum possible nonzero reaction rates v_i and thus uniquely define the set of irreducible elementary subnetworks of the mechanism. The cone can be spanned by more than $r - d$ frame vectors, $f \geq r - d = 24$ so the edges may not be all linearly independent. Moreover, certain edges span k -dimensional faces of \mathcal{C}_v , where $k = 2, \dots, 23$. The edges (or 1-faces) and k -faces constitute a natural hierarchy of increasingly complex subnetworks that may be used as a basis for reduced models of the full network. The software we use for decomposition of

the stoichiometric network, i.e. calculation of \mathbf{E} , is based on a pathway oriented algorithm [24]. The identification of the edges and faces is a first step when examining the stability of the (sub)networks at the steady state \mathbf{x}^0 .

The dynamical behavior of the system is described by Eq. (2). Dynamics sufficiently close to the steady state \mathbf{x}^0 follows the linearized form of Eq. (2),

$$\frac{d\boldsymbol{\zeta}}{dt} = \mathbf{J} \boldsymbol{\zeta}, \quad (4)$$

where $\boldsymbol{\zeta} = \mathbf{x} - \mathbf{x}^0$ is a small deviation from the steady state concentrations of species, and $\mathbf{J} \in \mathbb{R}^{n \times n}$ is the Jacobi matrix, which can be expressed in terms of new, so called convex parameters \mathbf{h} and \mathbf{j} as

$$\mathbf{J}(\mathbf{h}, \mathbf{j}) = \mathbf{S} \text{diag}(\mathbf{E} \mathbf{j}) \boldsymbol{\kappa}^T \text{diag}(\mathbf{h}), \quad (5)$$

where $\mathbf{h} \in \mathbb{R}_+^n$ is the vector of reciprocals of steady state concentrations, $h_i = \frac{1}{x_i^0}$.

The matrix $\boldsymbol{\kappa} = [\kappa_{ij}] \in \mathbb{R}^{n \times r}$ is called the kinetic matrix; its element κ_{ij} is the effective order of the j -th reaction with respect to the i -th species defined as

$$\kappa_{ij} \equiv \frac{\partial \ln v_j(\mathbf{x}, \mathbf{k})}{\partial \ln x_i}. \quad (6)$$

In general, linear stability of the steady state \mathbf{x}^0 is determined by eigenvalues of the Jacobi matrix. However, the SNA is adopting an approach of predicting stability prior specifying \mathbf{x}^0 (or equivalently \mathbf{h}). For mass action/power law kinetics, κ_{ij} is constant and independent of \mathbf{x}^0 . In addition, $\kappa_{ij} \leq \nu_{ij}$. Since these conditions apply to the TWC mechanism, the matrix $\mathbf{B} = -\mathbf{S} \text{diag}(\mathbf{E} \mathbf{j}) \boldsymbol{\kappa}^T$ is independent of \mathbf{h} and can be conveniently used for predicting stability of any (sub)network $\mathbf{v}^0 = \mathbf{E} \mathbf{j}$ without involving \mathbf{h} as would be the case when using eigenvalues of \mathbf{J} .

Stability of \mathbf{v}^0 can be inferred from \mathbf{B} by examining its principal subdeterminants β_l of order $l = 1, \dots, n$. There are $\binom{n}{l}$ different β_l s related to all choices of l species. If at least one β_l is negative, then at least one eigenvalue of \mathbf{J} has a positive real part and indicates an instability of the steady state \mathbf{x}^0 provided that the steady state concentrations of the corresponding l species are sufficiently small [22]. Because any steady state rate vector \mathbf{v}^0 is a convex combination of elementary subnetworks $\mathbf{v}^0 = \mathbf{E} \mathbf{j}$, the stability of the entire network depends on the stability of the elementary subnetworks and coefficients \mathbf{j} . Thus if there is a negative β_l for a (sub)network, then the SNA predicts that the (sub)network is capable of displaying a dynamical instability even prior specifying rate coefficients and steady state concentrations. There are two basic types of instabilities: occurrence of multiple steady states (via a saddle-node bifurcation) and occurrence of oscillations (via a Hopf bifurcation). The condition of a

negative β_l implies a positive feedback, which is a sufficient condition for occurrence of multistability. A combination of positive and negative feedback leading to oscillations via the Hopf bifurcation requires specific types of negative feedback, and knowledge of steady state concentrations. It is possible to formulate conditions ensuring the Hopf bifurcation in terms of inequalities for steady state concentrations [13, 25].

A rough but useful guide for a visual identification of both positive and negative feedbacks is a graphical representation of the network called a network diagram. Each reaction can be represented as a multi-headed multi-tailed arrow which is oriented from the reactants to the products. The number of feathers/barbs determines the stoichiometric coefficients of reactants/products. The number of left feathers determines the reaction order of the reacting species. The network diagram for an oscillatory network, i.e. a network having the capacity for occurrence of the Hopf bifurcation, possesses characteristic features such as autocatalytic cycles (positive feedback) and reactions that are tangent or exit with respect to the autocatalytic cycles (negative feedback) [26, 27].

At the Hopf bifurcation (specified by a pair of pure imaginary eigenvalues of \mathbf{J}), a classification and determination of the role of species in oscillations [26, 27] can be done, for example, by calculating mutual phase shifts of oscillating species, [28] or by other methods. [29, 30] To that purpose the phase shifts of oscillating species at the Hopf bifurcation were used in this work. The procedure of determining the phase shift signature is as follows. For each unstable edge or a low-dimensional face of a selected TWC (sub)system we verified whether it can provide oscillations by constructing a network $\mathbf{E}\mathbf{j}$ with nonzero values of all j_k , $k = 1, \dots, f$, but maintaining dominance of the unstable edge/face in question by setting the corresponding j_k s much larger than others. For such a network we set the reciprocal steady state vector \mathbf{h} so that its components specified by the negative β_l were large enough ensuring an unstable eigenvalue(s) of \mathbf{J} . Then we fine-tuned both \mathbf{j} and \mathbf{h} to find a pair of pure imaginary eigenvalues of \mathbf{J} . This procedure amounts to balancing positive feedback with a proper negative feedback to yield an oscillatory instability. The phase shifts of all species relative to a reference species are then determined from the complex conjugate eigenvectors associated with the pair of pure imaginary eigenvalues. Qualitatively, each of the n phase shifts can be characterized as being in-phase (small shifts), anti-phase (shifts near to π), phase advanced and phase delayed. We call the n -vector of qualitative phase shifts a shift signature.

Based on the signatures, the chemical oscillators can be classified as category 1 or 2 (suggesting first or second order autocatalysis), with subcategories B and C (suggesting batch and continuous conditions of operation). Simultaneously, the species can be classified as essential/nonessential for oscillations; if the former are held fixed (buffered) the oscillations are suppressed. The essential species are of three types: the autocatalytic, exit and negative feedback (denoted as X, Y

and Z, respectively). Type X species are typically forming a cyclic chain of linked reactions in the network diagram (current cycle), the type Y species reacts with and removes a type X species (direct inhibition) and the type Z species forms a negative cyclic feedback involving the X species (indirect inhibition) which makes the oscillations possible.

In the next step we examined the same TWC (sub)system by using bifurcation analysis to find a Hopf bifurcation, but instead of using convex parameters (i.e., \mathbf{j} and \mathbf{h}) we used direct parameters (i.e. rate coefficients at a given temperature and inflow rates of reactants). When the phase shifts determined by both methods are matching each other, we conclude that the oscillations are caused by the corresponding dominant unstable edge/face combined with a proper negative feedback. This conclusion is based on an idea verified repeatedly in our previous work that the shift signatures are constant and specific for each topologically distinct type of oscillatory (sub)network dominating the dynamics of the full network within certain (usually large) parameter domain bounded by Hopf bifurcation.

Software used for network analysis and classification of oscillators is homemade (written in Fortran and Matlab), additional dynamic and bifurcation analysis was done by using the program CONT [31].

4 Results

After visual inspection of the TWC reaction mechanism listed in Table 1, the system can be naturally separated into several subsystems: CO oxidation, CO & C₂H₂ oxidation, CO oxidation & NO_x reduction. Here we analyze these three subsystems. In all cases, we focus on the identification of the mechanistic sources of oscillatory instabilities which are compared with various modes of oscillatory dynamics of the kinetic model.

4.1 Network of CO oxidation

The CO oxidation subsystem as the subsystem of the TWC reaction mechanism was previously examined in the work by Marek *et al.* [23], where the network analysis of CO oxidation subsystem is compared with the previously cited experimental results [23].

The network of CO oxidation involves nine chemical reactions R₁–R₉, and 5 pseudoreactions R₃₁–R₃₅, and 11 chemical species, see Table 1. This network can be decomposed into 7 elementary subnetworks E_k, see Table 2. The first

Table 2. Elementary subnetworks E_k (edges) for CO oxidation subsystem; unstable ones are marked in boldface

	E_1	E_2	E_3	E_4	E_5	E_6	E_7
v_1	1	0	2	0	2	0	0
v_2	1	0	0	0	0	0	0
v_3	0	0	1	1	0	0	0
v_4	0	0	2	0	0	0	0
v_5	0	1	0	2	0	0	0
v_6	0	1	0	0	0	0	0
v_7	0	0	0	2	0	0	0
v_8	0	0	0	0	1	0	0
v_9	0	0	0	0	2	0	0
v_{31}	0	0	2	2	2	1	0
v_{32}	0	0	0	0	0	1	0
v_{33}	0	0	1	1	1	0	1
v_{34}	0	0	0	0	0	0	1
v_{35}	0	0	2	2	2	0	0

two E_k s represent reversible reaction pairs at equilibrium. The last two E_k s represent inflow/outflow steady state for the CO and O_2 . The subnetworks E_4 – E_6 involve genuine chemical pathways. E_3 involves reactions R_1 , R_3 , and R_4 balanced by pseudoreactions R_{31} , R_{33} , and R_{35} . This subnetwork represents the classical Langmuir-Hinshelwood mechanism of CO oxidation characterized by interaction of previously Pt-adsorbed carbon monoxide and oxygen. E_4 consists of reactions R_3 , R_5 , and R_7 and pseudoreactions R_{31} , R_{33} , and R_{36} . In contrast, this subnetwork represents the Eley-Rideal mechanism, characterized by interaction of Pt-adsorbed oxygen with gaseous CO. On the other hand, E_5 represents a pathway of CO oxidation with mixed catalysts whereby Pt-adsorbed CO^* is oxidized by Ce-adsorbed O^s . In addition, the E_k s form 36 different 2-faces and a number of higher-dimensional faces. Below we examine edges and 2-faces because higher-dimensional faces are unlikely to produce instability on their own.

A negative β_l indicating at least one unstable eigenvalue of \mathbf{J} marks an instability in the subnetworks represented by the edge E_3 and the 2-faces $F_{(1,4)}$ and $F_{(4,5)}$ shown as network diagrams in Fig. 1. The faces $F_{(1,4)}$ and $F_{(4,5)}$ are spanned by the edges E_1 & E_4 and the edges E_4 & E_5 , respectively. Each of these subnetworks accounts for multiple steady states and by combining any of them with certain stable subnetworks an oscillator emerges via Hopf bifurcation. In addition, the 2-face $F_{(4,5)}$ involves two topologically distinct oscillators in contrast to E_3 and $F_{(1,4)}$. It is therefore necessary to determine, which of these four options underlie the oscillatory behavior obtained by the direct simulations with a realistic choice of parameters [23].

The corresponding bifurcation diagram (see Ref. [23]) shows two regions of oscillatory dynamics, one at sub-stoichiometric and the other at super-stoichiometric constraints. According to the classification system of chemical oscillators [26,27],

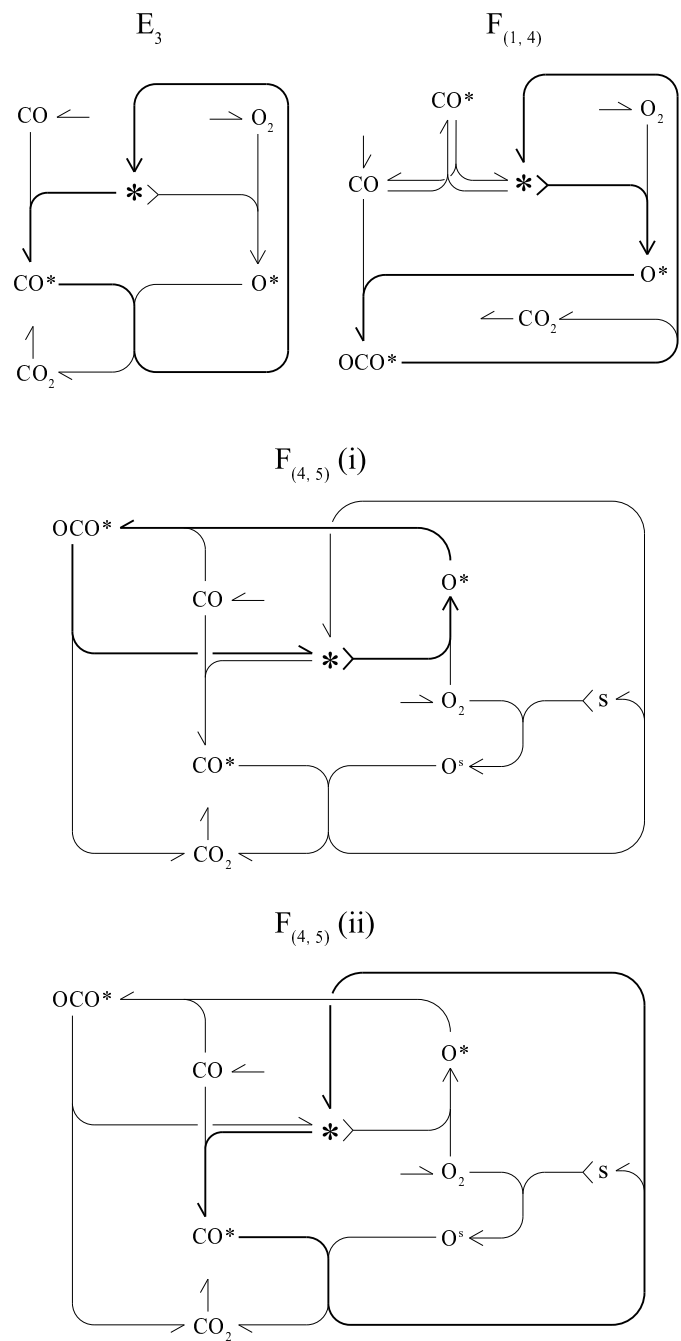


Figure 1. Network diagrams of oscillators in the CO oxidation mechanism. Autocatalytic cycles are emphasized by bold lines.

each of the two oscillatory regions is tied up with a particular topologically distinct oscillatory subnetwork detectable by comparing the phase shifts of essential species obtained from the network analysis and from the direct simulations, see Table 3.

Table 3. Classification deduced from phase shifts of chemical species relative to $*$ at the Hopf bifurcation in four oscillatory networks based on the E_3 , $F_{(1,4)}$ and $F_{(4,5)}$.

Subnetwork	Category	CO	CO*	OCO*	O ₂	O*	O*	*	s
E_3	1C	163.37 (Z)	30.54 (X)	152.35 (n)	175.83 (Y)	-47.08 (n)	161.76 (n)	0.00 (X)	-18.24 (n)
$F_{(1,4)}$	1C	-178.97 (Y)	-177.00 (n)	7.75 (X)	162.12 (Z)	3.33 (X)	110.68 (n)	0.00 (X)	-69.32 (n)
$F_{(4,5)}$ (i)	1C	-178.80 (Y)	-177.32 (n)	6.35 (X)	163.71 (Z)	3.14 (X)	113.40 (n)	0.00 (X)	66.61 (n)
$F_{(4,5)}$ (ii)	1C	157.70 (Z)	12.60 (X)	151.27 (n)	177.48 (Y)	-58.40 (n)	-179.71 (n)	0.00 (X)	0.29 (W)
θ_1^{sim}		-164.65	-128.14	59.32	179.98	28.49	178.29	0.00	-1.71
θ_2^{sim}		67.75	39.10	85.94	176.51	-113.15	26.97	0.00	-153.03

The vector of the simulated phase shifts θ_1^{sim} was computed near the Hopf bifurcation at $T = 477$ K and $y_{O_2}^{\text{in}} = 0.5$ %. Similarly, the vector of phase shifts θ_2^{sim} was computed near Hopf bifurcation at $T = 500$ K and $y_{O_2}^{\text{in}} = 0.673$ %.

When we look for the oscillator responsible for oscillatory behavior in the sub-stoichiometric region, phase shifts of all oscillators are compared with θ_1^{sim} , see Table 3. Both oscillators $F_{(1,4)}$ and $F_{(4,5)}$ (i) have almost same values of phase shifts except the species s and correspond to θ_1^{sim} quite well. The 2-faces $F_{(1,4)}$ and $F_{(4,5)}$ (i) involve the classical Eley-Rideal mechanism of CO oxidation over Pt. For both oscillators, the instability determining minor indicates that the species $*$, O^* , OCO^* and CO must have small steady state concentrations and thus are of autocatalytic (X) or exit (Y) type. The autocatalytic cycle involves the reactions R_3 , R_5 and R_7 and the autocatalytic species O^* , OCO^* and $*$. The reaction order of these species in the reactions R_3 , R_5 and R_7 is one and it is equal to their order in any reactions removing them from the cycle (here R_1). In this situation, an unstable steady state is achieved only if there exists an exit reaction which is a reaction of a non-cycle species with a cycle species removing that species [22]. This is provided by reaction R_1 and CO is then the exit species. Finally, the oscillatory instability is made possible by the presence of O_2 and its flow-controlled availability. There is a negative cycle feedback exerted by O_2 upon itself via the path through O^* , OCO^* and $*$ implying that the autocatalysis depletes the supply of O_2 , which must be replenished by the feed at a later time. During the autocatalytic phase CO is consumed, and as the autocatalysis reaches its peak, CO becomes depleted due to reaction R_1 . The overall effect is an oscillatory regime with the negative feedback species O_2 advancing the three autocatalytic species O^* , OCO^* and $*$, which are mutually in-phase, and the exit species CO being antiphase relative to the autocatalytic species. All the above species are thus essential for oscillations.

On the other hand, the unstable subnetwork E_3 shown in Fig. 1 is dominant in the oscillatory region where the amount of oxygen is just stoichiometric or in excess. Phase shifts of species θ_2^{sim} correspond to the unstable edge E_3 in the best way. The subnetwork E_3 involves the classical Langmuir-Hinshelwood mechanism of CO oxidation. Oscillations occurring under these circumstances have been examined earlier for the case of CO oxidation on a single crystal of Pt(100) or Pt(110) [13,32]. The instability determining minor indicates that the species $*$, CO^* and O_2 are of autocatalytic or exit type. Near the Hopf bifurcation the concentrations of species CO^* and $*$ oscillate relatively in-phase therefore they are autocatalytic species. Then the autocatalytic loop involves reactions R_1 and R_4 . Since oxygen is antiphase correlated with respect to the autocatalytic species it plays the role of the exit species in the exit reaction R_2 . The role of the negative feedback species is played by CO which controls the autocatalysis.

4.2 Subsystem of CO & C_2H_2 oxidation

This is a more complex subsystem of the TWC reaction mechanism where competition between different reactants for oxygen occurs. This network includes 19 chemical reactions R_1 – R_{19} , eight pseudoreactions R_{31} – R_{38} , and involves 13 chemical species from Table 1. The SNA decomposes the network of the CO & C_2H_2 oxidation subsystem into 28 elementary subnetworks E_k (the list is available upon request from the corresponding author). The 7 elementary subnetworks found in the CO oxidation network, (Table 2) occur naturally here since the CO network is a subnetwork of the CO & C_2H_2 system. Apart from that, there are two roughly separable groups of subnetworks, one representing different pathways of C_2H_2 oxidation to CO_2 and H_2O and the other involves pathways of partial oxidation of C_2H_2 to CO and H_2O .

Upon examining the stability of the network in the same manner as before, potentially unstable behavior is indicated in 15 edges. In this case no 2-face or higher order face shows an instability not already contained in the edges. Some of the edges display multiple unstable topologies based on different essential species. Altogether there are 37 different unstable topologies, 23 of them provide oscillatory behavior when a given unstable elementary subnetwork is mixed with some stable ones. The rest accounts for multiple steady states only (i.e., no Hopf bifurcation occurs). The list of the oscillatory subnetworks and their classification is shown in Table 4.

Using the eigenvectors associated with the pair of pure imaginary eigenvalues of the Jacobi matrix, we calculated mutual phase shifts of all species for the oscillators where a particular unstable subnetwork plays a dominant role. These phase shifts of the unstable subnetworks were then compared with those obtained from the kinetic model with realistic kinetics near the Hopf bifurcation, see Table 5. The vector of phase shifts θ_1^{sim} was computed near Hopf bifurcation at

Table 4. List of oscillators in CO & C₂H₂ oxidation subsystem

Subnetwork oscillator	Essential species (Roles of species)
E ₃ (i)	CO (Y), O* (X), * (X), O ₂ (Z)
E ₃ (ii)	CO* (X), O ₂ (Y), * (X), CO (Z)
E ₉	O* (X), * (X), C ₂ H ₂ (Y), C ₂ H ₂ * (Y), O ₂ (Z)
E ₁₀ (i)	CO (W), O* (X), * (X), C ₂ H ₂ (Y), C ₂ H ₂ * (Y), O ₂ (Z)
E ₁₀ (ii)	CO* (X), O* (X), * (X), C ₂ H ₂ (Y), C ₂ H ₂ * (Y), O ₂ (Z)
E ₁₀ (iii)	OCO* (X), O* (X), * (X), C ₂ H ₂ (Y), C ₂ H ₂ * (Y), O ₂ (Z)
E ₁₁	O* (X), * (X), C ₂ H ₂ (Y), C ₂ H ₂ * (Y), O ₂ (Z)
E ₁₂	O* (X), * (X), C ₂ H ₂ (Y), O ₂ (Z)
E ₁₃ (i)	O ₂ (Y), * (X), C ₂ H ₂ * (X), C ₂ H ₂ (Z)
E ₁₃ (ii)	CO* (X), OCO* (X), O* (X), * (X), C ₂ H ₂ (Y), O ₂ (Z)
E ₁₄ (i)	CO* (X), O ₂ (Y), * (X), C ₂ H ₂ * (X), C ₂ H ₂ (Z)
E ₁₄ (ii)	CO* (X), O* (X), * (X), C ₂ H ₂ (Y), O ₂ (Z)
E ₁₄ (iii)	O ₂ (Y), * (X), s (W), C ₂ H ₂ * (X), C ₂ H ₂ (Z)
E ₁₅ (i)	O* (X), * (X), O ₂ (Z)
E ₁₅ (ii)	CO* (X), O ₂ (Y), * (X), C ₂ H ₂ * (X), C ₂ H ₂ (Z)
E ₁₆	CO (W), CO* (X), OCO* (X), O ₂ (Y), * (X), C ₂ H ₂ * (X), C ₂ H ₂ (Z)
E ₁₈	O* (X), * (X), C ₂ H ₂ (Y), O ₂ (Z)
E ₁₉	CO* (X), OCO* (X), O* (X), * (X), C ₂ H ₂ (Y), O ₂ (Z)
E ₂₀	CO* (X), O* (X), * (X), C ₂ H ₂ (Y), O ₂ (Z)
E ₂₁	O* (X), * (X), C ₂ H ₂ (Y), C ₂ H ₂ * (Y), O ₂ (Z)
E ₂₂ (i)	O ₂ (Y), * (X), C ₂ H ₂ * (X), C ₂ H ₂ (Z)
E ₂₂ (ii)	CO* (X), O* (X), * (X), C ₂ H ₂ (Y), O ₂ (Z)
E ₂₄	CO* (X), O* (X), * (X), C ₂ H ₂ (Y), O ₂ (Z)

$T = 575$ K and $y_{O_2}^{\text{in}} = 0.5$ %. The vector of phase shifts θ_2^{sim} was computed near Hopf bifurcation at $T = 680$ K and $y_{O_2}^{\text{in}} = 0.841$ %.

As before, only two of those subnetworks correspond to the regions of oscillations in the bifurcation diagram obtained for realistic parameter values. They are shown in Fig. 2. The unstable subnetwork E₂₀ brings about oscillatory instability in the region of sub-stoichiometric oxygen concentration. Gaseous C₂H₂ is firstly adsorbed on O* and then C₂H₂O* is oxidized into CO*. CO* is oxidized by O^s. Negative β indicates that species CO*, O*, C₂H₂ and * are essential which means that they have relatively low concentrations. Autocatalytic species CO*, O* and * oscillate in-phase forming the autocatalytic cycle. The autocatalytic

Table 5. Phase shifts of chemical species relative to * at a Hopf bifurcation for the relevant unstable subnetworks

Subnetwork	Category	CO*	O ₂	O*	*	C ₂ H ₂
Sub-st. region						
E ₂₀	1C	3.76 (X)	141.91 (Z)	15.55 (X)	0.00 (X)	-175.37 (Y)
θ_1^{sim}		6.84	178.57	-6.73	0.00	-176.39
Subnetwork	Category	O ₂	*	s	C ₂ H ₂	C ₂ H ₂ *
Super-st. region						
E ₁₄ (ii)	1C	174.27 (Y)	0.00 (X)	-4.09 (W)	129.88 (Z)	-20.46 (X)
θ_2^{sim}		178.55	0.00	-51.79	-176.51	-3.38

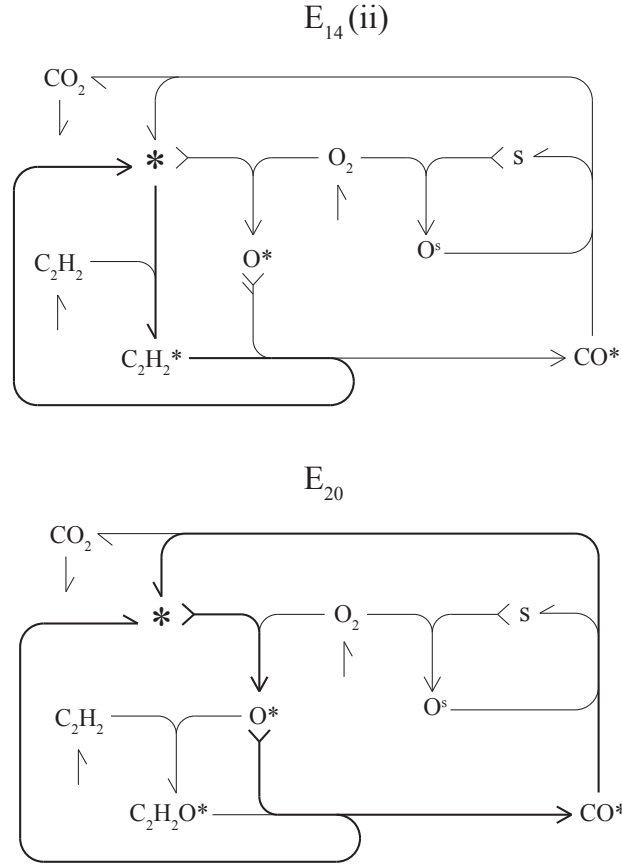


Figure 2. Unstable subnetworks of CO & C_2H_2 oxidation subsystem causing oscillatory behavior. Autocatalytic cycles are emphasized by bold lines.

loop is formed by reactions R_3 , R_9 and R_{19} . C_2H_2 decreases the concentration of O^* via the exit reaction R_{16} . Negative feedback species O_2 makes autocatalysis possible.

The oscillator $E_{14} \text{ (ii)}$ in Fig. 2 is responsible for oscillations in the surplus of oxygen. Gaseous C_2H_2 is firstly adsorbed on $*$ and then $C_2H_2^*$ is oxidized into CO^* via R_{14} . Here negative β indicates that there are four essential species $*$, s , O_2 and $C_2H_2^*$. Because concentrations of $C_2H_2^*$ and $*$ oscillate mutually in-phase and the species form a closed loop then $C_2H_2^*$ and $*$ must be autocatalytic species. The autocatalytic cycle involves reactions R_{10} and R_{14} . Since concentration of O_2 oscillates anti-phase respect to $*$ then species O_2 plays the role of exit species decreasing the number of free sites $*$. Negative feedback is provided by controlled inflow of C_2H_2 which makes autocatalysis possible.

4.3 Subsystem of CO oxidation and NO_x reduction

This subsystem of the TWC reaction mechanism allows for transfer of oxygen from nitrogen oxides to CO which may be seen as synergy between oxidation and reduction subnetworks. The network of the CO oxidation and NO_x reduction system is formed by 20 chemical reactions R₁–R₉, R₂₀–R₃₀, 10 pseudoreactions R₃₁–R₃₆ and R₃₉–R₄₂, and involves 13 chemical species from Table 1. This network can be decomposed into 31 elementary subnetworks E_k. Again, 7 of these elementary subnetworks are the same as the elementary subnetworks for the CO oxidation network in Table 2. Furthermore, 8 elementary subnetworks involve inflow of NO₂. Since the concentration of NO₂ is much lower than the concentration of NO these subnetworks play minor role in dynamical behavior.

The SNA indicates unstable behavior in 17 elementary subnetworks. The unstable elementary subnetworks include 60 different topologies out of which 29 can oscillate. Interestingly, E₁₄ (i), E₁₆ (i), E₁₆ (iii), E₁₈ (ii) are standalone oscillators, the rest displays oscillatory behavior when the unstable elementary subnetwork is combined with some stable ones. The list of all oscillatory subnetworks and their classification is found in Table 6

Selection of two oscillators whose phase shifts of oscillating species correspond to those for sub- and superstoichiometric region in the corresponding bifurcation diagram is based on Table 7. The vector of phase shifts θ_1^{sim} was computed near Hopf bifurcation at $T = 483$ K and $y_{\text{O}_2}^{\text{in}} = 0.5$ %. Similarly the vector of phase shifts θ_2^{sim} was computed near Hopf bifurcation at $T = 510$ K and $y_{\text{O}_2}^{\text{in}} = 0.647$ %.

The two dominant subnetworks accounting for the two oscillatory domains in the bifurcation diagram are shown in Fig. 3. The unstable subnetwork E₂₀ involves the oscillator E₂₀ (i) that is responsible for oscillatory behavior in the region of sub-stoichiometric oxygen concentration. The subnetwork E₂₀ represents an ideal situation when NO is reduced into N₂ while CO depletes supply of O* to produce CO₂. Negative β indicates that CO*, NO*, NO and * are essential species. Species CO* and * oscillate mutually in-phase and form the autocatalytic cycle. This autocatalytic loop is formed by reactions R₁ and R₄. Both species NO and NO* decrease the amount of free Pt-sites * via the exit reactions R₂₀ and R₂₂. Moreover, low concentration of NO* cause limited production of O* which is a necessary condition for oscillations here. A controlled inflow of CO provides for negative feedback.

The unstable subnetwork E₁₂ involves the oscillator E₁₂ (ii) that brings about oscillatory instability in the region of super-stoichiometric oxygen concentration, see Fig. 3. The subnetwork E₁₂ involves NO reduction with CO is oxidized into N₂O. Negative β indicates that there are four essential species CO*, N*, * and NO. Autocatalytic species CO*, N* and * form two autocatalytic loops acting in synchrony. These loops combine reactions R₁, R₄, R₂₂ and R₂₃. NO

Table 6. List of potential oscillators in CO & NO_x oxidation subsystem

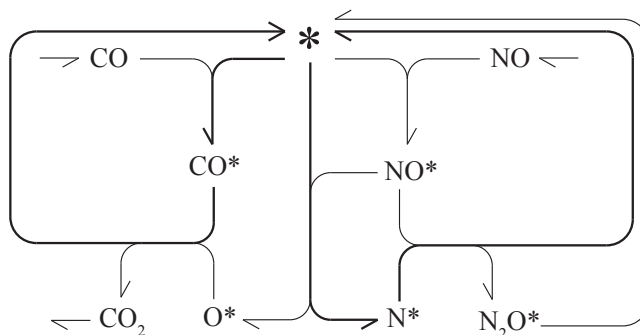
Subnetwork	Essential species (Roles of species)
E ₃ (i)	CO (Y), O* (X), * (X), O ₂ (Z)
E ₃ (ii)	CO* (X), O ₂ (Y), * (X), CO (Z)
E ₉	O* (X), * (X), NO (Y), N* (X), NO* (Z)
E ₁₀	O* (X), * (X), NO (Y), NO ₂ * (X), NO* (Z)
E ₁₁ (i)	O* (X), * (X), NO (Y), NO ₂ * (X), NO* (Z)
E ₁₁ (ii)	O* (W), * (X), NO (Y), N* (X), NO* (Z)
E ₁₂ (i)	CO (Y), O* (X), * (X), NO (Y), CO* (Z)
E ₁₂ (ii)	CO* (X), * (X), NO (Y), N* (X), CO (Z)
E ₁₂ (iii)	CO (Y), * (X), NO (Y), N* (X), N ₂ O* (X), NO* (Z)
E ₁₃	* (X), NO (Y), N* (X), N ₂ O* (X)
E ₁₄ (i)	CO* (X), * (X), NO (Y), NO ₂ (Y), CO (Z)
E ₁₄ (ii)	CO* (X), * (X), NO ₂ (Y), N* (X), CO (Z)
E ₁₄ (iii)	CO (Y), O* (X), * (X), NO (Y), NO ₂ (Y), NO* (Z)
E ₁₄ (iv)	CO (Y), O* (X), * (X), NO* (Y), NO ₂ (Y), N ₂ O* (W), CO* (Z)
E ₁₄ (v)	CO (Y), * (X), NO (Y), NO ₂ (Y), N* (X), N ₂ O* (X), CO* (Z)
E ₁₅	* (X), NO (Y), NO ₂ (Y), N* (X), N ₂ O* (X), NO* (Z)
E ₁₆ (i)	CO* (X), * (X), NO (Y), CO (Z)
E ₁₆ (ii)	CO (Y), O* (X), * (X), NO (Y), NO* (Z)
E ₁₆ (iii)	CO (Y), O* (X), * (X), NO* (Y), N ₂ O* (W), CO* (Z)
E ₁₆ (iv)	CO (Y), O* (X), * (X), N* (X), N ₂ O* (X), NO* (Z)
E ₁₈ (i)	CO (Y), O* (X), * (X), NO (Y), NO ₂ (Y), NO* (Z)
E ₁₈ (ii)	CO (Y), O* (X), * (X), NO* (Y), NO ₂ (Y), N ₂ O* (W), CO* (Z)
E ₁₈ (iii)	CO (Y), O* (X), * (X), NO ₂ (Y), N* (X), N ₂ O* (X), NO (Z)
E ₂₀ (i)	CO* (X), * (X), NO (Y), NO* (Y), CO (Z)
E ₂₀ (ii)	CO* (X), * (X), NO (Y), N* (X), CO (Z)
E ₂₂ (i)	CO* (X), * (X), NO (Y), NO ₂ (Y), CO (Z)
E ₂₂ (ii)	CO (Y), O* (X), * (X), NO ₂ (Y), N* (X), NO* (Z)
E ₂₅ (i)	CO* (X), * (X), NO ₂ (Y), CO (Z)
E ₂₅ (ii)	CO (Y), O* (X), * (X), NO ₂ * (X), NO ₂ (Z)

Table 7. Phase shifts of chemical species relative to * at a Hopf bifurcation for the relevant unstable subnetworks

Subnetwork	Category	CO	CO*	*	NO	NO*
Sub-stoichiometric region						
E ₂₀ (i)	1C	148.71 (Z)	45.46 (X)	0.00 (X)	174.25 (Y)	170.23 (Y)
θ_1^{sim}		6.84	101.93	0.00	-6.73	0.00
Super-stoichiometric region						
E ₁₂ (ii)	1C	151.25 (Z)	81.54 (X)	0.00 (X)	174.89 (Y)	-3.01 (X)
θ_2^{sim}		66.68	128.26	0.00	-52.62	-176.51

is indicated as exit species that decreases the concentration of * by binding to Pt-sites. Negative feedback is provided by controlled inflow of CO which makes autocatalysis possible.

E_{12} (ii)



E_{20} (i)

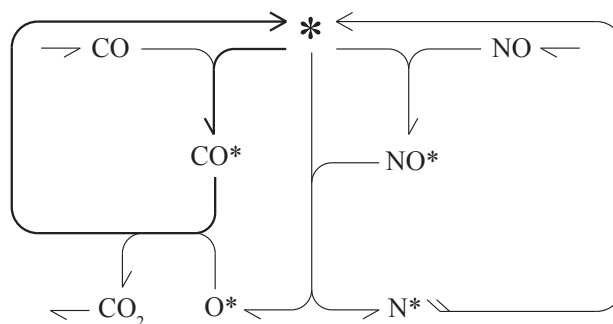


Figure 3. Unstable subnetworks of CO & NO_x subsystem causing oscillatory behavior. Autocatalytic cycles are emphasized by bold lines.

5 Conclusions

The application of the stoichiometric network analysis to the TWC proves an efficient tool in elucidating the nature of oscillatory dynamics predicted by direct simulations and by constructing bifurcation diagrams. In principle, the method enables to indicate all the potential oscillating subnetworks and provides criteria for selecting those that fit best either simulations or experimental observations.

References

1. G. Th. Fechner. Zür elektrochemie. *Schweigger's Journal für Chemie und Physik*, 53:129–151, 1828.
2. P. Hugo and M. Jakubith. Dynamisches Verhalten und Kinetik der Kohlenmonoxid-Oxidation am Platin-Katalysator. *Chemie Ingenieur Technik*, 44(6):383–387, 1972.
3. H. Beusch, P. Fieguth, and E. Wicke. Thermisch und kinetisch verursachte Instabilitäten im Reaktionsverhalten einzelner Katalysatorkörner. *Chemie Ingenieur Technik*, 44(7):445–451, 1972.
4. Marina Slinko and Nils Jaeger. Oscillatory Heterogeneous Catalytic Systems. *Catalysis Today*, 105(2):I–II, 2005.
5. M. M. Slinko. Oscillating reactions in heterogeneous catalysis: What new information can be obtained about reaction mechanisms? *Catalysis Today*, 154(1-2):38–45, 2010.
6. M. M. Slinko and N. I. Jaegar. *Oscillating Heterogeneous Catalytic Systems*. Elsevier, Amsterdam, 1994.
7. R. Imbihl and G. Ertl. Oscillatory kinetics in heterogeneous catalysis. *Chemical Reviews*, 95(3):697–733, 1995.
8. H. H. Rotermund, W. Engel, M. Kordesch, and G. Ertl. Imaging of spatio-temporal pattern evolution during carbon monoxide oxidation on platinum. *Nature*, 343(6256):355–357, 1990.
9. M. F. H. van Tol, G. Gielbert, and B. E. Nieuwenhuys. Oscillatory behaviour of the reduction of no by h₂ over rh. *Catalysis Letters*, 16(3):297–309, 1992.
10. R. M. Heck and R. J. Farrauto. Automobile exhaust catalysts. *Applied Catalysis A: General*, 221(1-2):443–457, 2001.
11. T. Engel and G. Ertl. Elementary steps in the catalytic oxidation of carbon monoxide on platinum metals. *Advances in Catalysis*, 28:1–78, 1979.
12. T. Gritsch, D. Coulman, R. Y. Behm, and G. Ertl. Mechanism of the CO-induced $1 \times 2 \rightarrow 1 \times 1$ structural transformation of Pt(110). *Physical Review Letters*, 63(10):1086–1089, 1989.
13. M. Eiswirth, J. Bürger, P. Strasser, and G. Ertl. Oscillating Langmuir-Hinshelwood mechanisms. *Journal of Physical Chemistry*, 100(49):19118–19123, 1996.
14. H. U. Onken and E. Wicke. Periodicity and chaos in a catalytic packed bed reactor for CO oxidation. *Chemical Engineering Sciences*, 43(8):2289–2294, 1988.
15. J. Kapička and M. Marek. Oscillations on individual catalytic pellet in a packed bed: CO oxidation on Pt/Al₂O₃. *Journal of Catalysis*, 119(2):508–511, 1989.
16. R. H. Nibbelke, A. J. Nievergeld, J. H. Hoebink, and G. B. Marin. Development of a transient kinetic model for the CO oxidation by O₂ over a Pt/Rh/CeO₂/γ-Al₂O₃ three-way catalyst. *Applied Catalysis B: Environmental*, 19(3-4):245–259, 1998.
17. J. M. Harmsen, J. H. Hoebink, and J. C. Schouten. Transient kinetic modeling of the ethylene and carbon monoxide oxidation over a commercial automotive exhaust gas catalyst. *Industrial & Engineering Chemistry Research*, 39(3):599–609, 2000.
18. J. M. Harmsen, J. H. Hoebink, and J. C. Schouten. Acetylene and carbon monoxide oxidation over a Pt/Rh/CeO₂/γ-Al₂O₃ automotive exhaust gas catalyst: kinetic modeling of transient experiments. *Chemical Engineering Science*, 56(6):2019–2035, 2001.
19. J. M. Harmsen, J. H. Hoebink, and J. C. Schouten. NO reduction by CO over automotive exhaust gas catalysts in the presence of O₂. *Catalysis Letters*, 71(1-2):81–90, 2001.

20. P. Kočí, M. Kubíček, and M. Marek. Modeling of three-way-catalyst monolith converters with microkinetics and diffusion in the washcoat. *Industrial & Engineering Chemistry Research*, 43(16):4503–4510, 2004.
21. P. Kočí, M. Kubíček, and M. Marek. Periodic forcing of three-way catalyst with diffusion in the washcoat. *Catalysis Today*, 98(3):345–355, 2004.
22. B. L. Clarke. Stability of complex reaction networks. *Advances in Chemical Physics*, 43:1–278, 1980.
23. M. Marek, M. Schejbal, P. Kočí, V. Nevorál, M. Kubíček, O. Hadač, and I. Schreiber. Oscillations, period doublings, and chaos in CO oxidation and catalytic mufflers. *Chaos*, 16(037107):1–13, 2006.
24. C. H. Schilling, D. Letscher, and B. Ø. Palsson. Theory for the systemic definition of metabolic pathways and their use in interpreting metabolic function from a pathway-oriented perspective. *Journal of Theoretical Biology*, 203(3):229–248, 2000.
25. K. Gatermann, M. Eiswirth, and A. Sense. Toric ideals and graph theory to analyze hopf bifurcations in mass action systems. *Journal of Symbolic Computation*, 40:1361–1382, 2005.
26. M. Eiswirth, A. Freund, and J. Ross. Mechanistic classification of chemical oscillators and the role of species. *Advances in Chemical Physics*, 80:127–199, 1991.
27. M. Eiswirth, A. Freund, and J. Ross. Operational procedure toward the classification of chemical oscillators. *Journal of Physical Chemistry*, 95(3):1294–1299, 1991.
28. T. Chevalier, I. Schreiber, and J. Ross. Toward a systematic determination of complex-reaction mechanisms. *Journal of Physical Chemistry*, 97(26):6776–6787, 1993.
29. J. D. Stemwedel, I. Schreiber, and J. Ross. Formulation of oscillatory reaction mechanisms by deduction from experiments. *Advances in Chemical Physics*, 89:327–388, 1995.
30. J. Ross, I. Schreiber, and M. O. Vlad. *Determination of Complex Reaction Mechanisms*. Oxford University Press, Inc., New York, 2006.
31. M. Kohout, I. Schreiber, and M. Kubíček. A computational tool for nonlinear dynamical and bifurcation analysis of chemical engineering problems. *Computers & Chemical Engineering*, 26(4-5):517–527, 2002.
32. M. Eiswirth. *Chaos in Chemistry and Biochemistry*, chapter Chaos in Surface-Catalyzed Reactions. World Scientific, Singapore, 1993. editors R. J. Field and L. Györgyi.

Acknowledgments: This work was supported by the project LH14009 of the Ministry of Education of Czech Republic.

The detection of Hopf bifurcations in large scale problems arising in computational fluid dynamics

Alastair Spence

Department of Mathematical Sciences, University of Bath, Bath, UK

Keywords: Linear Stability Analysis, Hopf Bifurcation, Inverse Iteration, Lyapunov Solvers

Abstract

The detection of a Hopf bifurcation in a large-scale dynamical system that depends on a physical parameter often consists of computing the right-most eigenvalues of a sequence of large sparse eigenvalue problems. This is not only a hugely expensive operation but many of the common numerical methods for this problem may be unreliable for large sparse matrices.

This talk will summarise some of the methods commonly used in applications and discuss their advantages and disadvantages. Next, we describe a recent approach that reformulates the problem using Kronecker products of matrices (see [1], [2]). This approach is based on inverse iteration but requires the solution of Lyapunov equations with low-rank right-hand sides at each step of the iteration. Numerical results will be presented for some large-scale problems arising from fluid dynamics and aeroelasticity.

This is joint work with Karl Meerbergen (KU Leuven), Howard Elman (Maryland) and Minghao Rostami (Worcester Polytechnic Institute).

References

1. K. MEERBERGEN AND A. SPENCE, *Inverse iteration for purely imaginary eigenvalues with application to the detection of Hopf Bifurcation in large scale problems*, SIAM J Matrix Anal Appl., Vol 31 (2010), pp.1982-1999.
2. H. C. ELMAN, K. MEERBERGEN, A. SPENCE AND M. WU, *Lyapunov inverse iteration for identifying Hopf bifurcations in models of incompressible flow*, SIAM J. Sci Comput., Vol 34 (2012), pp.A1584-A1606.

Cancer Diagnosis with PESI-Mass Spectrometry Data: A learning machine approach alternative to the morphology-based pathological method

Kunio Tanabe

Waseda University, Tokyo, Japan

Keywords: Machine learning, dPLRM, Mass Spectrometry, PESI, Cancer Diagnosis

Abstract

Currently cancer diagnosis ought to be carried out by qualified pathologists based mainly on morphological inspection of biological specimen taken from patients. We have developed a new automatic method of cancer diagnosis based on observation of multitude of bio-chemical compounds measured on a tiny tissue with a PESI-MS spectrometer. There have been many attempts of the diagnosis based on particular biological markers identified for particular cancers. But this approach is not very reliable, because it is based on a single (or a few) marker(s) and their combined thresholds are not clear. Presuming that a cancerous cell would produce multiple *unknown metabolites* different from the ones of normal cells, we applied the learning machine dPLRM for diagnosis.

dPLRM (dual Penalized Logistic Regression Machine(2001)) ([1-5] is a 'universal' inductive reasoning machine, which belongs to a family of *learning machines* such as Neural Networks(NN), Support Vector Machines(SVM). The concept of machine learning has recently arisen as an alternative to the *Hypothetico-Deductive Method* accompanied by the *Reductionism*, which has been held unequivocal for scientific inquiries. However, dPLRM and other learning machines follow *Anti-Reductionism*. These machines are intended for scientific inference in the fields whose subjects are too complex to allow contrived identification of causal chains of primitive elements, [1, 5].

When a set of multi-categorically classified data (in the cancer diagnosis case, pathologically diagnosed MS data) is fed into dPLRM, it produces inside the machine a mathematical model which relate data to category. This process is called *learning* with the training data set. Once this process is completed, the machine can tell you which categorical class a newly obtained unknown data should be classified.

Unlike NN and SVM, the machine PLRM and its dual machine, dPLRM, are based essentially on a statistical model, called *penalized logistic regression model*, and can give directly a *probabilistic estimate (or prediction)* of possible categorical classes of yet-to-be classified data. The statistical model adopted with dPLRM differ from the traditional statistical models representing very specific mathematical relationship between category and data. By presuming that the true mathematical relationship is not to be known, dPLRM adopts a set of very versatile and plastic models for relating data to category, resulting in the models with *kernel functions*, thus enabling us to infer categorical class of a data without resorting to heavily specific assumptions.

Three histological types, RCC, HCC, MUC of human tissue specimen were gathered and they were put into the **PESI module**, [6, 8, 9], directly connected to the single quadropole mass spectrometers, **SHIMADZU LCMS-2020** to obtain PESI-MS data of a large set of microscopic droplets picked up with the tip of a very fine acupuncture needle from pathologically diagnosed normal and cancerous tissues. We fed dPLRM with the full measurable range (from m/z 10 through 2000) spectrum data without any range truncation adjustment to histological types of the tissues. We found that the agreement rate of probabilistic diagnosis by dPLRM and diagnosis by pathologists is quite high for each histological type case, [10]. Besides, the diagnosing time of an unknown spectrum by our system is within a few minutes, in which dPLRM computing requires about 10 seconds for diagnosis.

References

1. K. TANABE, Penalized Logistic Regression Machines: New method for statistical prediction 1, ISM Cooperative Research Report, **143**, (2001),163-194.
2. K.TANABE, Penalized Logistic Regression Machines: New method for statistical prediction 2, Proceedings of 2001 Workshop on Information Based Induction Science(IBIS2001) (2001), 71-76.
3. K.TANABE, Penalized Logistic Regression Machines and Related Numerical Algebra, KOKYUROKU, Inst. for Math. Sci., Kyoto Univ., **1320** (2003), 239-249.
4. T. MATSUI ET AL., Speaker Recognition without Feature Extraction Process, Technical Report of IEICE, NLC2004-54, SP2004-94, Institute of Electronics, Information and Communication Engineers, (2004), 79-84.
5. K.TANABE, ‘Universal’ Induction Machine PLRM and dPLRM — Methodology, Model, Algorithm and Applications(in Japanese), System, Information and Control, **51**, **2** (2007), 87-95.
6. K.HIRAOKA ET AL., Development of Probe Electrospray using a Solid Needle, Rapid Commun. Mass Spectrom., **21**, (2007), 3139-3144.
7. O.BIRKENES ET AL., Penalized Logistic Regression with HMM Log-Likelihood Regressors for Speech Recognition, IEEE Transaction on Audio, Speech and Language Processing, **18**, **6** (2010), 1440-1454.
8. S.TAKEDA ET AL., Innovation in Analytical Oncology-Status quo of Mass Spectrometry-based Diagnostics for malignant Tymor, J. Anal. Oncol., **2012**, **1**, 74-80.

9. K. YOSHIMURA ET AL., Analysis of Renal Cell Carcinoma as a First Step for Developing Mass Spectrometry-based Diagnostics, *J. Am. Soc. Mass Spectrom.*, **23**, 1741-1749 (2012).
10. S. TAKEDA ET AL., Developing a Novel Cancer Diagnosis System Based on the Mass Spectrometry and Learning Machine (in Japanese), *SHIMADZU REVIEW*, (2013), 203-210.

Acknowledgments: This is a collaborate work by K.Tanabe¹, H.Hori², S.Takeda², K.Hiraoka², K.Yoshimura², S.Ninomiya², H.Izumi³, H.Nakajima³ (¹ Waseda University, ² University of Yamanashi, ³ Shimadzu Corporation)

Ecoepidemics with a nonlinear disease incidence

Ezio Venturino

Dipartimento di Matematica “Giuseppe Peano”,
Università di Torino, Italy.

Keywords: predator-prey models, transmissible diseases, incidence rates, herd behavior, ecoepidemics

Abstract We present two new models for interacting populations subject to a transmissible disease. The novelty lies in the assumption that herd behavior influences the disease incidence, rather than the demographic description of the interactions, as in previous related similar models. As it is already known from other ecoepidemiological situations, the epidemics may affect the system demographic outcomes.

1 Introduction

Ecoepidemiology studies the influence of diseases among interacting populations. This rather new field of research started about a quarter of a century ago, with investigations merging diseases in demographic models in different contexts, [3, 6, 9]. For a brief overview of the progress up to a few years ago, see Chapter 7 of [8].

Much more recently, a novel idea for modeling herd behavior has been introduced, [1, 2], and further explored in [4]. It is essentially based on the observation that individuals gathering in groups can generally be attacked by predators on the outskirts of the territory that they occupy, that is proportional to their size. The population occupies thus a two-dimensional manifold, while its boundary represents a one-dimensional one. The former is directly related to the population size, while the latter instead must be then related to its square root.

Rather than pursuing this idea in various circumstances in ecological situations, [2], following the idea of extending these demographic remarks to ecoepidemic situations, [4, 10], we want to exploit it here still in the ecoepidemic realm, but considering gatherings of infected individuals. In fact, we use the basic ideas on herd behavior, [2], in a different context. Specifically, in [10] as well as in [4, 5], it is still the demographic part of the system that is modeled according to herd behavior. Here, however, we assume that the infected lump together. Their herd

size grows due to the arrival of new individuals only through the susceptible contacts, wandering about independently of each other, with the infectious individuals positioned on the outskirts of the infected bunch. This may be plausible in the context of predators and prey interactions, because infected individuals, in general weaker and slower, may gather together. Hence, their new possible recruits would arrive precisely through the above mechanism. As stated above, assuming thus that these populations occupy a certain portion of ground, predation occurs on the border, i.e. the perimeter, of the lump of infected individuals, therefore it is expressed via a square root term of their size.

The paper is organised as follows. We briefly summarize the results on the classical predator-prey reference model in the next Section, then provide some basic information on the ecoepidemic models we want to introduce. In Section 4 we consider the case of infected prey that are harmless for predators. Section 5 contains the particular case in which the predators recognize and avoid infected prey. In Section 6 we present the model for which infected are toxic for the predators. Results on the boundedness of the systems' trajectories are derived in the next Section and a final summary of the results concludes the paper.

2 The classical predator-prey reference model

Let us consider the Lotka-Volterra predator-prey model with logistic correction for the prey Q . The predators P are assumed to be specialists, so that in the absence of Q they would starve to death. The model reads

$$\begin{aligned}\frac{dP}{dt} &= -mP + aPQ, \\ \frac{dQ}{dt} &= rQ \left(1 - \frac{Q}{K}\right) - aPQ.\end{aligned}\tag{1}$$

The parameters are defined as follows: m represents the predator's mortality rate, a is the predator's hunting rate, r is the prey reproduction rate, K is the prey carrying capacity.

This system dynamics is well known. There are only two possibly stable equilibria, since the origin is always unstable. Between the predator-free point $E_1^c = (0, K)$ and coexistence $\widehat{E}_*^c = (P_*^c, Q_*^c)$ there is a transcritical bifurcation. Whenever the predators' mortality rate falls below the threshold

$$m^* = aK\tag{2}$$

the predators invade the environment permanently, as E_*^c becomes feasible and is unconditionally stable, while instead E_1^c loses its stability. In each case, the only possible equilibrium is globally asymptotically stable.

3 Background on the ecoepidemic situation

In the ecoepidemic approach the main difference with the previous demographic model consists in the fact that the prey population is divided among infected I , that gather in herds, and susceptibles S . We also assume the presence in the ecosystem of a third population P that can predate on S as well as possibly on the I lumped together. With this we mean that predation occurs always on the border of the lump of I 's, as in other herd behavior systems, [2]. But the effect of predation on the infected can have different outcomes for the predators.

Three cases will be considered, as far as the behavior of P with respect to I is concerned: they do not recognize the infected, but their predation leaves the P 's unaffected, they recognize the I 's and avoid them, or finally the P 's predate the I 's and the latter harm the predators. We stress here once again that the novelty of this model is in using the herd behavior in the epidemiological terms, especially in contrast with what was done in [4,5], where the major issue was on the infected behavior, but still considered from the demographic behavior point of view.

The group gathering behavior is modeled as indicated above, via the square root of the infected population density \sqrt{I} . Disease transmission occurs through contacts among the infected lying on the boundary of the herd with the susceptibles. Assuming homogeneous mixing among these classes of individuals, the corresponding (modified) "mass action" term assumes the form $S\sqrt{I}$. Thus, our nonlinear disease incidence model could be regarded as a particular case of the $S^\alpha I^\gamma$ incidence, which has been proposed among other epidemiological population interaction possibilities, see [7]. The following are further general assumptions for all the three models considered here: the lump of I 's does not reproduce, it can grow only by recruiting newcomers from the class S . They are also too weak to exert any intraspecific competition on the healthy individuals S , nor feel their pressure for the search for resources, since they do not reproduce. We also assume that the predators do not have other food sources, being specialists. With respect to the loose population S the encounters with P are on a one to one basis, i.e. they are expressed via the usual mass action law.

4 Infected are harmless for predators.

The first model we investigate is the following one

$$\begin{aligned} \frac{dP}{dt} &= -mP + aPS + bP\sqrt{I}, \\ \frac{dS}{dt} &= -\beta S\sqrt{I} + rS \left(1 - \frac{S}{K}\right) - aPS, \\ \frac{dI}{dt} &= -\mu I + \beta S\sqrt{I} - bP\sqrt{I}. \end{aligned} \tag{3}$$

We define the meaning of all the parameters, because although we use the same notation as in (1), the interpretation of the parameters common to both (1) and (3) is at times slightly different. Here m represents the predator's mortality rate, a is the predator's hunting rate on healthy prey, b is the predation rate on the infected herds of prey, β is the disease incidence rate, r is the healthy prey reproduction rate, K is the carrying capacity of healthy prey, μ is the natural plus disease-related mortality rate of infected individuals.

In view of the fact that the prey modeled by the I 's lump together, predation on them is exerted only on the outer boundary of their herd, which is expressed by the square root term in the above first and third equations (3). We need to redefine the dependent variables, to avoid a possible singularity in the Jacobian when I vanishes. Singularity removal can be performed by defining $U = \sqrt{I}$. It leads to

$$\begin{aligned}\frac{dP}{dt} &= P(-m + aS + bU), \\ \frac{dS}{dt} &= S \left[-\beta U + r \left(1 - \frac{S}{K} \right) - aP \right], \\ \frac{dU}{dt} &= \frac{1}{2} (-\mu U + \beta S - bP).\end{aligned}\tag{4}$$

The Jacobian of (4) is

$$J^h = \begin{pmatrix} -m + aS + bU & aP & bP \\ -aS & -\beta U + r - 2\frac{r}{K}S - aP & -\beta S \\ -\frac{1}{2}b & \frac{1}{2}\beta & -\frac{1}{2}\mu \end{pmatrix}.\tag{5}$$

4.1 Equilibria and their analysis

The possible equilibria are the points E_0 , namely the system disappearance, the predator-free point

$$E_1 = \left(0, rK \frac{\mu}{\beta^2 K + r\mu}, rK \frac{\beta}{\beta^2 K + r\mu} \right),$$

and the coexistence equilibrium \hat{E}_* with population values

$$\begin{aligned}\hat{P}_* &= \frac{bKr\beta + aKr\mu - mr\mu - Km\beta^2}{a^2K\mu + b^2r}, & \hat{S}_* &= K \frac{am\mu + b^2r - bm\beta}{a^2K\mu + b^2r}, \\ \hat{U}_* &= \frac{bmr + aKm\beta - abKr}{a^2K\mu + b^2r}.\end{aligned}$$

Feasibility conditions for \hat{E}_* are

$$Kr(b\beta + a\mu) \geq m(r\mu + K\beta^2), \quad am\mu + b^2r \geq bm\beta, \quad m(br + aK\beta) > abKr.\tag{6}$$

The origin is unstable, since the eigenvalues of J^h are $-m, r, -\frac{1}{2}\mu$.

At E_1 the stability condition is regulated by the very first eigenvalue,

$$aS_1 + bU_1 \equiv m^\ddagger < m, \quad (7)$$

since the remaining ones come from a 2 by 2 submatrix J_2^h for which the Routh-Hurwitz conditions hold unconditionally, since they become

$$-tr(J_2^h) = \frac{r}{K}S_1 + \frac{1}{2}\mu > 0, \quad \det(J_2^h) = \frac{r}{K}S_1 + \frac{1}{2}\beta^2S_1 > 0. \quad (8)$$

Note that (7) is the opposite condition of the first inequality for the feasibility of \widehat{E}_* , (6), so that when the other two feasibility conditions (6) hold, we have a transcritical bifurcation for which \widehat{E}_* emanates from E_1 . It is clearly seen also that no Hopf bifurcation can arise here, in view of the strict inequality for the trace.

The coexistence equilibrium \widehat{E}_* is always stable, whenever feasible, since the characteristic equation (9) is the cubic

$$\sum_{k=0}^3 a_k \lambda^k = 0, \quad (9)$$

with the coefficients

$$\begin{aligned} a_0 &= \frac{1}{2} \left(a^2 \mu + b^2 \frac{r}{K} \right) S_* P_* > 0, & a_2 &= \frac{r}{K} S_* + \frac{1}{2} \mu > 0, \\ a_1 &= a^2 S_* P_* + \frac{1}{2} \left[b^2 P_3 + \left(\frac{r}{K} \mu + \beta^2 \right) S_* \right] > 0. \end{aligned} \quad (10)$$

In fact, also the last Routh-Hurwitz conditions holds unconditionally

$$a_2 a_1 - a_0 = \frac{r}{K} S_*^2 \left(a^2 P_* + \frac{r\mu}{2K} + \frac{1}{2} \beta^2 \right) + \frac{\mu}{4} \left(\frac{r\mu}{K} S_* + \beta^2 S_* + b^2 P_* \right) > 0 \quad (11)$$

and strictly, thus preventing also possible Hopf bifurcations.

5 No predation on infected prey

We briefly examine here the particular case of (3) in which $b = 0$, i.e. the infected are recognized and completely disregarded by the predators. The system with no singularity and its Jacobian are obtained just as particular cases of (4) and (5), setting in them $b = 0$.

The possible equilibria are again all the points found earlier, namely the origin and the predator-free equilibrium E_1 with the very same population values. Both these equilibria are always feasible. We also find coexistence, which now simplifies to

$$E^* = \left(\frac{arK\mu - m\beta^2K - mr\mu}{a^2K\mu}, \frac{m}{a}, \frac{\beta m}{\mu a} \right).$$

It is feasible only if

$$m < m^\dagger \equiv \frac{aKr\mu}{K\beta^2 + r\mu}. \quad (12)$$

This condition specifies that the predator's mortality must fall below a certain critical threshold. Note that m^\dagger coincides with m^\ddagger when the latter is evaluated for $b = 0$.

The origin E_0 retains its unconditional instability, in view of the very same eigenvalues we found for (4), namely $-m$, r , $-\frac{1}{2}\mu$.

One eigenvalue of E_1 is now $-m + aS_1$ giving the stability condition, as the last two conditions (6) now are trivially satisfied:

$$m^\dagger < m, \quad (13)$$

again a particular case of what we found for (4). For the remaining ones again the Routh-Hurwitz conditions hold unconditionally. Indeed the remaining ones come from the 2 by 2 submatrix $\tilde{J}_2^h = J_2^h$ for which the Routh-Hurwitz conditions hold unconditionally (8). Again, no Hopf bifurcation can arise here as well and for $m = m^\dagger$ there is a transcritical bifurcation for which E^* arises from E_1 .

At E^* the characteristic equation is the cubic (9) with coefficients that are obtained from (10) by setting $b = 0$. Therefore since all these coefficients are strictly positive and also the third Routh-Hurwitz stability condition holds, whenever feasible, the coexistence equilibrium is unconditionally stable. Also, in view of the above strict inequality in (11), no Hopf bifurcations can arise here as well.

6 The case of toxic infected.

In this case we assume that the infected prey are harmful for the predators when they come in contact. The model becomes then

$$\begin{aligned} \frac{dP}{dt} &= -mP + aPS - bP\sqrt{I}, \\ \frac{dS}{dt} &= -\beta S\sqrt{I} + rS \left(1 - \frac{S}{K} \right) - aPS, \\ \frac{dI}{dt} &= -\mu I + \beta S\sqrt{I} - bP\sqrt{I}. \end{aligned} \quad (14)$$

Again, all the parameters retain their meaning from (4), but note the change in sign in the last term of the first equation. Once again, the system with the removed singularity becomes

$$\begin{aligned}\frac{dP}{dt} &= P(-m + aS - bU), \\ \frac{dS}{dt} &= S \left[-\beta U + r \left(1 - \frac{S}{K} \right) - aP \right], \\ \frac{dU}{dt} &= \frac{1}{2} (-\mu U + \beta S - bP).\end{aligned}\tag{15}$$

The Jacobian of (15) is

$$J^t = \begin{pmatrix} -m + aS - bU & aP & -bP \\ -aS & -\beta U + r - 2\frac{r}{K}S - aP & -\beta S \\ -\frac{1}{2}b & \frac{1}{2}\beta & -\frac{1}{2}\mu \end{pmatrix}.$$

6.1 Equilibria and their analysis

Again the origin E_0 and the predator-free equilibria E_1 are unaltered from the previous case (4) and are therefore always feasible. Coexistence \tilde{E}_* settles instead at the following population values

$$\begin{aligned}\tilde{P}_* &= \frac{aKr\mu - mr\mu - Km\beta^2 - bKr\beta}{a^2K\mu - 2abK\beta - b^2r}, & \tilde{S}_* &= \frac{aKm\mu - bKm\beta - b^2Kr}{a^2K\mu - 2abK\beta - b^2r} \\ & & \tilde{U}_* &= \frac{aKm\beta + bmr - abKr}{a^2K\mu - 2abK\beta - b^2r}.\end{aligned}$$

Feasibility conditions are either one of these sets of inequalities

$$\begin{aligned}2abK\beta + b^2r &\geq a^2K\mu, & mr\mu + Km\beta^2 + bKr\beta &\geq aKr\mu, \\ bKm\beta + b^2Kr &\geq aKm\mu, & abKr &\geq bmr + aKm\beta;\end{aligned}\tag{16}$$

or

$$\begin{aligned}2abK\beta + b^2r &\leq a^2K\mu, & mr\mu + Km\beta^2 + bKr\beta &\leq aKr\mu, \\ bKm\beta + b^2Kr &\leq aKm\mu, & abKr &\leq bmr + aKm\beta.\end{aligned}\tag{17}$$

Stability of E_0 is once again unchanged, the eigenvalues are still the same, $-m, r, -\frac{1}{2}\mu$. For E_1 we find again the very same condition (7), as the remaining analysis on the 2 by 2 submatrix carries out unaltered.

At coexistence instead relevant changes occur, as the cubic (9) has here the coefficients

$$\begin{aligned}a_0 &= \frac{1}{2} \left(a^2\mu - b^2\frac{r}{K} - 2ab\beta \right) \tilde{S}_*\tilde{P}_*, & a_2 &= \frac{r}{K}\tilde{S}_* + \frac{1}{2}\mu, \\ a_1 &= a^2\tilde{S}_*\tilde{P}_* + \frac{1}{2} \left[\left(\frac{r}{K}\mu + \beta^2 \right) \tilde{S}_* - b^2\tilde{P}_* \right].\end{aligned}$$

They now must all be imposed to be positive. Note that $a_0 > 0$ is incompatible with the first feasibility condition for \tilde{E}_* (16). Also the condition $a_2 a_1 - a_0 > 0$ must be imposed, which now becomes

$$\frac{r}{K} \tilde{S}_*^2 \left(a^2 \tilde{P}_* + \frac{r}{2K} \mu + \frac{1}{2} \beta^2 \right) + \frac{1}{4} \mu \tilde{S}_* \left(\frac{r}{K} \mu + \beta^2 \right) + ab \beta \tilde{S}_* \tilde{P}_* > \frac{1}{4} \mu b^2 \tilde{P}_*. \quad (18)$$

It would therefore in principle be possible that Hopf bifurcations in this case could arise. However extended simulations attempting to violate this conditions were not successful. We have been able only to make it almost an equality, but never to reverse the above inequality (18), see Fig. 3.

We conjecture therefore that also in this case the coexistence equilibrium does not lead to Hopf bifurcations. Instead, mainly by rendering a_0 negative, we can destabilize the coexistence equilibrium. This in turn takes the system trajectories either to the predator-free equilibrium E_1 , when it is stable, namely for (7), or to limit cycles around it, see Fig. 1.

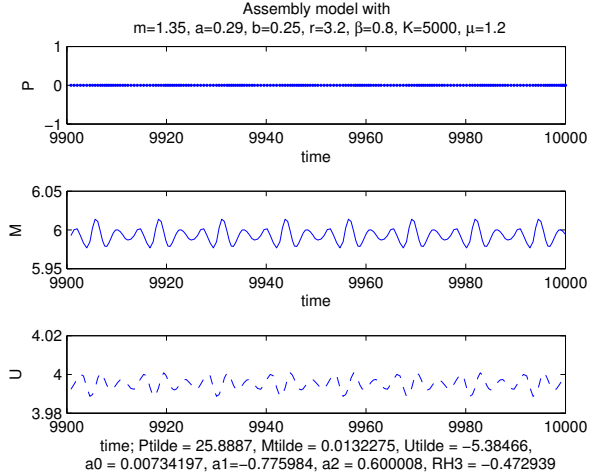


Figure 1. For the system (15), the prey subpopulations can thrive together, in absence of predators, also via tiny persistent oscillations, here obtained with the parameter values $m = 1.35$, $a = 0.29$, $b = 0.25$, $r = 3.2$, $\beta = 0.8$, $K = 5000$, $\mu = 1.2$. The coexistence equilibrium in this case is unfeasible, $\tilde{E}_* = (25.889, 0.013, -5.385)$. In this case $E_1 = (0, 5.993, 3.995)$ and $m < m^\ddagger = 2.737$, showing its instability, compare (7). Note that the oscillations shown are indeed around this predator-free equilibrium point. Top to bottom the populations P , S , U , as functions of time.

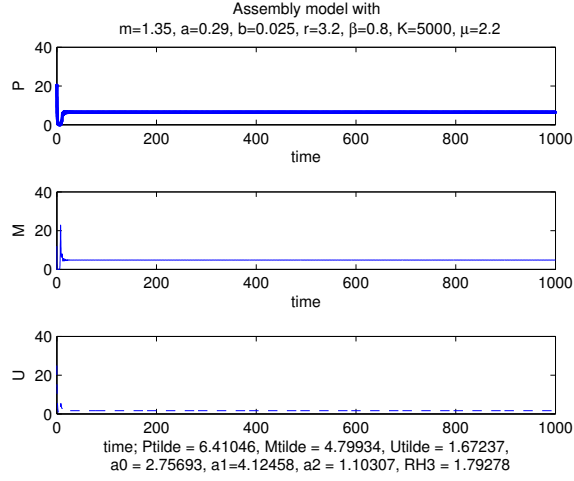


Figure 2. For the system (15), the coexistence equilibrium can be stably achieved for the parameter values $m = 1.35$, $a = 0.29$, $b = 0.025$, $r = 3.2$, $\beta = 0.8$, $K = 5000$, $\mu = 2.2$, at the level $\tilde{E}_* = (6.410, 4.799, 1.672)$. The Routh-Hurwitz conditions hold, since $a_0 = 2.667$, $a_1 = 4.125$, $a_2 = 1.103$ and $a_2 a_1 - a_0 = 1.882$. Top to bottom the populations P , S , U , as functions of time.

7 Boundedness

The finiteness of the trajectories can be shown for all three original models together as follows. Let $T = P + S + I$, by adding the differential equations it is then easy to show that for (3) and (14) the following inequality holds:

$$\frac{dT}{dt} \leq -mP + rS - \frac{r}{K}S^2 - \mu I.$$

Taking now an arbitrary $0 < q < \min\{\mu, m\} = M$, we find

$$\frac{dT}{dt} + qT \leq (r + q)S - \frac{r}{K}S^2 + (q - M)(P + I) \leq \Psi,$$

since $q - M < 0$ and where Ψ denotes the height of the vertex of the parabola in S on the left hand side, for which

$$\Psi = \frac{K}{4r}(r + q)^2.$$

It follows then that the solutions of the above differential inequality must lie below those of

$$\frac{dT}{dt} = \Psi - qT,$$

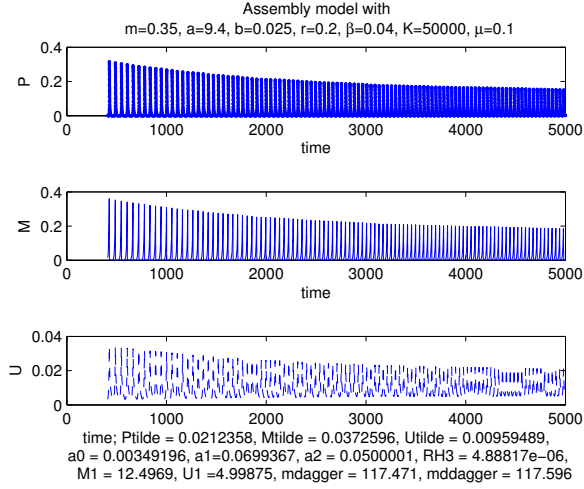


Figure 3. For the system (15), decaying oscillations involving all three sub-populations arise for the parameter values $m = 0.35$, $a = 9.4$, $b = 0.025$, $r = 0.2$, $\beta = 0.04$, $K = 50000$, $\mu = 0.1$, dampened toward the equilibrium $\tilde{E}_* = (0.0212, 0.0373, 0.0096)$. The Routh-Hurwitz conditions do however hold: $a_0 = 0.0035$, $a_1 = 0.0699$, $a_2 = 0.0500$ and $a_2 a_1 - a_0 = 8.607 \times 10^{-6}$. Top to bottom the populations P , S , U , as functions of time.

i.e.

$$T(t) = \frac{\Psi}{q} (1 - e^{-qt}) + T(0)e^{-qt} \leq \max \left\{ \frac{\Psi}{q}, T(0) \right\}.$$

8 Conclusions

The analysis shows that the system cannot possibly disappear, as the origin is always unstable. This is a good result in terms of ecological implications, and it is essentially implicit in the model assumptions, namely the logistic growth of the prey, as the positive eigenvalue of the Jacobian stems exactly from the susceptible prey reproduction equation.

The systems then have only two possible equilibria, related to each other via a transcritical bifurcation, which occurs when the predators' mortality falls below the threshold m^\ddagger , or its particular case m^\ddagger for the model of infected prey avoided by predators. When it is above it, the systems settles at the prey-only equilibrium, with endemic disease.

The predator-free equilibrium E_1^c of the classical predator-prey case can get destabilized by the disease presence, see the stability conditions for E_1 (7) and

(13). Note indeed that the thresholds m^\dagger and m^\ddagger contain the epidemiological parameters β and μ , while m^* obviously does not, compare (2) with (7) and (13). Note also that $m^\dagger = m^*$ for $\beta = 0$, i.e. in the absence of the disease. This destabilization never occurs in the classical case. This remark once more stresses the fact that epidemics have also demographic consequences at the ecological level and therefore cannot be easily neglected in ecological investigations too.

References

1. V. AJRALDI, E. VENTURINO, *Mimicking spatial effects in predator-prey models with group defense*, Proceedings of the 2009 International Conference on Computational and Mathematical Methods in Science and Engineering, J. Vigo Aguiar, P. Alonso, S. Oharu, E. Venturino, B. Wade (Editors), Gijón, Asturias, Spain, June 30th - July 3rd, 2009, p. 57-66. ISBN 978-84-612-9727-6
2. V. AJRALDI, M. PITTAVINO, E. VENTURINO, *Modeling herd behavior in population systems*, Nonlinear Analysis: Real World Applications, Vol. 12 (2011), pp. 2319-2338.
3. E. BELTRAMI, T. O. CARROLL, *Modelling the role of viral disease in recurrent phytoplankton blooms*, J. Math. Biol., Vol. 32 (1994), pp. 857-863.
4. E. CAGLIERO, E. VENTURINO, *Ecoepidemics with group defense and infected prey protected by the herd*, Proceedings of the 12th International Conference on Computational and Mathematical Methods in Science and Engineering, CMMSE 2012, J. Vigo-Aguiar, A.P. Buslaev, A. Cordero, M. Demiralp, I.P. Hamilton, E. Jeannot, V.V. Kozlov, M.T. Monteiro, J.J. Moreno, J.C. Reboredo, P. Schwerdtfeger, N. Stollenwerk, J.R. Torregrosa, E. Venturino, J. Whiteman (Editors) La Manga, Spain, July 2nd-5th, Vol. 1 (2012), pp. 247-266.
5. E. CAGLIERO, E. VENTURINO, *Ecoepidemics with infected prey in herd defense: the harmless and toxic cases*, submitted for publication (2013).
6. K. P. HADELER, H. I. FREEDMAN, *Predator-prey populations with parasitic infection*, J. Math. Biol., Vol. 27, (1989), pp. 609-631.
7. W. LIU, S. A. LEVIN AND Y. IWASA, *Influence of nonlinear incidence rates upon the behavior of SIRS epidemiological models*, Journal of Mathematical Biology, Vol. 23 (1986), pp. 187-204.
8. H. MALCHOW, S. PETROVSKII, E. VENTURINO, *Spatiotemporal patterns in Ecology and Epidemiology*, CRC, Boca Raton, 2008.
9. E. VENTURINO, *The influence of diseases on Lotka-Volterra systems*, Rocky Mountain Journal of Mathematics, Vol. 24, (1994), pp. 381-402.
10. E. VENTURINO, *A minimal model for ecoepidemics with group defense*, J. of Biological Systems, Vol. 19, No. 4, (2011), pp. 763-785.

Acknowledgments: This research has been partially supported by the project “Metodi numerici in teoria delle popolazioni” of the Dipartimento di Matematica “Giuseppe Peano”.

Microscopic traffic model on the infinite line with bottleneck: standing and traveling waves

Bodo Werner

University of Hamburg, Department of Mathematics,
Hamburg, Germany

Keywords: microscopic car following traffic model on the line, optimal velocity function, leading car model, quasi-stationary solution, standing waves, Poincaré N -model, Floquet multipliers.

Abstract

We study a very simple microscopic car following traffic model on the line with a leading car at the top, given by the infinite ODE system

$$\ddot{x}_j(t) = \frac{1}{\tau} (V(x_{j-1}(t) - x_j(t)) - \dot{x}_j(t)), \quad j = 2, 3, \dots,$$

where $V(h)$ is a certain optimal velocity function as proposed in [1]. The leading car ($j = 1$) has no car ahead and is governed by the simple ODE

$$\ddot{x}_1(t) = \frac{1}{\tau} (v_f - \dot{x}_1(t)),$$

where v_f is the speed it is aiming to.

This **line model** has a unique trivial solution – a quasi-stationary solution where all cars have speed v_f and headway h_f implicitly defined by $V(h_f) = v_f$. In comparison with an arbitrary infinite autocode (without a leading car), in our *leading car model* we extract a specific solution from all possible quasi-stationary solutions with constant headway h and speed v , where $v = V(h)$. The quantity $\rho_f := 1/h_f$ can be considered as a given average traffic density on the infinite line. In [4] we studied the stability of the quasi-stationary solution in dependence on the system parameter h_f .

In addition to [4] we introduce a bottleneck of strength ε at certain position in the same way as in [2] for the circle model. The bottleneck is modeled by replacing the optimal velocity function V by some function $V_{j,\varepsilon}$ for car No. j .

We are interested how ε and h_f influence the traffic dynamics. The first observation is that the quasi-stationary solution for $\varepsilon = 0$ is perturbed to a certain standing wave where all cars have the same dynamics. Their speed is locally reduced in the neighborhood of the bottleneck, see Fig. 1.

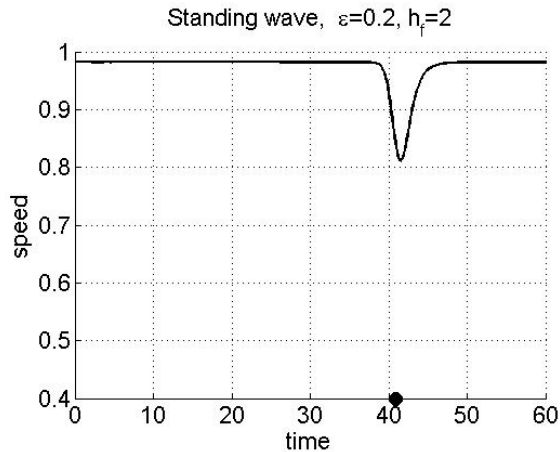


Figure 1. Standing wave: Speed-time dynamics of a single car for $h_f = 2$ and $\varepsilon = 0.2$.

Numerical experiments show a similar bifurcation phenomenon as reported in [4]: As far as an infinite autocade is considered, for a fixed ε the standing waves lose stability with decreasing h_f , and jam waves caused by the bottleneck are traveling upstream (We will present some movies). In [4] the loss of stability of the quasi-stationary solution was theoretically justified by investigating the spectrum of an infinite matrix. Based on these arguments it was shown that the bifurcation takes place at the Hopf bifurcation parameters in the circle model, [3]. Another observation in [4] is the coexistence of stable quasi-stationary solutions and certain jam waves – another analogy to the circle model when jam waves are replaced by periodic solutions. We will show that some results in [2] for the circle model still hold on the line. The natural analogy with so called POMs are standing waves. To handle their stability we use another approach as in [4]. Instead of the infinite ODE system we consider a simple **Poincaré N–model**: The Poincaré event is defined by the fact that the leading car of a finite autocade consisting of N cars passes certain fixed position behind the bottleneck. Then the leading car is removed from the autocade, the second car becomes the new leader and at the end of the autocade another car is added with headway h_f and speed v_f . This defines a Poincaré map on \mathbb{R}^{2N} . A standing wave is now a fixed point of this Poincaré map. Its stability can be studied numerically by the eigenvalues of its linearization. We call the eigenvalues **Floquet multipliers** of the standing waves.

Our numerical experiments show that for large enough N , say $N = 100$, our Poincaré N –model shows the same dynamical behavior as the infinite ODE system.

This enables us to follow numerically the standing waves in dependence on ε or

h_f and study their stability and possible bifurcations. An example of a solution diagram is given by Fig. 2, where the minimal speed v_{Min} of the standing wave is indicated on the vertical axis. The dashed line corresponds with stable standing waves. From Fig. 2 we conclude the coexistence of two stable standing waves for $\varepsilon = 0.25$.

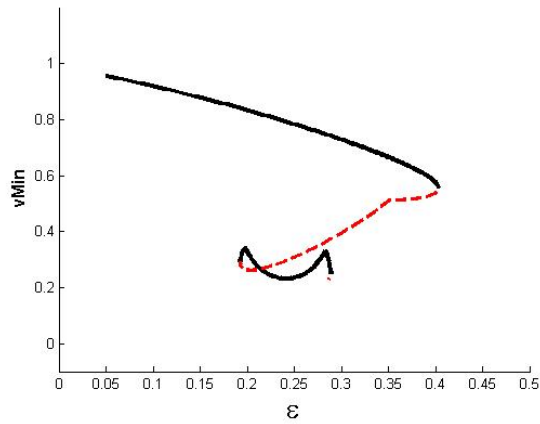


Figure 2. Solution diagram: Standing waves for $h_f = 2.1$ in dependence on ε .

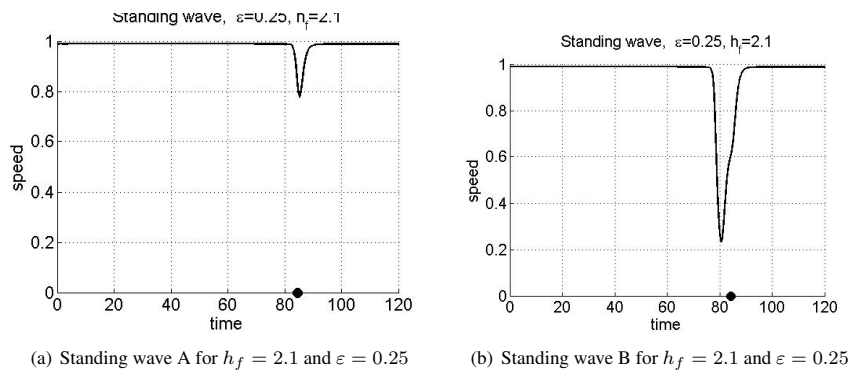


Figure 3. Time-speed dynamics for $h_f = 2.1$ and $\varepsilon = 0.25$.

Fig. 3 shows the two standing waves which are quite different with respect to the decrease of speed each car has to undergo by passing the bottleneck. The black dot on the time axis denotes the time when the car passes the center of

the bottleneck. The first one, standing wave A , is the result of a quasi-stationary autocade hitting the bottleneck. It is very stable, the Floquet multiplier with maximal modulus is $\mu = 0.8$. The second one was initiated by a rather large initial perturbation of the quasi-stationary autocade. Its Floquet multiplier with maximal modulus is $\mu = 0.98$. This indicates that its stability is rather weak. There exist parameter regions where there exist no stable standing wave. This can already occur for $\varepsilon = 0$ and small headways, see [4]. Then small perturbations of the quasi-stationary solution lead to so called jam waves. Also in case of bottlenecks coexistence of stable standing waves and jam waves can be observed.

References

1. M. BANDO, K. HASEBE, A. NAKAYAMA, A. SHIBATA, AND Y. SUGIYAMA, *Dynamical model of traffic congestion and numerical simulation*. Phys. Rev. E, 51:1035ff, 1995.
2. I. GASSER AND B. WERNER, *Dynamical phenomena induced by bottleneck*. Phil. Trans. R. Soc. A 368, 4543- 4562, 2010.
3. T. SEIDEL, I. GASSER, AND B. WERNER, *Microscopic car-following models revisited: from road works to fundamental diagrams*. SIAM J. Appl. Dyn. Sys. 8 (3),1305–1323, 2009.
4. B. WERNER, *Microscopic traffic model on the infinite line: Quasi-stationary solutions, their stability and jam waves*. Hamburger Beiträge zur Angewandten Mathematik 2013-12, 2013.

Some developments on the global conditional regularity of the Navier-Stokes equations concerning one velocity component

Šimon Axmann^{1,2}

Institute of Chemical Technology, Prague¹
Faculty of Mathematics and Physics, Charles University, Prague²

Keywords: incompressible Navier-Stokes equations, global regularity, regularity criteria

Abstract The Navier–Stokes system represents well established model for describing flows of viscous incompressible fluids. Although it is widely used in numerous applications, its mathematical analysis is far from being satisfactory. Recently, there have appeared many regularity criteria for weak solutions regarding one velocity component or/and part of its gradient. The aim of this review note is to give an introduction into this area and an overview of known results.

1 Introduction

We consider the Cauchy problem for the incompressible Navier–Stokes equations in three space dimensions, id est system of nonlinear partial differential equations for unknown vector velocity field \mathbf{v} and a scalar function p representing pressure; the constant kinematic viscosity $\nu > 0$ and the density of external force \mathbf{f} are given.

$$\left. \begin{aligned} \frac{\partial \mathbf{v}}{\partial t} + \mathbf{v} \cdot \nabla \mathbf{v} - \nu \Delta \mathbf{v} + \nabla p = \mathbf{f} \\ \operatorname{div} \mathbf{v} = 0 \end{aligned} \right\} \text{ in } (0, T) \times \mathbb{R}^3, \quad (1)$$
$$\mathbf{v}(0, \mathbf{x}) = \mathbf{v}_0(\mathbf{x}) \quad \text{in } \mathbb{R}^3,$$

Since the existence of classical solutions to the system (1) globally in time is generally not known¹, we move our attention to so called weak solutions which existence and main properties were proved by Jean Leray [20] in 1930's. Now,

¹ In fact, its existence is one of the Millenium problems of Clay institute, see [13].

we will recall briefly his main results. Further details, as well as other properties of the solutions and the definitions of involved spaces can be found in classical monographies (see e.g. [19], or [21]).

1.1 Weak, strong and classical solutions

In what follows we will assume for simplicity $\mathbf{f} = \mathbf{0}$. In fact, for the case of potential forces we can absorb it in the pressure, while for the nonpotential case it is easy to establish the assumptions on its behaviour so that all results remain valid.

Theorem and definition 1. *Let $\mathbf{v}_0 \in L^2_{\text{div}}(\mathbb{R}^3)$. Then there exists at least one weak solution to the Navier–Stokes equations corresponding to the initial value \mathbf{v}_0 , id est $\mathbf{v} \in L^2\left(0, T, (W^{1,2}_{\text{div}}(\mathbb{R}^3))\right) \cap L^\infty\left(0, T, (L^2(\mathbb{R}^3))\right)$ with $\frac{\partial \mathbf{v}}{\partial t} \in L^1\left(0, T, (W^{1,2}_{\text{div}}(\mathbb{R}^3))^*\right)$, such that*

$$\begin{aligned} & \left\langle \frac{\partial \mathbf{v}}{\partial t}, \boldsymbol{\varphi} \right\rangle_{(W^{1,2}_{\text{div}}(\mathbb{R}^3))^*, W^{1,2}_{\text{div}}(\mathbb{R}^3)} + \int_{\mathbb{R}^3} (\mathbf{v} \cdot \nabla \mathbf{v}) \cdot \boldsymbol{\varphi} \, dx \\ & + \nu \int_{\mathbb{R}^3} (\nabla \mathbf{v} : \nabla \boldsymbol{\varphi}) \, dx = 0, \quad \forall \boldsymbol{\varphi} \in W^{1,2}_{\text{div}}(\mathbb{R}^3), \text{ s.v. } t \in (0, T), \\ & \lim_{t \rightarrow 0^+} \int_{\mathbb{R}^3} \mathbf{v}(t, \cdot) \cdot \boldsymbol{\varphi} \, dx = \int_{\mathbb{R}^3} \mathbf{v}_0 \cdot \boldsymbol{\varphi} \, dx, \quad \forall \boldsymbol{\varphi} \in L^2_{\text{div}}(\mathbb{R}^3). \end{aligned}$$

Moreover, we are able to construct the solution in such a way that it satisfies the so called energy inequality,

$$\frac{1}{2} \int_{\mathbb{R}^3} |\mathbf{v}(t)|^2 \, dx + \nu \int_0^t \int_{\mathbb{R}^3} |\nabla \mathbf{v}|^2 \, dx \, dt \leq \frac{1}{2} \int_{\mathbb{R}^3} |\mathbf{v}_0|^2 \, dx, \quad \text{for a.a. } t \in (0, T)$$

in that case we call it the weak Leray–Hopf solution.

Remark 1. *Since we take in the weak formulation only solenoidal test functions, the pressure is in the weak formulation not present. However, it can be subsequently recovered from the velocity field, we omit further discussion concerning this feature.*

Remark 2. *It is not known whether there can exist a weak solution, which does not satisfy the energy inequality.²*

² Let us remark that in 2D setting due to a better integrability of the time derivative, we are able to test the weak formulation with the solution itself, to get the energy equality and consequently also uniqueness and full regularity.

Definition. We call a weak solution strong, if it additionally satisfies

$$\mathbf{v} \in L^\infty \left(0, T, (W_{\text{div}}^{1,2}(\mathbb{R}^3)) \right) \cap L^2 \left(0, T, (W^{2,2}(\mathbb{R}^3)) \right).$$

The following assertions possess really important role in understanding the possible behaviour of the solution and are crucial in proofs of regularity criteria.

Theorem 3. *Every strong solution satisfies even the energy equality, especially it is the Leray–Hopf solution, and it is also unique in the class of the weak Leray–Hopf solutions satisfying the corresponding initial condition.*

Theorem 4. *Let $\mathbf{v}_0 \in W_{\text{div}}^{1,2}(\mathbb{R}^3)$. Suppose that \mathbf{v} is a strong solution to the Navier–Stokes equations, then \mathbf{v} is as smooth as the data allow, hence in our case of the Cauchy problem with zero external force $\mathbf{v} \in C^\infty((0, T) \times \mathbb{R}^3)$.*

Theorem 5. *Let $\mathbf{v}_0 \in W_{\text{div}}^{1,2}(\mathbb{R}^3)$. Then there exists (possibly small) time $T^* = T^*(\|\mathbf{v}_0\|_{W_{\text{div}}^{1,2}(\mathbb{R}^3)}, \nu)$ so that on the time interval $(0, T^*)$, there exists a unique strong solution to the Navier–Stokes equations. Moreover, we have a lower bound on this time $T^* \geq \frac{C\nu^3}{\|\nabla \mathbf{v}_0\|_2^4}$.*

2 Regularity criteria

Generally speaking it is not known whether the class of weak solutions is a class of uniqueness of the solutions, or equivalently said, if it is possible that for some choice of initial data the singularity (blow-up) time occurs, meaning that time T^* is necessarily finite. Therefore, there naturally appears a question, under which additional conditions imposed on the general Leray–Hopf weak solution, is the weak solution regular, and consequently also unique. These conditions are in literature called *regularity criteria*, and a lot of mathematicians are focused on searching for them during the last fifteen years, in hope that it will help to shed light on the behaviour of a possible singularity. Unfortunately, not all the authors are familiar with already known results, and it is not rare to recognize that some of them just reobtain exactly the same result (compare e.g. [25] with more recent [33]).

The celebrated Prodi–Serrin conditions, guaranteeing the regularity as soon as there exist s and t such that

$$\mathbf{v} \in L^t \left(0, T, (L^s(\mathbb{R}^3)) \right), \quad \frac{2}{t} + \frac{3}{s} \leq 1, \quad s \geq 3 \quad (2)$$

have an interesting history.

First in early sixties, Prodi [27] proved uniqueness of the solutions in the class

$$\mathbf{v} \in L^t \left(0, T, (L^s(\mathbb{R}^3)) \right), \quad \frac{2}{t} + \frac{3}{s} < 1, \quad s \geq 3, \quad (3)$$

further Ohyama³ and Serrin [24, 29] showed for $s > 3$ also the regularity of the solution. Fabes, Jones and Rivière [12] then proved that for smoothness of \mathbf{v} it is enough to assume

$$\mathbf{v} \in L^t(0, T, (L^s(\mathbb{R}^3))), \quad \frac{2}{t} + \frac{3}{s} \leq 1, \quad s > 3.$$

The fact that the Prodi–Serrin conditions assures regularity also in the limit case $s = 3$, was showed more recently by Escauriaza, Seregin and Šverák [9] by transforming the problem into the backward uniqueness of the heat equation (see also [28]).

As a straightforward consequence of (2) we get by the Gagliardo–Nirenberg inequality the regularity also by assuming

$$\nabla \mathbf{v} \in L^t(0, T, (L^s(\mathbb{R}^3))), \quad \frac{2}{t} + \frac{3}{s} \leq 2, \quad s \in \left[\frac{3}{2}, 3\right), \quad (4)$$

this was generalized for $s \in [3, \infty)$ by Beirão da Veiga [3].

Thanks to the incompressibility condition $\operatorname{div} \mathbf{v} = 0$ it is relatively easy to show that it is enough to assume satisfaction of the classical Prodi–Serrin conditions only by two velocity components (see e.g. [2]), id est

$$v_1, v_2 \in L^t(0, T, (L^s(\mathbb{R}^3))), \quad \frac{2}{t} + \frac{3}{s} \leq 1, \quad s > 3, \quad (5)$$

and similarly for their gradients (see e.g. [8]):⁴

$$\nabla v_1, \nabla v_2 \in L^t(0, T, (L^s(\mathbb{R}^3))), \quad \frac{2}{t} + \frac{3}{s} \leq 2, \quad s \in \left(\frac{3}{2}, \infty\right), \quad (7)$$

note that this is a direct consequence of (5) for $s \in (\frac{3}{2}, 3)$.

Since in two dimensional setting, the regularity (and the uniqueness) of the solutions to the Navier–Stokes equations is well established, it is natural to search for the regularity criteria in terms of just one velocity component. The main aim of the following parts is to give a comprehensive overview of known results concerning one velocity component and/or its gradient.

³ Because of this article the conditions are sometimes called the Prodi–Ohyama–Serrin conditions.

⁴ See also [6] where the regularity is proved for

$$\nabla v_1, \nabla v_2 \in L^t(0, T, (L^s(\mathbb{R}^3))), \quad \frac{2}{t} + \frac{3}{s} \leq 1, \quad s \in [3, \infty]. \quad (6)$$

2.1 Conditions concerning one velocity component

We would like to expose an up to date summary of global regularity criteria to the Navier–Stokes equation in three space dimensions on the scale of the Lebesgue spaces, involving one velocity component or its derivatives. For the sake of clarity, we do not present the known results neither in higher space dimensions nor those expressed in other space norms (with one exception), since from our point of view, the proofs of these criteria usually do not bring anything new, but only reformulate already known results in terms of a bit finer spaces.⁵

The very first result concerning one velocity component regularity is due to Neustupa and Penel [23], who proved locally for suitable weak solution that if possible blow-up point occurs then there have to be all three velocity components unbounded. Globally this was proved independently by He [14] using the same idea⁶ based on the equation for the vorticity; more precisely He showed regularity of solution provided

$$v_3 \in L^\infty(0, T, (L^\infty(\mathbb{R}^3))).^7 \quad (8)$$

This pioneering result was then improved by a similar method upto

$$v_3 \in L^t(0, T, (L^s(\mathbb{R}^3))), \quad \frac{2}{t} + \frac{3}{s} \leq \frac{1}{2}, \quad s > 6, \quad (9)$$

see Neustupa, Novotný and Penel [22] for suitable weak solution, and Zhou [36] for a global regularity criterion for Cauchy’s problem.

In connection with the above mentioned results concerning one velocity component, there appeared also regularity criteria involving the gradient of one velocity component. The first result in this direction is due to He [14], who assumed

$$\nabla v_3 \in L^t(0, T, (L^s(\mathbb{R}^3))), \quad \frac{2}{t} + \frac{3}{s} \leq 1, \quad s \geq 3. \quad (10)$$

This was soon improved by Pokorný [26], and independently by Zhou [35], who proved regularity for

$$\nabla v_3 \in L^t(0, T, (L^s(\mathbb{R}^3))), \quad \frac{2}{t} + \frac{3}{s} \leq \frac{3}{2}, \quad s \geq 2, \quad (11)$$

(see also [30] for the special case $s = 3$ and $t = 4$). Note that for $s \in [2, 3)$ it is again just a consequence of the corresponding condition for the velocity (9).

Using a quite different technique based on the role of pressure and estimating it by parts Kukavica and Ziane [17] proved that as a global regularity criterion

⁵ See e.g. [32], where even the author in the abstract claims that his result is obvious.

⁶ Generally speaking, it is an interesting question whether it is possible to transform a given local regularity criterion to a global one and vice versa.

⁷ This can be also formally expressed as $v_3 \in L^t(0, T, (L^s(\mathbb{R}^3))), \quad \frac{2}{t} + \frac{3}{s} = 0$.

can be taken also the condition

$$v_3 \in L^t(0, T, (L^s(\mathbb{R}^3))), \quad \frac{2}{t} + \frac{3}{s} \leq \frac{5}{8}, \quad s > \frac{24}{5}, \quad (12)$$

or

$$\nabla v_3 \in L^t(0, T, (L^s(\mathbb{R}^3))), \quad \frac{2}{t} + \frac{3}{s} \leq \frac{11}{6}, \quad s \in \left[\frac{54}{23}, \frac{18}{5} \right]. \quad (13)$$

Note that in contrary to the previous works, in this case, the second criterion is not a direct consequence of the first one for any s .

A new approach to the problem was due to Cao and Titi [4], who by usage of the multiplicative Gagliardo–Nirenberg inequality proved regularity assuming only

$$v_3 \in L^t(0, T, (L^s(\mathbb{R}^3))), \quad \frac{2}{t} + \frac{3}{s} \leq \frac{2}{3} + \frac{2}{3s}, \quad s > \frac{7}{2}. \quad (14)$$

Let us note, that the authors proved the result for periodic boundary conditions, which can be however directly modified to a global regularity criterion; and further that the result is better than (12) (assuming less regularity), although it does not correspond to the natural scaling of the Navier–Stokes equations.

Using a combination of methods from [18] and [4], Zhou and Pokorný [38] showed the regularity even for

$$v_3 \in L^t(0, T, (L^s(\mathbb{R}^3))), \quad \frac{2}{t} + \frac{3}{s} \leq \frac{3}{4} + \frac{1}{2s}, \quad s < \frac{10}{3},^8 \quad (15)$$

and for

$$\nabla v_3 \in L^t(0, T, (L^s(\mathbb{R}^3))), \quad \frac{2}{t} + \frac{3}{s} \leq \begin{cases} \frac{19}{12} + \frac{1}{2s} & s \in \left(\frac{30}{19}, 3 \right) \\ \frac{3}{2} + \frac{3}{4s} & s \in (3, \infty); \end{cases} \quad (16)$$

and then by a slightly different technique, see [37], reobtain (15), and enlarge the regularity class concerning the gradient of one velocity component upto

$$\nabla v_3 \in L^t(0, T, (L^s(\mathbb{R}^3))), \quad \frac{2}{t} + \frac{3}{s} \leq \begin{cases} \frac{53}{18} - \frac{2}{s}, & s \in \left(\frac{90}{53}, \frac{54}{29} \right), \\ \frac{61}{24} - \frac{5}{4s}, & s \in \left[\frac{54}{29}, 2 \right), \\ \frac{23}{12}, & s \in [2, 3], \\ \frac{7}{4} + \frac{1}{2s}, & s \in \left(3, \frac{10}{3} \right], \\ \frac{3}{2} + \frac{4}{3s}, & s \in \left(\frac{10}{3}, \infty \right). \end{cases} \quad (17)$$

Note that except for $s \in [2, 3]$ the conditions do not correspond to the natural scaling of the Navier–Stokes equations.

⁸ Recently, Jia nad Zhou [16] proved also the limit case $s = \frac{10}{3}$.

Recently, Skalák [31] revisited the methods used in [37] and [38], and got the regularity assuming

$$\nabla v_3 \in L^t(0, T, (L^s(\mathbb{R}^3))), \quad \frac{2}{t} + \frac{3}{s} \leq \begin{cases} \frac{19}{10}, & s \in [\frac{30}{19}, \frac{10}{3}], \\ \frac{7}{4} + \frac{1}{2s}, & s \in (\frac{10}{3}, \infty]. \end{cases} \quad (18)$$

This is better than (17) for $s \in (\frac{30}{19}, \frac{150}{77}] \cup (\frac{10}{3}, \infty]$. Another modification of (17) is due to Jia and Jiang, see [15], where an anisotropic regularity criterion involving the derivatives of one velocity component was presented.

Very recently, Chemin and Zhang [7] following completely different idea with usage of anisotropic Littlewood-Paley theory, came to the following regularity criterion in homogeneous Sobolev space (σ denotes the order of differentiability) rather than Lebesgue space

$$v_3 \in L^t(0, T, (H^\sigma(\mathbb{R}^3))), \quad \sigma = \frac{1}{2} + \frac{2}{t}, \quad t \in (4, 6). \quad (19)$$

Let us emphasize that this norm is scaling invariant, and although there is a restriction on range of σ ⁹, it is in a certain sense on the same critical scale as (2) and (4). Actually, the limit case $t = 4$ would be equivalent to $\nabla v_3 \in L^4(0, T, (L^2(\mathbb{R}^3)))$.

In above mentioned article by Penel and Pokorný [25] there appeared among others also the very first regularity criterion concerning only one component of the gradient of one velocity component, more precisely they showed regularity of solutions satisfying

$$\partial_3 v_3 \in L^\infty(0, T, (L^\infty(\mathbb{R}^3))). \quad (20)$$

Later on, this result was markedly improved using the multiplicative Gagliardo–Nirenberg inequality independently by Zhou and Pokorný [38]

$$\partial_3 v_3 \in L^t(0, T, (L^s(\mathbb{R}^3))), \quad \frac{2}{t} + \frac{3}{s} < \frac{4}{5}, \quad s > \frac{15}{4}, \quad (21)$$

and by Cao and Titi [5], who assumed

$$\partial_3 v_3 \in L^t(0, T, (L^s(\mathbb{R}^3))), \quad \frac{2}{t} + \frac{3}{s} \leq \frac{3}{4} + \frac{3}{2s}, \quad s > 2, \quad (22)$$

in the latter article there also appeared the following condition imposing the nondiagonal components of the velocity gradient

$$\partial_j v_3 \in L^t(0, T, (L^s(\mathbb{R}^3))), \quad j \neq 3, \quad \frac{2}{t} + \frac{3}{s} \leq \frac{1}{2} + \frac{3}{2s}, \quad s > 3. \quad (23)$$

We can deduce that for $\partial_3 v_3$ and $s > 30$, the result (21) is better than (22); the results of Cao and Titi were further slightly improved by Fang and Qian [10].

⁹ Lately, the authors announced that they are able to show the result for all $\sigma \in (4, \infty)$.

Zhang [34] recently reobtain condition (22), using the method from [38], as a special case of the following more general criterion

$$\begin{aligned}
v_3 &\in L^{t_1}(0, T, (L^{s_1}(\mathbb{R}^3))), & \partial_3 v_3 &\in L^{t_2}(0, T, (L^{s_2}(\mathbb{R}^3))) \\
\frac{2}{t_1} + \frac{3}{s_1} &= \alpha, & \frac{2}{t_2} + \frac{3}{s_2} &= \beta, & p_1 < \infty \text{ or } p_2 < \infty & \quad (24) \\
\left(1 - \frac{1}{s_2}\right) s_1 &= \frac{1/t_2 + 3/8}{3/8 - 1/t_1} = \frac{9/4 - \beta}{\alpha - 3/4} > 1.
\end{aligned}$$

Setting $t_1 = \infty$, $s_1 = 2$, $\alpha = \frac{3}{2}$, $\beta = \frac{3}{4} + \frac{3}{2s_2}$ we immediately get the result from (22). This last criterion was further generalized by Fang and Qian [11] to anisotropic Lebesgue spaces concerning different integrability in different directions.

2.2 Possible generalizations

Introducing the regularity criteria concerning one velocity component, say v_3 , there appeared a natural question, to what extent the choice of the component $v_3 = e^3 \cdot \mathbf{v}(t, \mathbf{x})$ is crucial in the considerations. It is clear that all the criteria can be generalized to the corresponding condition imposed on the projection to constant nonzero vector field \mathbf{b} , id est $\mathbf{b} \cdot \mathbf{v}(t, \mathbf{x})$. However, assuming the reference field \mathbf{b} varying over space and time, the situation become more complex; the smoothness of \mathbf{b} have to be taken into account as well as the technique of the original criterion.

This problem was first touched by Beirão da Veiga in the article [3], where the conditions where imposed on the projection of the velocity into the vector field changing in time.

In the article [1], the authors showed that the criteria (9) and (11) from [26, 35, 36] for one velocity component can be generalized in such a way that the original condition can be replaced by a corresponding criteria concerning $\mathbf{b}(t, \mathbf{x}) \cdot \mathbf{v}(t, \mathbf{x})$, with vector field $\mathbf{b}(t, \mathbf{x}) : (0, T) \times \mathbb{R}^3 \mapsto \mathbb{R}^3$ sufficiently regular, but changing in time as well as in space. There remains an open problem, whether this can be done also for all other criteria and it is probably closely connected with possibility of transforming the criteria into a local version.

References

1. Š. AXMANN, M. POKORNÝ, *A generalization of some regularity criteria to the Navier–Stokes equations involving one velocity component*. accepted for publication in Recent Developments of Mathematical Fluid Mechanics Series: Advances in Mathematical Fluid Mechanics (edited by Giovanni P. Galdi, John G. Heywood and Rolf Rannacher), Birkhäuser Verlag, 2014.

2. H.-O. BAE, H. J. CHOE. *A regularity criterion for the Navier–Stokes equations*, Communications in Partial Differential Equations, 2007, Vol. 32, Issue 7, pp. 1173–1187.
3. H. BEIRÃO DA VEIGA, *On the smoothness of a Class of Weak solutions to the Navier–Stokes equations*, Journal of Mathematical Fluid Mechanics, 2000, Vol. 2, No. 4, pp. 315–323.
4. CH. CAO, E. S. TITI. *Regularity criteria for the three-dimensional Navier–Stokes equations*, Indiana University Mathematics Journal, 2008, Vol. 57, No. 6, pp. 2643–2660.
5. CH. CAO, E. S. TITI. *Global regularity criterion for the 3D Navier–Stokes equations involving one entry of the velocity gradient tensor*, Archive of Rational Mechanics and Analysis, 2011, Vol. 202, Issue 3, pp. 919–932.
6. D. CHAE, H.-J. CHOE. *Regularity of solutions to the Navier–Stokes equation*, Electronic Journal of Differential Equations, 1999, Vol. 1999, No. 5, pp. 1–7.
7. J.-Y. CHEMIN, P. ZHANG, *On the critical one component regularity for 3-D Navier–Stokes system*, preprint arXiv:1310.6442
8. B.-Q. DONG, Z.-M. CHEN. *Regularity criterion of weak solutions to the 3D Navier–Stokes equations via two velocity components*, Journal of Mathematical Analysis and Application, 2008, Vol. 338, Issue 1, pp. 1–10.
9. L. ESCAURIAZA, G. A. SEREGIN, V. ŠVERÁK. *$L_{3,\infty}$ -solutions of the Navier–Stokes equations and backward uniqueness*, Russian Mathematical Surveys, 2003, Vol. 58, No. 2, pp. 211–250.
10. D. FANG, C. QIAN. *The regularity criterion for 3D Navier–Stokes equations involving one velocity gradient component*, Nonlinear analysis: TMA, 2013, Vol. 78, pp. 86–103.
11. D. FANG, C. QIAN, *Several almost critical regularity conditions based on one component of the solutions for 3D N-S equations*, preprint arXiv:1312.7378
12. E. B. FABES, G. A. JONES, N. M. RIVIÈRE. *The initial value problem for the Navier–Stokes equations with data in L^p* , Archive for Rational Mechanics and Analysis, 1972, Vol. 45, No. 3, pp. 186–212.
13. CH. FEFFERMAN, *Existence and smoothness of the Navier–Stokes equation*[online]. [cit. 2012-04-10]. <<http://www.claymath.org/millennium/Navier-Stokes~Equations/navierstokes.pdf>>.
14. C. HE, *Regularity for solutions to the Navier–Stokes equations with one velocity component regular*, Electronic Journal of Differential Equations, 2002, Vol. 2002, No. 29, pp. 1–13, ISSN: 1072-6691.
15. X. JIA, Z. JIANG. *An anisotropic regularity criterion for the 3D Navier–Stokes equations*, Commun. Pure Appl. Anal., 2013, Vol. 12, No. 3, pp. 1299–1306.
16. X. JIA, Y. ZHOU. *Remarks on regularity criteria for the Navier–Stokes equations via one velocity component*, Nonlinear Analysis: Real World Applications, 2014, Vol. 15, pp. 239–245.
17. I. KUKAVICA, M. ZIANE. *One component regularity for the Navier–Stokes equations*, Nonlinearity, 2006, Vol. 19, No. 2, pp. 453–469.
18. I. KUKAVICA, M. ZIANE. *Navier–Stokes equations with regularity in one direction*, Journal of Mathematical Physics, 2007, Vol. 48, No. 6, 065203.
19. O. A. LADYŽENSKAJA, *The mathematical theory of viscous incompressible flow*. 2nd edition. New York-London-Paris: Gordon and Breach Science Publishers, 1969. 184 pp.
20. J. LERAY, *Sur le mouvement d’un liquide visqueux emplissant l’espace*, Acta Mathematica, 1934, Vol. 63, No. 1, pp. 193–248.

21. P.-L. LIONS, *Mathematical topics in fluid mechanics, Volume I: Incompressible models*. Oxford: Clarendon Press, 1996. 252 s. ISBN: 0-19-851487-5.
22. J. NEUSTUPA, A. NOVOTNÝ, P. PENEL, *An interior regularity of weak solution to the Navier–Stokes equations in dependence on one component of velocity*. *Quaderni in matematica*, 2002, vol. 10 Topics in mathematical fluid mechanics, pp. 163–183.
23. J. NEUSTUPA, P. PENEL, Regularity of a suitable weak solution to the Navier–Stokes equations as a consequence of regularity of one velocity component. In *Applied Nonlinear Analysis*, edited by Sequeira et al., New York: Kluwer Academic/Plenum Publishers, 1999. pp. 391–402.
24. T. OHYAMA, *Interior regularity of weak solutions of the time-dependent Navier–Stokes equation*, *Proceedings of the Japan Academy*, 1960, Vol. 36, No. 5, pp. 273–277.
25. P. PENEL, M. POKORNÝ. *Some new regularity criteria for the Navier–Stokes equations containing gradient of the velocity*, *Applications of Mathematics*, 2004, Vol. 49, No. 5, pp. 483–493.
26. M. POKORNÝ, *On the result of He concerning the smoothness of solutions to the Navier–Stokes equations*, *Electronic Journal of Differential Equations*, 2003, Vol. 2003, No. 11, pp. 1–8.
27. G. PRODI, Un teorema di unicità per le equazioni di Navier–Stokes. *Annali di Matematica Pura ed Applicata*, 1959, ser. IV, Vol. 48, No. 1, pp. 173–182.
28. G. SEREGIN, V. ŠVERÁK, *The Navier–Stokes equations and backward uniqueness, II*. In Honor of Professor O. A. Ladyzhenskaya (M. Sh. Birman et al., eds.), New York: Kluwer/Plenum, 2002, pp. 359–370.
29. J. SERRIN, *On the interior regularity of weak solutions of the Navier–Stokes equations*, *Archive for Rational Mechanics and Analysis*, 1962, Vol. 9, No. 1, pp. 187–195.
30. Z. SKALÁK, P. KUČERA. *A note on coupling of velocity components in the Navier–Stokes equations*, *Zeitschrift für Angewandte Mathematik und Mechanik*, 2004, Vol. 84, No. 2, pp. 124–127.
31. Z. SKALÁK, *On the regularity of the solutions to the Navier–Stokes equations via the gradient of one velocity component.*, *Nonlinear Analysis: TMA*, 2014, Vol. 104, pp. 84–89.
32. X. YIN, *A Note on the Regularity Criterion of Weak Solutions of Navier–Stokes Equations in Lorentz Space*, *Abstract and Applied Analysis*, 2012, Vol. 2012, 9 pages.
33. X. ZHANG, *A regularity criterion for the solutions of 3D Navier–Stokes equations*, *Journal of Mathematical Analysis and Applications*, 2008, Vol. 364, Issue 1, pp. 336–339.
34. Z. ZHANG, *A Serrin-type regularity criterion for the Navier–Stokes equations via velocity component*, *Communications on Pure and Applied Analysis*, 2013, Vol. 12, No. 1, pp. 117–124.
35. Y. ZHOU, *A new regularity criterion for the Navier–Stokes equations in terms of the gradient of one velocity component*, *Methods and applications of analysis*, 2002, Vol. 9, No. 4, pp. 563–578.
36. Y. ZHOU, *A new regularity criterion for weak solutions to the Navier–Stokes equations*, *Journal de Mathématiques Pures et Appliquées*, 2005, Vol. 84, No. 11, pp. 1496–1514.
37. Y. ZHOU, M. POKORNÝ. *On a regularity criterion for the Navier–Stokes equations involving gradient of one velocity component*, *Journal of Mathematical Physics*, 2009, Vol. 50, No. 12, 123514.

38. Y. ZHOU, M. POKORNÝ. *On the regularity criterion of the Navier–Stokes equations via one velocity component*, *Nonlinearity*, 2010, Vol. 23, No. 5, pp. 1097–1107.

Acknowledgments: The work was supported by the grant SVV-2014-260106.

Spiders on the vineyard with the ballooning effect

Martin Biák and Drahoslava Janovská

Institute of Chemical Technology, Prague

Keywords: population models, predator-prey models, ballooning, Filippov systems, sliding bifurcations

Abstract The population model of spiders hunting insect on the vineyard can be described as a set of four ordinary differential equations. This type of the model is known as a predator-prey model. We show how to integrate a human intervention into this model. We formulate Filippov system that includes both cases - with and without the intervention. Then we analyze this model using the piecewise-smooth dynamical system theory. We are looking for so-called local sliding bifurcations. All simulations are performed in Matlab. The solution diagram is computed in Matlab, too.

1 Model equations

The insect is considered to be pest in the vineyard but it is to be harmless in the surrounding woods. Insect population is under control of natural predators, spiders. The predator-prey model of spiders and insect on the vineyard is described as the following set of ordinary differential equations:

$$\dot{w} = \left(b \left(1 - \frac{w}{W} \right) - \ell s_w \right) w, \quad (1)$$

$$\dot{v} = \left(a \left(1 - \frac{v}{V} \right) - k s_v \right) v, \quad (2)$$

$$\dot{s}_w = \left(-c + \tilde{\ell} \left(1 - \alpha \frac{V}{V+W} \right) w \right) s_w + \alpha \tilde{k} \frac{W}{V+W} s_v v, \quad (3)$$

$$\dot{s}_v = \left(-e + \tilde{k} \left(1 - \alpha \frac{W}{V+W} \right) v \right) s_v + \alpha \tilde{\ell} \frac{V}{V+W} s_w w, \quad (4)$$

where $v(t)$ is the insect population on the vineyard, $w(t)$ is the insect population outside the vineyard, $s_v(t)$ is the spiders population on the vineyard, $s_w(t)$ is the population of the spiders outside the vineyard. For more information about

this model, see [1]. If man intervenes into the ecosystem by spraying to prevent an overgrowth of insect in the vineyard, equations (1)–(4) pass to the system

$$\dot{w} = \left(b \left(1 - \frac{w}{W} \right) - \ell s_w \right) w - h(1-q)w, \quad (5)$$

$$\dot{v} = \left(a \left(1 - \frac{v}{V} \right) - k s_v \right) v - hqv, \quad (6)$$

$$\dot{s}_w = \left(-c + \tilde{\ell} \left(1 - \alpha \frac{V}{V+W} \right) w \right) s_w + \alpha \tilde{k} \frac{W}{V+W} s_v v - hK(1-q)s_w, \quad (7)$$

$$\dot{s}_v = \left(-e + \tilde{k} \left(1 - \alpha \frac{W}{V+W} \right) v \right) s_v + \alpha \tilde{\ell} \frac{V}{V+W} s_w w - hKqs_v, \quad (8)$$

where an extra term in each equation represents the mortality caused by spraying. All parameters in (1)–(4) and (5)–(8) are positive real numbers.

The question is how to introduce the model that includes both cases (with and without spraying) and that keeps the insect population on the vineyard below a given limit. We will show that such a model is a type of Filippov system and it can be treated using the techniques stated e.g. in [2].

We put $\mathbf{x} = (w, v, s_w, s_v)^T$. Because only the positive values of $w(t)$, $v(t)$, $s_w(t)$, $s_v(t)$ have a physical meaning, our state space is

$$\mathcal{D} = \{\mathbf{x} \in \mathbb{R}^4 : x_j \geq 0, \quad j = 1, \dots, 4\}.$$

Let us have a scalar function $\varphi : \mathcal{D} \rightarrow \mathbb{R}$. The function φ divides the region \mathcal{D} into:

$$\begin{aligned} S_1 &= \{\mathbf{x} \in \mathcal{D} : \varphi(\mathbf{x}) > 0\}, \\ S_2 &= \{\mathbf{x} \in \mathcal{D} : \varphi(\mathbf{x}) < 0\}, \\ \Sigma &= \{\mathbf{x} \in \mathcal{D} : \varphi(\mathbf{x}) = 0\}. \end{aligned}$$

Our aim is to keep the population $v(t)$ of the insect on the vineyard below the given value $v_m \in \mathbb{R}$, $v_m > 0$. Therefore, our function $\varphi(\mathbf{x})$ will be

$$\varphi(w, v, s_w, s_v) = v_m - v. \quad (9)$$

We define the following Filippov system \mathcal{F} on $\mathcal{D} = S_1 \cup S_2 \cup \Sigma$,

$$\mathcal{F} : \dot{\mathbf{x}} = \begin{cases} \mathbf{g}^{(1)}(\mathbf{x}), & \mathbf{x} \in S_1, \\ \mathbf{g}^{(0)}(\mathbf{x}), & \mathbf{x} \in \Sigma, \\ \mathbf{g}^{(2)}(\mathbf{x}), & \mathbf{x} \in S_2, \end{cases} \quad (10)$$

where $\dot{\mathbf{x}} = (\dot{w}, \dot{v}, \dot{s}_w, \dot{s}_v)^T$, and where the vector fields $\mathbf{g}^{(i)} : \mathbb{R}^4 \rightarrow \mathbb{R}^4$, $i = 1, 2$, are

$$\mathbf{g}^{(1)} = \begin{bmatrix} \left(b \left(1 - \frac{w}{W}\right) - \ell s_w\right) w, \\ \left(a \left(1 - \frac{v}{V}\right) - k s_v\right) v, \\ \left(-c + \tilde{\ell} \left(1 - \alpha \frac{V}{V+W}\right) w\right) s_w + \alpha \tilde{k} \frac{W}{V+W} s_v v, \\ \left(-e + \tilde{k} \left(1 - \alpha \frac{W}{V+W}\right) v\right) s_v + \alpha \tilde{\ell} \frac{V}{V+W} s_w w. \end{bmatrix}$$

$$\mathbf{g}^{(2)} = \begin{bmatrix} \left(b \left(1 - \frac{w}{W}\right) - \ell s_w\right) w - h(1-q)w, \\ \left(a \left(1 - \frac{v}{V}\right) - k s_v\right) v - h q v, \\ \left(-c + \tilde{\ell} \left(1 - \alpha \frac{V}{V+W}\right) w\right) s_w + \alpha \tilde{k} \frac{W}{V+W} s_v v - h K(1-q) s_w, \\ \left(-e + \tilde{k} \left(1 - \alpha \frac{W}{V+W}\right) v\right) s_v + \alpha \tilde{\ell} \frac{V}{V+W} s_w w - h K q s_v. \end{bmatrix}.$$

If $\varphi(w, v, s_w, s_v) > 0$, no spraying occurs and the vector field $\mathbf{g}^{(1)}$ is in effect. If the insect population $v(t)$ on the vineyard exceeds the given value v_m , i.e. if $\varphi(w, v, s_w, s_v) < 0$, the spraying begins and the vector field $\mathbf{g}^{(2)}$ takes place. The spraying goes on until the value of $v(t)$ decreases below v_m , when $\mathbf{g}^{(1)}$ applies again.

Before we define the vector field $\mathbf{g}^{(0)}$, which determines the behavior of system (10) on the boundary Σ , it is necessary to distinguish two types of sets on Σ , see [2]. We define a scalar function $\sigma : \Sigma \rightarrow \mathbb{R}$,

$$\sigma(\mathbf{x}) = \langle \nabla \varphi, \mathbf{g}^{(1)} \rangle \langle \nabla \varphi, \mathbf{g}^{(2)} \rangle,$$

and we obtain two sets on Σ :

- the crossing set $\Sigma_c \subseteq \Sigma = \{\mathbf{x} \in \Sigma : \varphi(\mathbf{x}) = 0 \wedge \sigma(\mathbf{x}) > 0\}$,
- the sliding set $\Sigma_s \subseteq \Sigma = \{\mathbf{x} \in \Sigma : \varphi(\mathbf{x}) = 0 \wedge \sigma(\mathbf{x}) \leq 0\}$.

In our case, the scalar function $\sigma(w, v, s_w, s_v)$ reads

$$\begin{aligned} \sigma(w, v, s_w, s_v) &= \langle \nabla \varphi, \mathbf{g}^{(1)} \rangle \langle \nabla \varphi, \mathbf{g}^{(2)} \rangle, \\ \langle \nabla \varphi, \mathbf{g}^{(1)} \rangle &= - \left(a \left(1 - \frac{v_m}{V} \right) - k s_v \right) v_m, \\ \langle \nabla \varphi, \mathbf{g}^{(2)} \rangle &= - \left(a \left(1 - \frac{v_m}{V} \right) - k s_v - h q \right) v_m, \end{aligned}$$

where $\nabla \varphi(w, v, s_w, s_v) = (0, -1, 0, 0)$.

If $\mathbf{x}_0 \in \Sigma_s$, trajectory $\gamma_{\mathbf{x}_0}$ slides along the sliding set Σ_s . If $\mathbf{x}_0 \in \Sigma_c$, trajectory $\gamma_{\mathbf{x}_0}$ leaves the boundary and continues to S_1 or S_2 , depending on the vectors $\mathbf{g}^{(1)}(\mathbf{x}_0)$ and $\mathbf{g}^{(2)}(\mathbf{x}_0)$.

On Σ_c , we put

$$\mathbf{g}^{(0)} = \frac{1}{2} \left(\mathbf{g}^{(1)} + \mathbf{g}^{(2)} \right).$$

For $\mathbf{x} \in \Sigma_s$, we apply the Filippov convex method and define a smooth vector field

$$\mathbf{g}^{(0)} = (1 - \lambda) \mathbf{g}^{(1)} + \lambda \mathbf{g}^{(2)}, \quad \lambda = \frac{\langle \nabla \varphi, \mathbf{g}^{(1)} \rangle}{\langle \nabla \varphi, \mathbf{g}^{(1)} - \mathbf{g}^{(2)} \rangle}, \quad (11)$$

where $0 \leq \lambda \leq 1$.

Such points from Σ_s , in which $\sigma(w, v, s_w, s_v) = 0$ are called tangent points. We observe two sets of tangent points T_1 and T_2 on the boundary Σ :

$$\begin{aligned} T_1 &= \{ (w, v, s_w, s_v) : w \geq 0 \wedge v = v_m \wedge s_w \geq 0 \wedge s_v = s_{v_{T_1}} \}, \\ T_2 &= \{ (w, v, s_w, s_v) : w \geq 0 \wedge v = v_m \wedge s_w \geq 0 \wedge s_v = s_{v_{T_2}} \}, \end{aligned}$$

where

$$s_{v_{T_1}} = \frac{1}{k} a \left(1 - \frac{v_m}{V} \right), \quad s_{v_{T_2}} = \frac{1}{k} \left(a \left(1 - \frac{v_m}{V} \right) - h q \right). \quad (12)$$

Let us assume that $s_{v_{T_1}} \geq 0$ and $s_{v_{T_2}} \geq 0$. Because $s_{v_{T_1}} > s_{v_{T_2}}$, the sets T_1 and T_2 are planes that delimit the sliding set

$$\Sigma_s \subset \Sigma = \{ (w, v, s_w, s_v) : w \geq 0 \wedge v = v_m \wedge s_w \geq 0 \wedge 0 \leq s_{v_{T_2}} \leq s_v \leq s_{v_{T_1}} \}.$$

The sliding set Σ_s has a shape of a semi-infinite prism with the non-zero height $\frac{1}{k} h q$.

If we put $\mathbf{g}^{(0)}(\mathbf{P}) = 0$ in the convex combination (11), the points $\mathbf{P} \in \Sigma_s$ are called pseudo-equilibria of the Filippov system. They can be computed numerically. We are looking for a so-called inner pseudo-equilibrium, i.e. a point that have all its coordinates positive.

2 Simulations

In Table 1, the parameters used in all simulations are listed. In Figure 1, the structure of the sliding segment Σ_s with only nine trajectories is depicted for $v_m = 0.4$. In the next Figure 2, more of the trajectories are added to show

the dynamical behavior of the system \mathcal{F} on the sliding segment Σ_s . The inner pseudo-equilibrium can be seen on the sliding set Σ_s , in particular it can be classified as stable pseudo-focus-node.

In Figure 3, the integral curves for $v_m = 0.4$ ($w(0) = 0.0001$, $v(0) = 1.01498$, $s_w(0) = 0.00872759$, $s_v(0) = 0.75024$) are depicted.

We have performed many simulations to determine the dependence of the solution on the given parameter, namely the limit value of the insect population on the vineyard v_m . We have found that a local sliding bifurcation occurs for the value $v_m = 0.485$. The bifurcation is caused by the collision of a standard equilibrium of the system \mathcal{F} with the boundary Σ . The bifurcation point is called the boundary equilibrium X and can be seen in the solution diagram in Figure 4. All phase portraits were obtained using the event driven method in Matlab. More information about the event driven method can be found in [3]. The solution diagram was computed in Matlab. We used the same equations that were used in SlideCont, see Table I in [4].

Table 1. The parameters used for the simulation of the system \mathcal{F} .

Parameter	Value	Meaning
a	1.5	specific growth rate of the prey in the vineyards
b	1.0	specific growth rate of the prey in the woods
c	0.1	specific mortality rate of predators in the woods
e	0.1	specific mortality rate of predators in the vineyards
k	2	specific predation rate of predators in the vineyards
ℓ	2	specific predation rate of predators in the woods
\tilde{k}	0.1	specific reproduction rate of predators per 1 prey eaten in the vineyards
$\tilde{\ell}$	0.1	specific reproduction rate of predators per 1 prey eaten in the woods
α	0.5	fraction of newborns carried by the wind into the air (so called ballooning effect)
V	1000	carrying capacity of the vineyard insect, $V \gg W$
W	10	carrying capacity of the wood insect
h	0.6	effectiveness of the insecticide against the parasites
q	0.9	portion of insecticide sprayed directly on the vineyards
$1 - q$	0.1	portion which may accidentally be dispersed in the woods
K	0.01	smaller effect the insecticide should have on the spiders,
v_m	0.4	limit of the insect population on the vineyard

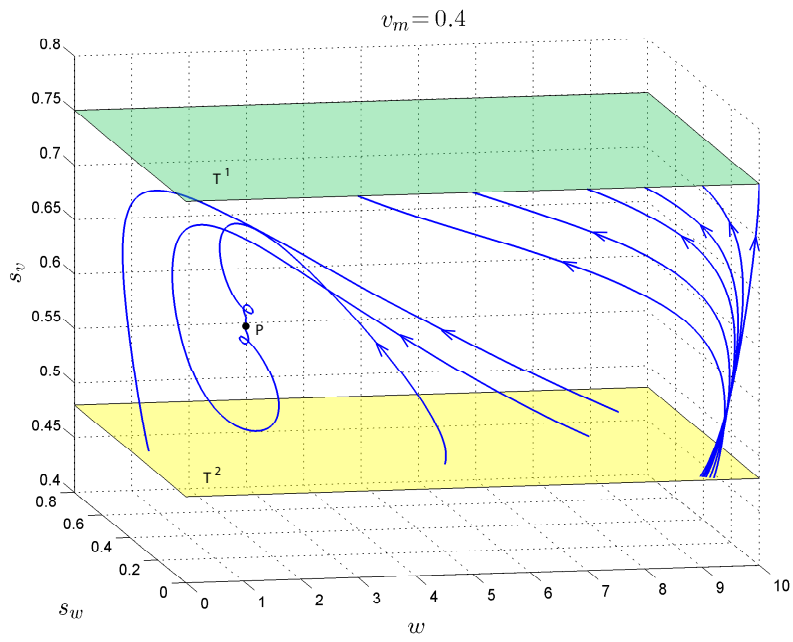


Figure 1. Sliding set Σ_s for $v_m = 0.4$ with only few trajectories.

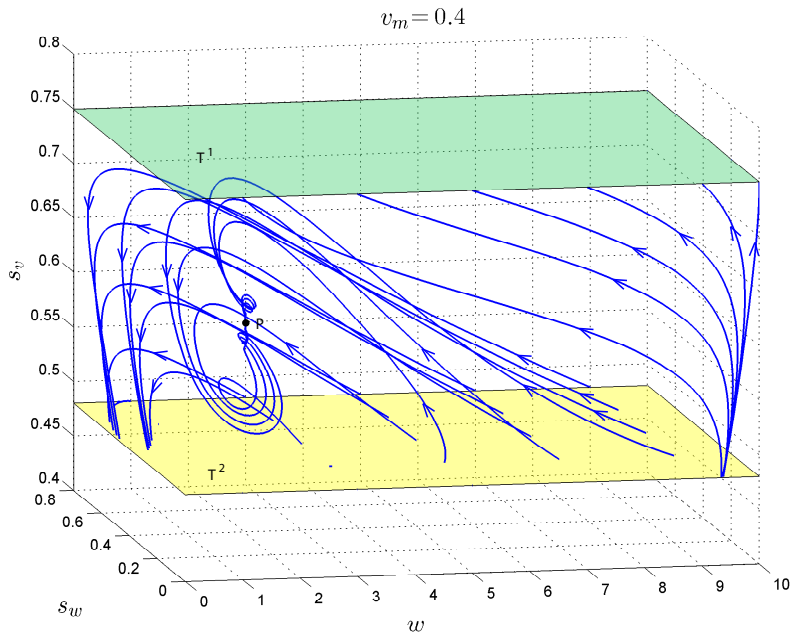


Figure 2. Sliding set Σ_s for $v_m = 0.4$ with more trajectories.

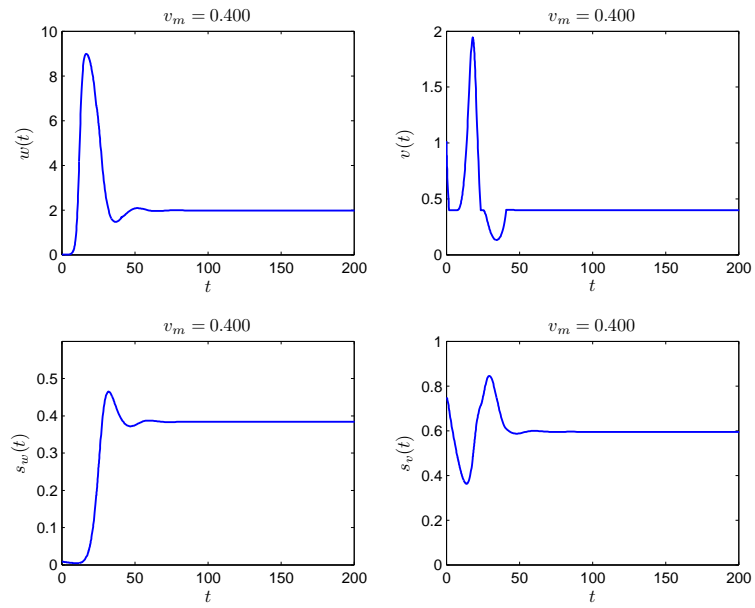


Figure 3. Integral curves for $v_m = 0.4$.

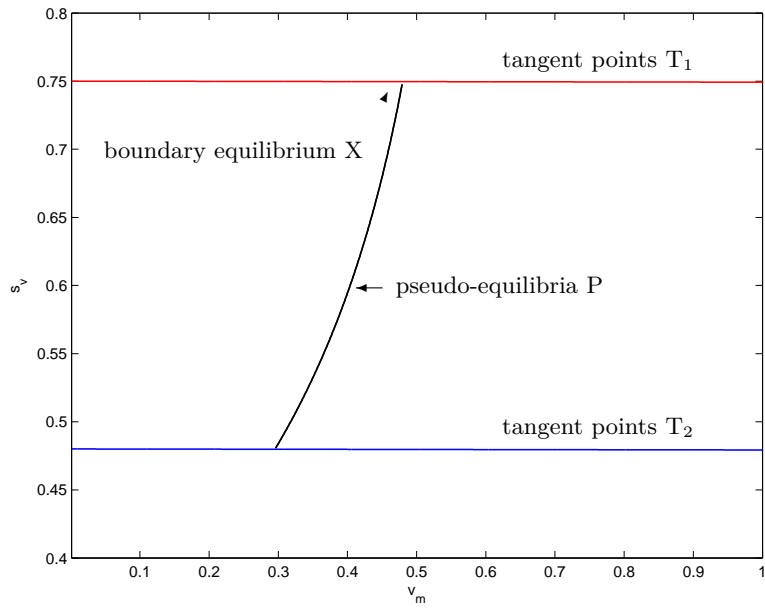


Figure 4. Solution diagram.

3 Conclusions

We have studied the structure of the sliding segment Σ_s and we have performed many simulations to determine the dependence of the solution on the given parameter (the limit value of the insect population v_m on the vineyard). We discovered the local sliding bifurcation in the population model of the spiders on the vineyard with the so-called ballooning effect. This bifurcation is caused by a collision of the standard equilibrium of the system \mathcal{F} with the boundary Σ . In the future, we plan to continue in the computations and simulations for detail analysis of the system.

References

1. E. VENTURINO, M. ISAIA, F. BONA, E. ISSOGLIO, V. TRIOLO, G. BADINO, *Modelling the spiders ballooning effect on the vineyard ecology*, Mathematical Modelling of Natural Phenomena, Vol.1. (2006), pp.133-155.
2. M. DI BERNARDO, C.J. BUDD, A.R. CHAMPNEYS, P. KOWALCZYK, *Piecewise-smooth Dynamical Systems: Theory and Applications*, Springer-Verlag, London (2008).
3. P.T. PIROINEN, YU.A. KUZNETSOV:, *An event-driven method to simulate Filippov systems with accurate computing of sliding motions*, ACM Trans. Math. Software, Vol.34, No.13. (2008), pp.1-24.
4. F. DERCOLE, YU.A. KUZNETSOV, *SlideCont: An AUTO97 driver for sliding bifurcation analysis*, ACM Trans. Math. Software, Vol.31. (2005), pp.95-119.

Maximization of schedule reliability under uncertain job processing times

Martin Branda¹

Department of Probability and Mathematical Statistics,
Faculty of Mathematics and Physics, Charles University in Prague¹

Keywords: Interval scheduling, stochastic delays, stochastic integer programming, robust coloring formulation

Abstract Interval scheduling problem aims at assigning jobs to machines where the job starting and finishing times are known. If random delays influence the job processing times, the objective can be to find a schedule which remains feasible with the highest possible probability. In this paper, we propose the formulations based on stochastic integer programming and robust coloring problems. The second one leads to a large scale binary-linear programming problem. We report first numerical results based on simulated instances.

1 Introduction

We deal with the problem of jobs scheduling on a set of available machines. We consider jobs with given starting and finishing times leading to a class of scheduling problems called interval scheduling, fixed interval scheduling or fixed jobs scheduling, cf. Kolen et al. [3], and Kovalyov et al. [4]. The goal can be to find a feasible jobs assignment to machines, leading to an operational problem, or to minimize the number of machines necessary to process all jobs, leading to a tactical problem, see Kroon et al [5, 6]. Such problems have many applications and arise in various areas such as crew scheduling, vehicle scheduling, telecommunication, scheduling of operating rooms in hospitals, and workers assignment to projects.

We focus on the operational problem where the number of machines is fixed. However, the finishing times of jobs can be influenced by unpredictable circumstances leading to uncertain (stochastic) delays. Our goal is then to find a “robust” schedule which remains feasible with the highest attainable probability. Such problems were introduced and investigated by Branda et al. [2]. In this paper, we review the mathematical programming formulations based on stochastic integer programming and robust coloring problem. The second one leads to a

large scale deterministic binary linear programming problem, thus it enables to compute the schedule reliability easily than the stochastic programming one.

The paper is organized as follows. In Section 2, we propose the stochastic integer programming formulation of the problem with schedule reliability maximization. A robust coloring formulation is reviewed in Section 3. A simple example is proposed for better understanding. In Section 4, we report first numerical results based on simulated test instances. Section 5 concludes the paper shortly.

2 A stochastic integer programming formulation

In our operational problem, the number of machines is already given and the goal is to find a schedule with the highest reliability, i.e. probability that it remains feasible with respect to the random delays. The planning period is considered in continuous time, i.e. $\mathcal{T} = [0, T]$. Let \mathcal{C} denote the set of machines and \mathcal{J} denotes the set of jobs with known starting times $s_j \in \mathcal{T}$. We consider a random finishing time $f_j(\xi)$ which is a sum of a prescribed finishing time $f_j^0 \in \mathcal{T}$ and a random delay $D_j(\xi)$, i.e.

$$f_j(\xi) = f_j^0 + D_j(\xi).$$

We assume that the distribution of the random delays P is known or well estimated with a support Ξ and a probability mass in zero, i.e. $D_j = 0$ has a positive probability. If the processing of a job j finishes at $f_j(\xi)$, a new job j' with starting time $s_{j'} \geq f_j(\xi)$ can be assigned to the same machine. Necessary machine breaks can be incorporated directly to the finishing times.

Let x_{jc} , $j \in \mathcal{J}$, $c \in \mathcal{C}$ be binary variables which are equal to one if job j is assigned to machine c , and it is equal to zero otherwise. The following random constraints ensure that in each time at most one job is processed by a machine

$$\sum_{j: s_j \leq t < f_j(\xi)} x_{jc} \leq 1, \quad t \in \hat{\mathcal{T}}, c \in \mathcal{C},$$

where $\hat{\mathcal{T}} = \{s_1, \dots, s_{|\mathcal{J}|}\}$ are known starting times. Branda et al. [2] introduced stochastic integer programming formulation where the probability of schedule feasibility with respect to the random delays is maximized:

$$\begin{aligned} \max_x P \left(\xi \in \Xi : \right. & \sum_{j: s_j \leq t < f_j(\xi)} x_{jc} \leq 1, \quad t \in \hat{\mathcal{T}}, c \in \mathcal{C} \left. \right) \\ & \sum_{j: s_j \leq t < f_j^0} x_{jc} \leq 1, \quad c \in \mathcal{C}, t \in \hat{\mathcal{T}}, \\ & \sum_{c \in \mathcal{C}} x_{jc} = 1, \quad j \in \mathcal{J}, \\ & x_{jc} \in \{0, 1\}, \quad c \in \mathcal{C}, j \in \mathcal{J}. \end{aligned} \tag{1}$$

The constraints ensure that there is at most one job assigned to a machine at each time with respect to the prescribed job processing times and a job is assigned to exactly one machine. However, the objective function leads to computation of multivariate integral which can be numerically untractable or can be highly time demanding, thus inappropriate for algorithms, see, e.g., Ruszczyński and Shapiro [7], Schultz [8] for general discussions. We show below that we can avoid this problem, although for a price of additional variables and constraints.

3 A robust coloring formulation

In this section, we propose an extended robust coloring formulation of the problem (1), which was introduced by Branda et al. [2]. The main advantage of the model is that the underlying randomness is transformed into penalty coefficients in the objective function leading to a deterministic integer (binary) problem.

The robust version of the vertex coloring problem was introduced by Yanez and Ramirez [9] and further investigated by Archetti et al. [1], and F. Wang and Xu [10]. The extended robust coloring formulation is also based on the interval graph which can be defined as follows. The set of jobs \mathcal{J} corresponds to vertices and the set of machines \mathcal{C} to colors. The set of undirected edges E contains all pairs of jobs $\{j, j'\}$ which overlap, i.e. $s_j \leq s_{j'} < f_j^0$. The complementary (directed) edge set \bar{E} contains all pairs $\{j, j'\}$ such that delay of job j could influence job j' if it is processed by the same machine, i.e. such that $f_j^0 \leq s_{j'}$. The set \bar{E} can be reduced for example in the case when the support of the random delays is bounded. It always holds $E \cap \bar{E} = \emptyset$.

We assume that the number of available machines (colors) is greater or equal to the chromatic number of the graph (\mathcal{J}, E) , i.e. the coloring of the graph without taking into account the random delays is possible. Under the assumption that the delays are mutually independent, Branda et al. [2] formulated an extended robust coloring problem, which is equivalent to the stochastic program-

ming problem (1):

$$\begin{aligned}
\min_{x,y,z} \quad & \sum_{\{j,j'\} \in \bar{E}} q_{jj'} z_{jj'} \\
& \sum_{c \in \mathcal{C}} x_{jc} = 1, \quad j \in \mathcal{J}, \\
& x_{jc} + x_{j'c} \leq 1, \quad \{j,j'\} \in E, \\
& x_{jc} + x_{j'c} \leq 1 + y_{jj'}, \quad \{j,j'\} \in \bar{E}, \\
y_{jj'} + \quad & \sum_{k: \{j,k\} \in \bar{E} \ \& \ s_k \geq f_j^0} z_{jk} \leq 1, \quad \{j,j'\} \in \bar{E}, \\
& \sum_{k: \{j,k\} \in \bar{E}} y_{jk} \leq |\mathcal{J}| \cdot \sum_{k: \{j,k\} \in \bar{E}} z_{jk}, \quad j \in \mathcal{J}, \\
& x_{jc} \in \{0,1\}, \quad c \in \mathcal{C}, j \in \mathcal{J}.
\end{aligned} \tag{2}$$

The complementary edges from the set \bar{E} are penalized if the connected vertices share the same color (machine). The binary variables x_{jc} have the same function as in the stochastic programming formulation. The variable $y_{jj'}$ is equal to one if the nodes j and j' share the same color. The additional binary variables z_{jk} are used to identify the subsequent job on the machine, thus they are important to set the right penalty. The following choice of the penalty coefficients was suggested by Branda et al. [2]:

$$q_{jj'} = -\ln(P(D_j \leq s_{j'} - f_j^0)).$$

The authors obtained that the objective function is equal to the minus logarithm of the whole schedule reliability, i.e.

$$\sum_{\{j,j'\} \in \bar{E}: z_{jj'}=1} q_{jj'} = -\ln \left(\prod_{\{j,j'\} \in \bar{E}: z_{jj'}=1} P(D_j \leq s_{j'} - f_j^0) \right).$$

Example 1. We present a simple example with five jobs and three machines, see Figures 1, 2, 3, 4. The interval graph shows hard edges connecting jobs, which cannot be processed by one machine, i.e.

$$E = \{\{1,2\}, \{1,3\}, \{2,3\}, \{3,4\}, \{4,5\}\}.$$

The rest of the edges belongs to the complementary set with assigned probabilities that the delay of a job influences the possible successor:

$$p_{14} = 0.2, \quad p_{15} = 0.1, \quad p_{24} = 0.4, \quad p_{25} = 0.2, \quad p_{35} = 0.4.$$

We propose four feasible assignments of jobs to machines and the corresponding coloring. Moreover, we can compute the schedule reliability explicitly. The worst coloring can be found in Figure 1 and the best one in Figure 4.

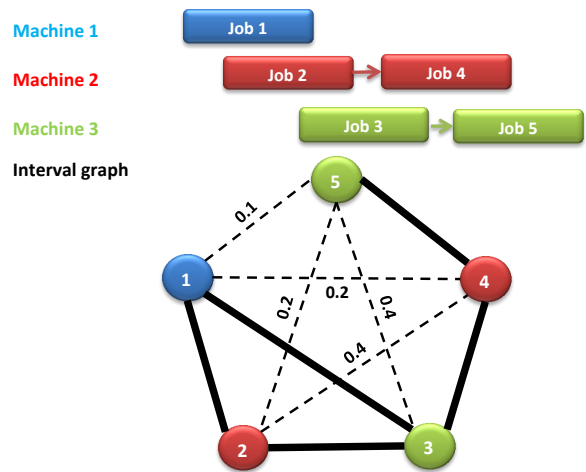


Figure 1. Feasible coloring with reliability $(1-0.4)(1-0.4) = 0.36$

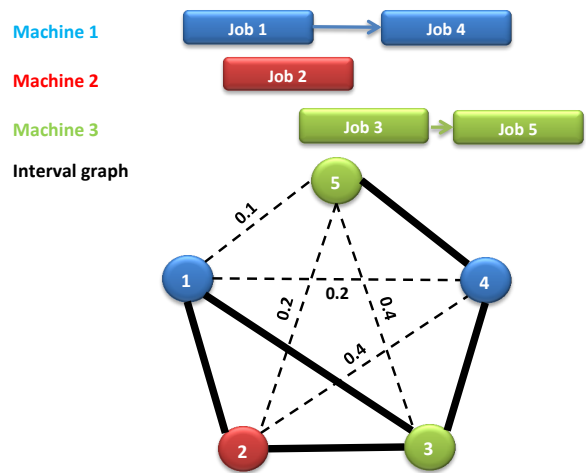


Figure 2. Feasible coloring with reliability $(1-0.2)(1-0.4) = 0.48$

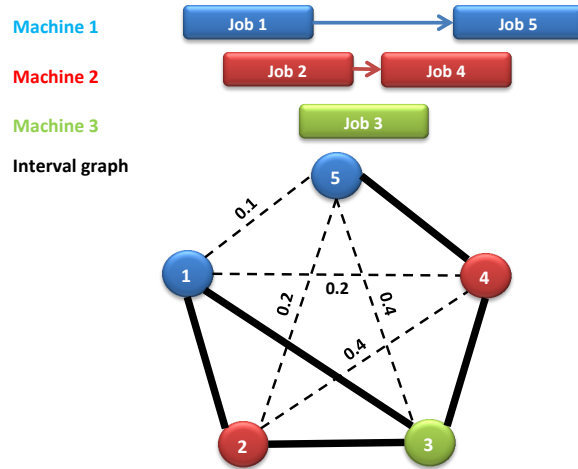


Figure 3. Feasible coloring with reliability $(1-0.1)(1-0.4) = 0.54$

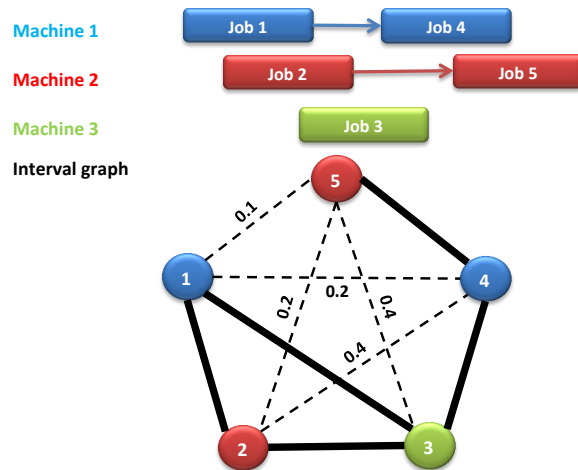


Figure 4. Feasible coloring with reliability $(1-0.2)(1-0.2) = 0.64$

4 A numerical study

In this section, we report first numerical results for the robust coloring formulation. The test instances were simulated using the exponential distribution for job processing times (with parameter $\lambda_1 = 0.2$) and breaks between jobs ($\lambda_2 = 0.05$). The exponential distribution ($\lambda_3 = 0.2$) is also used for the delays, where a probability mass 0.9 is added to zero, i.e. no delay appears with probability 0.9. We consider 30 random jobs assigned to 5 machines initially. We made also computations for first 20 and 25 jobs of these instances.

We solved the problems by the CPLEX 12.1 solver available in the modeling system GAMS 23.2. All computations were performed on PC with Intel Core i7 2.90 GHz CPU, 8 GB RAM and 64-bit Windows 7 Professional operational system. The results can be found in Table 1. The limit for the computations was set to 30 minutes. If the time limit was reached already for 25 jobs, the instance with 30 jobs was not solved. Reliability of the best found feasible solution is reported then. The instances with 30 jobs can be seen as highly demanding.

Test instances	20 jobs	25 jobs	30 jobs
1 (time)	0:47	9:22	LIMIT
1 (rel.)	0.897	0.883	0.883
2	0:14	3:13	7:09
2	0.951	0.947	0.946
3	0:43	1:49	LIMIT
3	0.839	0.837	0.833
4	0:38	1:46	LIMIT
4	0.857	0.837	0.816
5	0:28	10:33	17:24
5	0.914	0.911	0.911
6	0:25	LIMIT	-
6	0.947	0.933	
7	28:51	LIMIT	-
7	0.787	0.750	
8	0:17	11:13	16:35
8	0.949	0.939	0.939
9	0:13	2:40	16:23
9	0.951	0.946	0.946
10	0:7	3:46	LIMIT
10	0.977	0.962	0.958

Table 1. Test instances – computational time (mm:ss) and schedule reliability

5 A short conclusion

We have observed that the robust coloring formulation enables to solve to optimality or at least to find a good feasible solution for most the simulated problems with 30 and less jobs in a reasonable amount of time. However, the real life problems can comprise hundreds of jobs. Thus, future research will be devoted to new formulations as well as solution techniques.

References

1. C. ARCHETTI, N. BIANCHESI AND A. HERTZ, *A branch-and-price algorithm for the robust graph coloring problem*, Discrete Applied Mathematics, Vol. 165 (2014), pp. 49–59
2. M. BRANDA, J. NOVOTNÝ, A. OLSTAD AND P. POPELA, *Fixed interval scheduling under uncertainty – stochastic programming and robust coloring formulations*, Submitted (2014).
3. A.W.J. KOLEN, J.K. LENSTRA, CH.H. PAPADIMITRIOU AND F.C.R. SPIEKSMAN, *Interval scheduling: A survey*, Naval Research Logistics, Vol. 54, No. 5 (2007), pp. 530–543.
4. M.Y. KOVALYOV, C.T. NG AND T.C.E. CHENG, *Fixed interval scheduling: Models, applications, computational complexity and algorithms*, European Journal of Operational Research, Vol. 178 (2007), pp. 331–342.
5. L.G. KROON, M. SALOMON AND L.N. VAN WASSENHOVE, *Exact and approximation algorithms for the operational fixed interval scheduling problem*, European Journal of Operational Research, Vol. 82 (1995), pp. 190–205.
6. L.G. KROON, M. SALOMON AND L.N. VAN WASSENHOVE, *Exact and approximation algorithms for the tactical fixed interval scheduling problem*, Operations Research, Vol. 45, No. 4 (1997), pp. 624–638.
7. A. RUSZCZYNSKI AND A. SHAPIRO, *Stochastic Programming*, Handbook in Operations Research and Management Science Vol. 10, Elsevier, Amsterdam, 2003.
8. R. SCHULTZ, *Stochastic programming with integer variables*, Mathematical Programming, Ser. B, Vol. 97 (2003), pp. 285–309.
9. J. YANEZ AND J. RAMIREZ, *The robust coloring problem*, European Journal of Operational Research, Vol. 148 (2003), pp. 546–558.
10. F. WANG AND Z. XU, *Metaheuristics for robust graph coloring*, Journal of Heuristics, Vol. 19 (2013), pp. 529–548.

Acknowledgments: This work was supported by the Czech Science Foundation under the Grant GP13-03749P.

Numerical study of cooperating thermosolutal convection in a cylindrical annular geometry - Effect of thermal Rayleigh number

Bouchra Cheddadi¹ and Abdelkhalek Cheddadi²

Superior School of Technology, University Hassan II, Casablanca, Morocco¹
Mohammadia School of Engineers, University Mohammed V-Agdal, Morocco²

Keywords: Double diffusive convection, buoyancy ratio, cooperate thermal Rayleigh number, heat transfer, mass transfer,

Abstract A numerical investigation of double diffusive natural convection within a two-dimensional, horizontal annulus has been carried out. The A.D.I. method has been used to describe the symmetric solutions in terms of isotherms, streamlines and iso-concentrations. In this paper, we considered the case where the thermal and solutal buoyancy effects are cooperating. We restrict ourselves to analyze the influence of the thermal Rayleigh number on the flow structure and on the heat and mass transfer in the geometry considered.

1 Introduction

Double diffusive convection refers to the problems where the fluid flow is induced by the simultaneous presence of two diffusive components. These are the difference in temperatures and concentrations. Intensive research has been reported on double diffusive convection in confined spaces due to its many engineering and technological applications. Such as, the technologies involved in the chemical vapor deposition processes for the semiconductor device fabrications. Also, the migration of impurities in non-isothermal material processing applications has motivated many researches in exploring the characteristics of the associated species and energy transport process. There are also many important processes in nature where double diffusive convection plays a crucial role. The best known is thermohaline convection in oceans, driven by salinity gradients associated with temperature differences. Thermosolutal convection appears in many engineering applications, such as isotope separation in liquid and gaseous mixtures, identification and separation of crude oil components, coating of metallic items, etc. This phenomenon is supposed to play an important role in crystal growth. It also affects component separation in oil wells, solidifying metallic alloys, volcanic lava,

and in Earth mantle. Huppert and Turner [1] had presented an early review of the important developments in double diffusive convection and the result of a close interaction between theoreticians, laboratory experimenters and sea-going oceanographers. Most of early studies done on double diffusive convection were focused on rectangular enclosures with aiding or opposing solutal gradient. Bejan [2] reported a fundamental study of a scale analysis relative to heat and mass transfer within a rectangular enclosure when the buoyancy effect is due to density variations caused by either temperature or solute concentration variations. Other studies within rectangular cavities were carried by Lee and Hyun [3], Mamou et al. [4], Bennacer and Gobin [5], [6] and Ghorayeb and Mojtabi [7]. Recently, there has been a focus on cylindrical cavities as they are very present in the industry. For a vertical annulus, Ship et al. [8] conducted a numerical study for steady laminar double diffusive natural convection within a vertically mounted closed annulus with constant temperature and mass species differences imposed across the vertical walls. Later, the same authors [9] studied the effect of thermal Rayleigh number and Lewis number on double diffusive natural convection in a closed annulus. The results illustrated that the thermal Rayleigh number and the Lewis number were found to influence the buoyancy ratios at which flow transition and flow reversal occurred. Teamah and Shoukri [10] studied the effect of the radius ratio, aspect ratio and buoyancy ratio on the double diffusive natural convection in vertical annulus enclosures. Their results cover a radius ratio from 1 to 5, aspect ratio from 1 to 4 and buoyancy ratio from 10^{-3} to 10^3 . For cross double diffusive convection Shi and Lu [11] studied the double diffusive natural convection in a vertical cylinder with radial temperature and axial solutal gradients. Their investigation focused on the effect of the buoyancy ratio on the evolution of the flow field, temperature and solute field in the cavity.

2 Mathematical model

The geometry of the problem is shown in Fig.1. The two horizontal cylinders are considered long enough to neglect boundary effects and consider the flow as two-dimensional. Both of the two cylinders are held at constant temperatures and concentrations. The inner cylinder is considered the hot one ($T_c > T_f$). The temperature gradient generates the natural thermal diffusive force and the concentration gradient generates the natural solutal diffusive force. In addition, the flow in the annular space is considered to be Newtonian, steady and laminar. Also, all thermo-physical properties of the fluid are considered constant except for the fluid density variation in the buoyancy term, where the Boussinesq approximation is considered to be linearly proportional to both temperature and concentration so that :

$$\rho = \rho_0 (1 - \beta_T (T - T_0) - \beta_S (C - C_0)) \quad (1)$$

Where ρ_0 is the fluid density at temperature T_0 and concentration C_0 , and β_T and β_S are respectively the coefficients of thermal and solutal expansion, T_0 and C_0 are a temperature and a concentration of reference. The governing equations are written by employing a vorticity-stream function formulation. The stream function ψ and the vorticity ω (the unique component of the vector velocity $\boldsymbol{\Omega}$) are defined in terms of radial velocity u_r and tangential velocity u_φ as:

$$u_r = \frac{1}{r} \frac{\partial \psi}{\partial \varphi}, u_\varphi = -\frac{\partial \psi}{\partial r}, \omega = -\frac{\partial^2 \psi}{\partial r^2} - \frac{1}{r^2} \frac{\partial^2 \psi}{\partial \varphi^2} - \frac{1}{r} \frac{\partial \psi}{\partial r}. \text{ To cast the governing equations}$$

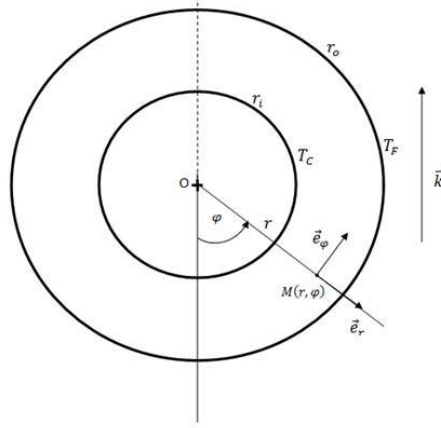


Figure 1. Definition diagram

in the dimensionless form, the following dimensionless variables are introduced to the governing equations: $r_a = \frac{r}{r_i}$, $t_a = \frac{a}{r_i^2} t$, $V_a = \frac{V}{V_0}$, $P_a = \frac{P^*}{\rho_0 V_0^2}$, $T_a = \frac{T - T_F}{T_c - T_F}$, $C_a = \frac{C - C_0}{C_1 - C_0}$ with $V_0 = \frac{a}{r_i}$ and $P^* = P + \rho_0 g z$. On the basis of the above assumption, the conservation equation for vorticity, stream-function, energy and species in dimensionless form are written as follows in polar coordinate [12].

Stream-function equation:

$$\Delta \psi + \omega = 0 \quad (2)$$

Vorticity equation:

$$\begin{aligned} \frac{\partial \omega}{\partial t} + \frac{1}{r} \left[\frac{\partial \psi}{\partial \varphi} \frac{\partial \omega}{\partial r} - \frac{\partial \psi}{\partial r} \frac{\partial \omega}{\partial \varphi} \right] = & Pr \Delta \omega + Ra_T Pr \left(\frac{\cos \varphi}{r} \frac{\partial T}{\partial \varphi} + \sin \varphi \frac{\partial T}{\partial r} \right) + \\ & + N Ra_T Pr \left(\frac{\cos \varphi}{r} \frac{\partial C}{\partial \varphi} + \sin \varphi \frac{\partial C}{\partial r} \right) \end{aligned} \quad (3)$$

Energy equation:

$$\frac{\partial T}{\partial t} + \frac{1}{r} \left[\frac{\partial \psi}{\partial \varphi} \frac{\partial T}{\partial r} - \frac{\partial \psi}{\partial r} \frac{\partial T}{\partial \varphi} \right] = \Delta T \quad (4)$$

Species equation:

$$\frac{\partial C}{\partial t} + \frac{1}{r} \left[\frac{\partial \psi}{\partial \varphi} \frac{\partial C}{\partial r} - \frac{\partial \psi}{\partial r} \frac{\partial C}{\partial \varphi} \right] = \frac{1}{Le} \Delta C \quad (5)$$

The dimensionless boundary conditions are:

$$\begin{aligned} r = 1: T = 1; C = 1; \psi = 0; \frac{\partial \psi}{\partial r} = 0; \frac{\partial^2 \psi}{\partial r^2} + \omega = 0 & \quad \forall \varphi \\ r = R: T = 0; C = 0; \psi = 0; \frac{\partial \psi}{\partial r} = 0; \frac{\partial^2 \psi}{\partial r^2} + \omega = 0 & \quad \forall \varphi \\ \varphi = 0 \text{ and } \varphi = \pi: \psi = 0; \frac{\partial T}{\partial \varphi} = 0; \frac{\partial C}{\partial \varphi} = 0; \omega = 0 & \quad \forall r \end{aligned}$$

The problem is characterized by 5 dimensionless parameters. They are: the thermal Rayleigh number: $Ra_T = g\beta\Delta T r_i^3 / \nu a$, the Lewis number: $Le = a/D$, the Prandtl number: $Pr = \nu/a$, the ratio: $N = \beta_s \Delta C / \beta_T \Delta T$, and the aspect ratio (the cylindrical raysâŽŽ ratio): $R = r_o/r_i$.

3 Results and discussion

The numerical code has been validated both by comparing the results to the pure thermal case and by analyzing the case of weak solutal buoyancies [13]- [14]. For positive values of the ratio N , the buoyancy forces induced by the thermal and solutal effects are cooperating, and their flows are aiding. In this paper, the effect of thermal Rayleigh number on the flow structure and on the heat and mass transfer in the geometry considered for a positive buoyancy ratio ($N > 0$) is investigated in detail and compared with the convection driven only by a thermal buoyancy ($N = 0$). All results were performed with Prandtl number $Pr = 0.7$ and aspect ratio $R = 2$.

3.1 Influence on the flow

The increase in thermal Rayleigh number leads always to more intense flow. Indeed, in the equation (2), the buoyancy force term is proportional to Ra_T . Fig.2 represents the variation of the maximum of the stream function ψ_{\max} in function of the thermal Rayleigh number Ra_T , for a value of buoyancy ratio $N = 1$ and different values of the Lewis number Le . The pure thermal case corresponding to $N = 0$ is represented for comparison. It is observed that for low values of thermal Rayleigh number Ra_T , the flow pattern is almost conductive and the fluid flow is not intense regarding the low values of ψ_{\max} . The increase in the

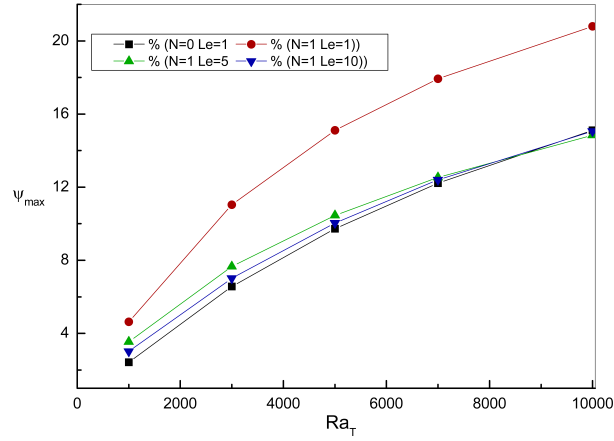


Figure 2. Effect of Ra_T on ψ_{\max} for $N = 1, Le = 1, 5$ and 10

thermal Rayleigh number causes the increase of flow's intensity. The figures Fig.3 and 4 represent the effect of thermal Rayleigh number on stream lines and isotherms. In order to highlight the effect of Ra_T alone, both Lewis number and buoyancy ratio were kept constant at values equal one. When Lewis number equals one, the thermal diffusivity equals the mass diffusivity. This means that the isothermal lines are congruent with the isoconcentration lines. Therefore, the isotherms were only presented. It is observed that the flow consists of a single convective cell crescent occupying a half annulus and rotating in the clockwise direction (we always consider the half-space on the right to represent the stream lines). The fluid rises against the hot inner cylinder. At the top, it cools down against the cold cylinder. Gradually, as the thermal Rayleigh number increases, the center of the convective cell, corresponding to the maximal value of the stream function, moves upwardly.

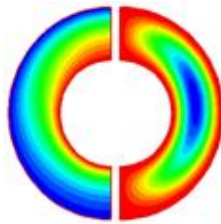


Figure 3. Isotherms and stream lines for $Ra_T = 1000, N = 1$ and $Le = 1$

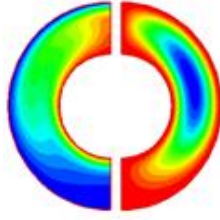


Figure 4. Isotherms and stream lines for $Ra_T = 10000$, $N = 1$ and $Le = 1$

For isotherms, there is a distortion when the thermal Rayleigh number Ra_T increases moving away increasingly pure conduction for which isotherms are concentric circles, meaning an increase in heat flux due to the increase in the flow intensity. The thermal boundary layers are developed near the cylindrical walls and becoming gradually thinner as the thermal Rayleigh number increases.

3.2 Influence on the heat transfer

The global Nusselt number Nug increases gradually as the thermal Rayleigh number increases (the convective flow is accentuated). The figure Fig. 5 illustrates the variation of the global number of Nusselt Nug as a function of the thermal Rayleigh number when the buoyancy ratio N is equal to 1 and for different values of the Lewis number. The pure thermal case is shown for comparison.

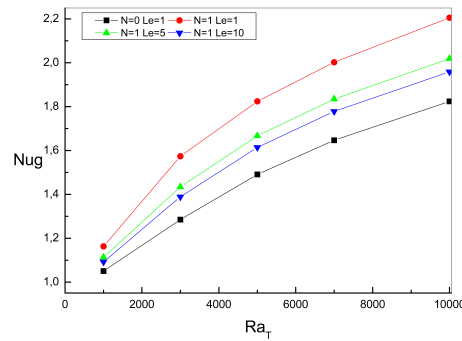


Figure 5. Effect of Ra_T on Nug for $N = 1$, $Le = 1, 5$ and 10

3.3 Influence on the mass transfer

The effect of the thermal Rayleigh number on the variation of the mass transfer is illustrated in Fig.6 for the values of the buoyancy ratio $N = 1$, and different values of the Lewis number. Pure thermal case is shown for comparison. It is

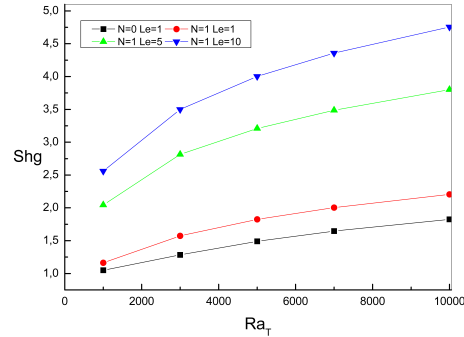


Figure 6. Effect of Ra_T on Sh_g for $N = 1$, $Le = 1, 5$ and 10

observed that there is also an increase in mass transfer, represented by the global number Sherwood, when the thermal Rayleigh number increases.

4 Conclusion

The problem of double diffusive natural convection in an annular cylindrical space with an aspect ratio of $R = 2$, was considered. The governing equations were given in polar coordinate and the ADI method has been implemented and used to describe the two-dimensional symmetric solutions in terms of isotherms, streamlines and iso-concentrations. The case when the solutal and thermal buoyancies are cooperating was considered. The work focuses on the effects of the thermal Rayleigh number on the characters of the flow, heat and mass transfer rates. It was shown that the increase of Ra_T accentuates the flow and that it follows a simultaneous increase of heat and mass transfer within the geometry studied.

References

1. H.E. HUPPER, J.S TURNER, *Double diffusive convection*, J.Fluid Mech., Vol.106, (1981), pp. 299-329.

2. A. BEJAN, *Mass and heat transfer by nature convection in a vertical cavity*, Int. J. Heat Fluid Flow, Vol.106, (1985), pp.149-159.
3. J.W. LEE, J.M. HYUN, *Time-dependent double diffusive in a stably stratified fluid under lateral heating*, Int. J. Heat Mass Transfer, Vol.34, (1991), pp.2409-2421.
4. M. MAMOU, P. VASSEUR, E. BILGEN, *Multiple Solutions for Double Diffusive Convection in a Vertical Porous Enclosure*, Int. J. Heat Mass Transfer, Vol.38, (1995), pp.1787-1798.
5. R. BENNACER, D. GOBIN, *Cooperating thermosolutal convection in enclosures-I. Scale analysis and mass transfer*, Int. J. Heat and Mass Transfer, Vol.39, (1996), pp.2671-2681.
6. D. GOBIN, R. BENNACER, *Cooperating thermosolutal convection in enclosures-II. Heat transfer and flow structure*, Int. J. Heat and Mass Transfer, Vol.39, (1996), pp.2683-2697.
7. C.K. GHORAYEB, H. KHALLOUF, A. MOJTABI, *Onset of oscillatory flows in double diffusive convection*, Int. J. Heat Mass Transfer, vol.42, (1999), pp.629-643.
8. P.W. SHIP, M. SHOUKRI, M.B. CARVER, *Double diffusive natural convection in a closed annulus*, Numer. Heat Transfer, Vol.24, (1993), pp.339-356.
9. P.W. SHIP, M. SHOUKRI, M.B. CARVER, *Effect of thermal Rayleigh and Lewis numbers on double diffusive natural convection in a closed annulus*, Numer. Heat Transfer, Vol 24, (1993), pp.451-465.
10. M.A. TEAMAH, M. SHOUKRI, *The effect of aspect and ratios on double diffusive natural convection in a vertical annulus*, Alexandria J., Vol.34, (1995), pp.95-105.
11. K.F. SHI, W.Q. LU, *Numerical simulation of double diffusive convection with cross gradients*, J. Eng. Thermophys., Vol.26, (2005), pp.328-330.
12. B. CHEDDADI, R. ABOULAICH, A. CHEDDADI, *Convection thermosolutale en géométrie annulaire cylindrique-résultats numériques préliminaires*, Physical and Chemical News, Vol.57, (2011), pp.71-75.
13. A. CHEDDADI A., J.P. CALTAGIRONE, A. MOJTABI, K. VAFAI *Free Two Dimensional Convective Bifurcation in a Horizontal Annulus*, ASME Journal of Heat Transfer, Vol.39, (1992), pp.99-106.
14. B. CHEDDADI, R. ABOULAICH, A. CHEDDADI, *Double diffusive convection in a cylindrical annular geometry - Validation and mesh sensibility*, Int. J. Computer Science Issues, Vol.11, (2014).

Solution of Advanced Model of Membrane Diffusion Processes

Miroslava Dubcová, Miroslav Zgažar

Institute of Chemical Technology, Prague

Keywords: partial differential equations, diffusion equation, Laplace transform, residues

Abstract The aim of this paper is to propose and solve the model of classical Fickian diffusion with dynamic correction of fluctuating concentration of penetrating substance on the surface of membrane, i.e. with the time dependent boundary condition. A generalized model of diffusion fluxes defined by Fredrickson [2] will be used. To solve the diffusion equation we apply the Laplace transform.

1 Diffusion model

The generalized model of diffusion fluxes defined by Fredrickson [2] has the form

$$j(t, x) = - \int_0^t \eta(t - \tau) \frac{dc(\tau, x)}{dx} d\tau, \quad (1)$$

where $\eta(t)$ is the diffusion relaxation function:

$$\eta(t) = D^i \delta(t) + \beta(D^0 - D^i) e^{-\beta t}, \quad (2)$$

where $\beta \in (0, 1)$ is the relaxing parameter, and D^i , and D^0 is an initial value and the final value of diffusion coefficient reached at infinity time, respectively. For ideal diffusion cases the diffusion relaxation function (2) devolves on $\eta(t) = D^i \delta(t)$. This form of the diffusion relaxation function was derived based on irreversible thermodynamics [4].

Now let us formulate the anomalous diffusion problem for permeation with dynamic correction $c(0, t)$ on the first boundary:

$$\begin{aligned}\frac{\partial c}{\partial t} &= \frac{\partial}{\partial x} \left[\int_0^t \eta(t-\tau) \frac{\partial c(x, \tau)}{\partial x} d\tau \right] \\ c(0, t) &= c_\infty(1 - e^{-\beta t}), \quad t \geq 0 \\ c(l, t) &= 0, \quad t \geq 0 \\ c(x, 0) &= 0, \quad x \in (0, l),\end{aligned}\tag{3}$$

where $c(x, t)$ is the concentration profile, c_∞ is the steady state concentration on the surface of membrane reached at infinity time. The choice of the boundary condition $c(0, t)$ is based on the experiments published in [3] which suggest that the surface concentration changes in time even though surrounding gas is maintained at constant pressure.

2 Solving the diffusion equation using the Laplace transform

By applying the Laplace transform to the diffusion problem (3) one derives:

$$\frac{d^2 \hat{c}(x, p)}{dx^2} - \frac{p}{\hat{\eta}(p)} \hat{c}(x, p) = 0\tag{4}$$

$$\hat{c}(0, p) = c_\infty \frac{\beta}{p(p + \beta)},\tag{5}$$

$$\hat{c}(l, p) = \lim_{x \rightarrow l} \hat{c}(x, p) = 0,\tag{6}$$

where

$$\hat{c}(x, p) = \int_0^\infty c(x, t) e^{pt} dt$$

is the Laplace transform of the concentration profile $c(x, t)$ and the Laplace transform of diffusional relaxation function $\eta(t)$ (2) is:

$$\hat{\eta}(p) = D^i + \frac{\beta(D^0 - D^i)}{p + \beta} = \frac{pD^i + \beta D^0}{p + \beta}.\tag{7}$$

The particular solution of (4) with the corresponding boundary conditions (5, 6) can be found in the form:

$$\hat{c}(x, p) = c_\infty \frac{\beta}{p(p + \beta)} \left[\cosh \left(\sqrt{\frac{p}{\hat{\eta}(p)}} x \right) - \frac{\cosh \left(\sqrt{\frac{p}{\hat{\eta}(p)}} l \right)}{\sinh \left(\sqrt{\frac{p}{\hat{\eta}(p)}} l \right)} \sinh \left(\sqrt{\frac{p}{\hat{\eta}(p)}} x \right) \right]\tag{8}$$

Because $\sinh(x - y) = \sinh x \cosh y - \cosh x \sinh y$, (8) can be rewritten as

$$\hat{c}(x, p) = c_\infty \frac{\beta}{p(p + \beta)} \frac{\sinh\left(\sqrt{\frac{p}{\hat{\eta}(p)}}(l - x)\right)}{\sinh\left(\sqrt{\frac{p}{\hat{\eta}(p)}}l\right)}. \quad (9)$$

In fact Bromwich showed that the inverse of Laplace transform (*Bromwich's integral*) can be expressed as the contour integral

$$c(x, t) = \frac{1}{2\pi i} \int_{\omega - i\infty}^{\omega + i\infty} \hat{c}(x, p) e^{pt} dp, \quad (10)$$

where ω is the Laplace convergence abscissa which is greater than the real part of any of the poles in (9). However, principally the inversion of (9) will be carried out by *Cauchy's residue theorem* [1]. Therefore, the poles of (9) require further attention. Two of the poles are $p = 0$ and $p = -\beta$; this can be easily derived from the term $\frac{\beta}{p(p+\beta)}$. The other poles are given by the equation

$$\sinh\left(\sqrt{\frac{p}{\hat{\eta}(p)}}l\right) = 0 \quad (11)$$

which implies

$$l\sqrt{\frac{p_k}{\hat{\eta}(p_k)}} = i k \pi, \quad k \in \mathbb{Z}. \quad (12)$$

The latter equation implies:

$$\frac{p_k}{\hat{\eta}(p_k)} = -\frac{k^2 \pi^2}{l^2}, \quad k \in \mathbb{N}. \quad (13)$$

Substitution of relation (7) into (13) results in quadratic equation

$$p^2 + (\beta - yD^i)p - y\beta D^0 = 0, \quad (14)$$

where $y = -k^2 \pi^2 / l^2$ and the solution is

$$p_k^\pm = -\frac{\beta - yD^i}{2} \pm \frac{1}{2}\sqrt{(\beta - yD^i)^2 + 4y\beta D^0}, \quad k \in \mathbb{N}. \quad (15)$$

The line integral (10) with the Bromwich contour lying parallel and slightly to the right of the imaginary axis can be converted into a closed contour using *Jordan's lemma* through the addition of an infinite semicircle joining $i\infty$ to $-i\infty$ [1]:

$$\int_{a-i\infty}^{a+i\infty} \hat{c}(x, p) e^{pt} dp = \oint_C \hat{c}(x, p) e^{pt} dp \quad (16)$$

Now *Cauchy's residue theorem* can be applied

$$\frac{1}{2\pi i} \oint_C \hat{c}(x, p) e^{pt} dp = \sum_{p_k^\pm = \text{pol}} \text{Res} [\hat{c}(x, p) e^{pt}; p_k^\pm] \quad (17)$$

and therefore the inverse of solution (9) has the following form with respect to (15):

$$c(x, p) = \text{Res} [\hat{c}(x, p) e^{pt}; 0] + \text{Res} [\hat{c}(x, p) e^{pt}; -\beta] + \sum_{p_k^\pm, k \in \mathbb{N}} \text{Res} [\hat{c}(x, p) e^{pt}; p_k^\pm] \quad (18)$$

The first residue in (18) can be found as

$$\begin{aligned} \text{Res} [\hat{c}(x, p) e^{pt}; 0] &= \lim_{p \rightarrow 0} p c_\infty \frac{\beta}{p(p + \beta)} \frac{\sinh\left(\sqrt{\frac{p}{\hat{\eta}(p)}}(l - x)\right)}{\sinh\left(\sqrt{\frac{p}{\hat{\eta}(p)}}l\right)} e^{pt} \\ &= \begin{cases} c_\infty \frac{l - x}{l} & x \neq l \\ 0 & x = l \end{cases} \end{aligned} \quad (19)$$

and the second one as

$$\begin{aligned} \text{Res} [\hat{c}(x, p) e^{pt}; -\beta] &= \lim_{p \rightarrow -\beta} (p + \beta) c_\infty \frac{\beta}{p(p + \beta)} \frac{\sinh\left(\sqrt{\frac{p}{\hat{\eta}(p)}}(l - x)\right)}{\sinh\left(\sqrt{\frac{p}{\hat{\eta}(p)}}l\right)} e^{pt} \\ &= \begin{cases} -c_\infty \frac{l - x}{l} e^{-\beta t} & x \neq l \\ 0 & x = l \end{cases} . \end{aligned} \quad (20)$$

The residues in the third term of (18) can be computed in similar way as follows:

$$\begin{aligned} \text{Res} [\hat{c}(x, p) e^{pt}; p_k^\pm] &= \lim_{p \rightarrow p_k^\pm} (p - p_k^\pm) c_\infty \left(\frac{\beta}{p(p + \beta)} \right) \frac{\sinh\left(\sqrt{\frac{p}{\hat{\eta}(p)}}(l - x)\right)}{\sinh\left(\sqrt{\frac{p}{\hat{\eta}(p)}}l\right)} e^{pt} \\ &= A \lim_{p \rightarrow p_k^\pm} \frac{p - p_k^\pm}{\sinh\left(\sqrt{\frac{p}{\hat{\eta}(p)}}l\right)}, \end{aligned} \quad (21)$$

where

$$A = c_\infty \left(\frac{\beta}{p_k^\pm (p_k^\pm + \beta)} \right) e^{p_k^\pm t} \sinh\left(\sqrt{\frac{p_k^\pm}{\hat{\eta}(p_k^\pm)}}(l - x)\right).$$

The latter limit can be computed by applying the L'Hospital rule:

$$\lim_{p \rightarrow p_k^\pm} \frac{p - p_k^\pm}{\sinh\left(\sqrt{\frac{p}{\hat{\eta}(p)}}l\right)} = \frac{1}{\cosh\left(\sqrt{\frac{p_k^\pm}{\hat{\eta}(p_k^\pm)}}l\right) \frac{l}{2\sqrt{\frac{p_k^\pm}{\hat{\eta}(p_k^\pm)}}} \frac{d}{dp} \left(\frac{p}{\hat{\eta}(p)} \right)_{p=p_k^\pm}} \quad (22)$$

Further, by (12), the general residue is

$$\text{Res} [\hat{c}(x, p)e^{pt}; p_k^\pm] = \frac{2ik\pi c_\infty \left(\frac{\beta}{p_k^\pm(p_k^\pm + \beta)} \right) e^{p_k^\pm t} \sinh(ik\pi \frac{l-x}{l})}{(-1)^k l^2 \frac{d}{dp} \left(\frac{p}{\hat{\eta}(p)} \right)_{p=p_k^\pm}}. \quad (23)$$

By the algebraic feature of hyperbolic sinus:

$$\begin{aligned} \sinh \left(ik\pi \frac{l-x}{l} \right) &= \sinh \left(ik\pi - \frac{x}{l} ik\pi \right) = \cos(ik\pi) \sinh \left(-\frac{x}{l} ik\pi \right) \\ &= \cos(k\pi) \sinh \left(-\frac{x}{l} ik\pi \right) = (-1)^k \sinh \left(-\frac{x}{l} ik\pi \right) \\ &= (-1)^{k+1} \sinh \left(\frac{x}{l} ik\pi \right), \end{aligned} \quad (24)$$

the general residue can be rewritten as:

$$\text{Res} [\hat{c}(x, p)e^{pt}; p_k^\pm] = \frac{-2ik\pi c_\infty \left(\frac{\beta}{p_k^\pm(p_k^\pm + \beta)} \right) e^{p_k^\pm t} \sinh(ik\pi \frac{x}{l})}{l^2 \frac{d}{dp} \left(\frac{p}{\hat{\eta}(p)} \right)_{p=p_k^\pm}}. \quad (25)$$

Hence, the corresponding concentration profile of anomalous permeation can be expressed as

$$c(x, t) = c_\infty \left[\frac{l-x}{l} (1 - e^{-\beta t}) - \frac{2}{l^2} \sum_{p_k^\pm, k \in \mathbb{N}} \frac{ik\pi, \beta}{p_k^\pm(p_k^\pm + \beta)} e^{p_k^\pm t} \frac{\sinh(ik\pi \frac{x}{l})}{\frac{d}{dp} \left(\frac{p}{\hat{\eta}(p)} \right)_{p=p_k^\pm}} \right]. \quad (26)$$

By applying the relation $\sinh(ik\pi \frac{x}{l}) = i \sin(k\pi \frac{x}{l})$ and by further manipulation one obtains the final form

$$c(x, t) = c_\infty \left[\frac{l-x}{l} (1 - e^{-\beta t}) + \frac{2\pi\beta}{l^2} \sum_{p_k^\pm, k \in \mathbb{N}} \frac{ke^{p_k^\pm t}}{p_k^\pm(p_k^\pm + \beta)} \frac{\sin(k\pi \frac{x}{l})}{\frac{d}{dp} \left(\frac{p}{\hat{\eta}(p)} \right)_{p=p_k^\pm}} \right]. \quad (27)$$

Because

$$\frac{d}{dp} \left(\frac{p}{\hat{\eta}(p)} \right) = \frac{d}{dp} \left(\frac{p(p+\beta)}{pD^i + \beta D^0} \right) = \frac{p^2 D^i + 2p\beta D^0 + \beta^2 D^0}{(pD^i + \beta D^0)^2}, \quad (28)$$

one can use (27) to depict the concentration profile of anomalous permeation. The 3D model of the concentration profile for the common values of diffusion coefficients $D^0 = 1, 2 \cdot 10^{-12} m^2 \cdot s^{-1}$ and $D^i = 1.10^{-13} m^2 \cdot s^{-1}$ together with the unit concentration at infinity, thickness of membrane $l = 60 \cdot 10^{-6} m$ and the relaxing parameter $\beta = 0,001 s^{-1}$, is included below:

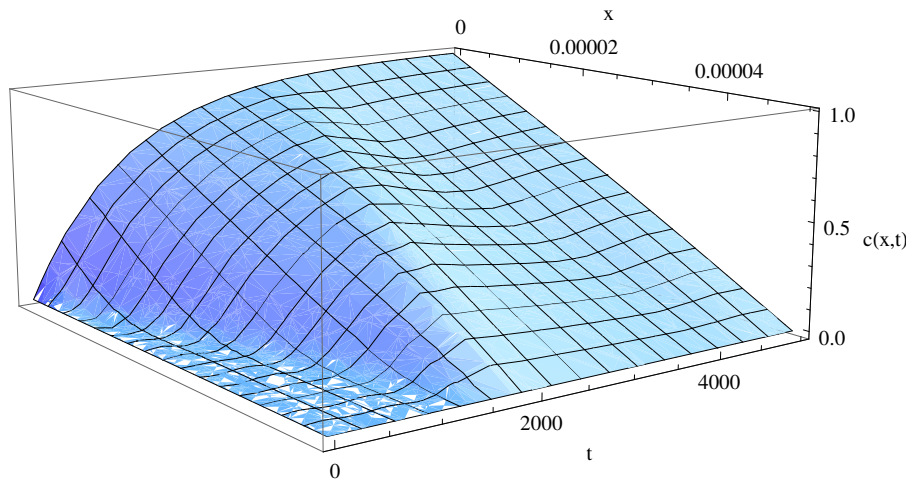


Figure 1. Concentration profile $c(t, x)$ for $\beta = 0,001s^{-1}$

References

1. D. G. Duffy, *Transform methods for solving partial differential equations*, Second Edition, Chapman & Hall/CRC, Florida, 2004, ISBN 1-58488-451-7
2. A. G. Fredrickson, *Principles and Applications of Rheology*, Prentice-Hall, Inc. (1974)
3. F. A. Long, D. Richman, *Concentration Gradients for Diffusion of Vapors in Glassy Polymers and Their Relation to Time Dependent Diffusion Phenomena*, J. Am. Chem. Soc., 82 (1960) 513
4. P. Neogi, *Irreversible Thermodynamics of Diffusion and Solution Processes*, AIChE Journal, 29/5 (1983) 829-833

Simplified model for a rivulet spreading down an inclined wetted plate

Martin Isoz

Institute of Chemical Technology, Prague

Keywords: rivulet, fluid dynamics, liquid spreading

Abstract Rivulet type flow down an inclined plate is of great importance in many engineering areas including packed columns design and catalytic reactors modeling. Combining a simplified solution of the Navier-Stokes equation for a rectilinear rivulet and the Cox-Voinov law for an axisymmetric spreading of a perfectly wetting liquid, we derived a semi-analytical model of the liquid flow in a spreading rivulet. The proposed model was used to characterize the flow of a liquid in dependence of the plate inclination angle, rivulet dynamic contact angle and liquid flow rate. The presented modeling method provides an insight on the liquid flow properties without the necessity of numerically solving the corresponding PDEs.

1 Introduction

Flow characteristics of a gravity driven, spreading trickle of a liquid, is of the key importance throughout many areas of chemical engineering, including the ones concerning the mass transfer [1], trickle bed reactors [2], heat exchangers [3] and various coating processes [4].

Eventhough the rivulet type flow can be modeled using various CFD methods [1, 5], such methods are still too complex to be used in the engineering practice and too computationally demanding for the parametric studies of the rivulet behavior.

A simplified solution to the problem of the rivulet type flow has been studied since 1960's. The pioneering studies by Towell and Rothfeld [6], Allen and Biggin [7], Bentwich et al. [8] and Fedotkin et al. [9] have led to a substantial amount of subsequent work on rectilinear rivulet flow. For example, Benilov [10] performed a stability analysis for the rivulet flow down an inclined substrate and Duffy and Moffat [11] used the solution available for the rectilinear rivulet flow to describe the flow with prescribed volume flux and non-zero contact angle over a

cylinder of large radius. For further informations on the topic of unidirectional (rectilinear) rivulet flow, see [12–15] and many references therein.

The problem of the physics of the contact line region of a rivulet was first taken into account by Davis [16] and revisited from another point of view by Shetty and Cerro [17]. However, a literature covering the topic of modeling the flow of a spreading rivulet is still limited to various CFD methods (e.g. [1,18,19]) or the spreading rivulet stability analysis (see [20] and references therein).

A rather different approach from the previous studies was taken in the presented work. We used the solution for the unidirectional flow of a slender and shallow rivulet with prescribed volume flux and non-zero contact angle to describe the locally unidirectional flow of a rivulet with slowly varying both contact angle and width. To link the change in contact angle with development of the rivulet width, we applied the Cox-Voinov law [21,22] for the axisymmetric spreading of a perfectly wetting liquid on a horizontal substrate in time coupled with an approximative transformation from time to a spatial coordinate.

A method for simulation of the flow in a spreading rivulet was derived for the case of a wetted plate inclined by an angle $\alpha \in (0; \pi)$ to the horizontal.

The studied problematics can be divided in two main parts: the specification of the rivulet gas-liquid (GL) interface shape and the calculation of the velocity field in it. Furthermore, it is convenient to analyze separately the case of a rivulet flowing on an inclined plate ($\alpha < \pi/2$), underneath it ($\alpha > \pi/2$) and the special case of a vertical plate ($\alpha = \pi/2$).

For the flow on a vertical plate or for a very shallow rivulet in which the gravity can be neglected, the problem of finding the shape of GL interface of the rivulet was reduced from the solution of the corresponding system of the Navier-Stokes equations to the repeated solution of one non-linear algebraic equation. The other cases have to be treated numerically. However, the proposed algorithms are all based on a solution of a single ordinary differential equation.

The velocity field in the spreading rivulet was obtained on a purely numerical basis. We used a technique based on a principle of particle image velocimetry (PIV), thoroughly described in a review [24], but with followed "particles" created numerically.

2 Coordinate system and simplifying assumptions

The case of a steady flow of a thin symmetric rivulet down an inclined wetted plate was studied in the Cartesian coordinate system $Oxyz$ with the x axis down the line of the greatest slope, the y axis horizontal and the z axis normal to the substrate $z = 0$. The used coordinate system as well as the most important symbols are depicted in the Fig. 1.

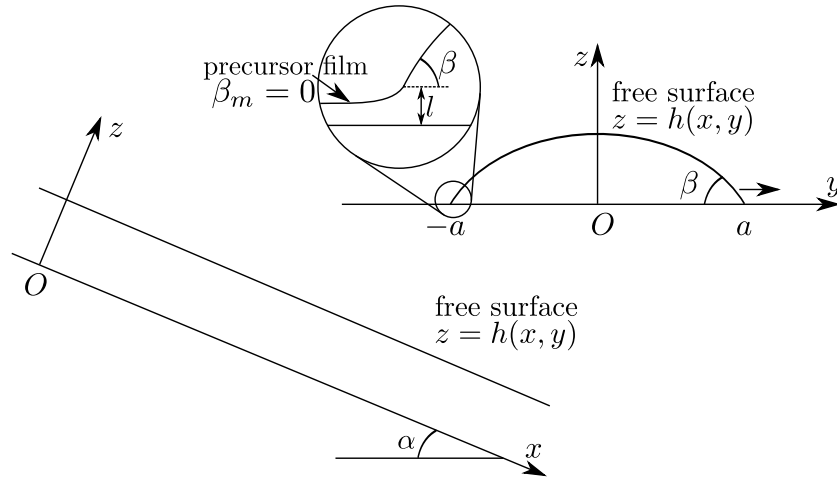


Figure 1. Used coordinate system with the basics of rivulet spreading notation. α is the plate inclination angle, β and β_m are the apparent (dynamic) and the microscopic contact angles, a is the rivulet half width.

The proposed method for modeling of a gravity driven spreading rivulet flow down an inclined wetted plate was derived under the following simplifications,

1. The studied liquid is Newtonian, ρ , μ and γ are constant.
2. The rivulet profile shape is constant in time. Furthermore, Q is constant not only in time, but also in all spatial directions.
3. There is no shear between the gas and liquid phases.
4. The liquid velocities in the directions transversal and normal to the plate are negligible in comparison to the one in its longitudinal direction, $u \gg v \sim w$. The inertial effects can be neglected in y and z directions.
5. The gravity is the only acting body force.
6. The rivulet is shallow. Its dynamic contact angles are assumed small, $\beta(x) \ll 1$, and its GL interface is nearly flat, $h_y(x, y) \ll 1$.
7. There is a thin precursor film of height l on the whole studied surface. Thus there is no contact angle hysteresis and $\beta_m = 0$. The height of the pre-

cursor film, l , can also be taken as the intermediate region length scale well separating the inner and outer solution for the profile shape [23].

3 Specification of the GL interface shape

With the above listed simplifying assumptions, the parallel between the spreading of a rivulet along an inclined plate and the spreading of a static objects in time can be found.

At first, the system of Navier-Stokes equations for an unidirectional flow, as presented by Duffy and Moffatt [11], is solved to obtain a local description of a spreading rivulet. Then, the Cox-Voinov law is used to describe the evolution of the boundary conditions, and thus the rivulet gas-liquid (GL) interface shape, along the plate.

3.1 Static rivulet

For the case of a rectilinear steady flow of a shallow rivulet, the Navier-Stokes equations can be simplified via 'thin-film theory' to,

$$\begin{aligned} 0 &= -p_x + \rho g \sin \alpha + \mu u_{zz} \\ 0 &= -p_y \\ 0 &= -p_z - \rho g \cos \alpha \end{aligned} \quad (1)$$

and integrated subject to the boundary conditions,

$$\begin{aligned} z &= 0 : & u &= u(y, z) = 0 \\ z &= h : & p &= p_A - \gamma h_{yy} \quad \text{and} \quad u_z = 0 \\ y &= \pm a : & h &= 0 \quad \text{and} \quad h_y = \pm \tan \beta. \end{aligned} \quad (2)$$

Solution of the system (1) with boundary conditions (2) yields the following equation describing the shape the GL interface of an uniform rivulet for the three cases of different plate inclination angles, $\alpha < \pi/2$, $\alpha = \pi/2$ and $\alpha > \pi/2$ indicated as (i), (ii) and (iii), respectively.

$$h(\zeta) = \begin{cases} \frac{a \tan \beta}{\sqrt{B}} \left(\frac{\cosh \sqrt{B} - \cosh \sqrt{B}\zeta}{\sinh \sqrt{B}} \right) & (i) \\ \frac{a \tan \beta}{2} (1 - \zeta^2) & (ii) \\ \frac{a \tan \beta}{\sqrt{B}} \left(\frac{\cos \sqrt{B}\zeta - \cos \sqrt{B}}{\sin \sqrt{B}} \right) & (iii) \end{cases} , \quad (3)$$

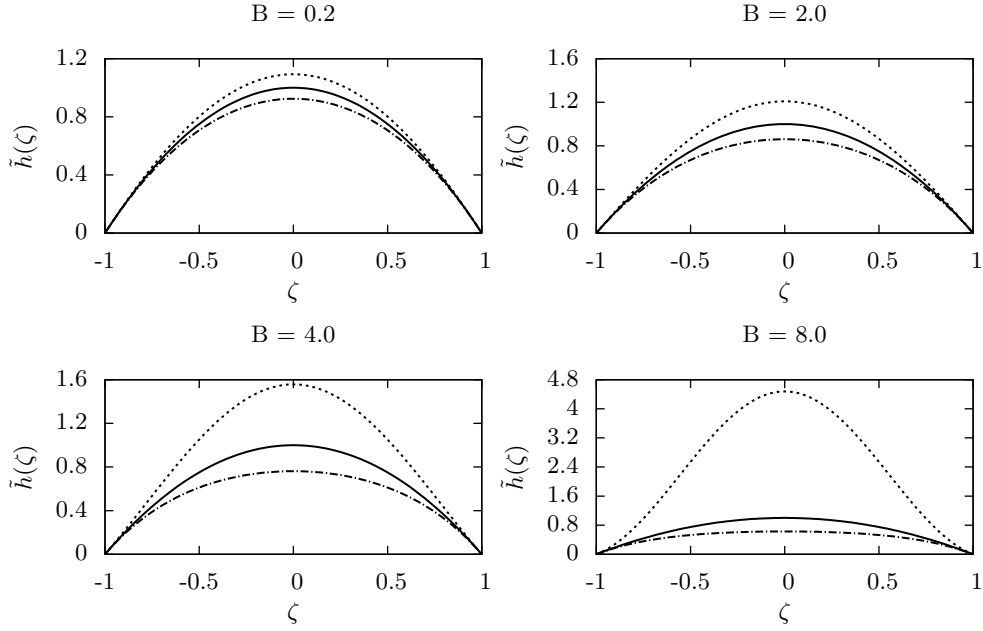


Figure 2. Scheme of the effects of changes in the Bond number on the rivulet GL interface shape. In the case (i) (---), the interface is flattened as the gravity effects grows stronger in comparison with the surface tension. In the case (iii) (.....) the increase of B has the narrowing effect on the rivulet GL interface. Case (ii) (—) is depicted for reference. Rivulet contact angle and semi-width are fixed at $\beta = 0.05$ and $a = 0.01$ m.

where B is the Bond number of the problem, defined as $B = a^2 \rho g |\cos \alpha| / \gamma$, representing the ratio of volume and surface forces in the rivulet and ζ is the y coordinate non-dimensionalized by the rivulet half-width, $\zeta = y/a$.

In addition, a multiplication factor useful for non-dimensionalization of the rivulet height arises from the case (ii) in the equation (3),

$$\tilde{h}(\zeta) = \frac{2h(\zeta)}{a \tan \beta} \quad (4)$$

Case (iii) of the solution (3) has a singularity at $B = \pi^2$ and thus is only sensible if B is restricted by $0 \leq B \leq \pi^2$. The singularity corresponds to the dripping of the liquid from the plate which occurs at high B, when the surface tension forces are not strong enough to keep the rivulet in contact with the plate. The effects of changes in the Bond number on the GL interface shape are depicted in the Fig. 2.

With the liquid volumetric flux taken as a fixed parameter, the rivulet half width, a , and its apparent contact angle, β , are bonded with the relation,

$$\frac{Q}{a} = \int_{-1}^1 \int_0^{h(\zeta)} u(\zeta, z) dz d\zeta = \int_{-1}^1 \int_0^{h(\zeta)} \frac{\rho g \sin \alpha}{2\mu} (2h(\zeta)z - z^2) dz d\zeta. \quad (5)$$

After the integration, one obtains the following equation for the rivulet contact angle and half width,

$$\frac{\mu Q}{a^4 \rho g \sin \alpha \tan^3 \beta} = F(B) \quad (6)$$

and

$$F(B) = \begin{cases} \frac{54\sqrt{B} \cosh \sqrt{B} + 6\sqrt{B} \cosh 3\sqrt{B} - 27 \sinh \sqrt{B} - 11 \sinh 3\sqrt{B}}{36B^2 \sinh^3 \sqrt{B}} & (i) \\ \frac{4}{105} & (ii) \\ \frac{27 \sin \sqrt{B} + 11 \sin 3\sqrt{B} - 54\sqrt{B} \cos \sqrt{B} - 6\sqrt{B} \cos 3\sqrt{B}}{36B^2 \sin^3 \sqrt{B}} & (iii) \end{cases} \quad (7)$$

Again, the liquid volumetric flow rate can be non-dimensionalized using the expression for the flow rate on a vertical plate,

$$\tilde{Q} = \frac{105\mu}{4a^4 \rho g \sin \alpha \tan^3 \beta} Q = \frac{105\rho g \mu \cos^2 \alpha}{4\gamma^2 \sin \alpha \tan^3 \beta B^2} \frac{Q}{B^2}. \quad (8)$$

The dependence of the liquid dimensionless flow rate, \tilde{Q} , on the plate inclination angle, α , is shown in the Fig. 3 (a) and the dependence of \tilde{Q} on the rivulet Bond number, B , in the Fig. 3 (b).

In the Fig. 3 (b), a different asymptotic behavior of the solution can be observed for the cases of a rivulet flowing on, (i), and under, (iii), an inclined plate,

$$\begin{aligned} (i) : \quad & \lim_{B \rightarrow \infty} \tilde{Q}(B) = 0 \\ (iii) : \quad & \lim_{B \rightarrow \pi_-^2} \tilde{Q}(B) = \infty \end{aligned} \quad (9)$$

Moreover, for rivulet flowing down a vertical plate or for a rivulet with neglectable effects of the gravity on its GL interface shape, the equation (6) can be solved analytically to obtain the following explicit relation between a and β ,

$$a = \eta \frac{1}{\tan^{3/4} \beta}, \quad \eta = \left(\frac{4\mu Q}{105\rho g \sin \alpha} \right)^{\frac{1}{4}}. \quad (10)$$

For the other cases, the equation (6) has to be solved numerically.

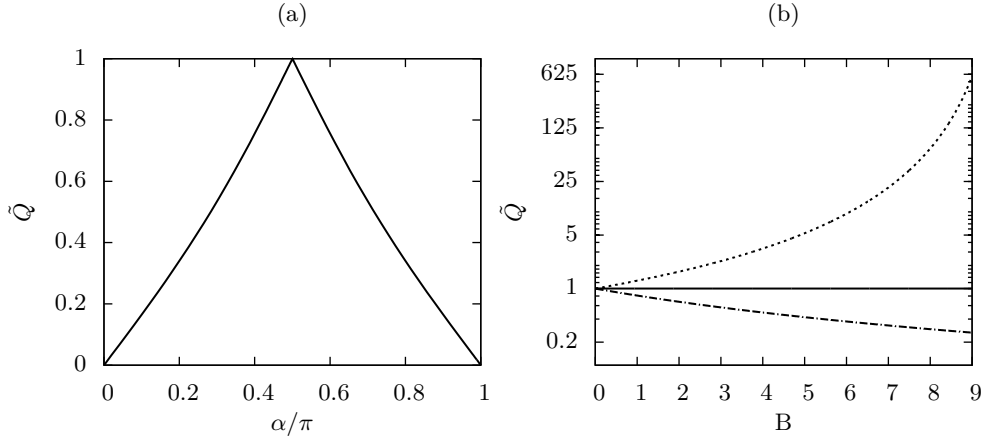


Figure 3. Dependence of the dimensionless flow rate, \tilde{Q} , on the plate inclination angle, (a), and on the Bond number, (b). In the Figure on the right side are distinguished the three different cases, (i) for $\alpha < \pi/2$ (---), (ii) for $\alpha = \pi/2$ (—) and (iii) for $\alpha > \pi/2$ (.....).

3.2 Spreading rivulet

In the previous section, the GL interface shape of a rectilinear steady rivulet was studied. In this section, the obtained results are used to locally describe the GL interface shape of a spreading rivulet. The local descriptions are bounded together by the Cox-Voinov law to obtain an approximate shape of the GL interface of a spreading rivulet.

The difference between a static, uniform, rivulet and the spreading one is in the formulation of the boundary conditions (2). For a static rivulet, β and a are constant all along the rivulet but for a spreading rivulet, these two become functions of the problem longitudinal coordinate, x .

Hence, for being able to profit from the solution for an uniform rivulet, it is necessary to provide a relation for the evolution of $\beta(x)$ and $a(x)$ along the rivulet.

In the review [23], the Cox-Voinov law for the case of a symmetric 2D object spreading on a horizontal substrate was derived in the form,

$$\beta(t)^3 = 9 \frac{da(t)}{dt} \frac{\mu}{\gamma} \ln \left(\frac{a(t)}{2e^{2l}} \right), \quad (11)$$

with $a(t)$ being the object characteristic dimension. For the case of a narrow axially symmetric stripe of a liquid, $a(t)$ represents its half width.

The resulting equation is a first order ordinary differential equation for two unknown functions, $\beta(t)$ and $a(t)$ and one free parameter, l , corresponding to the intermediate region length scale (see Fig. 1 and [21–23]).

In the case of a steady rivulet of a liquid flowing and spreading down an inclined wetted plate, the time coordinate in (11) can be transformed in the spatial coordinate, x .

Neglectable effects of the gravity The main thought of the modeling of a spreading rivulet GL interface is described using the simplest case of a vertical plate, or neglectable effects of gravity on the GL interface shape. With an assumption of a small contact angles all along the rivulet, $\beta(x) \ll 1, \forall x \in \langle 0; L \rangle$, the equation (10) can be simplified to

$$a \doteq \eta \frac{1}{\beta^{3/4}}. \quad (12)$$

Substituting for a from (12) to (11), one arrives at

$$\beta^{19/4} = -A \frac{d\beta}{dt} \ln \left(\frac{B}{\beta^{3/4}} \right), \quad \beta = \beta(t), \quad A = \frac{27}{4} \frac{\eta\mu}{\gamma}, \quad B = \frac{\eta}{2e^2 l}. \quad (13)$$

Solution of (13) yields an implicit relation for $\beta(t)$,

$$t - \frac{4}{15} \frac{A}{\beta_0^{15/4}} \left[\ln \left(\frac{B}{\beta^{3/4}} \right) - \frac{1}{5} \right] + C = 0. \quad (14)$$

The integration constant, C , is specified by the initial condition, $\beta(0) = \beta_0$,

$$C = \frac{4}{15} \frac{A}{\beta_0^{15/4}} \left[\ln \left(\frac{B}{\beta_0^{3/4}} \right) - \frac{1}{5} \right]. \quad (15)$$

Now, let us take the three phase point of one transversal cut through the rivulet and denote it as τ . The equation (14) describes the movement of τ in the direction of the y axis in time and the effects of this movement on the shape of the 2D GL interface of the chosen transversal cut.

For the description of the rivulet interface shape along the plate, the relation between the movement of τ in time and the movement of the chosen transversal cut along the plate has to be established.

The presented transformation from time to spatial coordinate arises from the last assumption in Coordinate system and simplifying assumptions (see page 104). We assume the presence of a precursor film of thickness equal to the intermediate region length scale, l , on the whole plate. Neglecting the long-range intermolecular forces, this precursor film can be taken as a free falling

film. The point τ is then considered not to be directly on the three phase line, as there is, in fact none, but in the height l above the plate. Hence, τ is moving along x axis with the speed of

$$u_\tau = \frac{\rho g \sin \alpha}{2\mu} l^2. \quad (16)$$

Using this estimate for the speed of τ , the needed transformation is,

$$t = \varpi x, \quad \varpi = \frac{2\mu}{\rho g \sin \alpha l^2}. \quad (17)$$

Substitution for t from (17) to (14) yields the equation defining the shape of the rivulet GL interface in the dependence on the plate longitudinal coordinate, x ,

$$x - \frac{\bar{A}}{\beta^{15/4}} \left[\ln \left(\frac{B}{\beta^{3/4}} \right) - \frac{1}{5} \right] + \bar{C} = 0, \quad \bar{A} = \frac{4}{15} \frac{A}{\varpi}, \quad \bar{C} = \frac{4}{15} \frac{C}{\varpi}. \quad (18)$$

With effects of the gravity If effects of the gravity on the shape of the rivulet GL interface cannot be neglected, specification of the interface shape becomes substantially more complicated. For the cases (i) and (iii), the equation (6) cannot be solved analytically and we cannot substitute for $a = a(\beta)$ in (11) as the relation is defined implicitly.

In the consequence, the equation (11) has to be solved numerically in the transformed coordinates $x = t/\varpi$. Moreover, the non-linear algebraic equation (6), defining the local contact angle $\beta = \beta(a(x))$, has to be solved in each iterator step.

Dimensionless coordinates and simulations All the variables except x were non-dimensionalized using the values at $x = 0$. For the non-dimensionalization of the plate longitudinal coordinate, x , the plate length, L , was used,

$$\xi = \frac{x}{L}, \quad \zeta = \frac{y}{a_0}, \quad \tilde{h} = \frac{h}{h_0^0}, \quad \tilde{\beta} = \frac{\beta}{\beta_0}, \quad (19)$$

where a_0 and β_0 are the rivulet halw-width and dynamic contact angle at $\xi = 0$ tight together by the condition of a prescribed volume flux (6) and h_0^0 is the rivulet height at $\zeta = \xi = 0$. As the rivulet is spreading down the plate, $\tilde{\beta}(\xi)$ is decreasing and $B(\xi)$ together with $\tilde{a}(\xi)$, are increasing as it is shown in the Fig. 4.

For the case of the plate inclination angle, α , greater than $\pi/2$, it can be seen, that the flow Bond number converges towards π^2 as the dynamic contact

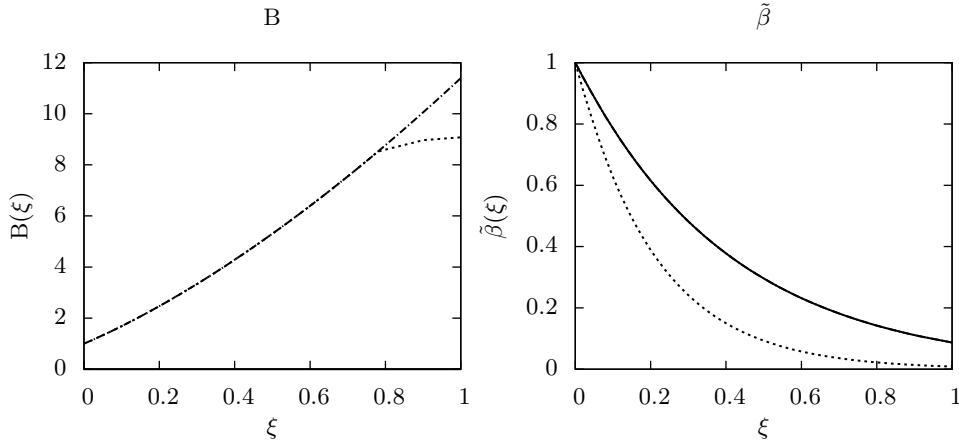


Figure 4. Change in the Bond number, $B(\xi)$, and in the reduced dynamic contact angle, $\tilde{\beta}(\xi)$, along the rivulet. The three cases, (i) (---), (ii) (—) and (iii) (····) are shown.

angle, $\tilde{\beta}$, vanishes. This corresponds to the fact, that for the case (iii), the GL interface is pulled from the plate by the gravity and

$$\lim_{\xi \rightarrow K \in \mathbb{R}^+} \tilde{\beta}(\xi) = 0, \quad (20)$$

meaning that at some finite distance, K , from the plate top, the surface tension and gravity forces reach an equilibrium and the spreading stops. This also follows directly from the analysis of the driving force for the spreading in the equation (11),

$$\frac{da(t)}{dt} = 0 \iff \beta(t) = 0. \quad (21)$$

During the simulations, we considered a shallow water rivulet on a wetted substrate. The volume flux in the rivulet was fixed at $Q = 0.01 \text{ ml s}^{-1}$, the initial dynamic contact angle at $\beta_0 = 0.05 \ll 1$ and the rivulet initial half-width, a_0 , was specified by the prescribed condition of $B = 1$ at $x = 0$. The inclined plate length, L , was taken equal to 0.1 m.

The remaining parameter of the model: the intermediate region length scale, l , was fixed at $l = 3 \cdot 10^{-5} \text{ m}$. The selection of the value of l was based on our previous work, [25, 26], and is in the agreement with literature on the topic (see [22, 27] and references therein).

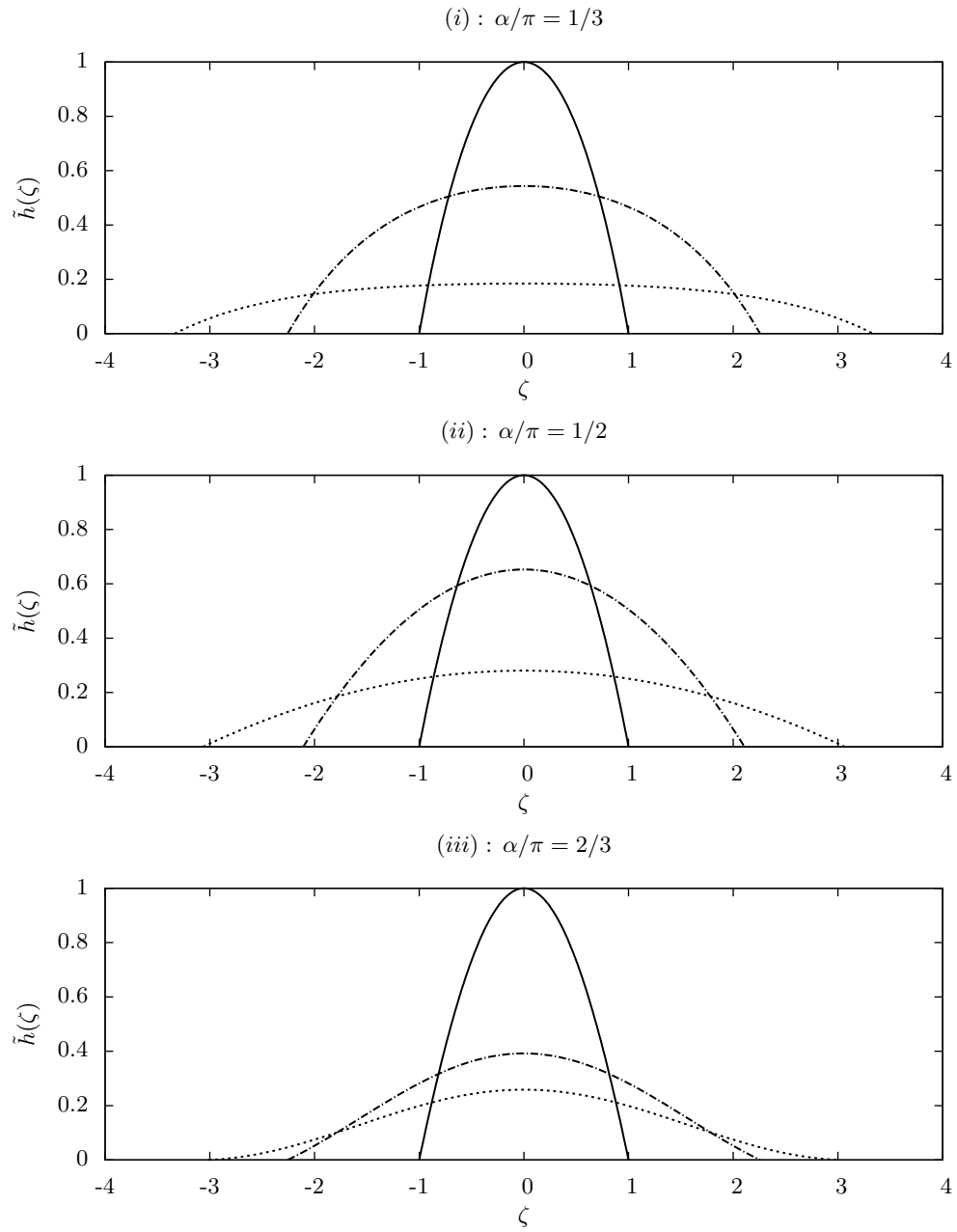


Figure 5. Evolution of the GL interface shape along the dimensionless plate longitudinal coordinate, ξ . Shapes of transversal cuts through the rivulet for the three cases are depicted at $\xi = 0$ (---), $\xi = 1/2$ (—) and $\xi = 1$ (.....).

4 Velocity field

The velocity field in a steady rectilinear rivulet with unidirectional flow of a liquid is in a form of $\mathbf{u} = u(y, z)$. With the assumptions listed in Sec. 2, the velocity field can be derived analytically by solving the Navier-Stokes equations [6, 11]. The obtained solution is in the form (consult the equation (5)),

$$u(\zeta, z) = \frac{\rho g \sin \alpha}{2\mu} (2h(\zeta)z - z^2). \quad (22)$$

However, let us now consider a spreading but locally rectilinear rivulet. The velocity field of such a rivulet consists of all the three components, $\mathbf{u}(\mathbf{x}) = (u(\mathbf{x}), v(\mathbf{x}), w(\mathbf{x}))$.

The u component of the velocity field is approximately defined, at each discrete point of the solution of the ODE (11), by the relation (22). The contours of the u velocity component in the water rivulet spreading down a plate inclined by an angle $\alpha = \pi/3$ to the horizontal are depicted in the Fig. 6. Further information on the selection of the simulation parameters can be found in the paragraph Dimensionless coordinates and simulations in the previous section. The u velocity field component was scaled using the velocity of the GL interface at the rivulet centerline, $\zeta = 0$, at the plate top, $\xi = 0$.

As for the v and w components of the velocity field, the presented method does not provide any approximate analytical solution. Thus, those two velocity components have to be simulated numerically. A technique similar to particle image velocimetry (PIV) was chosen.

PIV is an experimental technique which allows the velocity of fluid to be simultaneously measured throughout a region illuminated by a two-dimensional light sheet. Seeding particles are introduced into the flow and their motion is used to estimate the kinematics of the local fluid [24].

As the performed experiments were numerical, the seeding particles were defined artificially in a mesh-like manner. An algorithm for following the evolution of the v and w velocity field components is described below. The whole proposed cycle has to be repeated for all N transversal cuts of the rivulet placed at $i \delta \xi$ from the plate top, where $i = 1, 2, \dots, N$ and $\delta \xi$ is the time (distance) step prescribed by the solver used to treat the equation (11).

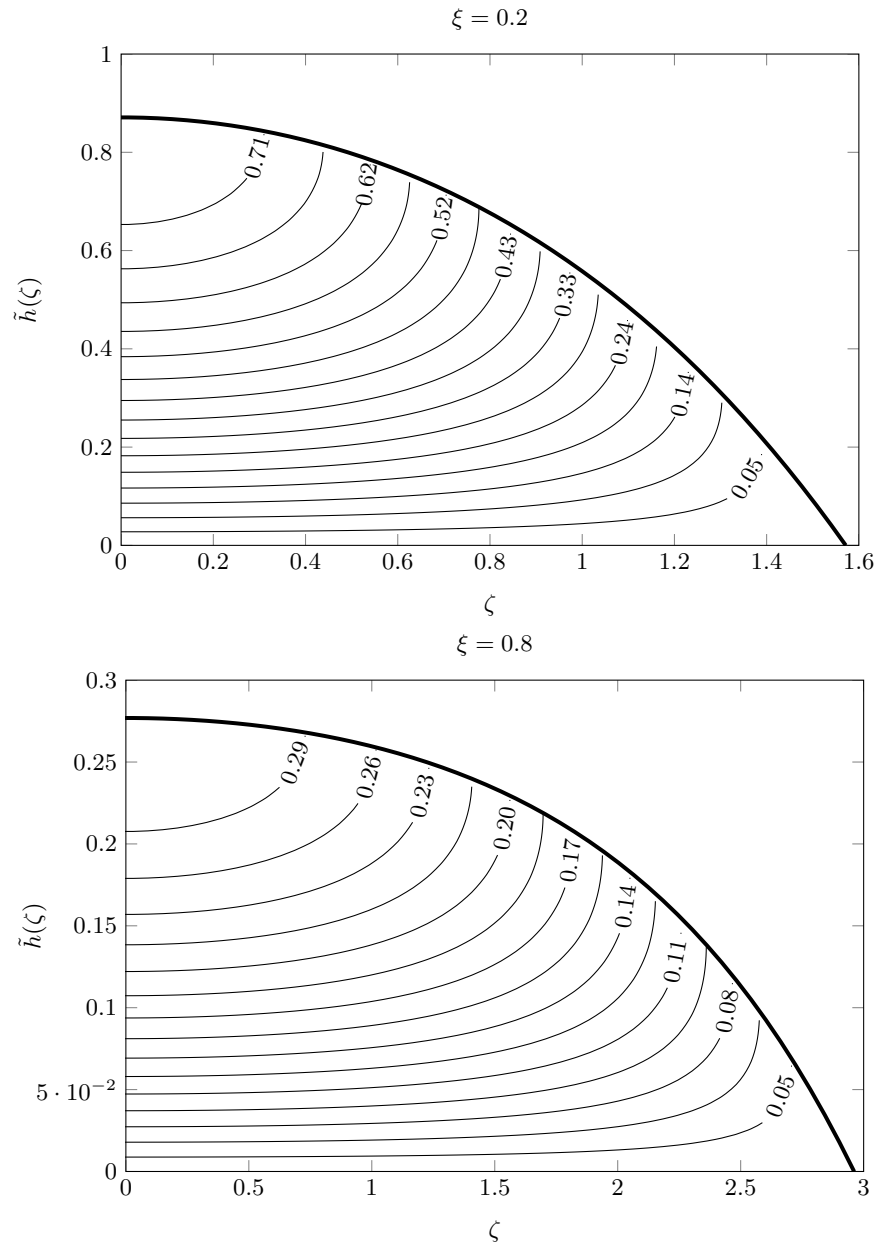


Figure 6. Contour plots of the \tilde{u} component of the velocity field in a water rivulet flowing down a plate inclined by an angle $\alpha = \pi/3$ to the horizontal. For more details on the simulation see the paragraph Dimensionless coordinates and simulations in the previous section. The cases of $\xi = 0.2$ and $\xi = 0.8$ are shown.

Velocity field tracking algorithm

- For each subrivulet do:
 1. Get the current width of the rivulet, ζ_i , from solution of the ODE (11).
 2. Calculate the current maximal rivulet height, \tilde{h}_i^0 , from the equation (3).
 3. Create a mesh on a domain Ω_i ,

$$\Omega_i = \{ (\zeta, \tilde{z}) : \zeta \in \langle 0; \zeta_i \rangle \mid \tilde{z} \leq \tilde{h}_i(\zeta) \}. \quad (23)$$

The domain Ω_i represents a right half of the rivulet at a distance $i \delta \xi$ from the plate top. The left side of the rivulet can be neglected as the problem is axisymmetric along the x axis. The mesh itself is obtained by discretizing the domain Ω_i equidistantly in each coordinate by M_1 and M_2 points, respectively. The set of discrete points, Ω_i^h , is obtained,

$$\Omega_i^h = \{ (\zeta^j, \tilde{z}^k) : \zeta^j \in \langle 0; \zeta_i \rangle \mid \tilde{z}^k \leq \tilde{h}_i(\zeta^j) \}_{j=1, \dots, M_1; k=1, \dots, M_2} \quad (24)$$

4. Save the current mesh, Ω_i^h .
- Having saved all the local meshes, Ω_i^h , $i = 1, \dots, N$, the velocity field in the $\zeta - \tilde{h}$ plane between individual transversal cuts can be calculated evaluating the change in the position of each mesh point along the rivulet.

In the Fig. 7, there are depicted the resulting velocity fields for the distances from the plate top $\xi = 0.2$ and $\xi = 0.8$ and the plate inclination angle $\alpha = \pi/3$. The slow down of the spreading can be observed as the contact angle, β , decreases.

Another interesting observation would be the fact, that the increase in the rivulet width is substantially quicker than the decrease in its height. This is due to the prescribed constant liquid flow rate and the parabolic velocity profile in the x axis direction.

5 Conclusion

Even with the continuous growth of the computing capacity of modern computers, there is still a need for simplified solutions to the complex problems of fluid mechanics. Such method for the simulation of a rivulet spreading down an inclined wetted plate was derived and used to study the dependence of the liquid flow properties on various process parameters. Moreover, the derived model was used to describe the spreading itself and the evolution of the flow along an inclined plate without the necessity of solving the corresponding system of Navier-Stokes partial differential equations with a complex boundary condition describing the behaviour of the three phase line.

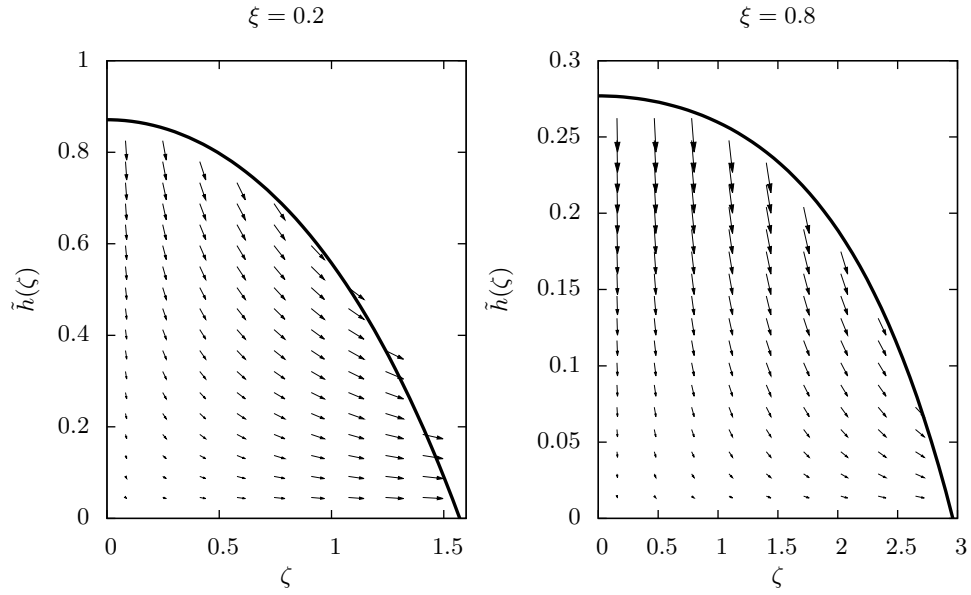


Figure 7. Comparison of the velocity fields in the $\zeta - \tilde{h}$ plane at $\xi = 0.2$ and $\xi = 0.8$. The case of a rivulet flowing down a plate inclined by $\alpha = \pi/3$ to the horizontal is depicted.

Nomenclature

a [m]	half-width of the rivulet	Greek letters α [-]	plate inclination angle
A, B, C , [s, -, -, -] constants	β [-] dynamic contact angle
B [-] Bond number	γ [N m ⁻¹] liquid surface tension
e [-] Euler's constant	δ [-] small difference
g [m s ⁻²] gravitational acceleration	η [m] constant defined in the equation (10)
h [m] height	ζ, ξ [-] dimensionless x, y coordinates
l [m] intermediate region length scale	μ [Pa s] liquid dynamic viscosity
L [m] total rivulet length	ϖ [m ⁻¹ s] transformation from t to x
M_1, M_2 [-] number of meshpoints	ρ [kg m ⁻³] liquid density
N [-] number of consecutive cuts	τ [-] contact point for 2D interface
p [Pa] pressure	Ω [-] domain of the rivulet transversal cut
Q [m ³ s ⁻¹] volumetric flow rate		
S [m ²] size of the interface		
t [s] time coordinate		
(u, v, w) [m s ⁻¹] velocity field		
x, y, z [m] coordinate system		

References

1. J. J. COOKE, S. GU, L. M. ARMSTRONG, K. H. LUO, *Gas-liquid flow on smooth and textured inclined planes*, World Ac. of Sc., Eng. and Technol., Vol.68. (2012), pp.1712-1719.
2. R. MAITI, R. KHANNA, K.D.P. NIGAM, *Hysteresis in trickle-bed reactors: a review*, Ind. Eng. Chem. Res., Vol.45. (2006), pp.5185-5198.
3. P. VLASOGIANNIS, G. KARAGIANNIS, P. ARGYROPOULOS, V. BONTOZO-GLOU, *Airwater two-phase flow and heat transfer in a plate heat exchanger*, Int. J. Multiph Flow, Vol.25. (2002), pp.757-772.
4. S.F. KISTLER, P.M. SCHWEIZER (EDS.). *Liquid Film Coating*, Chapman and Hall, London, (1997)
5. A. ATAKI, P. KOLB, U. BÜHLMAN, H. J. BART, *Wetting performance and pressure drop of structured packing: CFD and experiment*, I. Chem. E. – symp. series, Vol.152. (2009), pp.534-543.
6. G.D. TOWELL, L.B. ROTHFELD, *Hydrodynamics of rivulet flow*, A. I. Ch. E. J., Vol.12. (1966), pp.972-980.
7. R.F. ALLEN, C.M. BIGGIN, *Longitudinal flow of a lenticular liquid filament down an inclined plane*, Phys. Fluids, Vol.17. (1974), pp.287-291.
8. M. BENTWICH, D. GLASSER, J. KERN, D. WILLIAMS, *Analysis of rectilinear rivulet flow*, A. I. Ch. E. J., Vol.22. (1976), pp.772-779.
9. I. M. FEDOTKIN, G. A. MELNICHUK, F. F. KOVAL, E. V. KLIMKIN, *Hydrodynamics of rivulet flow on a vertical surface*, Inz.-Fiz. Zhurnal, Vol.46, No.1. (1984), pp.14-20.
10. E.S. BENILOV, *On the stability of shallow rivulets*, J. Fluid Mech., Vol.636. (2009), pp.455-474.
11. B.R. DUFFY, H.K. MOFFATT, *Flow of a viscous trickle on a slowly varying incline* Chem. Eng. J., Vol.60. (1995), pp.141-146.
12. P.A. KUIBIN, *An asymptotic description of the rivulet flow along an inclined cylinder*, Russ. J. Eng. Thermophys., Vol.6. (1996), pp.33-45.
13. C. A. PERAZZO, J. GRATTON, *Navier-Stokes solutions for parallel flow in rivulets on an inclined plane*, J. Fluid Mech., Vol.507. (2004), pp.367-379.
14. S. K. WILSON, J. M. SULLIVAN, B. R. DUFFY, *The energetics of the breakup of a sheet and of a rivulet on a vertical substrate in the presence of a uniform surface shear stress*, J. Fluid Mech., Vol.674. (2011), pp.281-306.
15. C. PATERSON, S. K. WILSON, B. R. DUFFY, *Pinning, de-pinning and re-pinning of a slowly varying rivulet*, Eur. J. Mech. B/Fluids, Vol.41. (2013), pp.94-108.
16. S.H. DAVIS, *Moving contact lines and rivulet instabilities, Part 1. The static rivulet*, J. Fluid Mech., Vol.90. (1980), pp.225-242.
17. S. A. SHETTY, R. L. CERRO *Spreading of liquid point sources over inclined solid surfaces* Ind. Eng. Chem. Res., Vol.34. (1995), pp. 4078-4086.
18. M. RENARDY, Y. RENARDY, J. LI, *Numerical simulation of moving contact line problems using a volume-of-fluid method*, J. Comp. Phys., Vol.171. (2001), pp.243-263.
19. K. V. MEREDITH, A. HEATHER, J. DE VRIES, Y. XIN, *A numerical model for partially-wetted flow of thin liquid films*, Comp. Meth. Multiph. Flow, Vol.70. (2011), pp.239-250.
20. J. A. DIEZ, A. G. GONZALES, L. KONDIC, *On the breakup of fluid rivulets*, Phys. Fluids, Vol.21. (2009), pp.1-15.

21. O. V. VOINOV, *Hydrodynamics of wetting*, Fluid Dyn., Vol.11. (1976), pp.714-721 (English translation).
22. R. G. COX, *The dynamics of spreading of liquids on a solid surface. Part 1. Viscous flow*, J. Fluid Mech., Vol.168 (1986), pp.169-194.
23. D. BONN, J. EGGERS, J. INDEKEU, J. MEUNIER, E. ROLLEY, *Wetting and spreading*, Rev. Mod. Phys., Vol.81. (2009), pp.739-805.
24. I. GRANT, *Particle image velocimetry: a review*, Proc. Inst. Mech. Engrs., Vol.211. (1997), pp.55-76.
25. M. ISOZ, *Study of the rivulet type flow of a liquid on an inclined plate*, Master thesis, ICT Prague, 2013
26. M. ISOZ, *Computationally inexpensive method to determine size of gas-liquid interfacial area of rivulet spreading on inclined wetted plate*, Proceedings of conference *Topical problems of fluid mechanics 2014*, Prague (2014), pp.59-62.
27. S. MIDDLEMAN, *Modeling axisymmetric flows*, Academic Press, London, 1995

Acknowledgments: The presented work was supported by IGA of ICT Prague, under the grant number A2_FCHI_2014_001.

On a Toeplitz structure of the characteristic polynomials

Drahoslava Janovská¹ and Gerhard Opfer²

Institute of Chemical Technology, Prague, Czech Republic¹
University of Hamburg, Faculty for Mathematics, Informatics, and Natural Sciences,
Hamburg, Germany ²

Keywords: Symmetric functions, characteristic polynomials, minimal polynomials, partitions, traces, Toeplitz form, characteristic polynomials of chemical graphs.

Abstract The $n + 1$ coefficients of the characteristic polynomial of a fixed real or complex matrix of order n can be expressed as a linear combination of products of traces of that matrix. We show that these coefficients form a matrix that has Toeplitz form. As tools we will be using results related to elementary, symmetric functions and to partitions. There will be a separate investigation on how to compute the trace formula for the determinant. Finally, we apply the theory to characteristic polynomials of chemical graphs.

1 Introduction

There exist investigations that show that a determinant of a matrix of order n can be expressed in form of a linear combination of all products of traces of fixed degree n . See Abramowitz-Stegun, [1]. For computing the trace formula for a determinant, we will alternatively develop a linear system of equations, the solution of which gives the wanted linear combination of the product of traces. In comparison with the standard algebraic manipulation (e.g. Krishnapriyan, [8]) of elementary, symmetric functions, the method is extremely simple and fast. We will show that it is sufficient to know the trace representation for the determinant up to order n , in order to find all coefficients of the corresponding characteristic polynomials up to degree n , due to a Toeplitz form of these formulas.

Throughout the paper, we will use the notation \mathbb{R}, \mathbb{C} for the field of real and complex numbers, respectively. And \mathbb{K} will stand for \mathbb{R} or \mathbb{C} . We also use \mathbb{Z} for the integers and \mathbb{N} for the positive integers. The set of matrices with m rows and n columns over \mathbb{K} will be denoted by $\mathbb{K}^{m \times n}$. We will mostly be concerned with square matrices of order n .

Let $\mathbf{A} \in \mathbb{K}^{m \times n}$ with entries a_{jk} , $j = 1, 2, \dots, m$; $k = 1, 2, \dots, n$. We say that \mathbf{A} has *Toeplitz form* if $a_{jk} = a_{j+\ell, k+\ell}$ for all $\ell = 1, 2, \dots$ as long as $j + \ell \leq m$, $k + \ell \leq n$. In other words, \mathbf{A} has Toeplitz form, if the entries of \mathbf{A} are constant down the diagonals parallel to the main diagonal. Matrices in Toeplitz form are uniquely determined by the entries in the first column and first row. By the definition, all matrices which consist only of one column or of one row have Toeplitz form. Thus, the notion Toeplitz form is mainly of interest for square matrices or for matrices which are close to square matrices.

2 Elementary, symmetric functions

Let $t \in \mathbb{K}$ and let $x_1, x_2, \dots, x_n \in \mathbb{K}$ be parameters for a fixed $n \in \mathbb{N}$. Define

$$f(t) := f(t; x_1, x_2, \dots, x_n) := \prod_{j=1}^n (1 - x_j t) \quad (1)$$

$$= 1 - \sigma_1^{(n)} t + \sigma_2^{(n)} t^2 - \dots + (-1)^n \sigma_n^{(n)} t^n, \text{ where for } j = 1, 2, \dots, n, \quad (2)$$

$$\sigma_j^{(n)} := \sigma_j^{(n)}(x_1, x_2, \dots, x_n) = \sum_{1 \leq k_1 < k_2 < \dots < k_j \leq n} x_{k_1} x_{k_2} \dots x_{k_j}. \quad (3)$$

Examples are $\sigma_1^{(n)} = x_1 + x_2 + \dots + x_n$, $\sigma_n^{(n)} = x_1 x_2 \dots x_n$. The functions $\sigma_j^{(n)}$, $j = 1, 2, \dots, n$, are called *elementary, symmetric functions* of the variables x_1, x_2, \dots, x_n . They are polynomials in n variables, where each term has the same degree j (thus, called *elementary*) and they are invariant under arbitrary permutations of the n variables (thus, called *symmetric*).

We define another, related function

$$g(t) := g(t; x_1, x_2, \dots, x_n) := t^n f\left(\frac{1}{t}\right) = t^n \prod_{j=1}^n \left(1 - \frac{x_j}{t}\right) = \prod_{j=1}^n (t - x_j) \quad (4)$$

$$= t^n - \sigma_1^{(n)} t^{n-1} + \sigma_2^{(n)} t^{n-2} - \dots + (-1)^{n-1} \sigma_{n-1}^{(n)} t + (-1)^n \sigma_n^{(n)}. \quad (5)$$

The apparent singularity of g at $t = 0$ is removable. Let $\mathbf{A} \in \mathbb{K}^{n \times n}$ with eigenvalues $\lambda_1, \lambda_2, \dots, \lambda_n$ and \mathbf{I} the identity matrix of the same size as \mathbf{A} . Then, the characteristic polynomial of \mathbf{A} is defined by

$$\chi_{\mathbf{A}}(t) := \det(t\mathbf{I} - \mathbf{A}) = \prod_{j=1}^n (t - \lambda_j) = g(t; \lambda_1, \lambda_2, \dots, \lambda_n) \quad (6)$$

$$= t^n - \sigma_1^{(n)} t^{n-1} + \sigma_2^{(n)} t^{n-2} - \dots + (-1)^{n-1} \sigma_{n-1}^{(n)} t + (-1)^n \sigma_n^{(n)} \quad (7)$$

where all $\sigma_j^{(n)}$, $j = 1, 2, \dots, n$, depend on $\lambda_1, \lambda_2, \dots, \lambda_n$. The polynomial $\chi_{\mathbf{A}}$, defined in (6), (7) is *monic*, which means that the coefficient of the highest

term, t^n , is one, which implies that $\chi_{\mathbf{A}}$ can never vanish identically. One of the important properties of $\chi_{\mathbf{A}}$ is expressed in the theorem by Cayley-Hamilton which says that

$$\chi_{\mathbf{A}}(\mathbf{A}) = \mathbf{A}^n - \sigma_1^{(n)} \mathbf{A}_{n-1} + \cdots + (-1)^{n-1} \sigma_{n-1}^{(n)} \mathbf{A} + (-1)^n \sigma_n^{(n)} \mathbf{I} = \mathbf{0}, \quad (8)$$

where $\mathbf{0}$ is the zero matrix of order n . See Horn and Johnson, [5]. A common technique to compute all coefficients $(-1)^j \sigma_j^{(n)}(\lambda_1, \lambda_2, \dots, \lambda_n)$, $j = 1, 2, \dots, n$, without using the eigenvalues is given by Leverrier (1840) and Faddejev (1949), see also Gantmacher's book, [4]. The algorithm uses $n - 1$ matrix \times matrix multiplications to compute all coefficients. It includes the computation of the determinant and of the inverse of \mathbf{A} if it exists. There is an extension by Schonhage, [10], to general fields of finite characteristic.

3 Partitions

Let n be a positive integer. In the sequel we will consider *monomials* in n variables x_1, x_2, \dots, x_n of the form

$$x_1^{k_1} x_2^{k_2} \cdots x_n^{k_n}, \quad 0 \leq k_j \leq k, j = 1, 2, \dots, n \text{ where } k = \sum_{j=1}^n k_j \quad (9)$$

is a fixed, nonnegative integer. We say, that the monomial has *degree* $d := k$. In order to determine all monomials of degree $d = k$ we have to find out all the possibilities of forming the sum $\sum_{j=1}^n k_j = k$. This brings us to the area of *partitions*.

Let n , as before, be a positive integer. The positive integer n can be written as a sum of *positive* integers

$$n = n_1 + n_2 + \cdots + n_\ell, \quad 1 \leq n_j \leq n, j = 1, 2, \dots, \ell \leq n \quad (10)$$

in various ways. Such a sum is called a *partition* of n . Let us assume that in (10) we use the order $n_1 \geq n_2 \geq \cdots \geq n_\ell$ for all possible partitions, then the number of all partitions is uniquely defined and the number of all such partitions is denoted by $p(n)$. Let us also agree that the list of all partitions is written in lexicographic order with respect to $1, 2, \dots$. Then, the whole list of all partitions including its order is uniquely defined. Let $\pi_j^{(n)}$ be the j th partition of n . For $n = 5$ we obtain the list

$$\underbrace{1+1+1+1+1}_{\pi_1^{(5)}} = \underbrace{2+1+1+1}_{\pi_2^{(5)}} = \underbrace{2+2+1}_{\pi_3^{(5)}} = \underbrace{3+1+1}_{\pi_4^{(5)}} = \underbrace{3+2}_{\pi_5^{(5)}} = \underbrace{4+1}_{\pi_6^{(5)}} = \underbrace{5}_{\pi_7^{(5)}}.$$

Thus, as a byproduct, we have $p(5) = 7$. Some examples are given in Table 1.

n	1	2	3	4	5	6	7	8	9	10	11	12	13	14	15	16	17
$p(n)$	1	2	3	5	7	11	15	22	30	42	56	77	101	135	176	231	297

Table 1. Partition numbers $p(n)$ for $1 \leq n \leq 17$

An algorithm for producing the whole list of partitions for a given positive integer n in the order described above is given by Zhogbi and Stojmenović, 1998, [14]. A more recent overview and a comparison of partition generating algorithms was given in 2009 by Kelleher and O’Sullivan, [7].

For later purpose we need some more notation. We associate with every $\pi_j^{(n)}$ an integer vector of length n , denoted by

$$\mu_j^{(n)} := (m_1, m_2, \dots, m_n), \quad j = 1, 2, \dots, p(n), \quad (11)$$

which counts, in its k th component m_k , how often k appears in $\pi_j^{(n)}$, $1 \leq k \leq n$, $0 \leq m_k \leq n$. For $n = 5$, we have $\mu_1^{(5)} = (5, 0, 0, 0, 0)$, $\mu_2^{(5)} = (3, 1, 0, 0, 0)$, $\mu_3^{(5)} = (1, 2, 0, 0, 0)$, $\mu_4^{(5)} = (2, 0, 1, 0, 0)$, $\mu_5^{(5)} = (0, 1, 1, 0, 0)$, $\mu_6^{(5)} = (1, 0, 0, 1, 0)$, $\mu_7^{(5)} = (0, 0, 0, 0, 1)$. The vector $\mu_j^{(n)} = (m_1, m_2, \dots, m_n)$, $j = 1, 2, \dots, p(n)$, has the property that $\sum_{k=1}^n m_k k = n$. For all $j = 1, 2, \dots, p(n)$, the sum

$$m := \sum_{k=1}^n m_k \quad (12)$$

is a count for the number of entries in $\pi_j^{(n)}$. It depends on n and on j and $1 \leq m \leq n$.

With the help of these numbers and the convention $0! := 1$ we construct a certain type of *multinomial coefficients* which are defined for a given partition $\pi_j^{(n)}$ by

$$M_j^{(n)} := \frac{n!}{1^{m_1} m_1! 2^{m_2} m_2! 3^{m_3} m_3! \dots n^{m_n} m_n!}, \quad j = 1, 2, \dots, p(n), \quad (13)$$

where the quantities m_k , $1 \leq k \leq n$, are defined in (11). For this definition see Abramowitz and Stegun, [1], and for numerical values for $n \leq 10$, denoted by M_2 , see Table 24.2 in [1]. Since $\mu_1^{(n)} = (n, 0, 0, \dots, 0)$, $\mu_2^{(n)} = (n-2, 1, 0, \dots, 0)$, $\mu_{p(n)-1}^{(n)} = (1, 0, 0, \dots, 0, 1, 0)$, $\mu_{p(n)}^{(n)} = (0, 0, 0, \dots, 1)$ for $n \geq 4$ we have

$$M_1^{(n)} = 1, M_2^{(n)} = \frac{(n-1)n}{2}, M_{p(n)-1}^{(n)} = (n-2)!n, M_{p(n)}^{(n)} = (n-1)! \quad (14)$$

for $n \geq 4$. For $n = 5$ the seven values of $M_j^{(5)}$ are: 1, 10, 15, 20, 20, 30, 24. We will return to the multinomial coefficients in the next section.

4 Properties of traces

Let $\mathbf{A} \in \mathbb{K}^{n \times n}$. Let us denote the diagonal elements of \mathbf{A} by $a_{11}, a_{22}, \dots, a_{nn}$. Then the *trace* of \mathbf{A} is denoted by tr and defined by

$$\text{tr}(\mathbf{A}) := \sum_{j=1}^n a_{jj}. \quad (15)$$

The trace is a linear function in the following sense: Let $\mathbf{A}, \mathbf{B} \in \mathbb{K}^{n \times n}$ be two matrices and let $\alpha, \beta \in \mathbb{K}$. Then

$$\text{tr}(\alpha\mathbf{A} + \beta\mathbf{B}) = \alpha\text{tr}(\mathbf{A}) + \beta\text{tr}(\mathbf{B}). \quad (16)$$

Let $\lambda_1, \lambda_2, \dots, \lambda_n$ be the eigenvalues of \mathbf{A} . Since the eigenvalues of \mathbf{A}^k , $k = 1, 2, \dots$ are $\lambda_1^k, \lambda_2^k, \dots, \lambda_n^k$, we have

$$t_k := \text{tr}(\mathbf{A}^k) = \sum_{j=1}^n \lambda_j^k, \quad k = 1, 2, \dots, \quad (17)$$

which means that $t_k = \sum_{j=1}^n \lambda_j^k$ can be computed only on the base of the matrix elements of \mathbf{A} . Another central property of the trace is, that it is defined for matrices of all orders. We will say that t_k has the *degree* $d := k$ and that the product $t_{k_1} \cdot t_{k_2} \cdots t_{k_\ell}$ of traces has the degree $d := k_1 + k_2 + \dots + k_\ell$.

Example 1. Let $n = 2$ and $\mathbf{A} := (a_{jk})$, $j, k = 1, 2$, with eigenvalues λ_1, λ_2 . Then, the characteristic polynomial $\chi_{\mathbf{A}}$ of \mathbf{A} (see (7)) has the coefficients

$$\begin{aligned} -\sigma_1^{(2)} &= -(\lambda_1 + \lambda_2) = -(a_{11} + a_{22}) = -\text{tr}(\mathbf{A}) = -t_1, \\ \sigma_2^{(2)} &= \lambda_1 \lambda_2 = \det(\mathbf{A}) = \chi_{\mathbf{A}}(0) = \frac{1}{2}(t_1^2 - t_2). \end{aligned}$$

Let $n = 3$ and $\mathbf{A} := (a_{jk}), j, k = 1, 2, 3$, with eigenvalues $\lambda_1, \lambda_2, \lambda_3$. Then, the characteristic polynomial $\chi_{\mathbf{A}}$ of \mathbf{A} (see (7)) has the coefficients

$$\begin{aligned} -\sigma_1^{(3)} &= -(\lambda_1 + \lambda_2 + \lambda_3) = -(a_{11} + a_{22} + a_{33}) = -\text{tr}(\mathbf{A}) = -t_1, \\ \sigma_2^{(3)} &= \lambda_1\lambda_2 + \lambda_1\lambda_3 + \lambda_2\lambda_3 = \frac{1}{2}(t_1^2 - t_2) \\ -\sigma_3^{(3)} &= -\lambda_1\lambda_2\lambda_3 = -\det(\mathbf{A}) = \chi_{\mathbf{A}}(0) = -\frac{1}{6}(t_1^3 - 3t_1t_2 + 2t_3). \end{aligned}$$

Let $n = 4$ and $\mathbf{A} := (a_{jk}), j, k = 1, 2, 3, 4$, has eigenvalues $\lambda_1, \lambda_2, \lambda_3, \lambda_4$. Then, the characteristic polynomial $\chi_{\mathbf{A}}$ of \mathbf{A} (see (7)) has the coefficients

$$\begin{aligned} -\sigma_1^{(4)} &= -t_1, \\ \sigma_2^{(4)} &= \frac{1}{2}(t_1^2 - t_2), \\ -\sigma_3^{(4)} &= -\frac{1}{6}(t_1^3 - 3t_1t_2 + 2t_3), \\ \sigma_4^{(4)} &= \frac{1}{24}(t_1^4 - 6t_1^2t_2 + 3t_2^2 + 8t_1t_3 - 6t_4). \end{aligned}$$

We see that all coefficients $\sigma_j^{(k)}, k = 2, 3, j = 1, 2, \dots, k$, can be expressed by linear combinations of products of traces of degree j , and the trace formulas are the same for $j = 1, 2, 3$. If we include also the case $n = 1$ we have

$$\begin{aligned} \sigma_1^{(4)} = \sigma_1^{(3)} = \sigma_1^{(2)} = \sigma_1^{(1)} &= t_1, \\ \sigma_2^{(4)} = \sigma_2^{(3)} = \sigma_2^{(2)} &= \frac{1}{2}(t_1^2 - t_2), \\ \sigma_3^{(4)} = \sigma_3^{(3)} &= \frac{1}{6}(t_1^3 - 3t_1t_2 + 2t_3). \end{aligned} \tag{18}$$

The given equations mean that the corresponding functions in each equation can be evaluated by the same trace formula, though the domain of definition changes and the values cannot be compared, too.

We will see in the sequel, that the results of the Example 1 show a general feature: All coefficients of the characteristic polynomial can be expressed by linear combinations of products of traces. And, in addition, the $n - 1$ trace formulas for the coefficients of the characteristic polynomial for the case $n - 1$ agree with the first $n - 1$ trace formulas for the case n . Let $n \in \mathbb{N}$ and let $\pi_j^{(n)}$ be the j th partition of n , where $j = 1, 2, \dots, p(n)$, and $p(n)$ is the number of partitions of n . We define the following products of traces of degree n :

$$T_j^{(n)} := \prod_{k \in \pi_j^{(n)}} t_k, \quad j = 1, 2, \dots, p(n). \tag{19}$$

If $\pi_j^{(n)} = (k_1, k_2, \dots, k_\ell)$ then the above product is $T_j^{(n)} := t_{k_1} \cdot t_{k_2} \cdots t_{k_\ell}$. We summarize the results in the following two theorems.

Theorem 1. Let $\mathbf{A} \in \mathbb{K}^{n \times n}$ and let $T_j^{(n)}$ be defined as in (19). Then, there are integers $x_1, x_2, \dots, x_{p(n)}$, independent of \mathbf{A} (but dependent on n) such that

$$n! \det(\mathbf{A}) = \sum_{j=1}^{p(n)} x_j T_j^{(n)}. \quad (20)$$

The integers have the property that

$$\sum_{j=1}^{p(n)} x_j = 0 \quad \text{for } n > 1, \quad (21)$$

$$\sum_{j=1}^{p(n)} |x_j| = n!. \quad (22)$$

Proof :

In Abramowitz and Stegun, [1], the last entry of Ch. 24.1.2 is

$$n! \det(\mathbf{A}) = \begin{vmatrix} t_1 & 1 & 0 & \dots & 0 \\ t_2 & t_1 & 2 & \dots & \cdot \\ t_3 & t_2 & t_1 & \ddots & \cdot \\ \vdots & \vdots & \vdots & \ddots & n-1 \\ t_n & t_{n-1} & t_{n-2} & \dots & t_1 \end{vmatrix} = \sum_{j=1}^{p(n)} (-1)^{n-m} M_j^{(n)} T_j^{(n)}, \quad (23)$$

where $M_j^{(n)}$ is defined in (13) and m in (12). We even obtain an explicit formula for all x_j . In order to show (21) put $\mathbf{A} = (a_{jk})$ and $a_{11} = 1, a_{jk} = 0$ otherwise. Then all traces and all $T_j^{(n)}$ are one and $\det(\mathbf{A}) = 0$, which implies (21). For showing (22) choose $\mathbf{A} = \text{diag}(e_1, e_2, \dots, e_n)$ where e_j are the solutions of $x_n + 1 = 0$. Then $\det(\mathbf{A}) = (-1)^n$, and $\text{tr}(\mathbf{A}^k) = 0$ for $k = 1, 2, \dots, n-1$, and $\text{tr}(\mathbf{A}^n) = -n$ with the consequence that $T_j^{(n)} = 0$ for all $j = 1, 2, \dots, p(n) - 1$ and $T_{p(n)}^{(n)} = \text{tr}(\mathbf{A}^n) = -n$. The result follows from (20) and from the last formula in (14). ■

Remark 1. In Abramowitz and Stegun, [1], we find also an explicit expression for x_j , namely

$$x_j = (-1)^{n-m} M_j^{(n)}, \quad (24)$$

where $M_j^{(n)}$ are the multinomial coefficients, defined in (13), and m is the number of entries in $\pi_j^{(n)}$ defined in (12).

We will see that the knowledge of this formula is sufficient to compute all coefficients of the characteristic polynomial.

Lemma 1. *Let \mathbf{A} be a matrix of order $n \in \mathbb{N}$. Then, all coefficients $(-1)^j \sigma_j^{(n)}$ of the corresponding characteristic polynomial can be expressed by linear combinations of products of traces of degree $j = 1, 2, \dots, n$. Thus, the traces t_1, t_2, \dots, t_n determine the characteristic polynomial uniquely.*

Proof :

See, Krishnapriyan, 1995, [8]. ■

Theorem 2. *Let*

$$\sigma^{(n)} := (\sigma_n^{(n)}, \sigma_{n-1}^{(n)}, \dots, \sigma_1^{(n)}, \sigma_0^{(n)}), \quad \sigma_0^{(n)} := 1, \quad (25)$$

be the vector of the coefficients of the characteristic polynomial of degree n (omitting the signs) of a matrix of order n in the trace form, where $\sigma_n^{(n)}$ denotes the constant term of the characteristic polynomial. Then the corresponding trace formulas for a matrix of order $n + 1$ satisfy

$$\sigma^{(n+1)} = (\sigma_{n+1}^{(n+1)}, \sigma_n^{(n)}, \sigma_{n-1}^{(n)}, \dots, \sigma_1^{(n)}, \sigma_0^{(n)}) = (\sigma_{n+1}^{(n+1)}, \sigma^{(n)}). \quad (26)$$

Let us put the $j+1$ trace formulas of the coefficients listed in (25) for all matrices of order $j = 1, 2, \dots, n$ in row j of an $(n \times n+1)$ matrix, augmented by $n-j$ zeros, then this matrix, denoted by Σ , has Toeplitz form. The matrix Σ is completely described by the trace formulas for $\sigma_j^{(j)}, j = 1, 2, \dots, n$, or, in other words, by the entries of the first column of Σ . See the following table.

j							
1	$\sigma_1^{(1)}$	1	0	0	0	...	0
2	$\sigma_2^{(2)}$	$\sigma_1^{(1)}$	1	0	0	...	0
3	$\sigma_3^{(3)}$	$\sigma_2^{(2)}$	$\sigma_1^{(1)}$	1	0	...	0
4	$\sigma_4^{(4)}$	$\sigma_3^{(3)}$	$\sigma_2^{(2)}$	$\sigma_1^{(1)}$	1	...	0
\vdots	\vdots	\vdots	\vdots	\ddots	\ddots	\ddots	\vdots
$n-1$							$\sigma_1^{(1)}$ 1
n	$\sigma_n^{(n)}$	$\sigma_{n-1}^{(n-1)}$	$\sigma_{n-2}^{(n-2)}$...		$\sigma_2^{(2)}$	$\sigma_1^{(1)}$

Table 2. Coefficients of characteristic polynomials in the trace form

Proof :

The form of Σ is a consequence of (26). One has to show, that the corresponding trace formulas are the same for

$$\sigma_j^{(n+1)} \quad \text{and for } \sigma_j^{(n)}, \quad n \in \mathbb{N}. \quad (27)$$

Let $\mathbf{A} \in \mathbb{K}^{n \times n}$ be given with eigenvalues $\lambda_1^{(n)}, \lambda_2^{(n)}, \dots, \lambda_n^{(n)}, n \in \mathbb{N}$. The basic formula for $\sigma_j^{(n)}$ is given in (3). It reads here

$$\sigma_j^{(\nu)} = \sum_{1_1 < k_2 < \dots < k_j \leq \nu} \lambda_{k_1}^{(\nu)} \lambda_{k_2}^{(\nu)} \dots \lambda_{k_j}^{(\nu)}, \quad \nu \in \{n, n+1\},$$

and we have

$$t_1^j = (\lambda_1^{(\nu)} + \lambda_2^{(\nu)} + \dots + \lambda_\nu^{(\nu)})^j = t_j + \nu! \sigma_j^{(\nu)} + R,$$

where R can be expressed independently of ν by the same trace formula. ■

5 Minimal polynomial

Let $\mathbf{A} \in \mathbb{K}^{n \times n}$ and let $\chi_{\mathbf{A}}$ be its characteristic polynomial as defined in (6). One of the important properties of $\chi_{\mathbf{A}}$ is that it annihilates \mathbf{A} , see (8). There may be other monic polynomials of degree at most n which also annihilate \mathbf{A} . The uniquely defined monic polynomial with minimum degree ν which annihilates \mathbf{A} is called *minimal polynomial* of \mathbf{A} and is denoted by $\mu_{\mathbf{A}}$, see Horn and Johnson [5]. Let \mathbf{I} be the identity matrix of the same size as \mathbf{A} . Then,

$$\mathbf{A}^j \in \text{span}\{\mathbf{I}, \mathbf{A}, \mathbf{A}^2, \dots, \mathbf{A}^{\nu-2}, \mathbf{A}^{\nu-1}\}, \quad j = 0, 1, \dots, \quad (28)$$

where ν is the degree of the minimal polynomial of \mathbf{A} . Formula (28) means, that all powers $j > 0$ of \mathbf{A} , regardless of the size of j can be expressed by a linear combination of powers of degree at most $\nu - 1$. Or in other words, the powers $\mathbf{A}^j, j \in \mathbb{N}$, span a space of dimension ν . For formula (28) see Horn and Johnson, [5, 6]. In the next theorem we will explicitly determine the linear combination which describes the power \mathbf{A}^j .

Theorem 3. *Let $\mathbf{A} \in \mathbb{K}^{n \times n}$ with $n \geq 2$ be given and let*

$$\mu_{\mathbf{A}}(t) = \sum_{k=0}^{\nu} b_k^{(\nu)} t^k, \quad b_{\nu}^{(\nu)} = 1, \quad (29)$$

be its minimal polynomial. Then, for all integers $j \geq 0$, there are numbers $\beta_k^{(j)}, k = 0, 1, \dots, \nu - 1$, such that

$$\mathbf{A}^j = \sum_{k=0}^{\nu-1} \beta_k^{(j)} \mathbf{A}^k, \quad \text{where} \quad (30)$$

$$\beta_k^{(\ell)} := \delta_{\ell, k}, \quad \ell < \nu \quad (\delta_{\ell, k} = \text{Kronecker symbol}), \quad (31)$$

$$\beta_0^{(\ell+1)} := -\beta_{\nu-1}^{(\ell)} b_0^{(\nu)}, \quad (32)$$

$$\beta_k^{(\ell+1)} := \beta_{k-1}^{(\ell)} - \beta_{\nu-1}^{(\ell)} b_k^{(\nu)}, \quad k = 1, 2, \dots, \nu - 1, \ell = 0, 1, \dots, j - 1. \quad (33)$$

If the coefficients $b_k^{(\nu)}$ of the minimal polynomial are real, then also all $\beta_k^{(j)}$ are real.

Proof :

The Cayley-Hamilton theorem (see (8)) applied to (29) implies

$$\mathbf{A}^\nu = - \sum_{k=0}^{\nu-1} b_k^{(\nu)} \mathbf{A}^k .$$

If we multiply (30) by \mathbf{A} and replace \mathbf{A}^ν with the right hand side of the last equation we obtain the recursion (31) to (33). That real $b_k^{(\nu)}$ imply real $\beta_k^{(j)}$ is obvious. ■

Example 2. Let

$$\mathbf{A} = \begin{bmatrix} 1 & 0 & 0 \\ 0 & 1 & 1 \\ 0 & 0 & 1 \end{bmatrix} .$$

Then the characteristic polynomial and minimal polynomial of \mathbf{A} are

$$\chi(t) = (t-1)^3 = t^3 - 3t^2 + 3t - 1, \quad \mu(t) = (t-1)^2 = t^2 - 2t + 1,$$

respectively, i.e., the coefficients of the minimal polynomial are $b_0 = 1, b_1 = -2$. The formulas of the theorem produce for \mathbf{A}^j the two coefficients $-(j-1)$ and j such that $\mathbf{A}^j = -(j-1)\mathbf{I} + j\mathbf{A}$, $j \geq 1$. We obtain

$$\mathbf{A}^j = \begin{bmatrix} 1 & 0 & 0 \\ 0 & 1 & j \\ 0 & 0 & 1 \end{bmatrix}, \quad j \geq 1.$$

6 Characteristic polynomials of chemical graphs

An organic molecule can be represented by a graph, which can be converted to several matrices by using various graph characteristics. Connectivity of atoms through bonds leads to adjacency matrices. Characteristic polynomials of these matrices may be treated as the signature of those molecules. The eigenvalues are also treated as molecular descriptors and have been used in studying quantitative structure properties of these molecules.

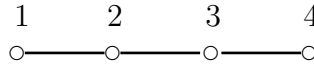


Figure 1. A molecular graph of butan

Example 3. *Let us consider the graph of butane in Fig. 1. The adjacency matrix \mathbf{A} is*

$$\mathbf{A} = \begin{bmatrix} 0 & 1 & 0 & 0 \\ 1 & 0 & 1 & 0 \\ 0 & 1 & 0 & 1 \\ 0 & 0 & 1 & 0 \end{bmatrix}.$$

By formulas (18), we obtain

$$\begin{array}{rcccc} t_1 & = & 0 & t_2 & = & 6 & t_3 & = & 0 & t_4 & = & 14 \\ \sigma_1 & = & 0 & \sigma_2 & = & -3 & \sigma_3 & = & 0 & \sigma_4 & = & 1 \end{array}$$

and the characteristic polynomial has the form $\chi_{\mathbf{A}}(t) = t^4 - 3t^2 + 1$.

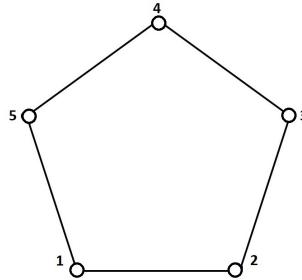


Figure 2. Peterson's graph

Example 4. *Now, let us consider the Peterson's graph in Fig. 2. The adjacency matrix \mathbf{A} is*

$$\mathbf{A} = \begin{bmatrix} 0 & 1 & 0 & 0 & 1 \\ 1 & 0 & 1 & 0 & 0 \\ 0 & 1 & 0 & 1 & 0 \\ 0 & 0 & 1 & 0 & 1 \\ 1 & 0 & 0 & 1 & 0 \end{bmatrix}.$$

By formulas (7), we obtain

$$\begin{array}{rcccccc} t_1 & = & 0 & t_2 & = & 10 & t_3 & = & 0 & t_4 & = & 30 & t_5 & = & 10 \\ \sigma_1 & = & 0 & \sigma_2 & = & -5 & \sigma_3 & = & 0 & \sigma_4 & = & 5 & \sigma_5 & = & -2 \end{array}$$

and the characteristic polynomial has the form $\chi_{\mathbf{A}}(t) = t^5 - 5t^3 + 5t - 2$.

The matrices in Examples 3 and 4 are symmetric with zero traces.

Remark 2. Square matrix \mathbf{Z} is called a commutator if and only if $\mathbf{Z} = \mathbf{XY} - \mathbf{YX}$ for some matrices \mathbf{X} and \mathbf{Y} (not determined uniquely by \mathbf{Z}). Then trace $\text{tr}(\mathbf{Z}) := \sum_i z_{ii} = 0$ because $\text{tr}(\mathbf{XY}) = \text{tr}(\mathbf{YX})$ for all matrices \mathbf{X} and \mathbf{Y} both of whose products \mathbf{XY} and \mathbf{YX} are square. Conversely, if $\text{tr}(\mathbf{Z}) = 0$ then \mathbf{Z} must be a commutator. This theorem has been proved in considerable generality; for instance see proofs by K. Shoda (1936), [11], and [12], and by A.A. Albert and B. Muckenhoupt (1957), [2].

j							
1	0	1	0	0	0	...	0
2	$-\frac{1}{2}t_2$	0	1	0	0	...	0
3	$\frac{1}{3}t_3$	$-\frac{1}{2}t_2$	0	1	0	...	0
4	$\frac{1}{8}(t_2^2 - 2t_4)$	$\frac{1}{3}t_3$	$-\frac{1}{2}t_2$	0	1	...	0
5	$\frac{1}{30}(6t_5 - 5t_2t_3)$	$\frac{1}{8}(t_2^2 - 2t_4)$	$\frac{1}{3}t_3$	$-\frac{1}{2}t_2$	0	\ddots	0
$n-1$	\vdots	\ddots	\ddots			0	1
n	$\sigma_n^{(n)}$	$\sigma_{n-1}^{(n-1)}$	$\sigma_{n-2}^{(n-2)}$...	$-\frac{1}{2}t_2$	0	

Table 3. Coefficients of characteristic polynomials of a commutator

Example 5. For a commutator, the formulae in Example 1 have the following form:

• $n = 2$, $\mathbf{A} := \begin{bmatrix} 0 & a_{12} \\ a_{21} & 0 \end{bmatrix}$. Then, the characteristic polynomial $\chi_{\mathbf{A}}$ of \mathbf{A} has the coefficients

$$\sigma_1^{(2)} = t_1 = 0, \quad \sigma_2^{(2)} = -\frac{1}{2}t_2.$$

• $n = 3$ and $\mathbf{A} := \begin{bmatrix} 0 & a_{12} & a_{13} \\ a_{21} & 0 & a_{31} \\ a_{31} & a_{32} & 0 \end{bmatrix}$. Then the coefficients are (see (7))

$$-\sigma_1^{(3)} = -t_1 = 0, \quad \sigma_2^{(3)} = -\frac{1}{2}t_2, \quad -\sigma_3^{(3)} = -\frac{1}{3}t_3.$$

• $n = 4$, $\mathbf{A} := (a_{jk})$, $j, k = 1, 2, 3, 4$, $a_{ii} = 0$ for $i = 1, 2, 3, 4$. Then, the characteristic polynomial $\chi_{\mathbf{A}}$ of \mathbf{A} (see (7)) has the coefficients

$$-\sigma_1^{(4)} = -t_1 = 0, \quad \sigma_2^{(4)} = -\frac{1}{2}t_2, \quad -\sigma_3^{(4)} = -\frac{1}{3}t_3, \quad \sigma_4^{(4)} = \frac{1}{8}(t_2^2 - 2t_4).$$

References

1. M. ABRAMANOVITZ AND I. A. STEGUN EDS., Handbook of mathematical functions with formulas, graphs, and mathematical tables, National Bureau of Standards, Applied Mathematics Series, **55** (1964), Tenth Printing, December 1972, with corrections, 1046 p.
2. A. A. ALBERT, B. MUCKENHOUPT, On matrices of trace zeros. Michigan Math. J. Volume 4, (1957), pp. 1–3.
3. K. BALASUBRAMANIAN *The use of Frame's method for the characteristic polynomials of chemical graphs*, Theoret. Chim. Acta (Berl.) **65** (1984), pp. 49–58.
4. F. R. GANTMACHER, Matrizenrechnung I, VEB Deutscher Verlag der Wissenschaften, Berlin, 1958.
5. R. A. HORN AND C. R. JOHNSON, Matrix Analysis, Cambridge University Press, Cambridge, 1992, 561 p.
6. R. A. HORN AND C. R. JOHNSON, Topics in Matrix Analysis, Cambridge University Press, Cambridge, 1991, 607 p.
7. J. KELLEHER AND B. O'SULLIVAN, *Generating all partitions: A comparison of two encodings*, Preprint, arXiv:0909.2331v1, 2009, 40 p.
8. H. K. KRISHNAPRIYAN, *On evaluating the characteristic polynomial through symmetric functions*, J. Chem. Inf. Comput. Sci, 35 (1995), pp. 196–198.
9. B. K. MISHRA, *Molecular (graph) characteristics of some hydrocarbons through graph theory*,
http://www.nrri.umn.edu/indouslecture/Kerala2007/pdf/Mishra_abs.pdf
10. A. SCHÖNHAGE, *Fast parallel computation of characteristic polynomials by Leverrier's power sum method adapted to fields of finite characteristic*, Lecture Notes in Computer Science, **700** (1993), pp.410–417.
11. K. SHODA, Einige Sätze über Matrizen, Jap. J. Math. vol. 13 (1936), pp. 361–365.
12. K. SHODA, Über den Kommutator der Matrizen, J. Math. Soc. Japan **3** (1951), 78–81 (German).
13. R. C. THOMPSON, Commutators in the special and general linear groups, Journal Trans. Amer. Math. Soc. **101** (1961), pp. 16–33.
14. A. ZOGHBI AND I. STOJMENOVIC, *Fast algorithms for generating integer partitions*, Intern. J. Computer Math., **70** (1998), pp. 319–332.

Acknowledgments: The research was supported by the German Science Foundation, DFG, under the contract number OP 33/19-1.

Lumped parameter friction models

Vladimír Janovský

Faculty of Mathematics and Physics, Charles University, Prague

Keywords: dry-friction, implicit constitutive laws, Filippov systems, Coulomb friction, unilateral contact, numerical simulation

Abstract We investigate two lumped parameter friction models: A dry-friction model (in 2-D) and a Coulomb friction model (in 8-D). The aim is a dynamical simulation of an initial value problem. Both models are formulated by means of differential inclusions. We consider alternative formulations which are better suited for numerical purposes: a) Standard equations of the motion completed by implicitly defined constitutive relationships. This leads to solving differential-algebraic equations (DAEs). b) Filippov systems of ordinary differential equations (ODEs) with discontinuous right-hand sides. For a numerical solution one can use the Filippov's convex method. We try to compare both approaches.

1 Introduction

We consider two lumped parameter friction models:

1. A dry-friction model
2. A Coulomb friction model.

The friction is an important physical phenomena which is concerned with elastodynamics. The parameter lumping can be understood as an averaging procedure. We may simply think of toy-problems with small degrees of freedom reflecting the phenomena called friction.

Both models are formulated as differential inclusions. The latter one is taken over from [5] and it will be formulated in Section 4. The former one is formulated as follows:

$$m x''(t) \in -k x(t) + f(t) - \mathcal{F} \text{Sign } x'(t), \quad (1)$$

where m , k , and \mathcal{F} are positive constants, $f = f(t)$ is a given function and $\text{Sign} : \mathbb{R} \rightrightarrows \mathbb{R}$ is the multivalued mapping,

$$\text{Sign } z = \begin{cases} \frac{z}{|z|} & \text{if } z \neq 0 \\ [-1, 1] & \text{if } z = 0 \end{cases} \quad (2)$$

see e.g. [2]. The next two sections will be devoted to alternative approaches to a numerical solution of (1)&(2).

In Section 2 we resume basic mechanical principles leading to the notion of dissipative force of Coulomb type. We shall follow the exposition in [3]: The idea is to introduce implicit constitutive relationship between this force and kinematic quantities namely the velocity. Hence, the balance of linear momentum is to be completed by this constitutive law. It leads to a system of semi-implicit differential-algebraic equations (DAEs). A numerical solutions of this DAEs is proposed. Note that the term of differential inclusion will not show up in this section. In Section 3, we formulate the problem (1)&(2) as a *Filippov system* i.e., the system of ordinary differential equations (ODEs) with discontinuous right-hand sides, [7]. The solution of this system is then defined by means of the Filippov's convex method, see e.g. [2]. As far as the numerical implementation is concerned, we integrate ODEs via standard solvers and concatenate smooth pieces of trajectories. We use a ready-made software [8]. We will try to compare both solution approaches (namely, the DAEs from Section 2 and the Filippov's one from Section 3).

In Section 4, we take on a lumped Coulomb friction model [5] which considers just one point on a contact with the rigid boundary, see the corresponding illustrative figure. The crucial issue of the analysis in [4, 5] was to preserve well-posedness of a semi-discretization scheme. We will investigate the possibility to formulate the lumped friction model as a Filippov system. We will exploit the ready-made solver [8].

2 Mechanical interpretation

Let m denote the mass. We represent the displacement of the mass by a function $x = x(t)$. The balance of linear momentum yields

$$x''(t) = \frac{1}{m} (f(t) - F_s(t) - F_d(t)) , \quad (3)$$

where a superposed prime denotes the time derivative. Let $f = f(t)$ denote the applied forces. Let $F_s = F_s(t)$ and $F_d = F_d(t)$, respectively, denote forces on the mass and dissipative forces. In particular, we consider $F_s(t) = kx(t)$ to be a spring force where $k > 0$.

Following [3], we transform (3) as follows: We set $v = v(t) = x'(t)$. Then

$$\begin{cases} v'(t) &= \frac{1}{m} (f(t) - F_s(t) - F_d(t)) \\ F_s'(t) &= k v(t) \end{cases} \quad (4)$$

and (3) are equivalent. The *constitutive relationship* which links F_d and v is defined *implicitly* as an implicit function $\beta : \mathbb{R} \times \mathbb{R} \mapsto \mathbb{R}$,

$$\beta(v(t), F_d(t)) = 0 \in \mathbb{R}, \quad (5)$$

see [11]. The system (4)&(5) is a system of semi-implicit *differential-algebraic equations* (DAEs). For the analysis and the numerical solution of DAEs, see e.g. [6].

Given $v^{\text{init}} \in \mathbb{R}$ and $x^{\text{init}} \in \mathbb{R}$ we solve the initial value problem

$$v(0) = x'(0) = v^{\text{init}}, \quad F_s(0) = kx(0), \quad x(0) = x^{\text{init}} \quad (6)$$

for DAEs (4)&(5). The objective is to solve this problem numerically by a time-stepping scheme.

In [3], such a scheme for a mass-spring-dashpot system was proposed. In [1], there was investigated an implicit constitutive law (5) of *Coulomb-type* which is related to the dry-friction. We shall resume the law and the numerical scheme, [1].

We consider the dissipation force F_d to be a Coulomb-type force labeled traditionally by F_c . Hence, $F_d(t) = F_c(t)$ is defined as

$$\begin{cases} F_c(t) &= \mathcal{F} \text{Sign } v(t) & \text{for } v(t) \neq 0 \\ v(t) &= 0 & \text{for } |F_c(t)| \leq \mathcal{F} \end{cases} \quad (7)$$

where \mathcal{F} is a positive constant. Obviously, (7) represents an implicit definition of the constitutive equation.

Next, we shall discretize the DAEs (4)&(7) in the spirit of [3]. Let $\{t_n\}_{n=0}^{+\infty}$ be the time-equidistant mesh $t_n = \tau n$ with a time-step $\tau > 0$. We denote v^n , F_e^n , f^n and $F_d^n \equiv F_c^n$, respectively, the function values $v(t_n)$, $F_e(t_n)$, $f(t_n)$ and $F_d(t_n) \equiv F_c(t_n)$. We use the implicit Euler scheme to approximate (4) i.e.,

$$v'(t_{n+1}) \sim \frac{v^{n+1} - v^n}{\tau}, \quad F_s'(t_{n+1}) \sim \frac{F_s^{n+1} - F_s^n}{\tau}$$

and hence

$$\begin{cases} \frac{v^{n+1} - v^n}{\tau} &= \frac{1}{m} (f^{n+1} - F_s^{n+1} - F_c^{n+1}) \\ \frac{F_s^{n+1} - F_s^n}{\tau} &= k v^{n+1} \end{cases} \quad (8)$$

We conclude that

$$\left(\frac{m}{\tau} + \tau k\right) v^{n+1} = \frac{m}{\tau} v^n + f^{n+1} - F_s^n - F_c^{n+1} \quad (9)$$

and

$$F_s^{n+1} = \tau k v^{n+1} + F_s^n. \quad (10)$$

We define an auxiliary function a "total force"

$$F_t^{n+1} = \frac{m}{\tau} v^n + f^{n+1} - F_s^n. \quad (11)$$

Hence (9) reads as

$$\left(\frac{m}{\tau} + \tau k\right) v^{n+1} = F_t^{n+1} - F_c^{n+1}. \quad (12)$$

The aim is to impose the constitutive law (7) namely,

$$\begin{cases} F_c^{n+1} = \mathcal{F} \text{Sign } v^{n+1} & \text{for } v^{n+1} \neq 0 \\ v^{n+1} = 0 & \text{for } |F_c^{n+1}| \leq \mathcal{F} \end{cases} \quad (13)$$

In other words, we need to show that the conditions (12)&(13) uniquely define a pair $\{v^{n+1}, F_c^{n+1}\}$. We need to provide an explicit formula.

Definition 1. Given a value of F_t^{n+1} in (11), we define the pair $\{v^{n+1}, F_c^{n+1}\}$ as follows:

if $|F_t^{n+1}| \leq \mathcal{F}$, set

$$\begin{cases} F_c^{n+1} = F_t^{n+1} \\ v^{n+1} = 0 \end{cases} \quad (14)$$

else

$$\begin{cases} F_c^{n+1} = \mathcal{F} \text{Sign } F_t^{n+1} \\ v^{n+1} = \left(\frac{m}{\tau} + \tau k\right)^{-1} (F_t^{n+1} - F_c^{n+1}) \end{cases} \quad (15)$$

end.

Lemma 1. A pair $\{v^{n+1}, F_c^{n+1}\}$ satisfies (12)-(13) provided that the pair is given by Definition 1.

Proof :

a) Let a pair $\{v^{n+1}, F_c^{n+1}\}$ be defined by Definition 1: Assuming (14) on the condition that $|F_t^{n+1}| \leq \mathcal{F}$, it yields (12) and the second requirement in (13).

Consider the pair defined via (15) on the condition that $|F_t^{n+1}| > \mathcal{F}$: If $F_t^{n+1} > \mathcal{F}$ then (15) implies (12) and

$$v^{n+1} = \left(\frac{m}{\tau} + \tau k\right)^{-1} (F_t^{n+1} - \mathcal{F}) > 0.$$

If $F_t^{n+1} < \mathcal{F}$ then (15) implies (12) and

$$v^{n+1} = \left(\frac{m}{\tau} + \tau k\right)^{-1} (F_t^{n+1} + \mathcal{F}) < 0.$$

Hence, $v^{n+1} \neq 0$ and $\text{Sign } v^{n+1} = \text{Sign } F_t^{n+1}$. We conclude that (12) and the first requirement in (13) hold.

b) Let a pair $\{v^{n+1}, F_c^{n+1}\}$ satisfy (11)-(13): Let us assume $v^{n+1} \neq 0$. The equation (12) implies the formula for v^{n+1} in (15). Due to the first condition in (13), the equation (12) yields

$$F_t^{n+1} = \left(\frac{m}{\tau} + \tau k\right) v^{n+1} + \mathcal{F} \text{Sign } v^{n+1}.$$

We conclude that $\text{Sign } F_t^{n+1} = \text{Sign } v^{n+1}$ and hence we get the formula for F_c^{n+1} in (15). If $v^{n+1} = 0$, then (12) implies (14). According to the assumption (13), $|F_c^{n+1}| \leq \mathcal{F}$. ■

Based on the above analysis, namely the formulas (11), (12), and (14), (15), we formulate a time-stepping algorithm:

Algorithm 1. *Initialization:* Given $v^{\text{init}} \in \mathbb{R}$ and $x^{\text{init}} \in \mathbb{R}$, set $v^0 = v^{\text{init}}$, $x^0 = x^{\text{init}}$, $F_s^0 = kv^0$. Set a stepsize $\tau > 0$. Define a forcing function $f = f(t)$ at $t = \tau n$, $n = 0, 1, \dots, \infty$, as a given sequence $\{f^n \equiv f(\tau n)\}_{n=0}^{\infty}$.

Define the sequences $\{v^n\}_{n=0}^{\infty}$ and $\{F_s^n\}_{n=0}^{\infty}$, (optional: record the sequences $\{x^n\}_{n=1}^{\infty}$ and $\{F_c^n\}_{n=1}^{\infty}$), by the recurrence:

$$\text{Given } v^n \text{ and } F_s^n, \text{ set } F_t^{n+1} = \frac{m}{\tau} v^n + f^{n+1} - F_s^n.$$

$$\text{if } |F_t^{n+1}| \leq \mathcal{F}, \text{ set } F_c^{n+1} = F_t^{n+1}, v^{n+1} = 0$$

else set

$$\begin{cases} F_c^{n+1} &= \mathcal{F} \text{Sign } F_t^{n+1} \\ v^{n+1} &= \left(\frac{m}{\tau} + \tau k\right)^{-1} (F_t^{n+1} - F_c^{n+1}) \end{cases}$$

end

$$F_s^{n+1} = \tau k v^{n+1} \text{ (optional: record } F_c^{n+1}, x^{n+1} = \frac{1}{k} F_s^{n+1}).$$

■

Remark 1. *The aim of [10] is to prove the unique solvability of the initial value problem (6) for DAEs (4)&(5) for a class of implicitly defined constitutive laws (5). The class includes Coulomb-type law (7) i.e., the problem (1)&(2).*

We will test the performance of Algorithm 1 on an example from [8], 4.1 A Dry-friction Oscillator.

Example 1. Data: $m = 1$, $k = 1$, $f(t) = \sin(\omega t)$, $\omega = 1/6$, $\mathcal{F} = 0.4$. The initial condition: $x^{\text{init}} = 4$, $v^{\text{init}} = 0$, time step: $\tau = 10^{-3}$, the solution time span: $[0, 10 * T]$, $T = 2\pi/\omega$. The results of the test-run of the Algorithm 1 are resumed in Figures 1-4.

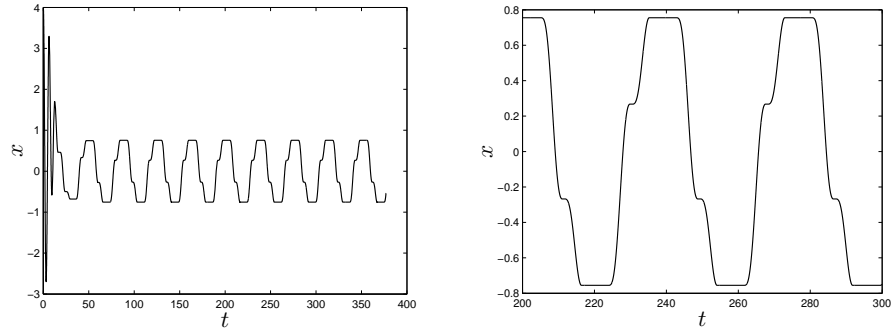


Figure 1. A plot of x versus time t . On the right: a zoom.

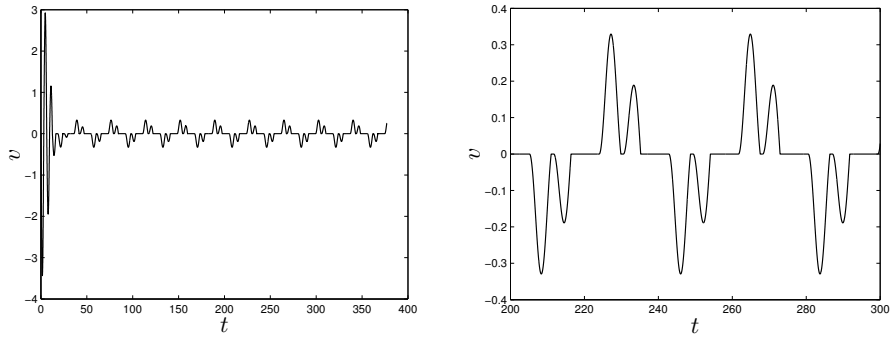


Figure 2. A plot of v versus time t . On the right: a zoom.

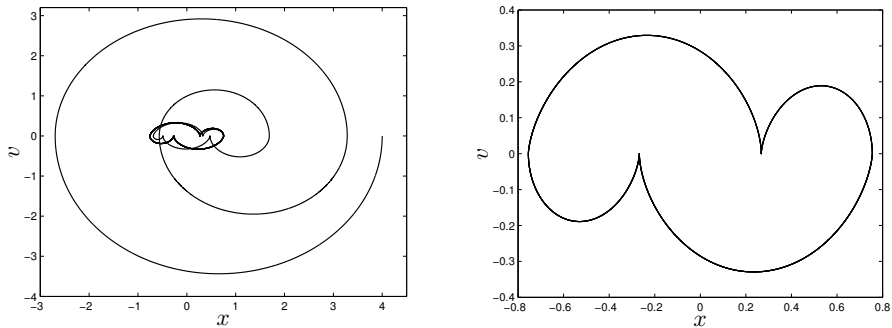


Figure 3. A phase plot of v versus x . On the right: cutting of the transients ($t \geq 200$).

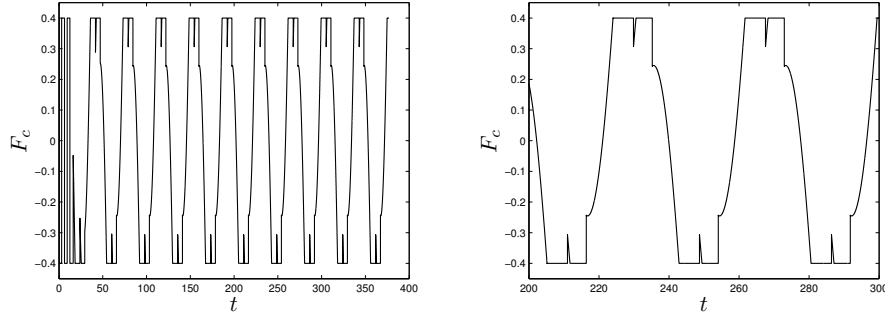


Figure 4. A plot of F_c versus time t . On the right: a zoom.

3 Filippov's method

We shall formulate the problem (1)&(2) as the system of (autonomous) ordinary differential equations (ODEs) with discontinuous right-hand sides, [7]. It is called *Filippov system*, see e.g. [2]. Let us elaborate:

We relabel the former state variables x , $v \equiv x'$ and time t as $x_1 = x$, $x_2 = x'$ and $x_3 = t$. We introduce vector fields $F_1 : \mathbb{R}^3 \rightarrow \mathbb{R}^3$ and $F_2 : \mathbb{R}^3 \rightarrow \mathbb{R}^3$ as

$$F_1 = \begin{bmatrix} x_2 \\ -\frac{k}{m}x_1 + \frac{1}{m}f(x_3) - \frac{1}{m}\mathcal{F} \\ 1 \end{bmatrix}, \quad F_2 = \begin{bmatrix} x_2 \\ -\frac{k}{m}x_1 + \frac{1}{m}f(x_3) + \frac{1}{m}\mathcal{F} \\ 1 \end{bmatrix}$$

and the level-set operator $H_{12} : \mathbb{R}^3 \rightarrow \mathbb{R}$,

$$H_{12}(x) = x_2.$$

The fields F_1 and F_2 , respectively, are defined on

$$S_1 = \{x \in \mathbb{R}^3 : H_{12}(x) > 0\} \quad \text{end} \quad S_2 = \{x \in \mathbb{R}^3 : H_{12}(x) < 0\}.$$

The set

$$\Sigma_{12} = \{x \in \mathbb{R}^3 : H_{12}(x) = 0\}$$

is called the *discontinuity surface*.

To the problem (1)&(2) we relate the Filippov system $x' = F(x)$,

$$x' = \begin{cases} F_1(x) & \text{for } x \in S_1 \\ F_2(x) & \text{for } x \in S_2 \end{cases} \quad (16)$$

This Filippov system can be understood as a short cut for the *differential inclusion*

$$x' \in \begin{cases} F_1(x), & x \in S_1 \\ \overline{\text{co}}(F_1, F_2), & x \in \Sigma_{12} \\ F_2(x), & x \in S_2 \end{cases} \quad (17)$$

where $\overline{\text{co}} = \{z \in \mathbb{R}^3 : z = \lambda F_1 + (1 - \lambda)F_2, \lambda \in [0, 1]\}$ is a convex hull.

Under generic assumptions, the solution of (17) generates a semi-flow: Let ϕ denote the semi-flow. Given an initial condition $x^0 \in \mathbb{R}^3$, the solution $x(t) = \phi(t, x^0)$, $t \geq 0$, of the initial value problem (17) is absolutely continuous and it is forward unique for almost all t in a finite time span, [7].

The solution can be constructed by the *Filippov's convex method*, see e.g. [2], solving ODEs on S_1, S_2 and on Σ_{12} , concatenating smooth trajectories as it is sketched in Figure 5: The trajectory here consists of nine smooth, oriented pieces. The thick parts of the trajectory correspond to the *sliding* i.e., integrating on the discontinuity surface Σ_{12} . The relevant vector field on Σ_{12} is defined by a proper convex combination of vector fields F_1 and F_2 via the above mentioned Filippov's method. The smooth trajectory pieces are numerically integrated up to points called *events*. They are related to discontinuities of the vector field. From the technical point of view, for each smooth trajectory piece there is defined a scalar function called *event function*. When integrating the piece, one check for zeros of the particular event function. The integration is stopped when a zero of the event function is reached in a prescribed tolerance. The classical ODE solvers can be augmented by *event location* tools (e.g., in the MATLAB ODE suit, [12]).

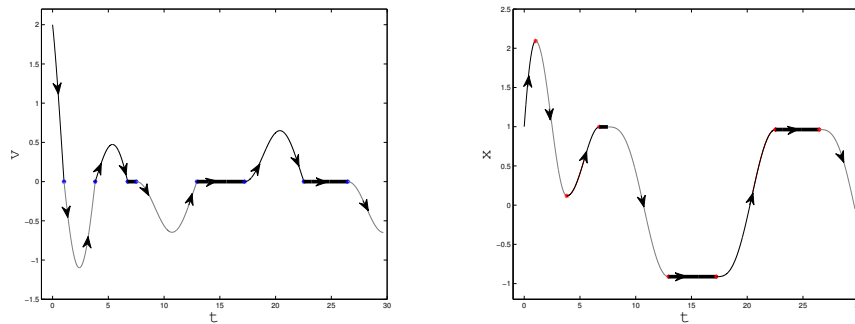


Figure 5. Example of a Filippov's solution of (16). Notation: $v = x'_1 = x_2$, $x = x_1$, $t = x_3$. The initial condition: $(1, 2, 0)^T$. The thick part of trajectory corresponds to sliding.

There is a ready-made MATLAB toolbox [8] for a numerical integration of Filippov's systems based on the ideas sketched above. The authors of the package speak about an *event-driven method*. Running the toolbox [8] on data from Example 1 show no apparent differences in plots of Figures 1, 2 and 3. (Please, mind the labeling of state variables x, v, t in Section 2 and x_1, x_2, x_3 in the current Section 3). Hence we will not present them. Nevertheless, unlike Figure 4, no information concerning the friction force $F_c = F_c(t)$ is supplied by the code [8] directly. The aim is to augment the current code introducing (apart of $x \in \mathbb{R}^3$) a new state variable F_c by means of the following

Definition 2. Given $x \in \mathbb{R}^3$, let $F_c = -kx_1 + f(x_3)$.

if $|F_c| \geq \mathcal{F}$, set $F_c = \text{Sign } \mathcal{F}$

else, set $F_c = -kx_1 + f(x_3)$.

When computing $x \in \mathbb{R}^3$ by the current time-stepping integration [8], we define F_c by Definition 2. The resulting $F_c = F_c(t)$ is shown in Figure 6. Comparing Figure 6 and Figure 4, the former one reveals finer details.

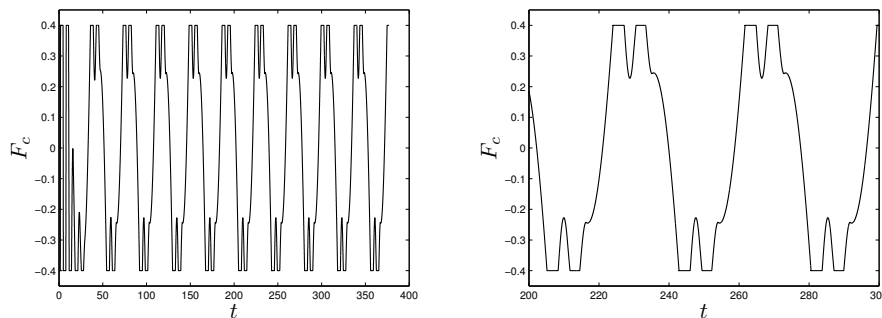


Figure 6. A plot of F_c versus time t via [8]. On the right: a zoom.

We can conclude that instead of solving an initial value problem for the inclusion (17) we solve an initial value problem for state variable $x \in \mathbb{R}^3$ and $F_c \in \mathbb{R}$ which consists of three ODEs for $x \in \mathbb{R}^3$

$$x' = \begin{bmatrix} x_2 \\ -\frac{k}{m}x_1 + \frac{1}{m}f(x_3) - \frac{1}{m}F_c \\ 1 \end{bmatrix} \quad (18)$$

depending on parameter F_c . The system (18) is completed by an *algebraic condition* for $x \in \mathbb{R}^3$ and $F_c \in \mathbb{R}$. The algebraic condition has a form of an *explicit formula* $x \in \mathbb{R}^3 \mapsto F_c \in \mathbb{R}$ given by Definition 2. As an initial condition we can prescribe any $x^0 \in \mathbb{R}^3$ and $F_c^0 \in \mathbb{R}$ such that $x_3^0 = 0$ and F_c^0 is defined by Definition 2 for the particular x^0 .

Remark 2. *The comparison favors the event-driven algorithm [8]: The numerical tests were done on PC with Intel T2300 1.66 GHz, dual core Centrino, using MATLAB version 7.1. As the test we considered Example 1. The performance of*

- *Algorithm 1: Elapsed time = 1995.06 secs, the number of time steps = 376991 (the fixed time step = 0.001)*
- *The event-driven algorithm [8]: Elapsed time = 24.38 secs, the number of time steps = 151204 (an adaptive time stepping), AbsTol: 1.0000 e-006, MaxStep: 0.01, RelTol: 1.0000 e-006.*

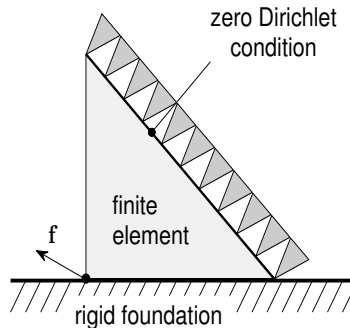
4 Coulomb friction

Apart from the multivalued mapping Sign we need to introduce a multivalued mapping $N_{\mathbb{R}_-^1} : \mathbb{R} \rightrightarrows \mathbb{R}$ called the *normal cone* with respect to the set $\mathbb{R}_-^1 = \{z \in \mathbb{R} : -\infty < z \leq 0\}$. It's action is defined as follows:

$$N_{\mathbb{R}_-^1} z = N z = \begin{cases} 0 & \text{if } z < 0 \\ (-\infty, 0] & \text{if } z = 0 \\ \emptyset & \text{if } z > 0 \end{cases} \quad (19)$$

The symbol N is a short-cut for $N_{\mathbb{R}_-^1}$.

We consider a finite element model of Coulomb friction with one contact point



see [5]. We seek for time-dependent functions $u_\nu, u_\tau, \lambda_\nu, \lambda_\tau : [0, T] \rightarrow \mathbb{R}$ such that

$$\mathbf{M} \begin{bmatrix} u_\nu''(t) \\ u_\tau''(t) \end{bmatrix} = \mathbf{A} \begin{bmatrix} u_\nu(t) \\ u_\tau(t) \end{bmatrix} + \begin{bmatrix} f_\nu(t) \\ f_\tau(t) \end{bmatrix} + \begin{bmatrix} \lambda_\nu(t) \\ \lambda_\tau(t) \end{bmatrix} \quad (20)$$

$$-\lambda_\nu(t) \in N u_\nu(t) \quad (21)$$

$$\lambda_\tau(t) \in \mathcal{F} u_\nu(t) \text{ Sign } u_\tau'(t) \quad (22)$$

almost everywhere (a.e.) in $[0, T]$ and an initial value condition

$$\begin{bmatrix} u_\nu(0) \\ u_\tau(0) \end{bmatrix} = \mathbf{u}^0, \quad \begin{bmatrix} u_\nu'(0) \\ u_\tau'(0) \end{bmatrix} = \mathbf{v}^0 \quad (23)$$

is satisfied for any given $\mathbf{u}^0 \in \mathbb{R}^2, \mathbf{v}^0 \in \mathbb{R}^2$. The unknowns of the model are

- $u_\nu(t)$ and $u_\tau(t)$ i.e., the normal and the tangential *displacement*
- $\lambda_\nu(t)$ and $\lambda_\tau(t)$ i.e., the normal and the tangential *stress*

components. The data are the given $f_\nu(t)$ and $f_\tau(t)$ i.e., the normal and the tangential *load* components.

Parameters of the model: The nonnegative friction coefficient \mathcal{F} , and the mass and stiffness matrices

$$\mathbf{M} = \begin{bmatrix} a & 0 \\ 0 & a \end{bmatrix}, \quad \mathbf{A} = \begin{bmatrix} b & c \\ c & b \end{bmatrix},$$

$$a = \frac{\rho l^2}{12}, \quad b = -\frac{\lambda + 3\nu}{2}, \quad c = \frac{\lambda + \nu}{2},$$

where ρ, l, λ and ν are positive parameters (the density, the diameter of the element, and two Lamé coefficients).

The condition (21) is called the *complementarity condition*. It can be interpreted as the **no contact** or the **contact**

$$\begin{cases} \lambda_\nu(t) = 0 & \text{for } u_\nu(t) < 0 & \dots \text{no contact} \\ \lambda_\nu(t) \leq 0 & \text{for } u_\nu(t) = 0 & \dots \text{contact} \end{cases} \quad (24)$$

with the rigid foundation. The condition (22) reads as

$$\begin{cases} \lambda_\tau(t) = \mathcal{F} \lambda_\nu(t) & \text{for } u_\tau'(t) > 0 \\ \lambda_\tau(t) = -\mathcal{F} \lambda_\nu(t) & \text{for } u_\tau'(t) < 0 \\ |\lambda_\tau(t)| \leq -\mathcal{F} \lambda_\nu(t) & \text{for } u_\tau'(t) = 0 \end{cases} \quad (25)$$

We resume that

1. In the case of **no contact** in (24), the condition (25) yields $\lambda_\nu(t) = \lambda_\tau(t) = 0$
2. In the case of **contact** in (24), the condition (25) can be interpreted as

$$\begin{cases} \lambda_\tau(t) = \mathcal{F} \lambda_\nu(t) & \text{for } u'_\tau(t) > 0 & \dots \text{contact-stick} \\ \lambda_\tau(t) = -\mathcal{F} \lambda_\nu(t) & \text{for } u'_\tau(t) < 0 & \dots \text{contact-stick} \\ |\lambda_\tau(t)| \leq -\mathcal{F} \lambda_\nu(t) & \text{for } u'_\tau(t) = 0 & \dots \text{contact-slip} \end{cases} \quad (26)$$

Let us analyze the latter case namely, assume that the body is in contact with the rigid foundation at a particular time $t_0 > 0$ including an open non-empty time interval $\mathcal{I}(t_0)$. It means that the equations (20) together with the conditions $\{\lambda_\nu(t) \leq 0, u_\nu(t) = 0\}$ and (26) are satisfied for $t \in \mathcal{I}(t_0)$.

The system (20) consists of two equations:

$$au''_\nu(t) = bu_\nu(t) + cu_\tau(t) + f_\nu(t) + \lambda_\nu(t) \quad (27)$$

$$au''_\tau(t) = cu_\nu(t) + bu_\tau(t) + f_\tau(t) + \lambda_\tau(t) \quad (28)$$

Since $u_\nu(t) = 0$ for all $t \in \mathcal{I}(t_0)$ then $u''_\nu(t) = 0$ for all $t \in \mathcal{I}(t_0)$. The equation (27) reduces to an algebraic constraint:

$$\lambda_\nu(t) = -cu_\tau(t) - f_\nu(t), \quad \lambda_\nu(t) \leq 0 \quad (29)$$

for $t \in \mathcal{I}(t_0)$. Finally, we have to employ (26) in the equation (28).

- If $u'_\tau > 0$ then $\lambda_\tau = \mathcal{F}\lambda_\nu$, see (26). The equations (28)&(29) yield

$$u''_\tau = \frac{b - \mathcal{F}c}{a} u_\tau + \frac{1}{a} (f_\tau - \mathcal{F}f_\nu)$$

- If $u'_\tau < 0$ then $\lambda_\tau = -\mathcal{F}\lambda_\nu$, see (26). Due to the equations (28)&(29)

$$u''_\tau = \frac{b + \mathcal{F}c}{a} u_\tau + \frac{1}{a} (f_\tau + \mathcal{F}f_\nu)$$

- If $u'_\tau = 0$ then $|\lambda_\tau| \leq \mathcal{F}\lambda_\nu$, see (26). We consider a convex combination of the above equations

$$u''_\tau = \frac{(1 - 2\lambda) + b}{a} u_\tau + \frac{1}{a} f_\tau + \frac{1 - 2\lambda}{a} \mathcal{F}f_\nu, \quad \lambda \in [0, 1].$$

Observe that the three above equations form a Filippov system for the unknowns u_τ and u'_τ . We have shown that $u_\nu \equiv u'_\nu \equiv 0$ and λ_ν depends on u_τ and f_ν by means of (29).

Let us relabel the state variables $x_1 = u_\nu$, $x_2 = u'_\nu$, $x_3 = u_\tau$ and $x_4 = u'_\tau$. Accordingly, we introduce vector fields $F_1 : \mathbb{R}^5 \rightarrow \mathbb{R}^5$ and $F_2 : \mathbb{R}^5 \rightarrow \mathbb{R}^5$ as

$$F_1 = \begin{bmatrix} 0 \\ 0 \\ x_4 \\ \frac{b - \mathcal{F}c}{a} x_3 + \frac{1}{a} (f_\tau - \mathcal{F}f_\nu) \\ 1 \end{bmatrix}, F_2 = \begin{bmatrix} 0 \\ 0 \\ x_4 \\ \frac{b + \mathcal{F}c}{a} x_3 + \frac{1}{a} (f_\tau + \mathcal{F}f_\nu) \\ 1 \end{bmatrix}$$

and the level-set operator $H_{12} : \mathbb{R}^5 \rightarrow \mathbb{R}$,

$$H_{12}(x) = x_4.$$

The fields F_1 and F_2 , respectively, are defined on

$$S_1 = \{x \in \mathbb{R}^5 : H_{12}(x) > 0\} \quad \text{end} \quad S_2 = \{x \in \mathbb{R}^5 : H_{12}(x) < 0\}.$$

The set $\Sigma_{12} = \{x \in \mathbb{R}^5 : H_{12}(x) = 0\}$ is the discontinuity surface. We consider the Filippov system

$$x' = \begin{cases} F_1(x) & \text{for } x \in S_1 \\ F_2(x) & \text{for } x \in S_2 \end{cases} \quad (30)$$

For a given initial condition $x^0 \in \mathbb{R}^5$, the Filippov's convex method gives the solution $x(t) = \phi(t, x^0)$, $t \geq 0$, of the system (30) on a time span for which the body stays in contact with the rigid obstacle i.e.,

$$\lambda_\nu(t) = -c x_3(t) - f_\nu(t) \leq 0.$$

It means that the initial condition $x^0 \in \mathbb{R}^5$ has to satisfy

$$x^0 = [0, 0, x_3^0, x_4^0, 0]^\top, \quad -c x_3^0(0) - f_\nu(0) < 0. \quad (31)$$

Example 2. *Data:* $a = 1$, $b = -1$, $c = 1$, $\mathcal{F} = 0.4$, $f_\tau(t) = \sin(\omega t)$, $\omega = 1/6$, $f_\nu = 1.3$. *The initial condition:* $x^0 = [0, 0, 1, 2, 0]^\top$. *The solution time span:* $[0, 10 * T]$, $T = 2\pi/\omega$. *Computation via the event-driven algorithm [8]. The results of the test-run are shown in Figures 7-10.*

In this particular numerical experiment the body stays in contact with the rigid obstacle for all times i.e., $\lambda_\nu < 0$ for any $t \geq 0$, see Figure 10. We distinguish two contact regimes:

- If $x_1(t) = x_2(t) = 0$ end $x_4(t) = 0$ then the body is in **contact-slip**
- If $x_1(t) = x_2(t) = 0$ end $x_4(t) \neq 0$ then the body is in **contact-stick**

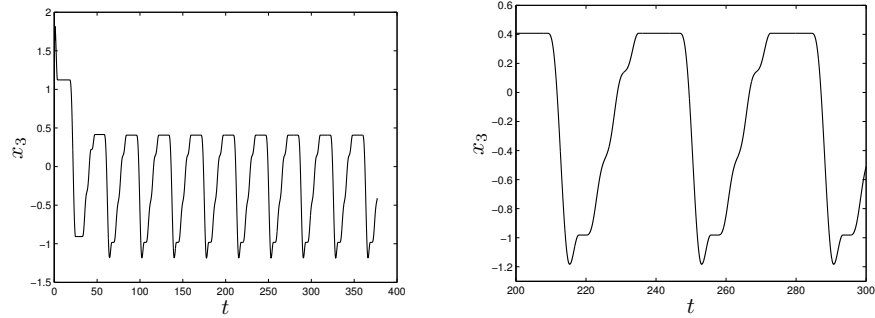


Figure 7. $f_\nu = 1.3$. A plot of x_3 versus time t . On the right: a zoom.

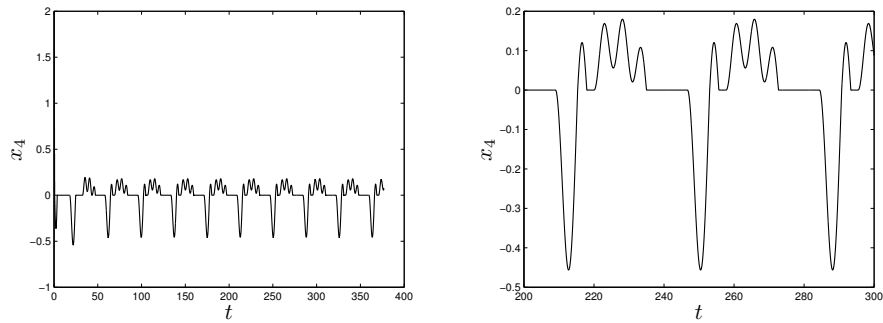


Figure 8. $f_\nu = 1.3$. A plot of x_4 versus time t . On the right: a zoom. Contact regime: If $x_4(t) = 0$ then **contact-slip**. If $x_4(t) \neq 0$ then **contact-stick**.

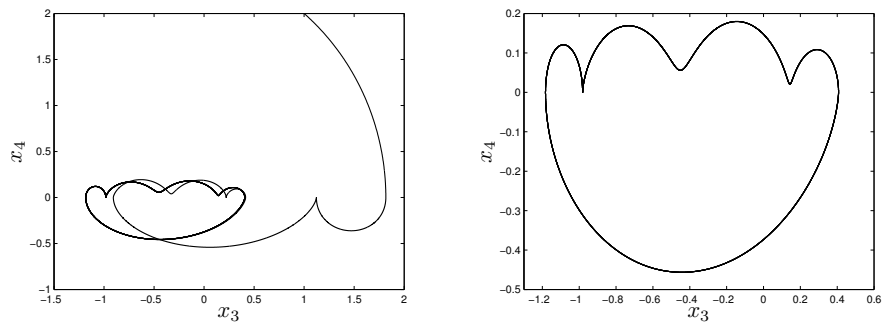


Figure 9. $f_\nu = 1.3$. A phase plot of x_4 versus x_3 . On the right: cutting of the transients.

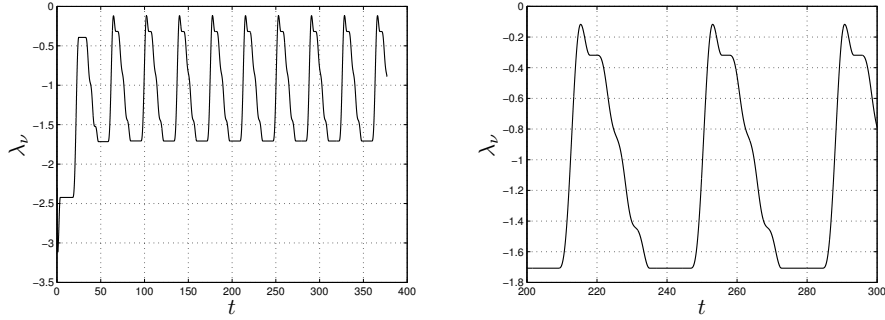


Figure 10. $f_\nu = 1.3$. A plot of λ_ν versus time t . On the right: a zoom.

regime, respectively. The former case was called the *sliding* in Section 3.

Consider the same data from Example 2 except for the normal load component f_ν . If the value of f_ν is positive and comparatively small then the solution may lose contact at a finite time:

Example 3. *Data:* $a = 1$, $b = -1$, $c = 1$, $\mathcal{F} = 0.4$, $f_\tau(t) = \sin(\omega t)$, $\omega = 1/6$, $f_\nu = 0.5$. *The initial condition:* $x^0 = [0, 0, 1, 2, 0]^\top$. *The solution time span:* $[0, 10 * T]$, $T = 2\pi/\omega$. *The first contact loss at* $t_E = 21.6095$, see Figure 11.

Figure 12 shows two solution trajectories for $t \in [0, t_E)$, $t_E = 21.6095$. Note that in the label t_E the subscript E stands for an *event*. What is this event (which happened in the particular time t_E)? In time sequels $t > t_E$ the body loses contact with the rigid obstacle. Hence, the model will be driven by different equations than the model (30). It means e.g. that $\lambda_\nu = 0$ for $t > t_E$.

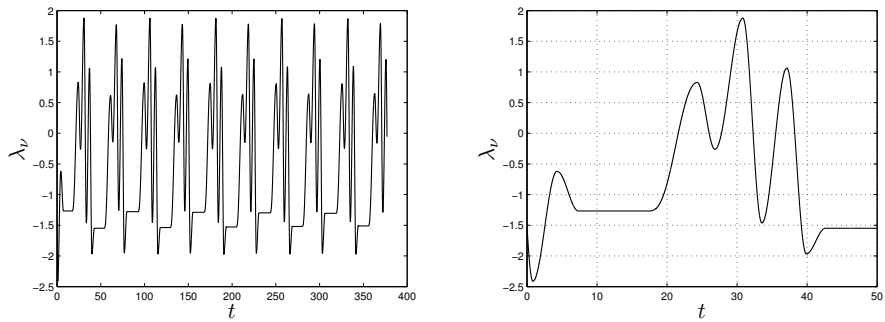


Figure 11. $f_\nu = 0.5$. A plot of λ_ν versus time t . On the right: a zoom. The first contact loss at $t_E = 21.6095$. Since the time t_E , the solution components are non-physical.

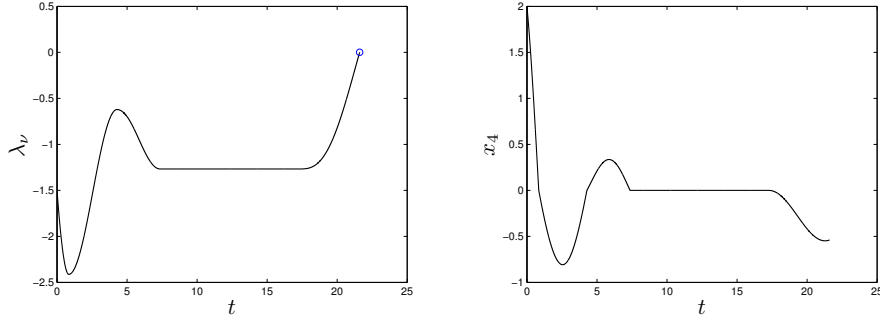


Figure 12. $f_\nu = 0.5$. The accepted solution trajectories in the interval $[0, t_E = 21.6095]$: A plot of λ_ν versus time t (on the left), a plot of x_4 versus time t (on the right).

Let us elaborate: Recall the original meaning of the state variables $x_1 = u_\nu$, $x_2 = u'_\nu$, $x_3 = u_\tau$ and $x_4 = u'_\tau$. Assume that the body is not in contact with the rigid foundations at a particular time $t_0 > 0$ including an open non-empty time interval $\mathcal{I}(t_0)$. Due to (24) (the option **no contact**) we can claim that $\{\lambda_\nu(t) = 0, u_\nu(t) < 0\}$ for $t \in \mathcal{I}(t_0)$. We already noted that $\lambda_\nu(t) = \lambda_\tau(t) = 0$ for $t \in \mathcal{I}(t_0)$, as a consequence of (25). Hence, the system (20) reduces to equations

$$au''_\nu(t) = bu_\nu(t) + cu_\tau(t) + f_\nu(t) \quad (32)$$

$$au''_\tau(t) = cu_\nu(t) + bu_\tau(t) + f_\tau(t) \quad (33)$$

for $t \in \mathcal{I}(t_0)$ provided that $u_\nu(t) < 0$. We formulate (32)&(33) as an autonomous system adding an extra equation $t' = 1$. Coming back to the variable $x \in \mathbb{R}^5$ we introduce vector fields $F_3 : \mathbb{R}^5 \rightarrow \mathbb{R}^5$ and $F_4 : \mathbb{R}^5 \rightarrow \mathbb{R}^5$ as

$$F_3 = \begin{bmatrix} x_2 \\ \frac{b}{a}x_1 + \frac{c}{a}x_3 + \frac{1}{a}f_\nu \\ x_4 \\ \frac{c}{a}x_1 + \frac{b}{a}x_3 + \frac{1}{a}f_\tau \\ 1 \end{bmatrix}, \quad F_4 = \begin{bmatrix} 0 \\ \frac{c}{a}x_3 + \frac{1}{a}f_\nu \\ x_4 \\ \frac{b}{a}x_3 + \frac{1}{a}f_\tau \\ 1 \end{bmatrix}$$

The fields F_3 and F_4 , respectively, are defined on

$$S_3 = \{x \in \mathbb{R}^5 : x_1 < 0\} \quad \text{end} \quad S_4 = \{x \in \mathbb{R}^5 : x_1 = 0\}.$$

The field F_3 is an immediate transcription of the equations (32)&(33) to the state variable $x \in \mathbb{R}^5$. The field F_4 reduces the flow to S_4 . The idea is that all four fields F_1 , F_2 , F_3 and F_4 will be concatenated by piecewise smooth trajectories. It will be the subject of a forthcoming paper.

5 Conclusions

We considered a dry-friction model (in 2-D) and a lumped parameter Coulomb friction model (in 6-D). In case of the dry-friction model we investigated two approaches for a numerical simulation:

- Solving DAEs, using an implicitly defined constitutive relation for the Coulomb friction force
- Solving the relevant Filippov system.

The comparison clearly favours the Filippov approach: We concatenate smooth solution branches computed by an optionally chosen ODEs solver with an adaptive step size. If DAEs approach were to be competitive then an adaptive step size should be implemented.

In case of the lumped Coulomb friction model we considered a Filippov formulation only. We have shown that the dry friction model is linked with the case of the `contact-stick` and the `contact-slip` solution modes on an open time interval. These two solution modes should be concatenated with `no contact` solution modes, which is not implemented yet. If the normal load components $f_\nu = f_\nu(t)$ is sufficiently high on an open time interval then we may expect solution being composed of concatenated `contact-stick` and `contact-slip` solution modes (as in Example 2).

References

1. J. BABOVÁKOVÁ, *Oscilace mechanických systému s implicitními konstitutivními vztahy*, Diplomová práce, Univerzita Karlova v Praze, Matematicko-fyzikální fakulta, 2012.
2. M. DI BERNARDO, C.J. BUDD, A.R. CHAMPNEYS AND P. KOWALCZYK, *Piecewise-smooth Dynamical Systems, Theory and Applications*, Springer, 2008.
3. S. DARBHA, K.B. NAKSHATRALA AND K.R. RAJAGOPAL, *On the vibrations of lumped parameter systems governed by differential-algebraic equations*, Journal of the Franklin Institute 347(2010), pp.87–101.
4. H.B. KHENOUS, P. LABORDE AND Y. RENARD, *Mass redistribution method for finite element contact problems in elastodynamics*, Eur. J. Mech., A/Solids 27(5) (2008), pp.918–932.
5. T. LIGURSKÝ AND Y. RENARD, *A Well-Posed Semi-Discretization of Elastodynamic Contact Problems with Friction*, Quarterly Journal of Mechanics and Applied Mathematics 64 (2011), pp.215–238.
6. K. KUNKEL AND V. MEHRMANN, *Differential-Algebraic Equations, Analysis and Numerical Solution*, EMS Textbooks in Mathematics, 2006.
7. A.F. FILIPPOV, *Differential Equations with Discontinuous Righthand Sides*, Kluwer Academic Publishes, 1988.

8. P.P. PIIRONEN AND Y.A. KUZNETSOV, *An event-driven method to simulate Filippov systems with accurate computing of sliding motions*, ACM Transactions on Mathematical Software Vol 34, No.3. Article13 (2008)
9. D. PRAŽÁK AND K.R. RAJAGOPAL, *Mechanical oscillators described by a system of differential-algebraic equations*, Appl. Math. 57 (2012), pp.129–142.
10. D. PRAŽÁK AND K.R. RAJAGOPAL, *Mechanical oscillators with fully implicit damping terms*, In preparation.
11. K.R. RAJAGOPAL, *A generalized framework for studying vibrations of lumped parameter systems*, Mechanics Research Communications 37 (2010), pp.463–466.
12. L.F. SHAMPINE AND M.W. REICHEL, *The MATLAB ODE suit*, SIAM J. Sci. Comput. 18, pp.1–18.

Acknowledgments: This work was supported by the Grant Agency of the Czech Republic (grant No. P201/12/0671).

On cover-incomparability graphs

Jana Maxová and Daniel Turzík

Institute of Chemical Technology, Prague

Keywords: poset, cover-incomparability graph, transitive orientation, NP-complete, chordal graph, simplicial vertex, Ptolemaic graph, distance-hereditary graph, k-tree

Abstract In this paper we deal with posets and graphs associated to them. We concentrate on so called cover-incomparability graphs. We prove that the C-I graph recognition problem is in general NP-complete. Then we present several classes of graphs (distance-hereditary graphs, Ptolemaic graphs, k -trees) for which the C-I graph recognition problem is polynomial.

1 Introduction

We deal with posets and graphs associated to them. There are several ways how to associate a graph G to a given poset P . The vertex set $V(G)$ is usually the set of points of P . Depending on the edge-set $E(G)$, we may obtain among others:

- the **comparability graph** of P (x and y are adjacent if and only if $x < y$ or $y < x$),
- the **incomparability graph** of P (x and y are adjacent if and only if x and y are incomparable),
- the **cover graph** of P (x and y are adjacent if and only if x covers y or vice versa) or
- the **cover-incomparability graph** of P (x and y are adjacent if and only if x covers y , or y covers x , or x and y are incomparable).

The incomparability graph of P is of course just the complement of the comparability graph, while the cover-incomparability graph of P is the union of the cover graph and the incomparability graph of G .

Example 1. Let $P = (\mathcal{P}(\{1, 2\}), \subseteq)$ be the poset of all subsets of $\{1, 2\}$ together with the relation \subseteq (being a subset). The following picture shows various graphs associated to this poset.

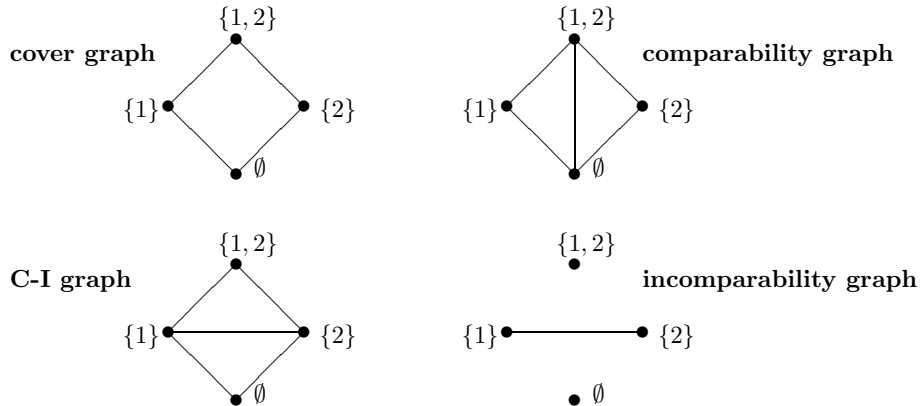


Figure 1. Poset P and various graphs associated to it

Cover graphs, comparability graphs and incomparability graphs are standard ways how to associate a graph to a given poset, while the notion of cover-incomparability graph (or shortly C-I graph) is new. It was introduced by Brešar et al. in 2008 [2]. This notion was motivated by the theory of transit functions on posets.

There are two basic ways how to approach the notion of C-I graphs. One possibility is to study posets whose C-I graphs have special properties. Posets whose C-I graphs are claw-free, chordal, distance-hereditary and Ptolemaic can be characterized using forbidden subsets [2].

The other direction is to try to answer questions such as: Which graphs are C-I graphs? Which chordal, interval, etc. graphs are C-I graphs? These questions seem to be much harder. In Section 3 we show that the problem of recognizing C-I graphs is in general NP-complete. On the other hand it is clearly polynomial for instance for trees (as in any C-I graph there are at most 2 vertices of degree 1). It is natural to ask the same question for some smaller classes of graphs such as chordal, interval, distance-hereditary or Ptolemaic graphs (see the list of open problems in [2]).

Brešar et al. [3] concentrated on two special subclasses of chordal graphs and proved that the recognition problem is polynomial if restricted to block graphs or to split graphs.

In Section 4 we continue the study of chordal C-I graphs in other direction. We found a simple necessary condition for a graph to be a C-I graph and show that for Ptolemaic graphs this condition is also sufficient. It follows that the problem of recognizing C-I graphs is polynomial among Ptolemaic graphs, and (with some more effort) also among all distance-hereditary graphs.

The last result of Section 4 is the solution of the C-I graph recognition problem for k -trees. A k -tree is a chordal graph all of whose maximal cliques are the same size $k + 1$ and all of whose minimal clique separators are also all the same size k . The k -trees are exactly the maximal graphs with a given treewidth, graphs to which no more edges can be added without increasing their treewidth.

2 Terminology and basic properties of C-I graphs

Let $P = (V, \leq)$ be a poset. We will use the following notation. For $u, v \in V$ we write:

- $u < v$ if $u \leq v$ and $u \neq v$.
- $u \triangleleft v$ if $u < v$ and there is no $z \in V$ such that $u < z < v$. We say that v covers u .
- $u \triangleleft \triangleleft v$ if $u < v$ and $\neg(u \triangleleft v)$.
- $u \parallel v$ if u and v are incomparable.

Definition 1. For a given poset $P = (V, \leq)$, let $G(P) = (V, E)$ be a graph with $E = \{\{u, v\} \mid u \triangleleft v \text{ or } v \triangleleft u \text{ or } u \parallel v\}$. Then we say that $G(P)$ is the **cover-incomparability graph** of P (or the *C-I graph* of P for short).

Note that for any $u, v \in V(G(P))$, $u \neq v$ we have $\{u, v\} \notin E(G(P)) \Leftrightarrow u \triangleleft \triangleleft v \text{ or } v \triangleleft \triangleleft u$.

For an undirected graph $G = (V, E)$ an orientation \vec{G} is the oriented graph $D = (V, A)$ that arises from G by replacing each edge uv by **one** of the arcs \vec{uv} or \vec{vu} . The orientation D is said to be *transitive* if for any two consecutive arcs $\vec{uv} \in A(D)$, $\vec{vw} \in A(D)$ also $\vec{uw} \in A(D)$.

Now let us list a few easy observations about C-I graphs [2, 8]. Their proofs follow mostly immediately from the definition.

Lemma 1. Let $P = (V, \leq)$ be a poset and $G(P) = (V, E)$ its C-I graph. Then

- (i) $G(P)$ is connected.

- (ii) If $U \subseteq V$ is an antichain in P , then U induces a complete subgraph in $G(P)$.
- (iii) If $I \subseteq V$ is an independent set in $G(P)$, then all points of I lie on a common chain in P .
- (iv) There are at most 2 vertices of degree 1 in $G(P)$.
- (v) $\overline{G(P)}$ (the complement of $G(P)$) admits a transitive orientation
- (vi) $G(P)$ contains no induced cycles of length greater than 4.

3 The recognition problem

The problem we are concerned with is the following:

C-I TESTING

Instance: A graph $G = (V, E)$.

Question: Is there a poset $P = (V, \leq)$ such that G is the C-I graph of P , i.e. $G = G(P)$?

The next theorem is the main result of this section.

Theorem 1. *The C-I testing problem, i.e. the decision whether a given graph is a C-I graph, is an NP-complete problem.*

Proof :

We prove this theorem by giving a polynomial-time transformation from Covering by complete bipartite subgraphs, which is an NP-complete problem, see e.g. [5]. This problem can be stated as follows.

COVERING BY COMPLETE BIPARTITE SUBGRAPHS

Instance: A bipartite graph $G = (V, E)$ and positive integer $k \leq |E|$.

Question: Are there k subsets V_1, \dots, V_k of V such that each V_i induces a complete bipartite subgraph of G and such that for each edge $uv \in E$ there is some V_i that contains both u and v ?

Given a bipartite graph $G = (V, E)$ and a positive integer $k, k \leq |E|$ we construct a graph $H = H_G^k = (W, F)$ such that H is a C-I graph if and only if G can be covered by k complete bipartite subgraphs. The exact construction of H_G^k together with the rest of the proof can be found in [8].

■

Before we close this section let us mention that the recognition problem for cover graphs is NP-complete [10, 11] or [4], while the recognition problem for comparability graphs (and hence also for incomparability graphs) is polynomial, see [1].

4 Chordal graphs and subclasses of chordal graphs

Chordal graphs present an extremely interesting class of graphs. Due to their simple structure (the existence of perfect elimination scheme) many NP-complete problems (as k -colorability, k -independent set, k -clique etc.) are polynomially solvable if restricted to chordal graphs.

A graph is said to be *chordal* if it has no induced cycles of length greater than 3. A vertex v is called *simplicial* if its neighborhood induces a complete subgraph. It is a well-known fact [6] that a chordal graph is either a clique or it contains a pair of independent (not adjacent) simplicial vertices.

A graph G is said to be *distance-hereditary* if for any two vertices u and v belonging to a connected induced subgraph H of G , some shortest path connecting u and v in G lies in H (so that the distance between u and v in H is the same as the distance in G). *Ptolemaic* graphs are distance-hereditary graphs without induced 4-cycles (i.e chordal distance-hereditary graphs).

Lemma 2. *Let P be a poset and $G(P) = (V, E)$ its C-I graph. Let v be a simplicial vertex in $G(P)$. Then v is a maximal or a minimal element of P .*

Proof :

Suppose v is neither a maximal nor a minimal element of P . Then there exist vertices $x, y \in V(G)$ such that $x \triangleleft v \triangleleft y$ in P . Vertices x and y are neighbors of v not connected by an edge, a contradiction with v being simplicial. ■

Lemma 3. *If G is a C-I graph then G does not contain 3 independent simplicial vertices.*

Proof :

Suppose there are 3 simplicial vertices in $G(P)$ that form an independent set. According to Lemma 1(iii) these 3 vertices lie on a common chain in the poset P . Hence one of them (the middle one) is neither a maximal or a minimal element of, a contradiction with Lemma 2. ■

Lemma 3 gives us a simple necessary condition for an arbitrary graph to be a C-I graph. This condition turns out to be sufficient if G is a Ptolemaic graph.

Theorem 2. *Let G be a Ptolemaic graph. G is a C-I graph if and only if G does not contain 3 independent simplicial vertices.*

Proof :

For the proof of Theorem 2, which exceeds the capacity of this article, see [9]. ■

It is easy to see that the condition from Theorem 2 can be checked in polynomial time. Hence we get the following corollary.

Corollary 1. *C-I graphs can be recognized in polynomial time in the class of all Ptolemaic graphs.*

For arbitrary distance-hereditary graph we are able to proof the following rather technical theorem (see [9] for the proof).

Theorem 3. *Let G be a distance-hereditary graph. G is a C-I graph if and only if one of the following two conditions holds:*

1. *diam $G = 2$ and the complement \overline{G} is a vertex disjoint union of b complete bipartite subgraphs and i isolated vertices and $i \geq b$, or*
2. *diam $G \geq 3$, G is chordal and G does not contain a triple of independent simplicial vertices.*

It follows that there are no other distance-hereditary C-I graphs with diam $G \geq 3$ other than Ptolemaic graphs. As both of these conditions can be checked in polynomial time we immediately have the following corollary.

Corollary 2. *C-I graphs can be recognized in polynomial time in the class of all distance-hereditary graphs.*

There is another interesting subclass of chordal graphs for which the recognition problem is known to be polynomial. This is the class of all k -trees.

A k -tree is a chordal graph all of whose maximal cliques are the same size $k + 1$ and all of whose minimal clique separators are also all the same size k . The k -trees are exactly the maximal graphs with a given treewidth, graphs to which no more edges can be added without increasing their treewidth. The graphs that have treewidth at most k are exactly the subgraphs of k -trees. For this reason they are called partial k -trees. A k -path is a k -tree with at most two simplicial vertices (or a complete graph on $k + 1$ vertices).

We first observe if a k -tree G is a C-I graph then G must be a k -path. This follows immediately from Lemma 3. We further show that a k -path is a C-I graph whenever k is odd. For k even, a k -path on n vertices is a C-I graph if and only if $n \leq 2k + 1$. Our observations are summarized in the following theorem for the proof see [7].

Theorem 4. For k odd, a k -tree G is a C-I graph if and only if G is a k -path. For k even, a k -tree G is a C-I graph if and only if G is a k -path and $n \leq 2k + 1$ where n is the number of vertices of G .

References

1. BRANDSTÄDT, A., LE, V.B., SPINARD, J., *Graph Classes*, SIAM, Philadelphia (1999)
2. BREŠAR, B., CHANGAT, M., KLAVŽAR, S., KOVŠE, M., MATHEWS, J., MATHEWS, A., *Cover-Incomparability Graphs of Posets*, *Order* **25** (2008), pp. 335-347
3. BREŠAR, B., CHANGAT, M., GOLOGRANC, T., MATHEWS, J., MATHEWS, A., *Cover-incomparability graphs and chordal graphs*, *Discrete Applied Mathematics* **158** (2010), pp. 1752-1759
4. BRIGTWELL, G., *On the complexity of Diagram Testing*, *Order* **10** (1993), pp. 297-303
5. GAREY, M.R., JOHNSON, D.S., *Computers and Intractability: A Guide to the Theory of NP-Completeness*, Freeman, New York (1979)
6. LEKKERKERKER, C.B. AND BOLAND, J.C., *Representation of finite graphs by a set of intervals on the real line*, *Fund. Math.* **51** (1962), pp. 45-64
7. MAXOVÁ, J., DUBCOVÁ, M., PAVLÍKOVÁ, P., TURZÍK, D., *Which k -trees are cover-incomparability graphs?*, *Discrete Applied Mathematics*, Volume 167 (2014), pp. 222-227
8. MAXOVÁ, J., PAVLÍKOVÁ, P., TURZÍK, D., *On the complexity of cover-incomparability graphs of posets* *Order* **26** (2009), pp. 229-236
9. MAXOVÁ, J., TURZÍK, D., *Which distance-hereditary graphs are cover-incomparability graphs*, *Discrete Applied Mathematics*, Volume 161, Issues 13Ú14 (2013), pp. 2095-2100
10. NEŠETŘIL, J., RÖDL, V., *Complexity of diagrams* *Order* **3** (1987), pp. 321-330
11. NEŠETŘIL, J., RÖDL, V., *More on the complexity of cover graphs*, *Comment.Math.Univ.Carol.* **36**, (1995), pp. 269-278

Study on Bi-Substrate Enzymatic Reactions through Variational Iteration Method

F A Basir[†] S Nandi[‡] Priti Kumar Roy[†] R Bhattacharyya[‡]
M K Ghosh[†]

[†]Center for Mathematical Biology and Ecology,
Department of Mathematics,
Jadavpur University,
Kolkata 700032, India.

[‡]Department of Chemistry
Narula Institute of Technology
Kolkata 700109, India.

Keywords: Enzyme Kinetics; Mathematical Modeling; Variational Iteration Method.

Abstract Enzymes constitute the most important functional aspect of all bio-chemical processes. It catalyzes numerous reactions taking place within the living organisms. Enzymatic reactions occur through the active sites which combine with the substrates to form intermediate complexes subsequently leading to products. In this research article, a single enzyme having dual active sites has been considered. These active sites offer room for combining with two substrates having varying reactivity in a sequential ordered mechanism. The enzyme first combines with the more reactive substrate to form the first intermediate complex. The complex then further reacts with the second substrate to yield the ultimate product via formation of a second intermediate complex. Mathematical modeling with its analytical and numerical analysis in this regard provides an idea to predict the behavior of the system. In this research article a mathematical model is formulated and approximate analytical solution for the reaction system is determined using Variational Iteration Method. Numerical simulation has also been done which is based on the analytical results.

1 Introduction

Enzymes play a significant role in controlling the extent of various chemical and biochemical reactions. It acts as a catalyst that increases the rate of a reaction without itself undergoing any change in its quantity. It modifies the rate of a

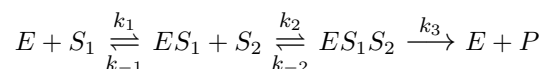
reaction by lowering the energy of activation required for a reaction [1]. In addition, enzymatic reactions do not leave any by-products which are an advantage for any system under consideration. Enzymes catalyze the reactions by combining with a substrate through an active site present on it forming an intermediate complex which ultimately leads to the product. The enzyme is reverted back at the end of the reaction.

Bi-substrate enzyme kinetic mathematical model has a long range application in the different fields of chemical production, drugs, pharmaceutical and polymers. LONZA, one of the reputed fine chemical producers in the world, routinely applies mathematical modeling to avoid formation of inhibiting by-products during enzymatic synthesis of fine chemicals. Additionally, dual substrate enzyme kinetic model provides an opportunity of a new dimension in the various scientific areas of chemical engineering, mathematics, medicine and other fields of interdisciplinary research. Catalytic power, specificity, time economization, regulation and reuse all contribute to the most important features of an enzyme in tailoring the mode of any biochemical processes. Mathematical modeling thus plays a considerable role in controlling the enzymatic reactions [2], [3], [4], [5] and specifically in case of dual substrate model, it helps us to understand the dependency of the system on system parameters [6], [7], [8].

In the present study, a model based mathematical approach with the bi-substrate enzyme kinetic model is introduced by considering the sequence of actions that lead to product formation [9]. With this view, a concentration relationship among the two substrates, enzyme, two complexes and the product have been established considering the significant importance of reaction. The proposed mathematical model for bi-substrate enzymatic reaction has been solved analytically with the help of Variational Iteration method [11]. The analytical results are supported numerically using Matlab.

2 Assumptions and Formulation of the Mathematical Model

Here we commence an enzyme kinetic model with two types of substrates S_1 , S_2 and enzyme E . The kinetic reaction is given by the following schematic diagram:



Here S_1 and S_2 are the two substrates, E is the enzyme, $ES_1(C_1)$ and $ES_1S_2(C_2)$ are the two intermediate enzyme-substrate complexes and P is the product. The rate constants for the formation of enzyme-substrate complexes C_1 and C_2 are denoted by k_1 and k_2 respectively and k_3 is the catalysis rate constant. Also we consider that the rate constant for backward reaction of the enzyme-substrate complexes C_1 and C_2 are k_{-1} and k_{-2} respectively. The above diagram states that one molecule of the substrate S_1 combines with one molecule of enzyme to form one molecule of enzyme-substrate complex C_1 . This complex may decompose back into enzyme and unmodified substrate S_1 or may combine with one molecule of substrate S_2 to form second enzyme-substrate complex C_2 . Finally this complex is transformed into product at a rate k_3 or may revert back into enzyme-substrate complex ES_1 and unmodified substrate S_2 or into ES_2 and S_1 . On the basis of the assumption that the reaction between E and S_1 is relatively faster than that between E and S_2 , the first one is considered as binding of E and S_1 is much stronger than that of E and S_2 at a particular time.

Considering s_1 , s_2 , e , c_1 , c_2 and p for $[S_1]$, $[S_2]$, $[E]$, $[ES_1]$, $[ES_1S_2]$ and $[P]$ respectively, where $[]$ denotes the concentration of a substance, from the law of mass action [7], the non linear system of differential equations for the above enzymatic reaction may be enunciated as follows:

$$\begin{aligned}
\frac{ds_1}{dt} &= -k_1es_1 + k_{-1}c_1, \\
\frac{ds_2}{dt} &= -k_2c_1s_2 + k_{-2}c_2, \\
\frac{de}{dt} &= -k_1es_1 + k_{-1}c_1 + k_3c_2, \\
\frac{dc_1}{dt} &= k_1es_1 - k_{-1}c_1 - k_2c_1s_2 + k_{-2}c_2, \\
\frac{dc_2}{dt} &= k_2c_1s_2 - k_{-2}c_2 - k_3c_2, \\
\frac{dp}{dt} &= k_3c_2
\end{aligned} \tag{1}$$

with initial conditions

$$\begin{aligned}
s_1(0) = s_{10}, s_2(0) = s_{20}, e(0) = e_0, \\
c_1(0) = 0, c_2(0) = 0 \text{ and } p(0) = 0,
\end{aligned} \tag{2}$$

where k_1 , k_2 , k_3 , k_{-1} , k_{-2} , s_{10} , s_{20} and e_0 are positive constants.

3 Boundedness, Existences and Uniqueness of the System

The right hand side of the equation (1) are smooth functions of the variables s_1, s_2, e, c_1, c_2, p and system parameters, as long as these quantities are non-negative, so local existence, uniqueness and continuous properties hold. In the next theorem we show that the linear combination of substrates, enzyme, complexes and product are less than a finite quantity or in other words, the solution of the system is bounded.

Theorem 1. *The solution $y(t)$ of (1), where $y = (s_1, s_2, e, c_1, c_2, p)$ is uniformly bounded for $y_0 \in R_{0,+}^6$*

Proof: We define the function $W(t): R_{0,+} \rightarrow R_{0,+}$ by

$$W(t) = s_1(t) + s_2(t) + e(t) + c_1(t) + c_2(t) + p(t). \quad (2.1)$$

Observe that W is well-defined and differentiable on some maximal interval $(0, t_f)$.

The derivative of (2.1) is

$$\begin{aligned} \frac{dW(t)}{dt} &= -k_1 e s_1 + k_{-1} c_1 + k_3 c_2 - k_2 c_1 s_2 + k_{-2} c_2. \\ \frac{dW(t)}{dt} + W(t) &= -k_1 e s_1 + k_{-1} c_1 + k_3 c_2 - k_2 c_1 s_2 + k_{-2} c_2 + s_1 + s_2 \\ &\quad + e(t) + c_1(t) + c_2(t) + p(t). \\ &\leq (k_3 + k_{-2} + 1)c_2 + (k_{-1} + 1)c_1 + s_1 + s_2 + p \end{aligned}$$

Now since the system is closed, mass will be preserved for all time. So,

$$\frac{dW(t)}{dt} + W(t) \leq k(s_{10} + s_{20} + e_0) = kW(0) = kW_0 \text{ for each } t \in (0, t_f).$$

Where, total mass of the system is $W_0 = (s_{10} + s_{20} + e_0)$.

and $k = \max(k_3 + k_{-2} + 1, k_{-1} + 1)$.

Let $G(t, y) = kW_0 - y(t)$, which satisfies Lipschitz condition everywhere, clearly

$$\frac{dW(t)}{dt} + W(t) \leq kW_0 \text{ for all } t \in (0, t_f).$$

Let,

$$\frac{dW(t)}{dt} = kW_0 - x(t) \text{ and } W(0) = W_0.$$

This linear ordinary differential equation has the solution

$$x(t) = m - (m - W_0)e^{-t}, \text{ where } m = kW_0.$$

It is clear that, $W(t)$ is bounded on $(0, t_f)$ By comparison theorem Brikhoff and Rota [10],

$$W(t) \leq m - (m - W_0)e^{-t}.$$

Now, suppose $t_f < \infty$, then $W(t_f) \leq x(t_f) < \infty$. But in this case the solution exists uniquely for some interval $(0, t_f)$ by *Picards – LindelofTheorem*.

3.1 Basic Idea of Variational Iteration Method

Here we can solve system (7) analytically using Variational Iteration Method [11] in the following way. Let us consider the system

$$Lz(t) + Nz(t) = g(t) \tag{3}$$

where L is a linear operator, N is a non linear operator and $g(t)$ is a given continuous function. Now using variational iteration method, we construct the correct functional form [11] as follows:

$$z_{n+1}(t) = z_n(t) + \int_0^t \eta [L(z_n(\xi)) + N(\tilde{z}_n(\xi)) - g(\xi)] d\xi \tag{4}$$

where η is the Lagrange multiplier [12]. We can identify η by the method of variational theory [11], [13]. Here z_n represents the n^{th} order approximate solution and \tilde{z}_n the restricted variation [13] i.e., $\delta\tilde{z}_n = 0$.

3.2 Detailed Analysis of the System

Now, using (4), we have the correction functional of (1) as given below,

$$s_{1,n+1}(t) = s_{1,n}(t) + \int_0^t \eta_1 [s'_{1,n}(\xi) + \overbrace{k_1 e_n(\xi) s_{1,n}(\xi)} - \overbrace{k_{-1} c_{1,n}(\xi) s_{2,n}(\xi)}] d\xi \tag{5a}$$

$$s_{2,n+1}(t) = s_{2,n}(t) + \int_0^t \eta_2 [s'_{2,n}(\xi) + \overbrace{k_2 s_{2,n}(\xi) c_{1,n}(\xi)} - \overbrace{k_{-2} c_{2,n}(\xi)}] d\xi, \quad (5b)$$

$$p_{n+1}(t) = p_n(t) + \int_0^t \eta_3 [p'_n(\xi) - \overbrace{k_3 c_{2,n}(\xi)}] d\xi \quad (5c)$$

where η_1, η_2, η_3 are Lagrange multipliers.

Here it is to be mentioned that for linear problems, using Variational Iteration Method, it's exact solution can be obtained by only one iteration. But for non linear problems, it's accurate solution can be obtained by iteration due to the fact that the Lagrange multipliers can only be identified approximately.

Considering the variation with respect to $s_{1,n}, s_{2,n}, p_n$, we have:

$$\delta s_{1,n+1}(t) = \delta s_{1,n}(t) + \delta \int_0^t \eta_1 [s'_{1,n}(\xi) + \overbrace{k_1 e_n(\xi) s_{1,n}(\xi)} - \overbrace{k_{-1} c_{1,n}(\xi) s_{2,n}(\xi)}] d\xi \quad (6a)$$

$$\delta s_{2,n+1}(t) = \delta s_{2,n}(t) + \delta \int_0^t \eta_2 [s'_{2,n}(\xi) + \overbrace{k_2 s_{2,n}(\xi) c_{1,n}(\xi)} - \overbrace{k_{-2} c_{2,n}(\xi)}] d\xi, \quad (6b)$$

$$\delta p_{n+1}(t) = \delta p_n(t) + \delta \int_0^t \eta_3 [p'_n(\xi) - \overbrace{k_3 c_{2,n}(\xi)}] d\xi \quad (6c)$$

Here $\overbrace{s_{1,n}(\xi) e_n(\xi)}$, $\overbrace{c_{1,n}(\xi) s_{2,n}(\xi)}$ and $\overbrace{c_{2,n}(\xi)}$ are considered as restricted variations. Under this consideration, the stationary conditions of the above correction functionals (6a), (6b), (6c) can be expressed as follows (here notice that $\delta c_{2,n}(0) = 0, \delta e_n(0) s_{1,n}(0) = 0, \delta c_{1,n}(0) s_{2,n}(0) = 0$)

$$\begin{aligned} \delta s_{1,n} : 1 + \eta_1(\xi)|_{\xi=t} &= 0, \\ \delta s_{1,n} : -\eta'_1(\xi) &= 0. \end{aligned} \quad (7a)$$

$$\begin{aligned} \delta s_{2,n} : 1 + \eta_1(\xi)|_{\xi=t} &= 0, \\ \delta s_{2,n} : -\eta'_1(\xi) &= 0. \end{aligned} \quad (7b)$$

$$\begin{aligned} \delta c_n : 1 + \eta_1(\xi)|_{\xi=t} &= 0, \\ \delta c_n : -\eta'_1(\xi) &= 0. \end{aligned} \quad (7c)$$

The Lagrange multipliers can be obtained using Lagrange-Euler equations from (13a), (13b), (13c) and (13d) as

$$\begin{aligned} \eta_1(\xi) &= -1, \\ \eta_2(\xi) &= -1, \\ \eta_3(\xi) &= -1. \end{aligned} \quad (8)$$

Using (8) and taking $n=0$ in the iteration formula (5a)-(5c) we have,

$$s_{1,1}(t) = s_{1,0}(t) + \int_0^t \eta_1 [s'_{1,0}(\xi) + \overbrace{k_1 e_0(\xi) s_{1,0}(\xi)} - \overbrace{k_{-1} c_{1,0}(\xi) s_{2,0}(\xi)}] d\xi \quad (9a)$$

$$s_{2,1}(t) = s_{2,0}(t) + \int_0^t \eta_2 [s'_{2,0}(\xi) + \overbrace{k_2 s_{2,0}(\xi) c_{1,0}(\xi)} - \overbrace{k_{-2} c_{2,0}(\xi)}] d\xi, \quad (9b)$$

$$p_1(t) = p_0(t) + \int_0^t \eta_3 [p'_0(\xi) - \overbrace{k_3 c_{2,0}(\xi)}]. \quad (9c)$$

We now consider the initial approximate solution satisfying (2) as

$$\begin{aligned} s_{1,0}(t) &= s_{10} e^{-m_1 t}, & s_{2,0}(t) &= s_{20} e^{-m_2 t}, \\ p_0(t) &= \frac{e^{-m_3 t} - e^{-m_4 t}}{m_4 - m_3}, & e_0(t) &= e_0 e^{-m_5 t}, \\ c_{1,0}(t) &= \frac{e^{-m_6 t} - e^{-m_7 t}}{m_7 - m_6}, & c_{2,0}(t) &= \frac{e^{-m_8 t} - e^{-m_9 t}}{m_9 - m_8}. \end{aligned} \quad (10)$$

where $m_i, i = 1, 2, \dots, 9$ are constants.

Thus from (9a)-(9c) along with initial condition (2) we have the approximate solution as given below:

$$s_1(t) \approx s_{10} + (a_1 e^{-b_1 t} - a_1) + a_2 \left\{ \left(\frac{e^{-b_2 t}}{b_2} - \frac{e^{-b_3 t}}{b_3} \right) - \left(\frac{b_3 - b_2}{b_2 b_3} \right) \right\}. \quad (11)$$

$$s_2(t) \approx s_{20} - a_3 \left(\frac{e^{-b_2 t}}{b_2} - \frac{e^{-b_3 t}}{b_3} - \left(\frac{b_3 - b_2}{b_2 b_3} \right) \right) + a_4 \left(\frac{e^{-m_9 t}}{m_9} - \frac{e^{-m_8 t}}{m_8} - \frac{m_8 - m_9}{m_8 m_9} \right). \quad (12)$$

$$p(t) \approx a_5 \left(\frac{e^{-m_9 t}}{m_9} - \frac{e^{-m_8 t}}{m_8} - \frac{m_8 - m_9}{m_8 m_9} \right). \quad (13)$$

where

$$\begin{aligned} a_1 &= \frac{k_1 s_{10}}{m_1 + m_5}, & a_2 &= \frac{k_{-1} s_{20}}{m_7 - m_6}, & a_3 &= \frac{k_2 s_{20}}{m_7 - m_6}, & a_4 &= \frac{k_{-2}}{m_9 - m_8}, \\ a_5 &= \frac{k_3}{m_9 - m_8}, & b_1 &= m_1 + m_5, & b_2 &= m_7 + m_2, & b_3 &= m_6 + m_2. \end{aligned} \quad (14)$$

The system we have considered here is a closed system. So mass will be preserved in this system for all time. Thus from system (1), equation (11-13) and initial condition(2), we get the following expressions:

$$\begin{aligned} e(t) &\approx s_1(t) + p(t) + (e_0 - s_{10}), \\ c_1(t) &\approx -s_1(t) + s_2(t) + (s_{10} - s_{20}), \\ c_2(t) &\approx -s_2(t) - p(t) + s_{20}. \end{aligned} \quad (15)$$

Thus equation (11) - (13) and (15) represent the complete solutions of the model system (1).

4 Numerical Simulation

The present study deals with kinetic reaction of two substrate enzyme kinetics. In this section, we investigate the effect of changes in the reaction parameters numerically which is based on analytical analysis of the reaction system. Numerical analysis represents the kinetic profile of the substrates, enzyme, complexes and product considering the parameter values as given in Table 1. All the numerical results are obtained by using *MATLAB* programming version 8.

Table 1 Values of parameters used for models dynamics calculations [2].

Parameter	Definition	Recommended Value
k_1	Rate constant for forward reaction	$5 \text{ (mole/litre)}^{-1} \text{hour}^{-1}$
k_2	Rate constant for forward reaction	$5 \text{ (mole/litre)}^{-1} \text{hour}^{-1}$
k_{-1}	Rate constant for backward reaction	1 hour^{-1}
k_3	Rate constant for product formation	5 hour^{-1}
k_{-2}	Rate constant for backward reaction	1 hour^{-1}

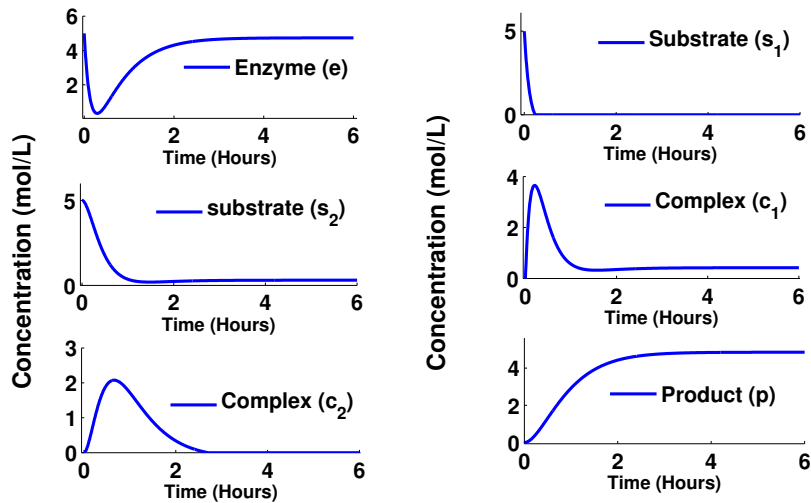


Figure 1. Normalized concentration profile of substrates, enzyme-substrate complexes, enzyme and product by VIM.

For numerical simulation we take $m_1 = 3.1; m_2 = 1.1; m_3 = 2; m_4 = 2; m_5 = 1; m_6 = 1.0005; m_7 = 0.94; m_8 = 1; m_9 = 1.03;$ and k_1, k_{-1} etc. as in Table 1. Moreover we assume that solutions of the system remain positive for all time.

Figure 1 represents the analytical expressions of concentrations of the substrates, enzyme, complexes and product for the parameter values as in Table 1. According to the enzyme behaviour of enzymatic reactions, the substrate concentration decreases initially with time and levels off to extinction nearly at $t = 0.25$ hours. The reaction is rapid at the initial stages of the reaction due to the high reactivity of the first substrate but it gradually falls off with time owing to its removal from the reaction medium to form the first intermediate complex. The concentration of the enzyme substrate complex (c_1) attains a maximum value (3.07 mole/L) at a particular intermediate step of the reaction. Henceforth, the second substrate (s_2) is triggered which interacts with the first complex and generates the second intermediate complex (c_2) in the course of reaction. Concentration of it gradually increase with time after reaching a maximum and levels off at a particular value of its concentration (2.06 mole/L) but it is worth notifying that the reactivity of second substrate S_2 always remains lower than that of S_1 . Due to the lower reactivity of S_2 at a given parametric condition as in Table 1, a finite quantity of it remains unchanged at the end of the reaction. The concentration profile of the second complex exhibits a much lesser variation compared to the first complex which is again indicative of the comparatively lower reactivity of the second complex.

Figure 2 represents the system behavior obtained by *ode45* solver in MATLAB, keeping the parameter values as in Table 1. From Figure 1 and Figure 2, we have made a comparative analysis between VIM and RK4 method. A very similar result is obtained by VIM compare to RK4 method.

5 Discussion and conclusion

In this paper, VIM method is applied to get the approximate solution of a nonlinear system of differential equations. We choose the conventional *RK4* method as standard, as it is widely accepted and used. We compare our results numerically with the results obtained by *ode45* solver. From this we can conclude that VIM method can be applied to solve linear and non-linear *ode* models. The obtained results demonstrate the simplicity, reliability and efficiency of VIM method and the faster convergence of this method as it gives continuous solution. From the numerical solution we see that the results from the proposed method are in an excellent agreement with the solution by *ode45* solver which is based on *RK4* method. VIM is the only method which gives exact solutions or solutions with

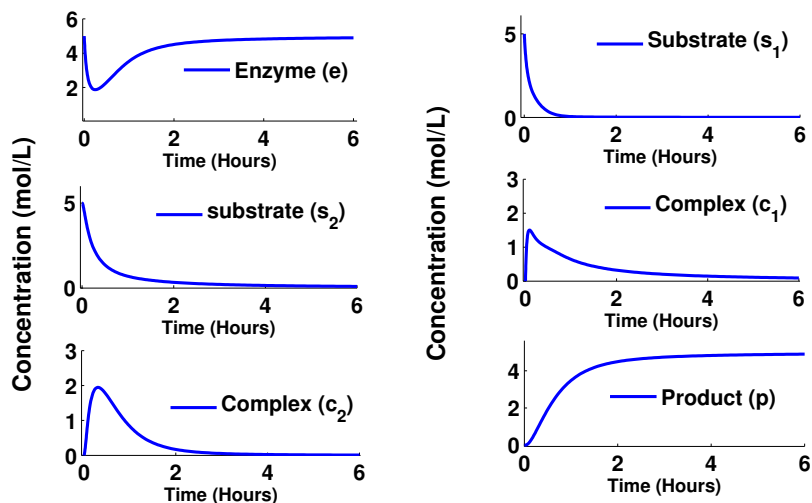


Figure 2. Normalized concentration profile of substrates, enzyme-substrate complexes, enzyme and product by RK4.

high accuracy in a single iteration.

In the chemical point of view, the kinetic profile of the bi-substrate reaction using single enzyme with multiple active sites is presented and the results show the analytical expressions for the concentration of substrates, complexes, product and enzyme after a definite time interval. The concentration curves also reveal significant information regarding yield of product by applying suitable reaction parameters at definite time interval. From the analytical result and numerical simulation of the concentration of different components, it can be concluded that our study can be helpful to understand the dynamical behavior bi-substrate enzymatic system in a better way.

References

1. J. M. Brass, F. W. J. M. M. Hoeks and M. Rohner, *Application of Modeling Techniques for the Improvement of Industrial Bioprocesses*, J. Biotechnol, Vol. 59, (1997), pp. 63-72.
2. R. M. Alicea, *A Mathematical Model for Enzyme Kinetics: Multiple Timescales Analysis*, Dynamics at the Horsetooth, Asymptotics and Perturbations, Vol. 2A, (2010).

3. G. Varadharajan and L. Rajendran, *Analytical Solution of Coupled Non-linear Second Order Reaction Differential Equations in Enzyme Kinetics*, Natural Science, Vol. 3, No. 6. (2011), pp. 459-465.
4. M. C. Hogan and J. M. Woodley, *Modeling of Two Enzyme Reactions in a Linked Cofactor Recycle System for Chiral Lactones Synthesis*, Chem. Engg., Vol.55, (2000), pp. 2001-2008.
5. A. J. J. Straathof, *Development of a Computer Program for Analysis of Enzyme Kinetics by Progress Curve Fitting*, Journal of Mol. Catalysis B:Enzymatic, Vol. 11, (2001), pp. 991-998.
6. S. I. Rubinow, *Introduction to Mathematical Biology*, Wiley, Newyork, (1975).
7. J. D. Murray, *Mathematical Biology*, Springer, Berlin, (1989), pp. 109.
8. L. A. Segel, *Mathematical Models in Molecular and Cellular Biology*, Cambridge University Press, Cambridge, (1980).
9. R. Gentry, L. Ye and Y. Nemerson, *A Mocroscopic Model of Enzyme Kinetics*, Biophysical Journal, Vol. 69, (1995), pp. 356-361.
10. Birkhoff, G., Rota, G.C., 1982, *Ordinary Differential Equations*, Ginn Boston.
11. J. H. He, *Variational Iteration Method-a kind of Non-linear Analytical Technique:Some examples*, International Journal of Non-Linear Mechanics, Vol. 34, (1999), pp. 699-708.
12. M. Inokuti, *General use of the Lagrange multiplier in non-linear mathematical physics: S. Nemat-Nasser (Ed.), Variational Method in the Mechanics of Solids*, Pergamon Press, Oxford, (1978), pp. 156-162.
13. B. A. Finlayson, *The Method of Weighted Residuals and Variational Principles*, Academic Press, New York, (1972).

Acknowledgement: *Research is supported by UGC DRS, Department of Mathematics, Jadavpur University, Kolkata - 700032, India.

Homomorphisms, Structural Ramsey Theory and Limits

Jaroslav Nešetřil

Computer Science Institute of Charles University, Prague

Abstract

In this talk we present 3 recent theorem in 3 seemingly different areas which nevertheless share common approach typical for structural combinatorics.

Seven Conjectures On Lucky Numbers

Pavla Pavlíková

Institute of Chemical Technology, Prague

Keywords: lucky number, prime number, labeling of graph, lucky and chromatic number of graph

Abstract The aim of this article is to present three different mathematical meanings of the term *lucky number* (lucky number of graph, lucky number of Ulam and lucky number of Euler) and comment seven conjectures about this kind of numbers.

*"Good mathematicians see analogies
between theorems or theories,
the very best ones see
analogies between analogies."*
STEFAN BANACH (1892–1945)

1 Introduction

It is very likely that you have heard that 3 or 7 are lucky numbers for somebody and 13 seems to be unlucky (this is not the case of Italians, they believe that 17 is unlucky number). But in this sense it is strictly individual problem. In this article we would like to present some mathematical aspects of the term *lucky number*.¹ We will focus on the lucky numbers in graph theory and number theory.

2 Lucky numbers in graph theory

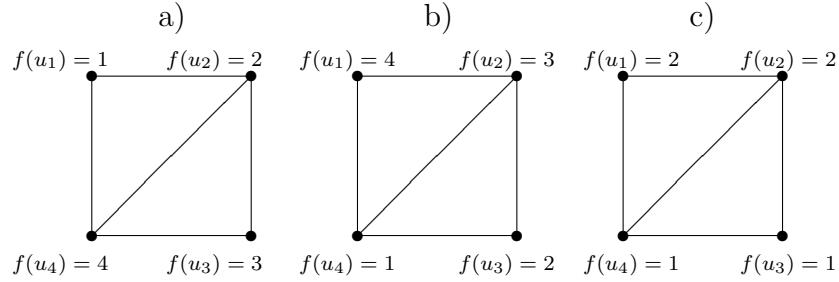
Let $G = (V(G), E(G))$ be undirected graph without loops or multiple edges. Let $f : V(G) \rightarrow \mathbb{N}$ be a labeling of its vertices. We call this labeling *lucky* if for every

¹ Please, be careful not to confuse these numbers with happy or Fortunate numbers (see [12] for more details).

edge $\{u, v\} \in E(G)$ holds the condition

$$\sum_{w \sim u} f(w) \neq \sum_{w \sim v} f(w).$$

We demonstrate it on the next picture.



The labeling in case a) is not lucky because

$$\sum_{w \sim u_1} f(w) = 6 = \sum_{w \sim u_4} f(w).$$

The same graph in case b) has lucky labeling $f : V(G) \rightarrow \{1, 2, 3, 4\}$. But we can see that it is not necessary to use so "large" set to become a lucky labeling of this graph. In case c) we have a "more economical" lucky labeling $f : V(G) \rightarrow \{1, 2\}$. This leads us to the definition of a lucky number of a graph.

Definition 1. *Lucky number of a graph G (denoted by $\eta(G)$) is the minimal number k such that G has lucky labeling $f : V(G) \rightarrow \{1, 2, \dots, k\}$.*

It is trivial to prove that lucky labeling exists for every undirected graph without loops or multiple edges. In [3] the authors have presented the following conjecture:

Conjecture 1. *For every graph G with the lucky number $\eta(G)$ and the chromatic² number $\chi(G)$ holds the condition $\eta(G) \leq \chi(G)$.*

The graph which we have studied on the picture above has the lucky number $\eta(G) = 2$ and the chromatic number $\chi(G) = 3$ (because it involves an odd cycle).

Studying the computational complexity of the lucky number problem is far from being easy. In [1] we can find a following theorem and subsequent conjecture:

² The *chromatic number* $\chi(G)$ of a graph G is the smallest number of colors needed to color the vertices of G so that no two adjacent vertices have the same color.

Theorem 1. *It is a NP-complete problem³ to decide if for a given planar 3-colorable⁴ graph G holds $\eta(G) = 2$.*

Conjecture 2. *It is a NP-complete problem to decide if for a given 3-regular⁵ graph G holds $\eta(G) = 2$.*

3 Lucky numbers in number theory

In 1956 Stanislaw Marcin Ulam (1909–1984) with his colleagues Verna L. Gardiner, Roger B. Lazarus and Nicolas C. Metropolis from Los Alamos Scientific Laboratory introduced in [5] a special sequence of natural numbers generated by a sieve⁶ similar to the sieve of Eratosthenes (for generating the prime numbers).

Here is the description of the sieving procedure: first we consider the sequence of all positive integers 1, 2, 3, ... Then we eliminate every second term by counting from 1. This step leads to the sequence of odd integers. The first integer (apart from 1) remaining is 3, so we next eliminate every third number not yet eliminated. After this step we get the sequence 1, 3, 7, 9, 13, 15, 19, 21, 25, etc., in which the first integer after 1 and 3 is 7. So we eliminate every seventh number (first eliminated is 19) in the next step. We can continue in this way indefinitely long. The numbers which survive the sieving procedure are called *lucky numbers*:

$$1, 3, 7, 9, 13, 15, 21, 25, 31, \dots$$

It is very interesting that lucky numbers have many properties analogous to the prime numbers. If we denote as p_n the n -th prime and l_n the n -th lucky number, then we get ([9]) two asymptotics

$$p_n = n \log n + n \log \log n + o(n \log \log n)$$

and

$$l_n = n \log n + \frac{1}{2}n(\log \log n)^2 + o(n(\log \log n)^2).$$

³ A problem \mathcal{P} is said to be *NP-complete* if it is in NP (the solution can be verified in non-deterministic polynomial time) and every problem from NP is reducible to \mathcal{P} in a polynomial time. The most famous NP-complete problems are the Hamiltonian path problem, the travelling salesman problem, the graph coloring problem, etc.

⁴ A graph G is said to be *3-colorable* if $\chi(G) \leq 3$.

⁵ We say that a graph G is *3-regular* (or *cubic*) if all its vertices have exactly three neighbors.

⁶ Sometimes it is called "sieve of Josephus Flavius" in the literature. The name is derived from the similarity with a special mathematical problem, called Josephus Problem, named after a Jewish historian Josephus Flavius (37–100). For the history of Josephus Problem see [13].

Then, for sufficiently large n , the condition $l_n > p_n$ holds, which S. Ulam predicted in [5]. There are infinitely many lucky numbers, but it is not known whether there are infinitely many primes among them.

Conjecture 3. *There are infinitely many lucky primes.*

We can call two lucky numbers which differ by 2 as *twin luckies* (similar as we define twin primes). It seems that the number of twin luckies and twin primes not exceeding given number N are almost the same. According to the twin-primes conjecture ([7]) we get:

Conjecture 4. *There exist infinitely many twin luckies.*

One of the most famous unsolved problems from number theory is the Goldbach conjecture⁷ which states that every even number greater than 2 can be written as a sum of two prime numbers ([8]). The team from Los Alamos studied in [5] the analogy for lucky numbers and proved that it holds for every even number up to 100 000. If it is true in general it is not known.

Conjecture 5. *Every even positive integer could be written as a sum of two lucky numbers.*

Denoting $L_2(n)$ as the number of ways how to write an even number n as a sum of two lucky numbers, Stein and Stein have found values of n for which $L_2(n) = k$ for all $k \leq 1769$ (see [14], [4]).

According to the quotation above we can write $l_1 = 1$, $l_2 = 3$, $l_3 = 7$, etc. The curious fact is that $l_3 = 7$ and 37 is also lucky number, $l_4 = 9$ and 49 is also lucky number, $l_6 = 15$ and 615 is lucky too, etc. In [2] have Ch. Ashbacher stated this conjecture:

Conjecture 6. *There exist infinitely many $k \in \mathbb{Z}$ such that $l_k = m$ is a lucky number and km is lucky too (that means: k is written before m , not k multiplied by m).*

It is well known that there does not exist a polynomial formula with integer coefficients generating only prime numbers (see [8]). Martin Gardner (1914–2002) guessed in [6] the following:

Conjecture 7. *There is no polynomial formula generating only lucky numbers.*

Sometimes we can find quadratic formulas generating restricted sequences of lucky numbers. If we use the method of S. Ulam, we can write the integers in

⁷ Tomás Oliviera e Silva have tested this conjecture on computer ([11]) and proved it for all $n < 4 \cdot 10^{18}$.

a spiral (it doesn't matter what number is in the center). From this spiral we can see that the lucky numbers tend to line up along diagonal lines. On the next picture there is an example of a part of such a spiral starting in number 13. The lucky numbers are bold-faced.

·	97	98	99	100	101	102	103
·	64	65	66	67	68	69	104
·	39	40	41	42	43	70	105
·	22	23	24	25	44	25	·
·	21	14	15	26	45	72	·
·	20	13	16	27	46	73	·
·	19	18	17	28	47	74	·
·	·	·	·	·	·	·	·

For example, the sequence of lucky numbers 13, 15, 25, 43, 69 on a diagonal can be generated by a quadratic formula $4x^2 - 2x + 13$ ($x = 0, 1, 2, 3, 4$).

Very famous is a formula $n^2 + n + 41$ of Leonhard Euler, which generates primes by letting $n = 0, 1, \dots, 39$. From this point there is just a small step to the last definition of lucky numbers.

4 Lucky numbers of Euler

Definition 2. We say that p is a lucky number of Euler if the values of a polynomial $n^2 - n + p$ are primes for every $n = 1, 2, \dots, p - 1$.

French chemical engineer and mathematician François Le Lionnais (1901–1984) stated in [10] that there exist only six such numbers, namely 2, 3, 5, 11, 17 and 41.

5 Conclusion

In spite of the fact that 70 is not a lucky number in the previous sense, we are glad that we can celebrate the 70th anniversaries of our dear colleagues during this colloquium and we would like to wish them that every number in their lives be lucky.

References

1. A. AHADI, A. DEGHAN, M. KAZEMI, E. MOLLAHMADI: *Computation of lucky number of planar graphs is NP-hard*. Inform. Process. Lett. 112 (2012), 109–112.
2. CH. ASHBACHER: *Collection of Problems on Smarandache Notions*, Erhus University Press, 1996, 51–52.
3. S. CZERWIŃSKI, J. GRYTCZUK, W. ŻELAZNY: *Lucky labeling of graphs*. Inform. Process. Lett. 109 (2009), 1078–1081.
4. C. J. EVERETT, P. R. STEIN: *On random sequences of integers*, Bull. AMS 76 (1970), no. 2, 349–351.
5. V. GARDINER, R. LAZARUS, N. METROPOLIS, S. ULAM: *On certain sequences of integers defined by sieves*, Math. Mag. 29 (1956), 117–122.
6. M. GARDNER: *Lucky numbers and 2187*, Math. Intell. 19 (1997), 26–29.
7. R. K. GUY: *Unsolved Problems in Number Theory*, 3rd ed., Springer-Verlag, 2004.
8. G. H. HARDY, E. M. WRIGHT: *An Introduction to the Theory of Numbers*, 5th ed., Oxford, Clarendon Press, 1979.
9. D. HAWKINS, W. E. BRIGGS: *The lucky number theorem*, Math. Mag. 31 (1957), no. 2, 81–84, 277–280.
10. F. LE LIONNAIS: *Les nombres remarquables*, Paris, Hermann, 1983.
11. T. OLIVEIRA E SILVA, S. HERZOG, S. PARDI: *Empirical verification of the even Goldbach conjecture and computation of prime gaps up to $4 \cdot 10^{18}$* , accepted for publication in Mathematics of Computation, 2013.
12. P. PAVLÍKOVÁ: *O čísle 13*, Sborník semináře Matematika na vysokých školách, Praha, ČVUT, 2013, 106–108.
13. P. PAVLÍKOVÁ: *O Josephově problému*, PMFA 57 (2012), 274–284.
14. M. L. STEIN, P. R. STEIN: *Tables of the number of binary decompositions of all even numbers $0 < 2n < 200\,000$ into prime numbers and lucky numbers*, Los Alamos Scientific Laboratory report LA-3106 (1965), vol. 1 and 2.

Fourier Invariants

Pavel Pokorný

Institute of Chemical Technology, Prague

Keywords: Fourier transform, iteration, fixed point

Abstract The simple structure of all functions invariant under Fourier transform is derived and illustrated.

Consider the Fourier transform \mathcal{F} for a complex-valued smooth absolutely integrable function s of one real argument

$$(\mathcal{F}s)(\nu) = \int_{-\infty}^{\infty} s(t) \exp(-i2\pi\nu t) dt = \int_{-\infty}^{\infty} s(t) (\cos(2\pi\nu t) - i \sin(2\pi\nu t)) dt$$

for $\nu \in R$, and its inverse

$$(\mathcal{F}^{-1}s)(\nu) = \int_{-\infty}^{\infty} s(t) \exp(+i2\pi\nu t) dt = \int_{-\infty}^{\infty} s(t) (\cos(2\pi\nu t) + i \sin(2\pi\nu t)) dt$$

for $\nu \in R$.

If s is even, i.e. $s(-t) = s(t)$ for all $t \in R$ then

$$(\mathcal{F}s)(\nu) = \int_{-\infty}^{\infty} s(t) \cos(2\pi\nu t) dt = (\mathcal{F}^{-1}s)(\nu)$$

and thus

$$\mathcal{F}^2 s = s$$

where $\mathcal{F}^2 s = \mathcal{F}\mathcal{F}s$ and

$$\mathcal{F}^4 s = s.$$

Similarly, if s is odd i.e. $s(-t) = -s(t)$ for all $t \in R$ then

$$(\mathcal{F}s)(\nu) = -i \int_{-\infty}^{\infty} s(t) \sin(2\pi\nu t) dt = -(\mathcal{F}^{-1}s)(\nu)$$

and thus

$$\mathcal{F}^2 s = -s$$

and again

$$\mathcal{F}^4 s = s.$$

As any function s can be written as a sum of an even function and of an odd function

$$s(t) = s_{\text{even}}(t) + s_{\text{odd}}(t) \quad t \in \mathbb{R}$$

where

$$s_{\text{even}}(t) = \frac{s(t) + s(-t)}{2}$$

and

$$s_{\text{odd}}(t) = \frac{s(t) - s(-t)}{2}$$

and due to linearity of \mathcal{F} we have $\mathcal{F}^4 s = s$ for any s . Thus we can formulate the following

Theorem 1. *The function*

$$u = s + \mathcal{F}s + \mathcal{F}^2 s + \mathcal{F}^3 s \tag{1}$$

is invariant under the Fourier transform.

Proof :

$$\mathcal{F}u = \mathcal{F}(s + \mathcal{F}s + \mathcal{F}^2 s + \mathcal{F}^3 s) = \mathcal{F}s + \mathcal{F}^2 s + \mathcal{F}^3 s + \mathcal{F}^4 s = \mathcal{F}s + \mathcal{F}^2 s + \mathcal{F}^3 s + s = u. \quad \blacksquare$$

Conversely, any invariant u of \mathcal{F} can be written in the form of (1) when we set $s = u/4$.

Also, note that due to

$$s + \mathcal{F}^2 s = 2s_{\text{even}}$$

any Fourier invariant is even.

Example 1. *It is well known that the Gaussian function*

$$g(t) = \exp(-\pi t^2)$$

is invariant under the Fourier transform. However, its shifted version

$$s(t) = \exp(-\pi(t-1)^2)$$

is not invariant. Still it can be used to construct an invariant by (1). We get

$$\begin{aligned} (\mathcal{F}s)(t) &= \exp(-\pi t^2 - i2\pi t) \\ (\mathcal{F}^2 s)(t) &= \exp(-\pi(t+1)^2) \\ (\mathcal{F}^3 s)(t) &= \exp(-\pi t^2 + i2\pi t) \end{aligned}$$

and then

$$u(t) = \exp(-\pi(t-1)^2) + \exp(-\pi(t+1)^2) + 2 \cos(2\pi t) \exp(-\pi t^2).$$

References

1. I. N. SNEDDON, *Fourier Transforms*, McGraw-Hill Book Company, 1951

Enhancement of Biodiesel Production from *Jatropha Curcas* oil: A Mathematical Study through Control on Backward Reaction Process

Priti Kumar Roy and Fahad Al Basir

Center for Mathematical Biology and Ecology,
Department of Mathematics,
Jadavpur University, Kolkata 700032, India.

Keywords: Biodiesel, *Jatropha Curcas* Oil, Transesterification, Optimization, Forward Reaction, Backward Reaction.

Abstract Biodiesel generates a lot of attention among the alternative renewable energy sources in the present depleting inclinations of non-renewable energy sources. Production of biodiesel from vegetable oil is a reversible process. Production of biodiesel from *Jatropha Curcas* oil depends considerably on reaction parameters such as temperature of reaction, molar ratio of oil to alcohol and mixing intensity. Control on backward reaction rate results enhancement of biodiesel production in the stipulated time period. Here we consider a set of differential equations for transesterification reaction kinetics. We apply mathematical control input parameter in the backward reaction for the cost effective production of biodiesel. Results from our analysis of the model are consistent with numerical observation.

1 Introduction

Generally, biodiesel is produced from *Jatropha Curcas* oil by means of catalytic transesterification process. Other methods of biodiesel production are much slower [1]. Thus catalytic transesterification process is used as it is the most economical and faster procedure. *Jatropha Curcas* oil contains mainly triglycerides which can be converted to biodiesel through transesterification with alcohol. Under normal condition, this reaction happens very slowly. Thus temperature, stirring and catalysts etc. are used to speed up the forward reaction.

Transesterification of *Jatropha* oil and alcohol is a reversible reaction. Some conditions (such as temperature, molar ratio etc,) increase the forward reaction and some conditions increase the backward reactions. If forward reaction

increases then production increases and if backward reaction increases then production decreases. Reaction rate is mainly depends on temperature, molar ratio, catalyst concentration, stirring. More explicitly, The rate of the reaction at lower temperature is slow. If we increase the temperature, forward reaction enhanced, which results a higher production of biodiesel. Stirrer speed is has a significant role in biodiesel production. At 600 rpm stirrer speed, biodiesel can be obtained at maximum level. If we increase or decrease the stirrer speed from 600 rpm, the backward reaction increases. Again to speed up the reaction, a catalyst can be used. It increases the rate reactions and so production can be obtained quickly. Thus we see that controlling factors (such as temperature, molar ratio, catalyst, stirring etc.) can be altered to increase or decrease reaction rate.

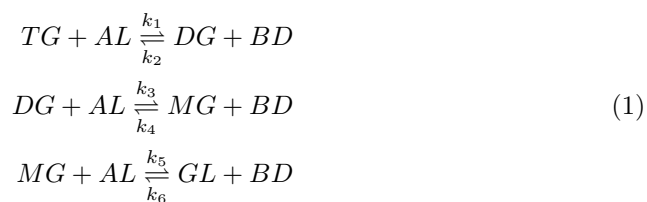
Transesterification or alcoholysis is commonly used to convert the Jatropha oil to biodiesel. There are many research articles based on the modeling strategies for biodiesel production. The development of kinetic models for transesterification reactions for biodiesel production were established by Nouredini and Zhu [2], Bambase [3], Berchmans [4], Vicente [5], Paola [6], Stamenkovic [7] and Diwekar [8]. Freedman et al., [9] observed that standard reaction conditions for the transesterification of soybean oils are molar ratio 6 : 1 of methanol to oil, 0.5 wt.% alkali catalyst (with respect to triglycerides), 600 rpm stirrer speed, 60°C reaction temperature and 60 minute reaction time to produce maximum methyl ester (biodiesel). Hifjur et al., [10] has shown that 99% yield of biodiesel having properties like diesel can be obtained from Jatropha oil at 60°C, keeping alcohol to oil molar ratio 6 : 1 with 88 minutes as reaction time. In his research work, Nipong showed that at 6 : 1 molar ratio, 60°C reaction temperature and 40 minutes reaction time 98.6%w/w yield of biodiesel can be obtained. Culshaw [11] used NaOH to oil as alkaline catalyst to produce biodiesel at 60°C. The final yield of methyl esters was 90% in 120 minute. Tiwari et al., [12] have studied that the equilibrium conversions of triglycerides was observed to be in the range of 50%-83% biodiesel from Jatropha oil. The equilibrium conversions were achieved in less than 45 minutes for both oils. It was also observed that the temperature and molar ratio had a positive influence on the reaction. But to get maximum production of biodiesel, a mere obstruction is the revert reaction which is the causal effect for less production of biodiesel. On that outlook control mathematical approach in reverse reaction is very much essential, which is not yet been explored.

It has been observed that temperature, molar ratio, catalyst concentration, stirring are important factors for biodiesel production. To get maximum production of biodiesel, a mere obstruction is the revert reaction which is a reason for less production of biodiesel. On that outlook control mathematical approach in reverse reaction is very much essential, which is not yet been explored. In this research article we want to find out a control policy that can be changed

with time by using the dynamic optimization. Here, the model equations are analyzed in two different ways viz. analytical and numerical simulation. For the determination of optimal control policy, ‘‘Pontryagin Minimum Principle’’ has been adopted. Numerical simulation has been done to analyze the system conditions for which the backward rate of reaction can be reduced and maximum biodiesel production can be obtained.

2 Formulation of the Mathematical Model

Biodiesel is produced by the transesterification of triglycerides with methanol in presence of NaOH. This reaction consists of three step wise reversible reactions, where three moles of methanol react with one mole of triglycerides. In the first step triglycerides (TG) is converted to diglycerides (DG), in second step diglycerides (DG) is converted to monoglycerides (MG) and in the final step monoglycerides (MG) is converted glycerol(GL). At each reaction step, one molecule of biodiesel (BD) is produced for each molecule of methanol consumed [2], [13]. The reaction steps and overall reaction are given below by schematic diagram, where k_1 to k_6 are the reaction rate constants.



Here k_1 , k_3 and k_5 are forward reaction rate constants and k_2 , k_4 and k_6 are backward reaction rate constants. The values of k_1 to k_6 are shown in Table 1. We denote the concentrations of triglycerides, diglycerides, monoglycerides, biodiesel (methyl ester), methanol(alcohol) and glycerol by x_T, x_D, x_M, x_B, x_A and x_G respectively. Using the law of mass action, we get the following mathematical model which characterize the stepwise reactions,

$$\begin{aligned}
\frac{dx_B}{dt} &= k_1x_Tx_A - k_2x_Dx_B + k_3x_Dx_A - k_4x_Mx_B + k_5x_Mx_A - k_6x_Gx_B, \\
\frac{dx_T}{dt} &= -k_1x_Tx_A + k_2x_Dx_B, \\
\frac{dx_D}{dt} &= k_1x_Tx_A - k_2x_Dx_B - k_3x_Dx_A + k_4x_Mx_B, \\
\frac{dx_M}{dt} &= k_3x_Dx_A + k_4x_Mx_B - k_5x_Mx_A + k_6x_Gx_B, \\
\frac{dx_A}{dt} &= -k_1x_Tx_A + k_2x_Dx_B - k_3x_Dx_A + k_4x_Mx_B - k_5x_Mx_A + k_6x_Gx_B, \\
\frac{dx_G}{dt} &= k_5x_Mx_A + k_6x_Gx_B.
\end{aligned} \tag{2}$$

Here the reaction constants k_1 , k_3 , k_5 are forward and k_2 , k_4 and k_6 are backward reaction rate constants. Model system (2) characterizes the transes-terification dynamics without any control inputs.

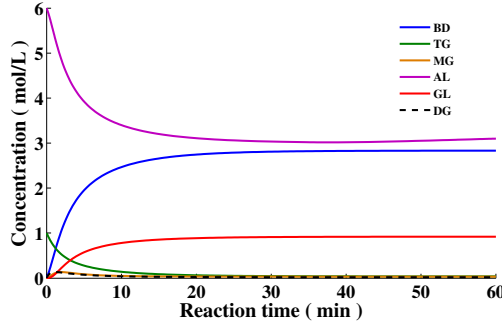
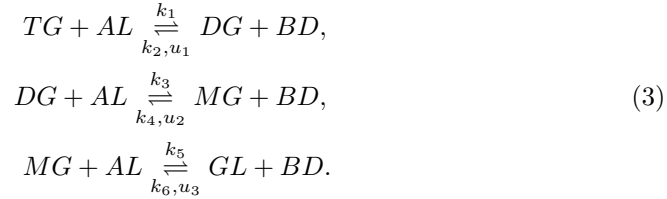


Figure 1. Concentration profiles of BD, TG, DG, MG, AL, and GL as a function of time for various values of reaction parameters given in Table 1 (without control).

3 The Optimal Control Problem

The reaction constants $k_1 - k_6$ can be expressed by the equation $k_i = a_i e^{-\frac{b_i}{T}}$, where T is the reaction temperature, a_i is the frequency factor and $b_i = \frac{Ea_i}{R}$ in which Ea_i is the activation energy for each component and R is the universal gas constant. Here, reaction constants are functions of temperature. Backward

reaction constants k_2, k_4, k_6 can be controlled by temperature. It is shown that reaction rates depend on mass transfer resistance rate [14]. It has been shown that reaction dynamics highly depends on mixing conditions [15]. Thus we can consider that the backward reaction rate can be reduced using control $u(t)$. Here we have introduced three control parameters $u_1(t)$, $u_2(t)$ and $u_3(t)$ in the backward reaction of first step, second step and third step respectively. The corresponding reaction mechanism is given by the following schematic diagram:



We apply the control inputs $u_1(t)$, $u_2(t)$ and $u_3(t)$ to reduce the rate of backward reaction, so that we can get more biodiesel in each step of transesterification reaction. Here $u_i(t)$ represents control input with values normalized between 0 and 1 [11]. Also $u_i(t) = 1$ represents the maximal use of control and $u_i(t) = 0$, which signifies no control. These control parameters are introduced to minimize the backward reaction, eventually which will maximize the production of biodiesel concentration. From mechanism (3) and law of mass action, we have the following control induced mathematical model of transesterification process:

$$\begin{aligned}
 \frac{dx_B}{dt} &= k_1 x_T x_A - k_2(1 - u_1) x_D x_B + k_3 x_D x_A - k_4(1 - u_2) x_M x_B \\
 &\quad + k_5 x_M x_A - k_6(1 - u_3) x_G x_B, \\
 \frac{dx_T}{dt} &= -k_1 x_T x_A + k_2(1 - u_1) x_D x_B, \\
 \frac{dx_D}{dt} &= k_1 x_T x_A - k_2(1 - u_1) x_D x_B - k_3 x_D x_A + k_4(1 - u_2) x_M x_B, \\
 \frac{dx_M}{dt} &= k_3 x_D x_A + k_4(1 - u_2) x_M x_B - k_5 x_M x_A + k_6(1 - u_3) x_G x_B, \\
 \frac{dx_A}{dt} &= -\frac{dx_B}{dt}, \\
 \frac{dx_G}{dt} &= k_5 x_M x_A + k_6(1 - u_3) x_G x_B,
 \end{aligned} \tag{4}$$

with initial conditions: $x_B(0) = x_{B_0}$, $x_T(0) = x_{T_0}$, $x_D(0) = x_{D_0}$, $x_M(0) = x_{M_0}$, $x_A(0) = x_{A_0}$, $x_G(0) = x_{G_0}$.

The cost function is thus formulated as:

$$J(u_1, u_2, u_3) = \int_{t_i}^{t_f} [Pu_1^2(t) + Qu_2^2(t) + Ru_3^2(t) - Sx_B^2(t)]dt. \quad (5)$$

The parameters P , Q and R are the positive weight constants on the benefit of the cost of production and S is the penalty multiplier. The benefit is based on the minimization of cost together with maximization of biodiesel concentration. Our aim is to find out the optimal control triplet $u^*=(u_1^*, u_2^*, u_3^*)$ such that

$$J(u_1^*, u_2^*, u_3^*) = \min (J(u_1, u_2, u_3) : (u_1, u_2, u_3) \in U),$$

where $U = U_1 \times U_2 \times U_3$,

$$U_1 = \{u_1(t) : u_1 \text{ is measurable and } 0 \leq u_1 \leq 1, t \in [t_i, t_f]\},$$

$$U_2 = \{u_2(t) : u_2 \text{ is measurable and } 0 \leq u_2 \leq 1, t \in [t_i, t_f]\},$$

$$\text{and } U_3 = \{u_3(t) : u_3 \text{ is measurable and } 0 \leq u_3 \leq 1, t \in [t_i, t_f]\}.$$

Here we use ‘‘Pontryagin Minimum Principle’’ [16] to find $u^*(t)$. The Hamiltonian is given by

$$\begin{aligned} H = & [Pu_1^2(t) + Qu_2^2(t) + Ru_3^2(t) - Sx_B^2(t)] + \\ & \xi_1 \{k_1x_Tx_A - (1 - u_1)k_2x_Dx_B + k_3x_Dx_A - (1 - u_2)k_4x_Mx_B \\ & + k_5x_Mx_A - k_6(1 - u_3)x_Gx_B\} + \xi_2 \{-k_1x_Tx_A + (1 - u_1)k_2x_Dx_B\} \\ & + \xi_3 \{k_1x_Tx_A - (1 - u_1)k_2x_Dx_B - k_3x_Dx_A + (1 - u_2)k_4x_Mx_B\} \\ & + \xi_4 \{k_3x_Dx_A + (1 - u_2)k_4x_Mx_B - k_5x_Mx_A + (1 - u_3)k_6x_Gx_B\} \\ & + \xi_5 \{-(k_1x_Tx_A - (1 - u_1)k_2x_Dx_B + k_3x_Dx_A - (1 - u_2)k_4x_Mx_B \\ & + k_5x_Mx_A - k_6(1 - u_3)x_Gx_B)\} + \xi_6 \{k_5x_Mx_A \\ & + k_6(1 - u_3)x_Gx_B\}. \end{aligned} \quad (6)$$

Where, ξ_1 , ξ_2 , ξ_3 , ξ_4 , ξ_5 and ξ_6 are adjoint variables.

Theorem 1. *The objective cost function $J(u_1^*, u_2^*, u_3^*)$ over U is minimum for the optimal control u^* corresponding to the interior equilibrium $(x_B^*, x_T^*, x_D^*, x_M^*, x_A^*, x_G^*)$ and also there exist adjoint variables $\xi_1, \xi_2, \xi_3, \xi_4, \xi_5$ and ξ_6 which satisfy the following equations:*

$$\begin{aligned}
\frac{d\xi_1}{dt} &= -[-Sx_B + \xi_1(-k_2(1-u_1)x_D - k_6(1-u_3)x_G - k_4(1-u_2)x_M + \\
&\quad \xi_2k_2(1-u_1)x_D + \xi_3(-k_2(1-u_1)x_D + k_4(1-u_2)x_M) + \\
&\quad \xi_4(-k_4(1-u_2)x_M + k_6x_G) + \xi_5(k_2x_D + k_6(1-u_3)x_G) \\
&\quad + \xi_6(-k_6(1-u_3)x_G)], \\
\frac{d\xi_2}{dt} &= -[\xi_1k_1x_A + \xi_3k_1x_A - \xi_5k_1x_A], \\
\frac{d\xi_3}{dt} &= -[-\xi_1k_4(1-u_2)x_B + \xi_1k_3x_A + \xi_2k_2(1-u_1)x_B - \xi_3k_2(1-u_1)x_B \\
&\quad - \xi_3k_3x_A + \xi_4k_3x_A + \xi_5(k_2(1-u_1)x_B - k_3x_A)], \\
\frac{d\xi_4}{dt} &= -[-\xi_1k_4(1-u_2)x_B + \xi_3k_4(1-u_2)x_B + \xi_4(-k_5x_A \\
&\quad - k_4(1-u_2)x_B) + \xi_5(-k_5x_A + k_4(1-u_2)x_B) + \xi_6k_5x_A], \\
\frac{d\xi_5}{dt} &= -[\xi_1(k_1x_T + k_3x_D + k_5x_M) - \xi_2k_1x_T - \xi_3k_3x_A + \xi_4(k_3x_D \\
&\quad - k_5x_M) + \xi_5(-k_1x_T - k_3x_A - k_5x_M) + \xi_6k_5x_M], \\
\frac{d\xi_6}{dt} &= -[-\xi_1k_6(1-u_3)x_B + \xi_4k_6(1-u_3)x_B + \xi_5k_6(1-u_3)x_B \\
&\quad - \xi_6k_6(1-u_3)x_B], \tag{7}
\end{aligned}$$

along with the transversality condition $\xi_i(t_f) = 0$ for $i = 1, 2, 3, 4, 5, 6$.

According to the Pontryagin Minimum Principle [17], the unconstrained optimal control variables u_1^* , u_2^* and u_3^* satisfy

$$\frac{\partial H}{\partial u_i^*} = 0, i = 1, 2, 3. \tag{8}$$

Thus from (6) and (8), we have

$$\begin{aligned}
u_1^*(t) &= \frac{k_2x_Bx_D(\xi_2 + \xi_5 - \xi_1 - \xi_3)}{P}, \\
u_2^*(t) &= \frac{k_2x_Bx_M(\xi_3 + \xi_5 - \xi_1 - \xi_4)}{Q}, \\
u_3^*(t) &= \frac{k_2x_Bx_G(\xi_4 + \xi_5 - \xi_1 - \xi_6)}{R}. \tag{9}
\end{aligned}$$

Due to the boundedness of the standard control [11],

$$u_1^*(t) = \begin{cases} 0, & \frac{k_2 x_B x_D (\xi_2 + \xi_5 - \xi_1 - \xi_3)}{P} \leq 0, \\ \frac{k_2 x_B x_D (\xi_2 + \xi_5 - \xi_1 - \xi_3)}{P}, & 0 < \frac{k_2 x_B x_D (\xi_2 + \xi_5 - \xi_1 - \xi_3)}{P} < 1, \\ 1, & \frac{k_2 x_B x_D (\xi_2 + \xi_5 - \xi_1 - \xi_3)}{P} \geq 1. \end{cases}$$

Hence the compact form of $u_1^*(t)$ is

$$u_1^*(t) = \max(0, \min(1, \frac{k_2 x_B x_D (\xi_2 + \xi_5 - \xi_1 - \xi_3)}{P})). \quad (10)$$

In a similar way, we have the compact form of $u_2^*(t)$ and $u_3^*(t)$ as

$$u_2^*(t) = \max(0, \min(1, \frac{k_2 x_B x_M (\xi_3 + \xi_5 - \xi_1 - \xi_4)}{Q})), \quad (11)$$

$$u_3^*(t) = \max(0, \min(1, \frac{k_2 x_B x_G (\xi_3 + \xi_5 - \xi_1 - \xi_4)}{Q})). \quad (12)$$

According to ‘‘Pontryagin Minimum Principle’’ [16], we can write

$$\frac{d\xi_i}{dt} = -\frac{\partial H}{\partial x_i}, \quad i = 1, 2, 3, 4, 5, 6. \quad (13)$$

where $x_i \equiv (x_B, x_T, x_D, x_M, x_A, x_G)$

and the necessary condition satisfying the optimal control $u^*(t)$ are

$$H(x_i(t), u^*(t), \xi_i(t), t) = \min_{u \in U} (H(x_i(t), u(t), \xi_i(t), t)), \quad i = 1, 2, 3, 4, 5, 6. \quad (14)$$

So the system of equations (7) can be obtained from the relation (13). According to Pontryagin Minimum Principle, the adjoint variables satisfied the condition $\xi_i(t_f) = 0$, ($i = 1, 2, 3, 4, 5, 6$).

Table 1. Values of parameters used for numerical simulation at 323K [8]

Parameters	Recommended Value (Unit)
k_1	0.0500 ($mol^{-1}lit \ min^{-1}$)
k_2	0.1099 ($mol^{-1}lit \ min^{-1}$)
k_3	0.1220 ($mol^{-1}lit \ min^{-1}$)
k_4	0.2147 ($mol^{-1}lit \ min^{-1}$)
k_5	0.2420 ($mol^{-1}lit \ min^{-1}$)
k_6	0.0070 ($mol^{-1}lit \ min^{-1}$)

4 Numerical Simulation

The reaction system equations of transesterification are analyzed using numerical methods in MATLAB. The present study deals with the application of control theory with an objective to maximize the biodiesel production. In this section, we have investigated the change of reaction dynamics with the parameters through the optimal control approach.

Figure 1 represents the concentration profile of the BD , TG , DG , MG , AL and GL in the absence of any control parameters. TG concentration falls off with time as it is consumed with the progress of the reaction. However the consumption is rapid at the initial stages due to initial higher rate of collision between alcohol and triglycerides but gradually becomes slow with time possibly due to the backward reversible reaction. Biodiesel concentration increases rapidly at the beginning due to higher rate of collision between alcohol and triglycerides but gradually becomes slow. After 60 minute of reaction time, there is no significant change in biodiesel concentration due to the backward reversible reaction. Same situation is also happens for other components. there is no further change occurs after reaching this time. That means the system is in equilibrium condition. If control input is applied to backward reversible reaction in each step to reduce the reaction rate, the production of biodiesel is maximized. Furthermore, TG concentration is expected to be minimum implementing control policy.

Optimization and quantization of biodiesel is quite valuable by applying control theoretic approach. Our numerical results reveal that the production of biodiesel through control measures from initial stage of reaction is much higher rather than the final phase of reaction. So it is obvious to get maximum biodiesel within a short period of time by adopting this approach.

Figure 2 illustrates how the control triplet (u_1^*, u_2^*, u_3^*) act on the system with time. From this figure we see that the control approach on third step is more essential except the other two steps. Glycerol is produced in this step. If we replace it then the backward rate of reaction will decrease.

Finally, Figure 3 represents the concentration profile of biodiesel. Here we are comparing the concentration profiles in two different venues which are mentioned as without control and at the optimal control level. From this figure, it is observed that the control induced system give more production of biodiesel with respect to time. Our result shows that at 50 minute of reaction time, the concentration of biodiesel at optimal level reaches its maximum value as 2.961 mole, while the

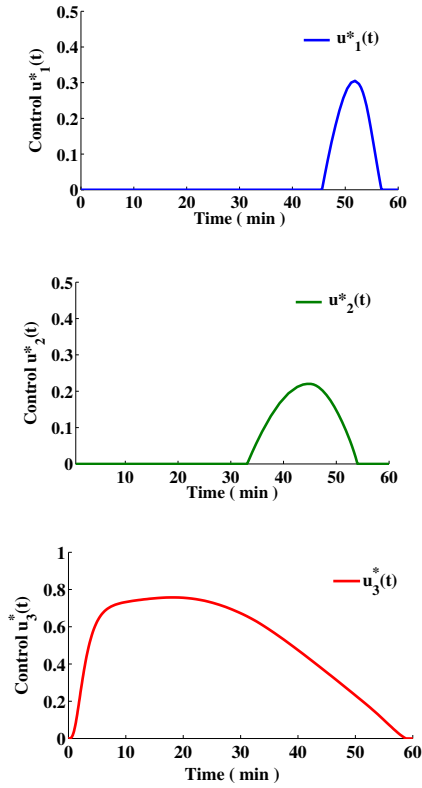


Figure 2. Optimal control effect $u^*(t)$ is plotted as a function of time.

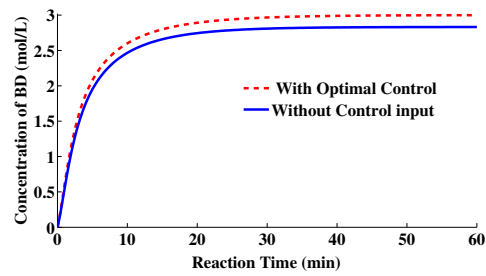


Figure 3. Comparison between two cases: (1) BD concentration with optimal control, and (2) BD concentration without control.

maximum concentration is 2.854 mole if there is no control policy like change of temperature, molar ratio, catalyst, stirring etc. present on the reaction.

5 Discussion and Conclusion

In this research article, optimal control approach is applied to get maximum biodiesel through transesterification process. Pontryagin minimum principle is used to solve the optimal control problem. The advantage of this method is that it avoid the solution of second order differential and partial differential equations that are required in other methods, such as dynamic programming and calculus of variation. Based on our analytical results, numerically we see that, 50 minutes of reaction time is required to reach the maximum concentration of biodiesel. It is also exposed that in this period the concentration value of biodiesel increased about 8%. It should be noted here that the concentration with optimal control reached 2.961 mole at 50 minute, which is implied a reduction of 10 minute of reaction time. Analytically, it can be easily established that the optimal control triplet are unique and derive the condition for which the system has its unique optimal control variables.

The control induced model of transesterification provide an idea of obtaining the maximum amount of biodiesel. This concept of experimental researches for biodiesel production is based on that prediction. Hence if we introduce the control in backward reaction of transesterification, then it will be helpful to produce maximum amount of biodiesel in the global aspect.

References

1. Marc, A., "Acid-Catalyzed Transesterification of Canola Oil to Biodiesel under Single and Double Phase Reaction Condition," *Energy and Fuel*, Vol. 21, pp. 2450-2459, 2007. (Article)
2. Nouredini, H., Zhu, D., " Kinetic of transesterification of soybean oil," *Journal of the American Oil Chemists' Society*, vol. 74, pp. 1457-1463, 1997. (Article)
3. Bambase, M. E., Nakamura N., Tanaka J., Matsumura M., "Kinetics of hydroxide-catalyze methanolysis of crude sunflower oil for the production of fuel-grade methyl ester," *Journal of chemical technology and biotechnology*, Vol. 82, pp. 273-280, 2007. (Article)
4. Berchmans, H., Shizuko, H., "Biodiesel production from crude *Jatropha curcas* L. seed oil with a high content of free fatty acids," *Bioresource Technology*, Vol. 99, pp. 1716-1721, 2008. (Article)
5. Vicente, G., Martínez, M., Aracil, J., Esteban, A., "Kinetics of sun flower oil methanolysis. *Industrial & Engineering Chemistry Research (ACS Publications)*", Vol. 44, pp. 5447-5454, 2005. (Article)

6. Paola, M. D., Ricca, E., Calabro, V., Curcio, S., Iorio, G., "Factor analysis of Transesterification reaction of waste oil for biodiesel production," *Bioresource Technology*, Vol. 100, pp. 5126-5131, 2009. (Article)
7. Stamenkovic, O. S., Todorovic, Z. B., Lazic, M. L., Veljkovic, V. B., Skala, D. U., "Kinetics of sun flower oil methanolysis at low temperatures," *Bioresource Technology*, Vol. 99, pp. 1131-1140, 2008. (Article)
8. Diwekar, U., Benavides P., "Optimal control of biodiesel production in a batch reactor Part 1: Deterministic control," *Fuel*, Vol. 94, pp. 211-217, 2012. (Article)
9. Freedman, B., Butterfield, R. O. "Transesterification Kinetics of Soybean Oil," *J. Am. Oil Chem. Soc.*, Vol. 63, pp. 1375-1380, 1986. (Article)
10. Hifjur, R., Kumar, A., "Biodiesel production from Jatropha oil with high free acid: an optimize process," *Biomass and Bioenergy*, Vol. 31, pp. 569-575, 2007. (Article)
11. Culshaw, R. V., Rawn, S., Spiteri, R. J., "Optimal HIV treatment by maximising immuno response," *Journal Mathematical Biology*, Vol. 48, pp. 545-562, 2004. (Article)
12. Tiwari, P., Kumar, R., Garg, S., "Transesterification, Modeling and Simulation of Batch Kinetics of Non-Edible Vegetable Oils for Biodiesel Production", Department of Chemical Engineering, IIT Kanpur, India. (Book chapter)
13. Berchmans, H. J., Morishta K., Takarada T., "Kinetic study of hydroxide-catalyze methanolysis of jatropha curcas waste food oil mixture for biodiesel production," *Fuel*, Vol. 104, pp. 46-52, 2013. (Article)
14. Roy, P. K., Datta, S., Nandi, S., Basir, F. A., "Effect of mass transfer kinetics for maximum production of biodiesel from Jatropha Curcas oil: A mathematical approach", Vol. 134, pp. 39-44, 2014.
15. Brasio, A. S. R., Andrey, R., Lino O. S., "Fernandes Natercia CP. Modeling the effect of mixing in biodiesel production", *Bioresource Technol*, Vol. 102, pp. 6508-6514, 2012.
16. Pontryagin, L. S., Boltyanskii, V. G., Gamkrelidze, R. V., Mishchenko, E. F. "Mathematical Theory of Optimal Process," Gordon and Breach Science Publishers, Vol. 4. (Book)
17. Fleming, W. H., Rishel, R. W., "Deterministic and Stochastic optimal control," Springer Verlag. (Book)

Acknowledgment: I desire to acknowledge one of my research scholars Abhirup Datta for his technical support. The research work is supported by UGC Major Research Project, F. No. 41-768/2012 (SR), dated: 18 July 2012.

Theory of multipoint boundary value problem and some of its applications

Carmen Simerská

Institute of Chemical Technology, Prague

Keywords: multipoint boundary value problem, existence and uniqueness, elastic beam

Abstract In [1] the problem of existence and uniqueness of L-splines was transformed to a general multipoint boundary value problem for a system of linear ordinary differential equations

$$\mathbf{x}'(t) + \mathbf{A}(t)\mathbf{x}(t) = \mathbf{f}(t) \quad \text{a.e. in } (a, b),$$

where the components of $\mathbf{A}(t)$ and $\mathbf{f}(t)$ are Lebesgue integrable and the boundary conditions cover the mixed and transition cases

$$\sum_{a \leq \xi_i^+ < b} M_i \mathbf{x}(\xi_i^+) + \sum_{a < \xi_i^- \leq b} N_i \mathbf{x}(\xi_i^-) = \mathbf{m}.$$

In this paper the theory giving the conditions under which the solution exists and is unique will be applied to some problems taken from mechanics.

1 Problem formulation

First, the multipoint boundary value problem is specified for a system of linear ordinary differential equations

$$\mathbf{x}'(t) + \mathbf{A}(t)\mathbf{x}(t) = \mathbf{f}(t) \quad \text{a.e. in } (a, b), \quad (1)$$

where $\mathbf{x}(t)$ and $\mathbf{f}(t)$ are vectors of length S , and $\mathbf{A}(t)$ is a matrix of type $S \times S$ (generally complex with a real t). The components of $\mathbf{A}(t)$ and $\mathbf{f}(t)$ are assumed to be Lebesgue integrable functions on (a, b) .

The formulation of the boundary conditions is more general than the standard approach. This enables to cover also transition conditions at inner points of the interval, where the relations between the limit values of the solution from the left and from the right-hand sides are prescribed. Moreover, we consider a possibility of binding these conditions. The following definitions are necessary for the determination of the set of solutions we are looking for.

Definition 1. We shall say that a function x is **piecewise absolutely continuous (PAC)** on the interval $\langle a, b \rangle$ with respect to the partition $\{t_i\}_{i=1}^N$, where $a = t_1 < t_2 < \dots < t_N = b$, iff there exist functions x_i , $i = 1, \dots, N - 1$, such that for $i = 1, \dots, N - 1$ holds:

1. the functions x_i are absolutely continuous on $\langle t_i, t_{i+1} \rangle$
2. $x(t) = x_i(t)$ for $t \in (t_i, t_{i+1})$.

Definition 2. We say that a vector $\mathbf{x}(t)$ is **PAC** on $\langle a, b \rangle$ with respect to the partition $\{t_i\}_{i=1}^N$ of $\langle a, b \rangle$ iff all components of $\mathbf{x}(t)$ are PAC on $\langle a, b \rangle$ with respect to $\{t_i\}_{i=1}^N$.

Definition 3. Let us suppose that N points $\{\xi_i\}_{i=1}^N$ are given in the interval $\langle a, b \rangle$ which form the partition Δ

$$a = \xi_1 < \xi_2 < \dots < \xi_N = b. \quad (\Delta)$$

Let matrices $\mathbf{M}^{(p)}$, $p = 1, \dots, 2(N - 1)$, be of the $J \times S$ type and a vector \mathbf{m} of length J . The problem of finding the vector function $\mathbf{x}(t)$ for which the following conditions a)-c) hold is said to be the **N -point boundary value problem (N-BVP)** iff:

- a) $\mathbf{x}(t)$ is PAC on $\langle a, b \rangle$ with respect to $\{\xi_i\}_{i=1}^N$,
- b) $\mathbf{x}(t)$ satisfies the differential equation (1),
- c) $\mathbf{x}(t)$ satisfies J boundary conditions

$$\sum_{i=1}^{N-1} \mathbf{M}^{(2i-1)} \mathbf{x}(\xi_i^+) + \sum_{i=1}^{N-1} \mathbf{M}^{(2i)} \mathbf{x}(\xi_{i+1}^-) = \mathbf{m}, \quad (2)$$

where $\mathbf{x}(\xi_i^+)$ and $\mathbf{x}(\xi_i^-)$ denote the respective one-side limits.

The matrices $\mathbf{M}^{(p)}$ with odd indices operate on the limit values of the vector $\mathbf{x}(t)$ at the points $\{\xi_i\}_{i=1}^{N-1}$ from the right-hand side, and similarly for even indices they operate on the limit values of $\mathbf{x}(t)$ at the points $\{\xi_i\}_{i=2}^N$ from the left-hand side.

The conditions (2) formally represent J equations with $2S(N - 1)$ unknowns. It is reasonable to require the system be solvable for any right-hand side \mathbf{m} , regardless of the differential equation (1). This will be the case if the rank of the matrix of the system

$$\mathbf{M} \equiv [\mathbf{M}^{(1)}, \mathbf{M}^{(2)}, \dots, \mathbf{M}^{(2N-2)}] \quad (3)$$

is maximal, i.e., is equal to the number of its rows. Therefore, further on we shall assume $r(\mathbf{M}) = J$.

Now, let's suppose real functions $p_i = p_i(t)$, $i = 0, \dots, n$, are given such that $\frac{1}{p_0}, p_1, \dots, p_n$ are from $\mathcal{L}(a, b)$. Let ℓ be a differential operator defined by the formal expression

$$\ell \equiv \sum_{i=0}^n (-1)^i \frac{d^i}{dt^i} \left(p_{n-i} \frac{d^i(\cdot)}{dt^i} \right). \quad (4)$$

Throughout the paper we will deal with the N -point boundary value problem only for the differential equation of the order $2n$

$$\ell y(t) = q(t) \quad \text{a.e. in } (a, b). \quad (5)$$

Then let us transform this $2n$ -order equation (5) to the system of $2n$ ordinary linear differential equations by the standard way and formulate the N -BVP for the equation (5).

Let us define $\mathbf{H}(t) \equiv \mathbf{H}$ of the type $2n \times 2n$,

$$\mathbf{H} = \begin{bmatrix} 0 & -1 & 0 & \dots & 0 & 0 & \dots & \dots & \dots & 0 \\ \vdots & \ddots & \ddots & & \vdots & \vdots & & & & \vdots \\ \vdots & & \ddots & \ddots & 0 & \vdots & & & & \vdots \\ \vdots & & & \ddots & -1 & 0 & \dots & \dots & \dots & 0 \\ 0 & \dots & \dots & \dots & 0 & -1/p_0 & 0 & \dots & \dots & 0 \\ 0 & \dots & \dots & 0 & -p_1 & 0 & 1 & 0 & \dots & 0 \\ \vdots & & \cdot & \cdot & 0 & \vdots & \ddots & \ddots & & \vdots \\ \vdots & \cdot & \cdot & \cdot & \vdots & \vdots & & \ddots & \ddots & 0 \\ 0 & \cdot & \cdot & & \vdots & \vdots & & & \ddots & 1 \\ -p_n & 0 & \dots & \dots & 0 & 0 & \dots & \dots & \dots & 0 \end{bmatrix}$$

and the vector of length $2n$

$$\mathbf{f}(t) = \begin{bmatrix} 0 \\ \vdots \\ 0 \\ -q(t) \end{bmatrix}. \quad (6)$$

Now we shall consider the problem of finding a solution of N -BVP, where the matrix $\mathbf{H}(t)$ replaces $\mathbf{A}(t)$ in (1) and $\mathbf{f}(t)$ is given by (6). Such a system with the boundary conditions (2) we shall denote by Ψ .

Further, denote the components of the solution \mathbf{x} of this problem with $\mathbf{y}(t) = (y_1(t), \dots, y_{2n}(t))^\top$. By specifying the equation

$$\mathbf{y}'(t) + \mathbf{H}(t)\mathbf{y}(t) = \mathbf{f}(t) \quad \text{a.e. in } (a, b). \quad (7)$$

we obtain the following relations valid a.e. on (a, b) :

$$\begin{aligned} y_2 &= y_1' && \text{R1} \\ y_3 &= y_2' = y_1'' && \text{R2} \\ &\vdots && \\ y_n &= y_{n-1}' = y_1^{(n-1)} && \text{R}(n-1) \\ y_{n+1} &= p_0 y_n' = p_0 y_1^{(n)} && \text{Rn} \\ &\vdots && \\ y_{n+k+1} &= p_k y_{n-k+1} - (y_{n+k})' = \sum_{i=0}^k (-1)^i (p_{n-i} y_1^{(n-k+i)})^{(i)} && \text{R}(n+k) \\ &\vdots && \\ q &= p_n y_1 - (y_{2n})' = \sum_{i=0}^n (-1)^i (p_{n-i} y_1^{(i)})^{(i)}. && \text{R2n} \end{aligned}$$

Obviously $y(t) = y_1(t)$. The functions $y_i(t)$, $i = 1, \dots, 2n$, are said to be quasiderivatives of y of the order $i - 1$. We shall denote by $y^{[k]}$, $k = 0, \dots, 2n - 1$ the quasiderivatives of the order k of the function $y(t)$, i.e.

$$\mathbf{y} = \begin{bmatrix} y^{[0]} \\ \vdots \\ y^{[2n-1]} \end{bmatrix}.$$

For this technique see [3]. Each of $R1 - R(2n - 1)$ equations represents the equality between absolutely continuous functions. These equations hold a.e. on (a, b) . Let us define the $2n$ -th quasiderivative of y as

$$y^{[2n]} \equiv p_n y^{[0]} - (y^{[2n-1]})'.$$

Then from the equation (5) we can write $y^{[2n]} = q$ a.e. in (a, b) . Further on we shall restrict ourselves to functions y that satisfy $y^{[2n]} \in \mathcal{L}_2(a, b)$.

Definition 4. For an arbitrary Δ and functions p_i , $i = 0, \dots, n$, with properties mentioned above we define the following set of functions

$D = \{y : \text{there exists a PAC vector } \mathbf{y} \text{ of quasiderivatives of } y \text{ on } \langle a, b \rangle \text{ with respect to } \Delta \text{ and the functions } p_i, i = 0, \dots, n, \text{ and } y^{[2n]} \in \mathcal{L}_2(a, b)\}$.

We denote by Λ the operator that corresponds to the conditions (2), i.e.:

$$\Lambda y = \sum_{i=1}^{N-1} \mathbf{M}^{(2i-1)} \mathbf{y}(\xi_i^+) + \sum_{i=1}^{N-1} \mathbf{M}^{(2i)} \mathbf{y}(\xi_{i+1}^-). \quad (8)$$

We call **the solution of N -BVP Ψ** a function y from D that satisfies the N -BVP Ψ : (5) and $\Lambda y = \mathbf{m}$.

Remark 1. The boundary conditions of the type (2) $\Lambda y = \mathbf{m}$ cover all conditions represented as a linear combination of (quasi)derivatives (one sided (quasi)derivatives) at a point ξ_i . They include also the transition conditions at the partition points Δ . These conditions can describe, e.g., the continuity of quasiderivatives at the point ξ_i of Δ .

The coefficients in the differential expression (4) can have discontinuities.

Let us deal with the problem Ψ . In practice, it is necessary to know the conditions on Λ that guarantee the existence and uniqueness of the solution of the problem. In [1], [2] it was shown that there exists a large class of conditions on the matrix \mathbf{M} for which the existence and uniqueness of the N -BVP Ψ is fulfilled and the required assumptions on the operator Λ are easy to verify.

By introducing the notation $\mathbf{y}_{i,2j-1}$, $\mathbf{y}_{i,2j}$, $i = 1, 2$, $j = 1, \dots, N - 1$,

$$\mathbf{y}_{1,2j-1} = \begin{bmatrix} y(\xi_j^+) \\ \vdots \\ y^{(n-1)}(\xi_j^+) \end{bmatrix}, \quad \mathbf{y}_{2,2j-1} = \begin{bmatrix} y^{[n]}(\xi_j^+) \\ \vdots \\ y^{[2n-1]}(\xi_j^+) \end{bmatrix},$$

$$\mathbf{y}_{1,2j} = \begin{bmatrix} y(\xi_{j+1}^-) \\ \vdots \\ y^{(n-1)}(\xi_{j+1}^-) \end{bmatrix}, \quad \mathbf{y}_{2,2j} = \begin{bmatrix} y^{[n]}(\xi_{j+1}^-) \\ \vdots \\ y^{[2n-1]}(\xi_{j+1}^-) \end{bmatrix}.$$

and $\mathbf{y}_1^\top \equiv (\mathbf{y}_{1,1}^\top, \dots, \mathbf{y}_{1,2(N-1)}^\top)$, $\mathbf{y}_2^\top \equiv (\mathbf{y}_{2,1}^\top, \dots, \mathbf{y}_{2,2(N-1)}^\top)$, we have a map that assigns each function $y \in D$ to the vector \mathbf{y} , of length $4n(N - 1)$,

$$\mathbf{y} \equiv \begin{bmatrix} \mathbf{y}_1 \\ \mathbf{y}_2 \end{bmatrix}. \quad (10)$$

It is useful to introduce the antidiagonal matrix $\mathbf{T} = \begin{bmatrix} 0 & 1 \\ 1 & 0 \end{bmatrix}$ of type $n \times n$ and matrices \mathbf{B} (type $2n(N - 1) \times 2n(N - 1)$) and \mathbf{A} ($4n(N - 1) \times 4n(N - 1)$)

$$\mathbf{B} \equiv \begin{bmatrix} -\mathbf{T} & & & \mathbf{0} \\ & \mathbf{T} & & \\ & & \ddots & \\ & & & -\mathbf{T} \\ \mathbf{0} & & & \mathbf{T} \end{bmatrix}, \quad \mathbf{A} \equiv \begin{bmatrix} \mathbf{0} & -\mathbf{B} \\ \mathbf{B} & \mathbf{0} \end{bmatrix}. \quad (11)$$

2 The existence of the N-BVP solution

Let $L \equiv (D_L, \ell)$ denote an operator L restricted to the domain D_L determined by $4n(N-1)$ homogeneous conditions $D_L = \{y \in D; \mathbf{y} = \mathbf{0}\}$. Theorem 1 characterizes all self-adjoint extensions of the operator L .

Theorem 1. *For every self-adjoint extension $\tilde{L} \equiv (D_{\tilde{L}}, \ell)$ of the operator L there exists a matrix \mathbf{W} such that the domain $D_{\tilde{L}}$ satisfies*

$$D_{\tilde{L}} = \{\varphi \in D; \mathbf{W}\varphi = \mathbf{0}\} \quad (12)$$

and the matrix \mathbf{W} has the following properties

- (i) \mathbf{W} is of the type $J \times 2J$, where $J = 2n(N-1)$,
- (ii) $r(\mathbf{W}) = 2n(N-1)$,
- (iii) $\mathbf{WAW}^* = \mathbf{0}$ (for \mathbf{A} see (11)).

Conversely, if the matrix \mathbf{W} with the properties (i), (ii), (iii) is given then the self-adjoint extension of the operator L exists such that in its domain $D_{\tilde{L}}$ the relation (12) holds.

Remark 2. *If $\mathbf{W} = (\mathbf{W}_1, \mathbf{W}_2)$, where \mathbf{W}_i , $i = 1, 2$ are matrices of the type $J \times 2n(N-1)$, $J \leq 4n(N-1)$, then the assumption (iii) can be written in the following way*

$$(iii') \quad \mathbf{W}_1\mathbf{BW}_2^* - \mathbf{W}_2\mathbf{BW}_1^* = \mathbf{0}, \quad \text{i.e. } \mathbf{W}_1\mathbf{BW}_2^* \text{ is a Hermitian matrix.}$$

The boundary conditions are usually given by $\mathbf{M}^{(p)}$, $p = 1, \dots, 2(N-1)$. Let us rewrite these matrices in the form $\mathbf{M}^{(p)} = (\mathbf{M}_1^{(p)}, \mathbf{M}_2^{(p)})$, where $\mathbf{M}_i^{(p)}$, $i = 1, 2$ are of the type $J \times n$. Further, let $\mathbf{W}_1 \equiv (\mathbf{M}_1^{(1)}, \mathbf{M}_1^{(2)}, \dots, \mathbf{M}_1^{(2N-2)})$, $\mathbf{W}_2 = (\mathbf{M}_2^{(1)}, \mathbf{M}_2^{(2)}, \dots, \mathbf{M}_2^{(2N-2)})$.

Now, we can rewrite $Ay = \mathbf{m}$ as an equivalent relation

$$\mathbf{W}\mathbf{y} = \mathbf{W}_1\mathbf{y}_1 + \mathbf{W}_2\mathbf{y}_2 = \mathbf{m}. \quad (2')$$

Let us have the N -BVP: (5), (2'). Let us denote the corresponding operator by L_A , i.e., $\boxed{L_A \equiv (\mathcal{D}, \ell)}$, where $\mathcal{D} = \{y \in D; \mathbf{W}\mathbf{y} = \mathbf{0}\}$, \mathbf{W} is a matrix of the type $J \times 4n(N-1)$, $r(\mathbf{W}) = J$.

In [2] we proved that the conditions (i), (ii), (iii) in Theorem 1 are also necessary conditions for L_A to be a self-adjoint operator.

Further suppose that the functions p_i satisfy

$$p_i \geq 0 \quad \text{a.e. in } (a, b) \quad \text{for all } i = 0, \dots, n \quad (13)$$

and the operator L_Λ is self-adjoint. The next theorem specifies the condition for the positive-semidefiniteness of L_Λ , i.e.

$$(\ell y, y) \geq 0 \quad \text{for all } y \in \mathcal{D}. \quad (14)$$

Theorem 2. *Let a self-adjoint operator $L_\Lambda \equiv (\mathcal{D}, \ell)$ be defined on the set of functions determined by the matrices $\mathbf{W} = (\mathbf{W}_1, \mathbf{W}_2)$. Then L_Λ is a positive-semidefinite operator, if the matrices $\mathbf{W}_1, \mathbf{W}_2$ fulfil the condition*

$$(iv) \quad \mathbf{W}_1 \mathbf{B} \mathbf{W}_2^* = \mathbf{W}_2 \mathbf{B} \mathbf{W}_1^* \text{ is a positive-semidefinite matrix.}$$

Moreover the condition (iv) is a necessary condition for the operator L_Λ to be positive-semidefinite for all coefficients in (4) satisfying (13).

The following theorem characterises all matrices \mathbf{W} that determine the self-adjoint operator with the condition (iv). These matrices \mathbf{W} directly imply the existence of solutions of N -BVP Ψ problem.

Theorem 3. *Let the matrix \mathbf{U} of the type $2n(N-1) \times 2n(N-1)$ be Hermitian and let its spectrum $\sigma(\mathbf{U})$ fulfil*

$$\sigma(\mathbf{U}) \subset \langle 0, 1 \rangle, \quad (15)$$

then the matrix

$$\mathbf{W} = \mathbf{K}(\mathbf{U}, (I - \mathbf{U})\mathbf{B}), \quad (16)$$

where \mathbf{K} is any regular matrix, is a matrix with the properties (i) – (iv).

On the contrary, all \mathbf{W} that fulfil (i) – (iv) can be written in the form (16), where \mathbf{K} is regular and \mathbf{U} is some Hermitian matrix (type $2n(N-1) \times 2n(N-1)$), the spectrum of which fulfils (15).

3 The uniqueness of the N -BVP solution

When investigating the uniqueness of the solution of N -BVP Ψ for any q and \mathbf{m} , it is sufficient, due to linearity, to study only the case when the homogeneous problem: $\ell y = 0$ a.e. in (a, b) and $Ay = \mathbf{0}$ has only the zero solution.

The operator L_Λ being positive semidefinite, we would be interested in finding for which functions y from the set $\mathcal{D} = \{y \in \mathcal{D} : \mathbf{W}y = \mathbf{0}\}$ the following equality holds

$$(\ell y, y) = 0. \quad (17)$$

Before stating the theorem on the uniqueness of the solution let us introduce the following notation:

To every interval (ξ_i, ξ_{i+1}) we will assign a number l_i : If

- $\int_{\xi_i}^{\xi_{i+1}} p_n dt > 0$, then $l_i \equiv 0$.
- $p_n = \dots = p_{n-k-1} = 0$ a.e. in (ξ_i, ξ_{i+1}) and $\int_{\xi_i}^{\xi_{i+1}} p_{n-k} dt > 0$, where $k \in \{1, \dots, n\}$, then $l_i \equiv k$.

Such an assignment always exists, because $p_0 > 0$ a.e. in $(\xi_i, \xi_{i+1}) \forall i$.

Further we denote by $\mathbf{R}_k = \begin{bmatrix} 0 & 1 & & 0 \\ & & \ddots & \\ & & & \ddots \\ 0 & & & 1 \\ & & & & 0 \end{bmatrix}$ the matrix of the type $k \times k$.

We shall distinguish two disjunctive cases:

- a) $l_i = 0$ for $\forall i = 1, \dots, N-1$,
- b) the set of indices $\mathcal{A} = \{i : 1 \leq i \leq N-1, l_i \neq 0\}$ is not empty.

For $i \in \mathcal{A}$ we define matrices \mathbf{S}_i and \mathbf{U}_i , of type $n \times l_i$, $l_i < n$, by the prescription

$$\mathbf{S}_i \equiv \begin{bmatrix} e^{\xi_i \mathbf{R}_{l_i}} \\ \mathbf{0}_{n-l_i, l_i} \end{bmatrix}, \quad \mathbf{U}_i \equiv \begin{bmatrix} e^{\xi_{i+1} \mathbf{R}_{l_i}} \\ \mathbf{0}_{n-l_i, l_i} \end{bmatrix},$$

where $\mathbf{0}_{k,j}$ is the null matrix of the type $k \times j$.

If $l_i = n$, let $\mathbf{S}_i \equiv e^{\xi_i \mathbf{R}_{l_i}}$, $\mathbf{U}_i \equiv e^{\xi_{i+1} \mathbf{R}_{l_i}}$. Let's denote $d \equiv \sum_{i=1}^{N-1} l_i$.

In case **b)**, it holds $d = \sum_{i \in \mathcal{A}} l_i > 0$ and we can define the matrix \mathbf{F} of type $2n(N-1) \times d$ by $\mathbf{F} \equiv \begin{bmatrix} \mathbf{F}_1 \\ \vdots \\ \mathbf{F}_{N-1} \end{bmatrix}$, where \mathbf{F}_i , $i = 1, \dots, N-1$ are matrices of the type $2n \times d$ that

- if $l_i = 0$, then $\mathbf{F}_i \equiv \mathbf{0}_{2n,d}$

– if $l_i \neq 0$, then

$$\mathbf{F}_i = \begin{bmatrix} \mathbf{0}_{2n, \sum_{p < i} l_p} & \left| \frac{\mathbf{S}_i}{\mathbf{U}_i} \right| & \mathbf{0}_{2n, d - \sum_{p \leq i} l_p} \end{bmatrix}. \quad (18)$$

Theorem 4. *Let us have the N -BVP Ψ , resp. (5), (2') where p_i satisfy (13) and the boundary conditions are determined by a matrix $\mathbf{W} = (\mathbf{W}_1, \mathbf{W}_2)$ satisfying (i) – (iv).*

*If **a)** holds, the problem has a unique solution. In case of **b)**, the problem has an unique solution in the set D iff*

$$(v) \quad r(\mathbf{W}_1 \mathbf{F}) = \sum_{i=1}^{N-1} l_i.$$

Moreover, if the problem is uniquely solvable, the operator L_A is positive-definite.

Example of a 2-point boundary problem with mixed conditions

$$\ell y = -(p_0 y')' + p_1 y = q \quad \text{a.e. in } (a, b), \quad \text{where } 1/p_0, p_1 \in \mathcal{L}(a, b) \quad (19)$$

$$\begin{aligned} \alpha_1 y(a) + \beta_1 p_0(a) y'(a) + \gamma_1 y(b) + \delta_1 p_0(b) y'(b) &= m_1, \\ \alpha_2 y(a) + \beta_2 p_0(a) y'(a) + \gamma_2 y(b) + \delta_2 p_0(b) y'(b) &= m_2, \end{aligned} \quad (20)$$

where $\alpha_i, \beta_i, \gamma_i, \delta_i \in \mathbb{R}$ ($i = 1, 2$).

In this case $N = 2$, $n = 1$, $y^{[1]} = p_0 y'$ and

$$\mathbf{y} = \begin{bmatrix} y(a^+) \\ y(b^-) \\ y^{[1]}(a^+) \\ y^{[1]}(b^-) \end{bmatrix}.$$

The corresponding operator L_A is self-adjoint iff the matrix

$$\mathbf{W} = (\mathbf{W}_1, \mathbf{W}_2) = \begin{bmatrix} \alpha_1 & \gamma_1 & \beta_1 & \delta_1 \\ \alpha_2 & \gamma_2 & \beta_2 & \delta_2 \end{bmatrix}$$

satisfies (i), (ii) and (iii) of Theorem 1, i.e., the rows of the matrix \mathbf{W} are linearly independent and

$$\alpha_2 \beta_1 - \alpha_1 \beta_2 = \gamma_2 \delta_1 - \gamma_1 \delta_2$$

(see e.g. [4], Chap. XI, Ex. 1.).

Now let's investigate when the operator is positive semidefinite. For that, suppose $p_i \geq 0$, $i = 0, 1$, a.e. in (a, b) .

Theorems 2 and 3 say that the operator will be positive semidefinite for all admissible coefficients p_0, p_1 if and only if $\mathbf{W} = \mathbf{K}(\mathbf{U}, (I - \mathbf{U})\mathbf{B})$, where \mathbf{K} is

an arbitrary regular matrix (2×2) , $\mathbf{B} = \begin{bmatrix} -1 & 0 \\ 0 & 1 \end{bmatrix}$, and where the symmetric matrix $\mathbf{U} = \begin{bmatrix} \alpha_1 & \alpha_2 \\ \alpha_2 & \gamma_2 \end{bmatrix}$ is such that all its eigenvalues lie in the interval $(0, 1)$, i.e.

$$\begin{aligned} 0 &\leq \gamma_2 + \alpha_1 + \sqrt{(\gamma_2 - \alpha_1)^2 + 4\alpha_2^2} \leq 2 \\ 0 &\leq \gamma_2 + \alpha_1 - \sqrt{(\gamma_2 - \alpha_1)^2 + 4\alpha_2^2} \leq 2. \end{aligned} \quad (21)$$

Every matrix \mathbf{W} of boundary conditions satisfying (i) – (iv) is characterised only by three numbers $\alpha_1, \alpha_2, \gamma_2$ and these conditions can be written in the original form

$$\begin{aligned} \alpha_1 y(a) - (1 - \alpha_1)p_0(a)y'(a) + \alpha_2 y(b) - \alpha_2 p_0(b)y'(b) &= m_1, \\ \alpha_2 y(a) + \alpha_2 p_0(a)y'(a) + \gamma_2 y(b) + (1 - \gamma_2)p_0(b)y'(b) &= m_2, \end{aligned} \quad (20')$$

where the coefficients $\alpha_1, \alpha_2, \gamma_2$ fulfil (21).

Particularly, all separated boundary conditions ($\alpha_2 = 0$) guaranteeing the validity of (i) – (iv) are given by the conditions of the form (or by their linear combinations):

$$\begin{aligned} \alpha_1 y(a) - (1 - \alpha_1)p_0(a)y'(a) &= m_1, \\ \gamma_2 y(b) + (1 - \gamma_2)p_0(b)y'(b) &= m_2, \end{aligned} \quad (20'')$$

where $0 \leq \alpha_1 \leq 1$ and $0 \leq \gamma_2 \leq 1$.

If $\int_a^b p_1 dt > 0$, then the problem (19), (20'), resp. (19), (20''), is uniquely solvable for all right-hand sides q and $\mathbf{m} = \begin{bmatrix} m_1 \\ m_2 \end{bmatrix}$.

If $p_1 = 0$ a.e. in (a, b) , then the problem (19), (20'), resp. (19), (20''), is uniquely solvable iff

$$r(\mathbf{U}\mathbf{F}) = r\left(\begin{bmatrix} \alpha_1 & \alpha_2 \\ \alpha_2 & \gamma_2 \end{bmatrix} \begin{bmatrix} 1 \\ 1 \end{bmatrix}\right) = r\begin{bmatrix} \alpha_1 + \alpha_2 \\ \alpha_2 + \gamma_2 \end{bmatrix} = 1$$

(see Theorem 4). It will be the case only when

$$\alpha_1 + \alpha_2 \neq 0 \quad \text{or} \quad \alpha_2 + \gamma_2 \neq 0.$$

4 An application of the theory of N-BVP

Boundary value problems for ODE arise in different areas of applied mathematics and physics. Some applications can be written as the N -BVP Ψ , i.e., in the form: $\ell y = q$ a.e. in (a, b) , where $q \in \mathcal{L}(a, b)$, and

$$Ay = \sum_{j=1}^{2(N-1)} \mathbf{M}^{(j)} \mathbf{Y}_j = \mathbf{m}.$$

For a special differential operator ℓ , where $p_0 \equiv 1$, $p_1 = \dots = p_n = 0$, the vectors \mathbf{Y}_k , describing the left- or right-hand side limits of the derivatives of y at $\{\xi_j\}_{j=2}^{N-1}$, are in the following form

$$\mathbf{Y}_{2j-2} = \begin{bmatrix} y(\xi_j^-) \\ \vdots \\ y^{(n-1)}(\xi_j^-) \\ y^{(n)}(\xi_j^-) \\ \vdots \\ (-1)^{n-1}y^{(2n-1)}(\xi_j^-) \end{bmatrix}, \quad \mathbf{Y}_{2j-1} = \begin{bmatrix} y(\xi_j^+) \\ \vdots \\ y^{(n-1)}(\xi_j^+) \\ y^{(n)}(\xi_j^+) \\ \vdots \\ (-1)^{n-1}y^{(2n-1)}(\xi_j^+) \end{bmatrix}$$

$$j = 2, \dots, N - 1.$$

The investigation of the existence and uniqueness of the Ψ solution reduces to checking simple conditions on matrices that define the boundary problem.

Multipoint boundary conditions are often separated and can be expressed in the matrix form as

$$\begin{aligned} E^{(1)}\mathbf{Y}_1 &= \mathbf{w}_1 \\ \mathbf{E}^{(2j-2)}\mathbf{Y}_{2j-2} + \mathbf{E}^{(2j-1)}\mathbf{Y}_{2j-1} &= \mathbf{w}_j, \quad j = 2, \dots, N - 1 \\ \mathbf{E}^{(2N-2)}\mathbf{Y}_{2N-2} &= \mathbf{w}_N, \end{aligned}$$

where $\mathbf{E}^{(k)}$, $k = 1, \dots, 2N - 2$, are matrices with $2n$ columns, matrices $\mathbf{E}^{(2j-2)}$ and $\mathbf{E}^{(2j-1)}$, $j = 2, \dots, N - 1$ have equal number of rows and $\mathbf{w}_1, \dots, \mathbf{w}_N$ are given vectors.

As an example of a multipoint boundary problem in physics one can mention that of a thin beam on the interval $\langle a, b \rangle$ in the equilibrium state. The deflection of the beam can be described by a function $y = y(x)$ on $\langle a, b \rangle$ that satisfies a fourth-order differential equation

$$\frac{d^2}{dx^2} \left[E(x)I(x) \frac{d^2 y}{dx^2} \right] + Q(x)y = f(x) \quad \text{in } (a, b), \quad (22)$$

where E is the modulus of elasticity, I the moment of inertia of the cross section about its bending axis, Q the coefficient of pliability of the subsoil, and f is the vertical load of the beam, which may have discontinuities. This can be rewritten in the form

$$(p_0 y'')'' + p_2 y = q(x) \quad \text{for } x \in (a, b) \setminus \{\xi_i\}_{i=1}^N, \quad (23)$$

where p_0, p_2, f are PAC functions.

For the deflection y to be uniquely given it is necessary to specify the boundary conditions.

Example 1. The simply supported beam at $\{\xi_i\}_{i=2}^{N-1}$ clamped at $a = \xi_1$ and $b = \xi_2$ and loaded with piecewise continuous force $q = q(t)$.

We seek the solution of

$$(p_0 y'')''(t) = q(t) \quad \text{a.e. in } (a, b),$$

where $p_0 = p_0(t) > 0$ is piecewise constant with respect to the partition Δ , such that

1. $y(\xi_i) = v_i$, for given positions v_i
2. y is continuous in $\langle a, b \rangle$
3. y' is continuous in $\langle a, b \rangle$
4. $p_0 y''$ is continuous in $\langle a, b \rangle$, y''' is continuous in $(a, b) \setminus \{\xi_i\}_{i=2}^{N-1}$.

In case of a cantilever beam at a and b the conditions are:

$$y(a) = y'(a) = y(b) = y'(b) = 0. \quad (24)$$

Because of $y^{[2]} = p_0 y''$, it must hold at the partition points that

$$y^{[2]}(\xi_i^-) - y^{[2]}(\xi_i^+) = 0,$$

whereas for $y^{[3]} = -(p_0 y'')$ ' at ξ_i no condition is required. The matrix notation of the boundary conditions is:

$$\mathbf{E}^{(1)} = \mathbf{E}^{(2N-2)} = [I_2, \mathbf{0}_{22}]$$

$$\mathbf{E}^{(2j-2)} = \left[\begin{array}{cc|cc} 1 & 0 & & \\ 0 & 0 & & \\ \hline 0 & 1 & 0 & 0 \\ 0 & 0 & 1 & 0 \end{array} \right], \quad \mathbf{E}^{(2j-1)} = \left[\begin{array}{cc|cc} 0 & 0 & & \\ 1 & 0 & & \\ \hline 0 & -1 & 0 & 0 \\ 0 & 0 & -1 & 0 \end{array} \right].$$

Example 2. The beam on elastic supports ξ_i , $i = 1, \dots, N$, and under the load of piecewise continuous force q . The solution of

$$y^{(4)}(t) = q(t) \quad \text{a.e. in } (a, b), \quad (25)$$

is sought so that the (quasi)derivatives y , y' , y'' are continuous on $\langle a, b \rangle$ and (quasi)derivative y''' is continuous in $(a, b) \setminus \{\xi_i\}_{i=2}^{N-1}$ and has jumps described by

$$y'''(\xi_j^-) - y'''(\xi_j^+) = k_j (y(\xi_j) - v_j), \quad j = 2, \dots, N-1, \quad (26)$$

where the coefficients k_j are the characteristics of spring stiffness and v_j are specified values of the equilibrium positions.

Then $n = 2$, $\ell \equiv \frac{d^4}{dt^4}$, $p_0 \equiv 1$, $p_2 \equiv 0$. The matrix notation of the boundary conditions is:

$$\mathbf{E}^{(1)} = \mathbf{E}^{(2N-2)} = [I_2, \mathbf{0}_{22}], \quad \mathbf{E}^{(2j-2)} = I_4,$$

$$\mathbf{E}^{(2j-1)} = \begin{bmatrix} -1 & 0 & 0 & 0 \\ 0 & -1 & 0 & 0 \\ 0 & 0 & -1 & 0 \\ k_j & 0 & 0 & -1 \end{bmatrix}, \quad \text{where } j = 2, \dots, N-1,$$

$$\mathbf{w}_j^T = [0, 0, 0, k_j v_j].$$

Example 3. *The simplified three-point boundary problem for the clamped beam, where the angular deflection of the beam in ξ_2 ($a = \xi_1 < \xi_2 < \xi_3 = b$) satisfies the condition*

$$y'(\xi_2) = v, \quad v \text{ is a given value,}$$

can be written as (25), (24) where the (quasi)derivatives y , y' , y''' are continuous on $\langle a, b \rangle$, the (quasi)derivative y'' is continuous on $\langle a, b \rangle \setminus \xi_2$, whereas for $y''(\xi_2)$ no condition is required.

As in Example 2, $n = 2$ and $\ell \equiv \frac{d^4}{dt^4}$, and the notation of $\mathbf{E}^{(k)}$, $k = 1, \dots, 4$ would be similar.

Sometimes it is better to try to formulate the boundary conditions directly in the matrix form as $\mathbf{W} = [\mathbf{U}, (I - \mathbf{U})\mathbf{B}]$, where \mathbf{U} is a Hermitian matrix with the property (15). Then it is not necessary to verify the properties (i) – (iv).

We can write the conditions in Example 3 as:

$$\mathbf{U} = \begin{bmatrix} 1 & 0 & & & & & & 0 \\ 0 & 1 & & & & & & \\ & & 1/2 & 0 & -1/2 & 0 & & \\ & & 0 & 1 & 0 & 0 & & \\ & & -1/2 & 0 & 1/2 & 0 & & \\ & & 0 & 0 & 0 & 1 & & \\ 0 & & & & & & 1 & 0 \\ 0 & & & & & & 0 & 1 \end{bmatrix},$$

$$(I - \mathbf{U})\mathbf{B} = \begin{bmatrix} 0 & 0 & & & & & & 0 \\ 0 & 0 & & & & & & \\ & & 0 & 1/2 & 0 & -1/2 & & \\ & & 0 & 0 & 0 & 0 & & \\ & & 0 & 1/2 & & -1/2 & & \\ & & 0 & 0 & 0 & 0 & & \\ & & & & & & 0 & 0 \\ 0 & & & & & & 0 & 0 \end{bmatrix},$$

where \mathbf{U} is a Hermitian matrix satisfying $\sigma(\mathbf{U}) \subset \langle 0, 1 \rangle$.

The verification of the condition (i) is trivial. When investigating (ii), the rank of \mathbf{W} is usually known. In Examples 1, 2, and 3 the condition (ii) is obviously satisfied. Often it happens that all matrices in (iii') are null (Example 1, 3). Then the conditions (iii) and (iv) hold true automatically. In Example 2 this is the case if $k_j \geq 0, \forall j = 2, \dots, N - 1$.

The difficulty of verifying the condition (v) depends on the integrals of coefficients $p_i, i = 0, \dots, n$, over the subintervals $(\xi_j, \xi_{j+1}), j = 1, \dots, N - 1$. In Example 2 and 3 the matrix \mathbf{F} can be constructed more or less easily, because $p_0 \equiv 1, p_1 \equiv 0, p_2 \equiv 0$ in the whole interval $\langle a, b \rangle$. So,

$$\mathbf{F} = \begin{bmatrix} 1 & \xi_1 & & & 0 \\ 0 & 1 & & & \\ 1 & \xi_2 & & & \\ 0 & 1 & & & \\ & & \ddots & & \\ & & & 1 & \xi_{N-1} \\ & & & 0 & 1 \\ & & & 1 & \xi_N \\ 0 & & & 0 & 1 \end{bmatrix}$$

and the condition (v), guaranteeing the uniqueness of the solution, can be easily verified.

References

1. C. SIMERSKÁ, *Generalized L-splines as a Solution of an N-point Boundary Value problem*, North-Holland Mathematics Studies 133, North-Holland, Amsterdam (1987), pp.151-160.
2. C. SIMERSKÁ, *Zobecněné L-spliny a vícebodová okrajová úloha*, Kandidátská disertační práce, Praha, (1986)
3. J. TAUFER, *Lösung der Randwertprobleme für Systeme von linearen Differentialgleichungen*, Prague, (1973)
4. E.A. CODDINGTON, N. LEVINSON, *Theory of Ordinary Differential Equations*, Mc.Graw-Hill, New York, (1955).

One example of correspondence between deterministic and stochastic differential equations

Jana Šnupárková

Institute of Chemical Technology, Prague

Keywords: Geometric Brownian Motion, Fractional Geometric Brownian Motion, Stochastic Differential Equations in Hilbert Space, Strong Solution

Abstract Although it is possible to reduce the problem of finding solution to one type of stochastic differential equation to the problem of solving certain deterministic differential equation in the Wiener case, this technique fails in the case of fractional Brownian motion.

1 Introduction

Let $(\Omega, \mathcal{F}, \mathbb{P})$ be a complete probability space and let $W = \{W_t, t \geq 0\}$ and $B^H = \{B_t^H, t \geq 0\}$ be centered Gaussian processes with covariance functions

$$\begin{aligned}\mathbb{E}[W_t W_s] &= \min\{s, t\}, \quad s, t \geq 0, \\ \mathbb{E}[B_t^H B_s^H] &= \frac{1}{2}(s^{2H} + t^{2H} - |s - t|^{2H}), \quad s, t \geq 0,\end{aligned}$$

respectively. Process W is called **Wiener process** or **Brownian motion** and B^H is called **fractional Brownian motion** with Hurst parameter $H \in (0, 1)$. Fractional Brownian motion is a generalization of a Wiener process because

$$B^{1/2} = W$$

holds. Nevertheless this generalization is not trivial because B^H is not a semimartingale nor a Markov process for $H \neq 1/2$. These processes have Hölder continuous trajectories \mathbb{P} -a.s. with exponent $\alpha < H$ and the trajectories are nowhere differentiable \mathbb{P} -a.s..

Let V be a separable Hilbert space. Consider the equations

$$dX_t^W = AX_t^W dt + BX_t^W dW_t, \quad X_0^W = x_0, \quad (1)$$

$$dX_t^B = AX_t^B dt + BX_t^B dB_t^H, \quad X_0^B = x_0, \quad (2)$$

where $A : \text{Dom}(A) \subset V \rightarrow V$ and $B : \text{Dom}(A) \subset V \rightarrow V$ are linear operators and $x_0 \in V$ is a deterministic initial value. The stochastic integral in equation (1) is supposed to be a classical Itô-type integral. Equation (2) is considered in the regular case only (i.e. $H > 1/2$) and the stochastic integral is understood in the Skorokhod sense. For the definitions and basic properties see e.g. monographs [4] and [1]. Note that the Skorokhod integral is a generalization of the Itô one for integrands which may not be necessarily progressively measurable.

The solutions to equations (1) and (2) can be viewed as random processes with values in a separable Hilbert space V and corresponding to the deterministic theory there are three notions of the solution – strong, weak and mild. However, in this paper, the concept of the strong solution will only be discussed.

Suppose that

(A) linear operator A is closed and densely defined with the domain $D := \text{Dom}(A)$.

Definition 1. A $(\mathcal{B}([0, T]) \otimes \mathcal{F})$ -measurable stochastic process $\{X_t, t \in [0, T]\}$ is said to be a **strong solution** to the equation (1) or (2) if $X_t \in D$ \mathbb{P} -a.s. for all $t \in [0, T]$ and

$$X_t = x_0 + \int_0^t AX_r dr + \int_0^t BX_r dW_r \quad \mathbb{P} - a.s.$$

for all $t \in [0, T]$, or

$$X_t = x_0 + \int_0^t AX_r dr + \int_0^t BX_r dB_r^H \quad \mathbb{P} - a.s.$$

for all $t \in [0, T]$, respectively.

Note that strong solutions exist very rarely. In the Wiener case (1) the problem of existence of a strong solution can be reduced to finding a solution to the corresponding deterministic equation. Unfortunately, this technique can not be applied to the fractional Brownian motion case (2) due to the term with the Malliavin derivative.

The solution to the equation (1) for $V = \mathbb{R}$ is well-known geometric Brownian motion which is important in many fields. The solution to the equation (2) is its fractional analogue called fractional Brownian motion.

2 Itô formula

The analogue of a deterministic chain rule is a stochastic chain rule called Itô formula.

Suppose that Y is a strong solution to the equation (1) or (2) with operators \tilde{A}, \tilde{B} and initial value \tilde{x}_0 . Let $V : [0, T] \times V \rightarrow \mathbb{R}$ be in $\mathcal{C}^{1,2}([0, T] \times V)$. Define

$$\mathcal{L}(V(t, Y_t)) = \frac{\partial V}{\partial t}(t, Y_t) + \langle \tilde{A}Y_t, D_x V(t, Y_t) \rangle_V + \frac{1}{2} \langle D_{xx}^2 V(t, Y_t) \tilde{B}Y_t, \tilde{B}Y_t \rangle_V$$

or

$$\mathcal{L}(V(t, Y_t)) = \frac{\partial V}{\partial t}(t, Y_t) + \langle \tilde{A}Y_t, D_x V(t, Y_t) \rangle_V + \langle D_{xx}^2 V(t, Y_t) \tilde{B}Y_t, D_t^\varphi Y_t \rangle_V,$$

respectively, where

$$D_t^\varphi Y_t = \int_0^T \varphi(t, r) D_r^H Y_t dr$$

and $D^H F$ is the Malliavin derivative of a random variable $F : \Omega \rightarrow V$ (for the definition see [1]) and

$$\varphi(t, r) = H(2H - 1)|t - r|^{2H-2}.$$

Then the process $\{V(t, Y_t), t \in [0, T]\}$ is a strong solution to the equation

$$dV(t, Y_t) = (\mathcal{L}V)(t, Y_t)dt + \langle D_x V(t, Y_t), \tilde{B}Y_t \rangle_V dW_t, \quad V(0, Y_0) = V(0, \tilde{x}_0),$$

or

$$dV(t, Y_t) = (\mathcal{L}V)(t, Y_t)dt + \langle D_x V(t, Y_t), \tilde{B}Y_t \rangle_V dB_t^H, \quad V(0, Y_0) = V(0, \tilde{x}_0),$$

respectively.

3 Reduction to deterministic system

Assume that

- (B) linear operator B is closed and densely defined and generates a strongly continuous group $\{S_B(u), u \in \mathbb{R}\}$ on V ,
- (AB) $\text{Dom}((B^*)^2)$ is dense in V where B^* is the adjoint operator of B and $D \subset \text{Dom}(B^2)$.

The technique how to pass from the deterministic system

$$v'(t) = S_B(-W_t) \left(A - \frac{1}{2} B^2 \right) S_B(W_t) v(t), \quad v(0) = x_0, \quad (3)$$

to the stochastic system (1) is described in [2], Chapter 6.

Theorem 1. Assume that (A), (B) and (AB) hold. Let v be a classical solution to the equation (3) \mathbb{P} -a.s. which is a predictable process with trajectories in $C^1([0, T]; V)$ \mathbb{P} -a.s. Then the process $\{X_t, t \in [0, T]\}$ given as

$$X_t = S_B(W_t)v(t), \quad t \in [0, T],$$

is a strong solution to the equation (1).

Proof :

Let $\zeta \in \text{Dom}((B^*)^2)$. Define the process $Z_\zeta = \{Z_\zeta(t), t \in [0, T]\}$ as

$$Z_\zeta(t) = S_B^*(W_t)\zeta, \quad t \in [0, T].$$

Clearly, applying the Itô formula to the process $\langle Z_\zeta(t), \xi \rangle_V$ (for any fixed $\xi \in V$) one gets that Z_ζ is a strong solution to the equation

$$dZ_\zeta(t) = \frac{1}{2}(B^*)^2 Z_\zeta(t)dt + B^* Z_\zeta(t)dW_t, \quad Z_\zeta(0) = \zeta.$$

Set

$$\begin{aligned} Y &= (v, Z_\zeta), \\ V(t, Y_t) &= \langle v(t), Z_\zeta(t) \rangle_V, \quad t \in [0, T], \\ \bar{A}(t) &= \begin{pmatrix} S_B(-W_t) \left(A - \frac{1}{2}B^2 \right) S_B(W_t) & 0 \\ 0 & \frac{1}{2}(B^*)^2 \end{pmatrix}, \quad \bar{B} = \begin{pmatrix} 0 & 0 \\ 0 & B^* \end{pmatrix}, \end{aligned}$$

and let

$$\bar{W} = (W_1, W)^T$$

be a two-dimensional Wiener process. Then the process Y is a strong solution to the equation

$$dY_t = \bar{A}(t)Y_t dt + \bar{B}d\bar{W}_t, \quad Y_0 = (x_0, \zeta).$$

Since

$$\begin{aligned} \bar{A}(t)Y_t &= \left(S_B(-W_t) \left(A - \frac{1}{2}B^2 \right) S_B(W_t)v(t), \frac{1}{2}(B^*)^2 Z_\zeta(t) \right)^T, \\ \bar{B}Y_t &= (0, B^* Z_\zeta(t))^T, \end{aligned}$$

then

$$\begin{aligned} \langle \bar{A}(t)Y_t, D_x V(t, Y_t) \rangle_V &= \left\langle S_B(-W_t) \left(A - \frac{1}{2}B^2 \right) S_B(W_t)v(t), Z_\zeta(t) \right\rangle_V \\ &\quad + \left\langle v(t), \frac{1}{2}(B^*)^2 Z_\zeta(t) \right\rangle_V \\ &= \left\langle \left(A - \frac{1}{2}B^2 \right) X_t, \zeta \right\rangle_V + \frac{1}{2} \langle B^2 X_t, \zeta \rangle_V \\ &= \langle AX_t, \zeta \rangle_V, \\ \frac{1}{2} \langle D_{xx}^2 V(t, Y_t) \bar{B}Y_t, \bar{B}Y_t \rangle_V &= \frac{1}{2} \left(\langle 0, B^* Z_\zeta(t) \rangle_V + \langle 0, B^* Z_\zeta(t) \rangle_V \right) = 0, \\ \langle D_x V(t, Y_t), \bar{B}Y_t \rangle_V &= \langle 0, Z_\zeta(t) \rangle_V + \langle v(t), B^* Z_\zeta(t) \rangle_V = \langle BX_t, \zeta \rangle_V. \end{aligned}$$

Thus applying again the Itô formula to the process $\{V(t, Y_t), t \in [0, T]\}$ the equality

$$\begin{aligned} dV(t, Y_t) &= d\langle v(t), Z_\zeta(t) \rangle_V = d\langle X_t, \zeta \rangle_V \\ &= \langle AX_t, \zeta \rangle_V dt + \langle BX_t, \zeta \rangle_V dW_t, \quad \langle v(0), Z_\zeta(0) \rangle_V = \langle x_0, \zeta \rangle_V, \end{aligned}$$

holds \mathbb{P} -a.s. for all $t \in [0, T]$. Since $\text{Dom}((B^*)^2)$ is dense in V and $\zeta \in \text{Dom}((B^*)^2)$ was chosen arbitrary the process $\{X_t, t \in [0, T]\}$ is a strong solution to the equation (1). \blacksquare

Remark 1. *Under some additional assumptions the statement of Theorem 1 can be reversed, i.e. given a strong solution to the equation (1) there exists a classical solution to the equation (3) for almost all $\omega \in \Omega$ defined as*

$$v(t) = S_B(-W_t)X_t, \quad t \in [0, T].$$

If one wants to follow the previous procedure in the case of fractional Brownian motion the problems with the form of Itô formula for fractional Brownian motion appear. The process $Z_\zeta = \{Z_\zeta(t), t \in [0, T]\}$ is now defined as

$$Z_\zeta(t) = S_B^*(B_t^H)\zeta, \quad t \in [0, T].$$

It can be shown that it is a strong solution to the equation

$$dZ_\zeta(t) = Ht^{2H-1}(B^*)^2 Z_\zeta(t)dt + B^* Z_\zeta(t)dB_t^H, \quad Z_\zeta(0) = \zeta.$$

The corresponding deterministic equation is

$$v'(t) = S_B(-B_t^H) (A - Ht^{2H-1}B^2) S_B(B_t^H)v(t), \quad v(0) = x_0.$$

Redefine the operator \bar{A} and the process \bar{W}

$$\begin{aligned} \bar{A}(t) &= \begin{pmatrix} S_B(-B_t^H) (A - Ht^{2H-1}B^2) S_B(B_t^H) & 0 \\ 0 & Ht^{2H-1}(B^*)^2 \end{pmatrix}, \\ \bar{B}^H &= (B_1^H, B^H)^\top, \end{aligned}$$

respectively, where \bar{B}^H is a two-dimensional fractional Brownian motion. Since

$$D_r^H Y_t = (D_r^H v(t), D_r^H Z_\zeta(t))^\top = (D_r^H v(t), B^* Z_\zeta(t) I_{[0,t]}(r))^\top,$$

where $I_{[0,t]}$ denotes the indicator function of the interval $[0, t]$, the equality

$$\begin{aligned} \langle D_{xx}^2 V(t, Y_t) \bar{B} Y_t, D_t^\varphi Y_t \rangle_V &= \langle 0, Ht^{2H-1} B^* Z_\zeta(t) \rangle_V \\ &\quad + \left\langle \int_0^T \varphi(t, r) D_r^H v(t) dr, B^* Z_\zeta(t) \right\rangle_V \end{aligned}$$

holds. Unfortunately, the second summand is not in general equal to zero because v is not a constant process \mathbb{P} -a.s. and therefore the Malliavin derivative of v is not zero.

Remark 2. Since v is a solution to the equation

$$v(t) = x_0 + \int_0^t S_B(-B_u^H) (A - Hu^{2H-1}B^2) S_B(B_u^H)v(u)du,$$

$D_r^H v(t)$ can be described as a solution to the equation

$$\begin{aligned} D_r^H v(t) &= \int_0^t -BS_B(-B_u^H)I_{[0,u]}(r) (A - Hu^{2H-1}B^2) S_B(B_u^H)v(u)du \\ &\quad + \int_0^t S_B(-B_u^H) (A - Hu^{2H-1}B^2) BS_B(B_u^H)I_{[0,u]}(r)v(u)du \\ &\quad + \int_0^t S_B(-B_u^H) (A - Hu^{2H-1}B^2) S_B(B_u^H)D_r^H v(u)du. \end{aligned}$$

Hence the Itô formula for fractional Brownian motion applied to the process $\{V(t, Y_t), t \in [0, T]\}$ yields

$$\begin{aligned} d\langle v(t), Z_\zeta(t) \rangle_V &= \langle X_t, \zeta \rangle_V = \langle AX_t, \zeta \rangle_V dt + \langle BX_t, \zeta \rangle_V dB_t^H \\ &\quad + \left\langle \int_0^T \varphi(t, r) D_r^H v(t) dr, B^* Z_\zeta(t) \right\rangle_V dt, \\ \langle v(0), Z_\zeta(0) \rangle_V &= \langle x_0, \zeta \rangle_V, \end{aligned}$$

where

$$X_t = S_B(B_t^H)v(t), \quad t \in [0, T],$$

so that this technique does not give the desired result in the case of fractional Brownian motion.

Remark 3. These difficulties can be overcome by modification of this technique and adding some natural assumptions, e.g.

- (AB1) the system of operators $\{A - Ht^{2H-1}B^2, t \in [0, T]\}$ generates a strongly continuous evolution system $\{U(t, s), 0 \leq s \leq t \leq T\}$ (for the definition see e.g. [5]),
- (AB2) the operators A and $\{S_B(u), u \in \mathbb{R}\}$ commute on the domain D , i.e.

$$S_B(u)Ay = AS_B(u)y$$

for any $u \in \mathbb{R}$ and $y \in D$.

Then the process

$$X_t = S_B(B_t^H)U(t, 0)x_0, \quad t \in [0, T],$$

is a strong (and also weak) solution to the equation (2). For the details see [3] in the regular case $H > 1/2$. The singular case $H < 1/2$ is more complicated and only a weak solution can be obtained (see [6]).

The condition (AB2) is satisfied e.g. in examples of partial differential equations where

- the operators A and B are differential operators,
- A generates an analytical semigroup on V and B is an identity operator.

References

1. F. BIAGINI, Y. HU, B. ØKSENDAL, T. ZHANG, *Stochastic Calculus for Fractional Brownian Motion and Applications*, Springer–Verlag, London, 2008.
2. G. DA PRATO, J. ZABCZYK, *Stochastic Equations in Infinite Dimensions*, Cambridge University Press, Cambridge, 1992.
3. T.E. DUNCAN, B. MASLOWSKI, B. PASIK–DUNCAN, *Stochastic equations in Hilbert space with a multiplicative fractional Gaussian noise*, *Stochastic Process. Appl.*, 115 (2005), 1357–1383.
4. B. ØKSENDAL, *Stochastic Differential Equations*, Fifth Ed., Springer–Verlag, New York, 1998.
5. A. PAZY, *Semigroups of Linear Operators and Applications to Partial Differential Equations*, Springer–Verlag, New York, 1983.
6. J. ŠNUPÁRKOVÁ, *Stochastic bilinear equations with fractional Gaussian noise in Hilbert space*, *Acta Univ. Carolin. Math. Phys.*, 51 (2010), 49–68.

Acknowledgments: This problem was studied during the author’s doctoral studies. The author would like to thank her supervisor B. Maslowski.

The number of symmetric colorings of the dihedral group D_4

Iryna Kashuba¹ and Yuliya Zelenyuk²

Institute of Mathematics, University of São Paulo, Caixa Postal 66281 CEP
05314-970, São Paulo, Brazil¹

School of Mathematics, University of the Witwatersrand, Private Bag 3, Wits 2050,
South Africa²

Keywords: Dihedral group, symmetric coloring, optimal partition, Möbius function, lattice of subgroups

Abstract Let r be a positive integer, then the r -coloring of a finite group G is a mapping $\chi : G \rightarrow \{1, \dots, r\}$. A coloring χ is symmetric if there exists $g \in G$ such that $\chi(gx^{-1}g) = \chi(x)$ for any $x \in G$. We compute the number of symmetric r -colorings and the number of equivalence classes of symmetric r -colorings of the dihedral group D_4 .

1 Introduction

The subject discussed in this paper is related to colorings of algebraic and geometric objects endowed with certain symmetries. In 1931 S. Sidon posed the following problem: given a subset $A \subset \mathbb{N}$ and a number $n \in \mathbb{N}$ estimate the quantity of solutions $(x, y) \in A \times A$ of the equation $x + y = n$. Essentially it is a question about symmetric subsets of A , since the set $S(n) = \{x \in A : n - x \in A\}$ is symmetric with respect to the point $\frac{n}{2}$ and its cardinality is the number of solutions of the original equation. Thus the Sidon question can be reformulated in terms of symmetry: given a subset $A \subset \mathbb{N}$ estimate the size of a maximal symmetric subset of A . We shall treat symmetry using the methods of Ramsey Theory (see [2] and references therein), but instead of partitions of A into r pieces, it is more convenient to speak about colorings of A in r colors.

Let G be a finite group and r be a positive integer. A *coloring* (an *r -coloring*) of G is any mapping $\chi : G \rightarrow \mathbb{N}$ ($\chi : G \rightarrow \{1, \dots, r\}$). The group G naturally acts on the colorings, namely for any $g \in G$, the coloring χg is defined by

$$\chi g(x) = \chi(xg^{-1}).$$

As usual $[\chi]$ and $St(\chi)$ denote the orbit and the stabilizer of a coloring χ , that is,

$$[\chi] = \{\chi g : g \in G\} \text{ and } St(\chi) = \{g \in G : \chi g = \chi\}.$$

In particular we have that

$$|[\chi]| = |G : St(\chi)| \text{ and } St(\chi g) = g^{-1}St(\chi)g.$$

Let \sim denote the equivalence on the colorings corresponding to the partition into orbits, that is, $\chi \sim \varphi$ if and only if there exists $g \in G$ such that $\chi(xg^{-1}) = \varphi(x)$ for all $x \in G$.

Obviously, the number of all r -colorings of G is $r^{|G|}$. To calculate the number of equivalence classes of r -colorings of G we apply Burnside's Lemma [1, I, S3]

$$\frac{1}{|G|} \sum_{g \in G} r^{|\langle g \rangle|}.$$

Here $\langle g \rangle$ is the subgroup generated by g .

Suppose G is an Abelian group, then analogously to Sidon question we call a coloring χ of G *symmetric* with respect to an element $g \in G$ if $\chi(2g - x) = \chi(x)$ for any $x \in G$. In the case of regular polygon with n vertices (i.e. $G = \mathbb{Z}_n$) we obtain the following geometric interpretation of the symmetric coloring: a coloring is symmetric if it is invariant in respect to some mirror symmetry with an axis crossing the center of polygon and one of its vertices. Generalizing it to the case of non-abelian group we say that a coloring χ of G is *symmetric* if there exists $g \in G$ such that

$$\chi(gx^{-1}g) = \chi(x)$$

for all $x \in G$. That is, a coloring is symmetric if it is invariant under some symmetry, and a symmetry is any mapping of the form

$$G \ni x \mapsto gx^{-1}g \in G,$$

where $g \in G$. A coloring equivalent to a symmetric one is also symmetric (see [5, Lemma 2.1]). Let $S_r(G)$ denote the set of all symmetric r -colorings of G .

Theorem 1. [3, Theorem 1] *Let G be a finite Abelian group. Then*

$$|S_r(G)| = \sum_{X \leq G} \sum_{Y \leq X} \frac{\mu(Y, X)|G/Y|}{|B(G/Y)|} r^{\frac{|G/X|+|B(G/X)|}{2}},$$

$$|S_r(G)/\sim| = \sum_{X \leq G} \sum_{Y \leq X} \frac{\mu(Y, X)}{|B(G/Y)|} r^{\frac{|G/X|+|B(G/X)|}{2}}.$$

Here, X runs over subgroups of G , Y over subgroups of X , $\mu(Y, X)$ is the Möbius function on the lattice of subgroups of G , and $B(G) = \{x \in G : x^2 = e\}$.

Given a finite partially ordered set, the Möbius function is defined as follows:

$$\mu(a, b) = \begin{cases} 1 & \text{if } a = b \\ -\sum_{a < z \leq b} \mu(z, b) & \text{if } a < b \\ 0 & \text{otherwise.} \end{cases}$$

See [1, IV] for more information about the Möbius function.

In case of \mathbb{Z}_n formulas can be reduced to elementary ones [3, Theorem 2].

Recently Theorem 1 was generalized to an arbitrary finite group G [5]. The approach is based on constructing the partially ordered set of so called optimal partitions of G .

Given a partition π of G , the *stabilizer* and the *center* of π are defined by

$$St(\pi) = \{g \in G : \text{for every } x \in G, x \text{ and } xg^{-1} \text{ belong to the same cell of } \pi\},$$

$$Z(\pi) = \{g \in G : \text{for every } x \in G, x \text{ and } gx^{-1}g \text{ belong to the same cell of } \pi\}.$$

$St(\pi)$ is a subgroup of G and $Z(\pi)$ is a union of left cosets of G modulo $St(\pi)$. Furthermore, if $e \in Z(\pi)$, then $Z(\pi)$ is also a union of right cosets of G modulo $St(\pi)$ and for every $a \in Z(\pi)$, $\langle a \rangle \subseteq Z(\pi)$. We say that a partition π of G is *optimal* if $e \in Z(\pi)$ and for every partition π' of G with $St(\pi') = St(\pi)$ and $Z(\pi') = Z(\pi)$, one has $\pi \leq \pi'$. The latter means that every cell of π is contained in some cell of π' , or equivalently, the equivalence corresponding to π is contained in that of π' . The partially ordered set of optimal partitions of G can be naturally identified with the partially ordered set of pairs (A, B) of subsets of G such that $A = St(\pi)$ and $B = Z(\pi)$ for some partition π of G with $e \in Z(\pi)$. For every partition π , we write $|\pi|$ to denote the number of cells of π .

Theorem 2. [5, Theorem 2.11] *Let P be the partially ordered set of optimal partitions of G . Then*

$$|S_r(G)| = |G| \sum_{x \in P} \sum_{y \leq x} \frac{\mu(y, x)}{|Z(y)|} r^{|x|},$$

$$|S_r(G)/\sim| = \sum_{x \in P} \sum_{y \leq x} \frac{\mu(y, x) |St(y)|}{|Z(y)|} r^{|x|}.$$

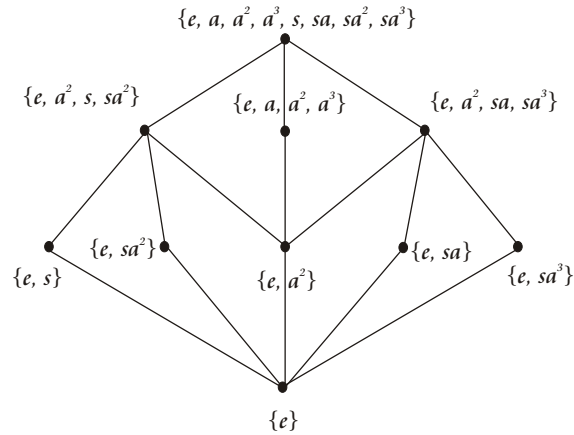
The partially ordered set of optimal partitions π of G together with parameters $|St(\pi)|$, $|Z(\pi)|$ and $|\pi|$ can be constructed by starting with the finest optimal partition $\{\{x, x^{-1}\} : x \in G\}$ and using the following fact:

Let π be an optimal partition of G and let $A \subseteq G$. Let π_1 be the finest partition of G such that $\pi \leq \pi_1$ and $A \subseteq St(\pi_1)$, and let π_2 be the finest partition of G such that $\pi \leq \pi_2$ and $A \subseteq Z(\pi_2)$. Then the partitions π_1 and π_2 are also optimal.

In this note we compute explicitly the numbers $|S_r(D_4)|$ and $|S_r(D_4)/\sim|$ where $D_4 = \{e, a, a^2, a^3, s, sa, sa^2, sa^3\}$ is the dihedral group of order 8, $a^4 = e$, $s^2 = e$, $sa^i = a^{-i}s$, $i = 0, 1, 2, 3$. For the number of symmetric colorings of the quaternion group, see [4].

2 Optimal partitions of D_4

Recall that the Hasse diagram of D_4 is the following:



Now we list all optimal partitions π of D_4 together with $St(\pi)$, $Z(\pi)$.

The finest partition:

$$\begin{aligned} \pi &: \{e\}, \{s\}, \{sa\}, \{sa^2\}, \{sa^3\}, \{a^2\}, \{a, a^3\}, \\ St(\pi) &= \{e\}, Z(\pi) = \{e, a^2\}, \\ |St(\pi)| &= 1, |Z(\pi)| = 2. \end{aligned}$$

Three partitions with six cells:

$$\begin{aligned} \pi &: \{e, a^2\}, \{s\}, \{sa\}, \{sa^2\}, \{sa^3\}, \{a, a^3\}, \\ St(\pi) &= \{e\}, Z(\pi) = \{e, a, a^2, a^3\}, \\ |St(\pi)| &= 1, |Z(\pi)| = 4. \end{aligned}$$

Three partitions with five cells:

$$\begin{aligned}\pi &: \{e, a^2\}, \{s, sa^2\}, \{sa\}, \{sa^3\}, \{a, a^3\}, \\ St(\pi) &= \{e\}, Z(\pi) = \{e, a, a^2, a^3, sa, sa^3\}, \\ |St(\pi)| &= 1, |Z(\pi)| = 6.\end{aligned}$$

Four partitions with three cells:

$$\begin{aligned}\pi &: \{e, s\}, \{a, sa^3, a^3, sa\}, \{a^2, sa^2\}, \\ St(\pi) &= \{e, s\}, Z(\pi) = \{e, a^2, s, sa^2\}, \\ |St(\pi)| &= 2, |Z(\pi)| = 4.\end{aligned}$$

One partition with four cells:

$$\begin{aligned}\pi &: \{e, a^2\}, \{s, sa^2\}, \{a, a^3\}, \{sa, sa^3\}, \\ St(\pi) &= \{e, a^2\}, Z(\pi) = D_4, \\ |St(\pi)| &= 2, |Z(\pi)| = 8.\end{aligned}$$

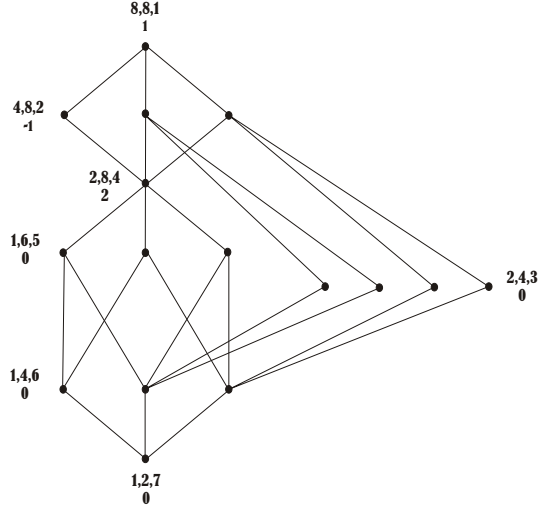
Three partitions with two cells:

$$\begin{aligned}\pi &: \{e, a, a^2, a^3\}, \{s, sa, sa^2, sa^3\}, \\ St(\pi) &= \{e, a, a^2, a^3\}, Z(\pi) = D_4, \\ |St(\pi)| &= 4, |Z(\pi)| = 8.\end{aligned}$$

And the coarsest partition

$$\begin{aligned}\pi &: \{D_4\}, \\ |St(\pi)| &= 8, |Z(\pi)| = 8.\end{aligned}$$

The picture below represents the partially ordered set of optimal partitions π , to each vertex π we assign a vector $\begin{bmatrix} |St(\pi)|, |Z(\pi)|, |\pi| \\ \mu(a, 1) \end{bmatrix}$, where μ is a Mobius function.



Finally, by the formulae from Theorem 2, we obtain that

$$\begin{aligned}
|S_r(D_4)| &= |D_4| \sum_{x \in P} \sum_{y \leq x} \frac{\mu(y, x)}{|Z(y)|} r^{|x|} \\
&= 8\left(\frac{1}{2}r^7 + 3r^6\left(\frac{1}{4} - \frac{1}{2}\right) + 3r^5\left(\frac{1}{6} - \frac{2}{4} + \frac{1}{2}\right) + r^4\left(\frac{1}{8} - \frac{3}{6} + \frac{3}{4} - \frac{1}{2}\right)\right) \\
&\quad + 4r^3\left(\frac{1}{4} - \frac{1}{4} + 0\frac{1}{2}\right) + r^2\left(\frac{1}{8} - \frac{1}{8} + 0\frac{3}{6} + 0\frac{3}{4} + 0\frac{1}{2}\right) \\
&\quad + 2r^2\left(\frac{1}{8} - \frac{1}{8} - \frac{2}{4} + 0\frac{3}{6} + 0\frac{2}{4} + \frac{2}{4} + 0\frac{1}{2}\right) + r\left(\frac{1}{8} - \frac{3}{8} + \frac{2}{8} + 0\frac{3}{6} + 0\frac{4}{4} + 0\frac{3}{4} + 0\frac{1}{2}\right) \\
&= 8\left(\frac{r^7}{2} - \frac{3}{4}r^6 + \frac{r^5}{2} - \frac{r^4}{8} + 0r^3 + 0r^2 + 0r\right) \\
&= 4r^7 - 6r^6 + 4r^5 - r^4,
\end{aligned}$$

$$\begin{aligned}
|S_r(D_4)/\sim| &= \sum_{x \in P} \sum_{y \leq x} \frac{\mu(y, x)|St(y)|}{|Z(y)|} r^{|x|} \\
&= \frac{1}{2}r^7 + 3r^6\left(\frac{1}{4} - \frac{1}{2}\right) + 3r^5\left(\frac{1}{6} - \frac{2}{4} + \frac{1}{2}\right) + r^4\left(\frac{2}{8} - \frac{3}{6} + \frac{3}{4} - \frac{1}{2}\right) \\
&\quad + 4r^3\left(\frac{2}{4} - \frac{1}{4} + 0\frac{1}{2}\right) + r^2\left(\frac{4}{8} - \frac{2}{8} + 0\frac{3}{6} + 0\frac{3}{4} + 0\frac{1}{2}\right) \\
&\quad + 2r^2\left(\frac{4}{8} - \frac{2}{8} - \frac{4}{4} + 0\frac{3}{6} + 0\frac{2}{4} + \frac{2}{4} + 0\frac{1}{2}\right) \\
&\quad + r\left(\frac{8}{8} - \frac{12}{8} + \frac{4}{8} + 0\frac{3}{6} + 0\frac{8}{4} + 0\frac{3}{4} + 0\frac{1}{2}\right) \\
&= \frac{1}{2}r^7 - \frac{3}{4}r^6 + \frac{1}{2}r^5 + r^3 - \frac{1}{4}r^2.
\end{aligned}$$

Proposition 1. For every $r \in \mathbb{N}$,

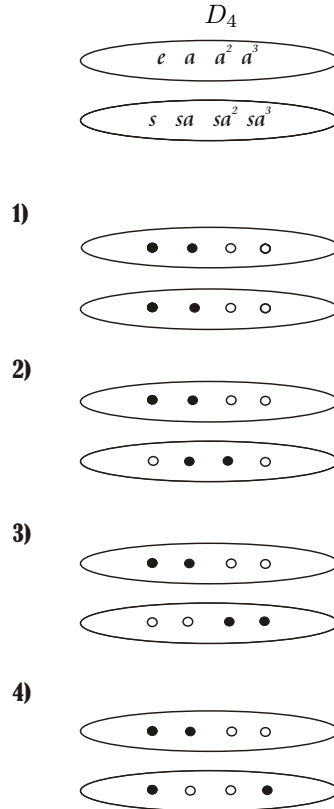
$$|S_r(D_4)| = 4r^7 - 6r^6 + 4r^5 - r^4,$$

$$|S_r(D_4)/\sim| = \frac{1}{2}r^7 - \frac{3}{4}r^6 + \frac{1}{2}r^5 + r^3 - \frac{1}{4}r^2.$$

The number of all r -colorings of D_4 is r^8 and the number of equivalence classes of all r -colorings of D_4 is

$$\frac{1}{|D_4|} \sum_{g \in D_4} r^{|D_4/\langle g \rangle|} = \frac{1}{8}(r^8 + 5r^4 + 2r^2).$$

In particular, the number of all 2-colorings of D_4 is $2^8 = 256$, the number of equivalence classes of all 2-colorings of D_4 is $\frac{1}{8}(2^8 + 5 \cdot 2^4 + 2 \cdot 2^2) = 43$, while the number of all symmetric 2-colorings of D_4 is $|S_2(D_4)| = 240$ and the number of equivalence classes of all symmetric 2-colorings of D_4 is $|S_2(D_4)/\sim| = 39$. The list of all asymmetric 2-colorings of D_4 up to equivalence is below.



References

1. M. Aigner, *Combinatorial Theory*, Springer-Verlag, Berlin-Heidelberg-New York, 1979.
2. T. Banakh, *Symmetry and colorings: some results and open problems, II*, arXiv:1111.1015, preprint.
3. Y. Gryshko (Zelenyuk), *Symmetric colorings of regular polygons*, *Ars Combinatoria*, **78** (2006), 277-281.
4. Y. Zelenyuk, *The number of symmetric colorings of the quaternion group*, *Symmetry*, **2** (2010), 69-75.
5. Y. Zelenyuk, *Symmetric colorings of finite groups*, *Proceedings of Groups St Andrews 2009, Bath, UK, LMS Lecture Note Series*, **388** (2011), 580-590.

Acknowledgments:

The first-named author was supported by CNPq 308090/2010-1, the second-named author was supported by NRF grant IFR1202220164 and FAPESP 2012/17010-6.

Segment Point Processes

Markéta Zikmundová

Institute of Chemical Technology, Prague
Faculty of Mathematics and Physics, Charles University, Prague

Keywords: point process, Poisson point process, interacting particles, density function, length distribution, U -statistic

Abstract We introduce some facts about U -statistics of union of interacting line segments and integral formulas for moments of characteristics of union of interacting line segments. Further we illustrate a behavior of lengths of segments driven by different choices of multidimensional parameter.

Modelling in stochastic geometry has many applications in seismology, neurophysiology, urban development, etc. This paper is a brief summary of selected results from [1] and doctoral thesis [6]. At first we set some basic definitions from theory of point processes, in the second part the model of interacting segments is defined and in the last section is a small simulation study. The proofs of Lemma 1 and Theorem 1 one can find in [6] and more theory of U -statistics in [2].

1 Definitions

Definition 1. Let E be separable locally compact complete metric space equipped with Borel σ -field $\mathcal{B} = \mathcal{B}(E)$. Locally finite measure on E is such measure which is finite on all bounded Borel sets of E . We denote \mathcal{M} the set of all locally finite measures on $(E, \mathcal{B}(E))$.

Definition 2. On space $(E, \mathcal{B}(E))$ let us define set \mathcal{N} of all locally finite measures taking the non-negative integer values or infinity

$$\mathcal{N} \equiv \{\mu \in \mathcal{M}; \mu(B) \in \mathbb{N} \cup \{0, \infty\} \text{ for all } B \in \mathcal{B}\}.$$

On spaces \mathcal{M}, \mathcal{N} define σ -fields

$$\begin{aligned} \mathfrak{M} &= \sigma\{\mu \mapsto \mu(B) \text{ measurable, } B \in \mathcal{B}\}, \\ \mathfrak{N} &= \{M \cap \mathcal{N} : M \in \mathfrak{M}\}. \end{aligned}$$

\mathfrak{M} is the smallest σ -field on \mathcal{M} for which the mapping $\mathcal{M} \rightarrow \mathbb{R}$, $\mu \mapsto \mu(B)$ is measurable for all $B \in \mathcal{B}$.

Definition 3. Let $(\Omega, \mathcal{A}, \mathbb{P})$ be a probability space. Point process on E is a measurable mapping $\mu : (\Omega, \mathcal{A}, \mathbb{P}) \rightarrow (\mathcal{N}, \mathfrak{N})$.

Distribution of point process is a probability measure p_μ given by $p_\mu(B) = \mathbb{P}(\mu \in B)$, $B \in \mathfrak{N}$.

We say that point process is simple if $\mathbb{P}(\mu \in \mathcal{N}^*) = 1$, where

$$\mathcal{N}^* = \{\gamma \in \mathcal{N} : \gamma(\{x\}) \leq 1; \forall x \in E\}.$$

Definition 4. Let $\Lambda \in \mathcal{M}$ and let η be a point process on E such that for all $n \in \mathbb{N}$ and bounded $B_1, \dots, B_n \in \mathcal{B}$ pairwise disjoint

- (i) the random variables $\eta(B_1), \dots, \eta(B_n)$ are independent,
- (ii) for all $i \in \mathbb{N}$ has $\eta(B_i)$ Poisson distribution with parameter $\Lambda(B_i)$.

Then η is called Poisson point process on E with intensity measure Λ .

Definition 5. Let Λ be the intensity measure such that there exists its density with respect to Lebesgue measure, i.e. $\Lambda(A) = \int_A \lambda(x) dx$, $A \in \mathcal{B}$, then λ is called intensity function.

Definition 6. Point process μ on E is finite if $\mu(E) < \infty$ almost surely.

Definition 7. Let η be the Poisson point process with an intensity measure Λ . A point process μ is given by a density $p : \mathcal{N} \rightarrow \mathbb{R}$ with respect to the Poisson point process η if

$$p(\mu \in B) = \int_B p(\mathbf{x}) p_\eta(d\mathbf{x}), \quad B \in \mathfrak{N}.$$

Definition 8. Let $\mu : \mathcal{N} \rightarrow E$ be a finite point process and $k \in \mathbb{N}$. Define random variable $F(\mu)$ as

$$F(\mu) = \sum_{(x_1, \dots, x_k) \in \mu_{\neq}^k} f(x_1, \dots, x_k),$$

where f is a symmetric function from $L^1(\Lambda^k)$ and $(x_1, \dots, x_k) \in \mu_{\neq}^k$ denotes all k -tuples of pairwise different points from μ . Then $F(\mu)$ is called U -statistic of order k .

2 Segment point processes

Each line segment s of finite length in \mathbb{R}^2 can be uniquely represented by its reference point $z \in \mathbb{R}^2$ (e.g. lexicographical minimum or maximum), positive

length l and direction ψ . Let $S \in \mathbb{R}^2$ be a bounded set and $0 < D_o < \infty$. Then segment point process on S can be identified with the points in $S \times (0, D_o] \times [0, \pi)$.

Denote η a stationary Poisson segment process on S with intensity measure $\Lambda(ds) = \rho(z)dzD(dl)\vartheta(d\psi)$, where ρ is an intensity function of reference points, D the length distribution with support in a bounded set $(0, D_o)$ and ϑ distribution of directions. Now consider a process μ of interacting line segments given by density function p with respect to the process η . Assume that for any finite configuration \mathbf{y} is the density in exponential form

$$p_{\mathbf{x}}(\mathbf{y}) = c_{\mathbf{x}}^{-1} \exp(\theta \cdot T(U_{\mathbf{y}})), \quad (2.1)$$

where $U_{\mathbf{y}}$ denotes union of segments in configuration \mathbf{y} , $T(U_{\mathbf{y}})$ vector of geometrical characteristics of the union $U_{\mathbf{y}}$ and $c_{\mathbf{x}}^{-1}$ is a normalising constant. In Figure 1 are drawn the realizations of process μ with various choices of parameter \mathbf{x} .

For the remaining text assume that

$$T(U_{\mathbf{y}}) = (N(U_{\mathbf{y}}), L(U_{\mathbf{y}}), N_{is}(U_{\mathbf{y}})),$$

where

- N ... number of intersection of $U_{\mathbf{y}}$
- L ... total length of all segments in $U_{\mathbf{y}}$
- N_{is} ... number of isolated segments in $U_{\mathbf{y}}$.

For statistics N and L we can define random variables $N(\eta)$, $N(\mu)$ and $L(\eta)$, $L(\mu)$, respectively, by formulas

$$\begin{aligned} L(\mu) &= \sum_{x \in \mu} l(x) \\ N(\mu) &= \frac{1}{2} \sum_{(x_1, x_2) \in \mu_{\neq}^2} \mathbf{I}_{[x_1 \cap x_2 \neq \emptyset]}. \end{aligned}$$

Obviously these variables are U -statistics of orders 1 and 2, respectively. The following lemma says for which values of parameter \mathbf{x} is the distribution of μ well defined.

Lemma 1. *Let $\mathbf{x} \in \mathbb{R} \times (-\infty, 0] \times \mathbb{R}$. Then we have*

- (i) $p \in L^2(p_{\eta})$
- (ii) $L(\eta), N(\eta), N_{is}(\eta) \in L^2(p_{\eta})$,

Definition 9. *A function $f : \mathcal{N} \rightarrow \mathbb{R}$ is called hereditary if for all finite configurations $\mathbf{x}, \tilde{\mathbf{x}} \in \mathcal{N}$ such that $\tilde{\mathbf{x}} \subset \mathbf{x}$, it holds that $f(\tilde{\mathbf{x}}) > 0$ whenever $f(\mathbf{x}) > 0$.*

Definition 10. Let μ be a point process with a hereditary density p with respect to a Poisson point process η . For $\mathbf{x} \in \mathcal{N}$ define Papangelou conditional intensity of order n

$$\lambda_n^*(u_1 \dots u_n, \mathbf{x}) = \frac{p(\mathbf{x} \cup \{u_1 \dots u_n\})}{p(\mathbf{x})}, \quad u_1 \dots u_n \in E.$$

Since L and N are U -statistics the following integral formulas for their first, second and mixed moments can be derived.

Theorem 1. For $L(\mu)$, $N(\mu) \in L^2(p_\eta)$ and $p \in L^2(p_\eta)$ we have

$$\begin{aligned} \mathbb{E} L(\mu) &= \int_E l(x) \mathbb{E} [\lambda_1^*(x; \mu)] \Lambda(dx) \\ \mathbb{E} L^2(\mu) &= \int_E l^2(x) \mathbb{E} [\lambda_1^*(x; \mu)] \Lambda(dx) \\ &\quad + \int_{E^2} l(x_1) l(x_2) \mathbb{E} [\lambda_2^*(x_1, x_2; \mu)] \Lambda(d(x_1, x_2)) \\ \mathbb{E} N(\mu) &= \frac{1}{2} \int_{E^2} \mathbf{I}_{[x_1 \cap x_2 \neq \emptyset]} \mathbb{E} [\lambda_2^*(x_1, x_2; \mu)] \Lambda(d(x_1, x_2)) \\ \mathbb{E} N^2(\mu) &= \frac{1}{2} \int_{E^2} \mathbf{I}_{[x_1 \cap x_2 \neq \emptyset]} \mathbb{E} [\lambda_2^*(x_1, x_2; \mu)] \Lambda(d(x_1, x_2)) \\ &\quad + \int_{E^3} \mathbf{I}_{[x_1 \cap x_2 \neq \emptyset]} \mathbf{I}_{[x_1 \cap x_3 \neq \emptyset]} \mathbb{E} [\lambda_3^*(x_1, x_2, x_3; \mu)] \Lambda(d(x_1, x_2, x_3)) \\ &\quad + \frac{1}{4} \int_{E^4} \mathbf{I}_{[x_1 \cap x_2 \neq \emptyset]} \mathbf{I}_{[x_3 \cap x_4 \neq \emptyset]} \mathbb{E} [\lambda_4^*(x_1, \dots, x_4; \mu)] \Lambda(d(x_1, \dots, x_4)) \\ \mathbb{E} L(\mu) N(\mu) &= \int_{E^2} l(x_1) \mathbf{I}_{[x_1 \cap x_2 \neq \emptyset]} \mathbb{E} [\lambda_2^*(x_1, x_2; \mu)] \Lambda(d(x_1, x_2)) \\ &\quad + \frac{1}{2} \int_{E^3} l(x_1) \mathbf{I}_{[x_2 \cap x_3 \neq \emptyset]} \mathbb{E} [\lambda_3^*(x_1, x_2, x_3; \mu)] \Lambda(d(x_1, x_2, x_3)). \end{aligned}$$

3 Length intensity

To provide the reader an idea of behavior of lengths of segments in μ for various choices of parameter \mathbf{x} we introduce a length intensity of the process.

Definition 11. For point process μ define length intensity

$$\gamma = \mathbb{E} \int H^1(\mathbf{x} \cap [0, 1]^d) \mu(d\mathbf{x}),$$

where H^1 denotes Hausdorff measure of dimension 1.

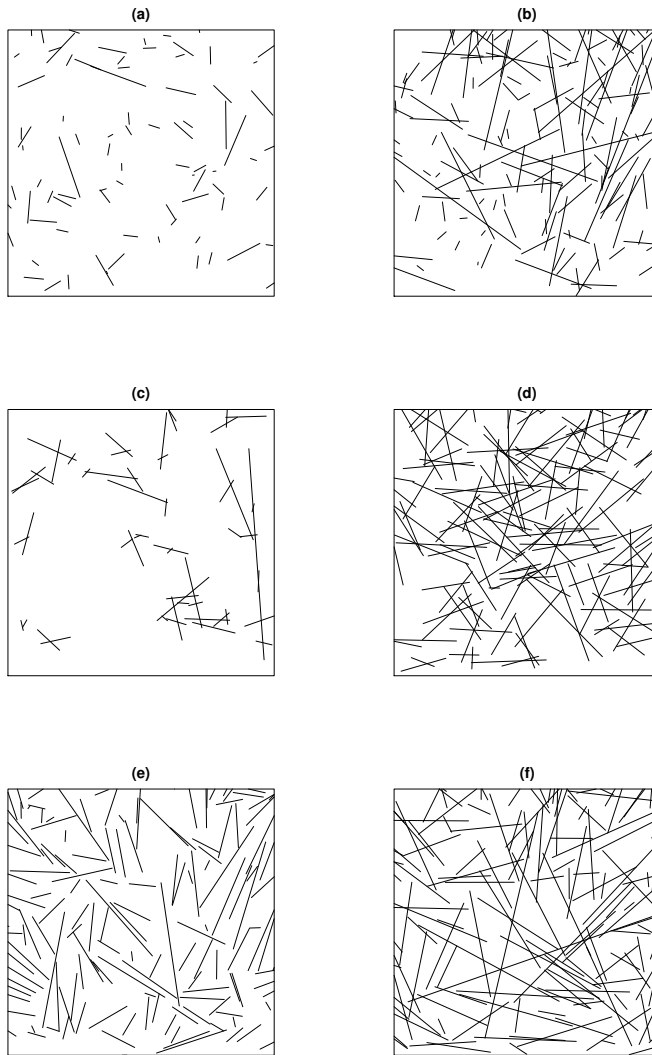


Figure 1. Simulated models with interacting line segments with various parameters \mathbf{x} , S is a square of size 10×10 . Here D is uniformly distributed on $(0, 10)$, the distribution of directions is uniform on $[-\pi/2, \pi/2)$ and $\rho = 1.5$ is constant. Number of iterations $It = 100.000$. The parameter vector (a) $\mathbf{x} = (0, -1, 0)$, (b) $\mathbf{x} = (3, 0, 0)$, (c) $\mathbf{x} = (0, 0, -10)$, (d) $\mathbf{x} = (3, 0, -10)$, (e) $\mathbf{x} = (3, 0, 1)$, (f) $\mathbf{x} = (3, -1, -3)$.

For Poisson segment process with intensity function $\rho(z) = \rho$

$$\gamma = \rho \mathbb{E}l$$

holds. The natural estimation of length intensity γ in a bounded observation window $|W|$ is then

$$\hat{\gamma} = \frac{1}{|W|} \sum_{\mathbf{x} \in \mu} H^1(\mathbf{x} \cap W).$$

Figure 2 shows the changes of length intensity of the process for various choices of parameter \mathbf{x} . Recall that parameter of the number of intersection cannot take positive values, in the other case the density p would not be integrable with respect to the intensity measure Λ .

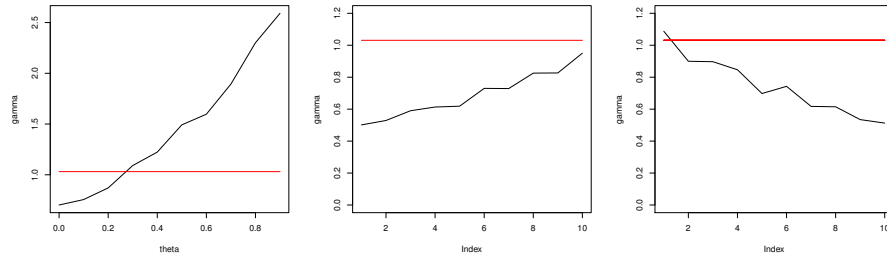


Figure 2. The estimation of length intensity for various development of parameter \mathbf{x} . (1) The parameter of total length L grows from zero to one, (2) the parameter of total length L grows from -0.5 to 0.5 and the parameter of number of intersections N decreases from 0 to -0.5 , (3) contrariwise to (2). A straight line denotes the length intensity of reference Poisson process. The observation window is a square of size 10×10 .

4 Conclusion

Analogical integral formulas can be derived for another models of interacting particles, e.g. for union of intercatating circular surfaces in \mathbb{R}^3 , see [6]. On the other hand the geometrical characteristics of the union of interacting discs in \mathbb{R}^2 ([3]) are not fully observable through any k -tuples of discs and that is why the theory of U -statistics cannot be used for estimation of their moments. In the present, unions of interacting particles are in a great field of study, see e.g. [4] or [5].

References

1. V. BENEŠ, M. ZIKMUNDOVÁ, *Functionals of spatial point processes having a density with respect to the Poisson process*, Kybernetika, submitted, arXiv:1401.2783.
2. G. LAST, M. PENROSE, *Poisson process Fock space representation, chaos expansion and covariance inequalities*, Probability Theory Related Fields, **150**, 663–690, 2011.
3. J. MØLLER, K. HELISOVÁ, *Likelihood inference for unions of interacting discs*, Scandinavian Journal of Statistics, **37**, 365–381, 2010.
4. K. STAŇKOVÁ HELISOVÁ, J. STANĚK, *Dimension reduction in extended Quermassinteraction process*, Methodology and Computing in Applied Probability, Online first, DOI 10.1007/s11009-013-9343-x.
5. M. ZIKMUNDOVÁ, K. STAŇKOVÁ HELISOVÁ, V. BENEŠ, *On the Use of Particle Markov Chain Monte Carlo in Parameter Estimation of Space-Time Interacting Discs*, Methodology and Computing in Applied Probability, **16(2)**, 451–463, 2014.
6. M. ZIKMUNDOVÁ, *Time-Space Point Processes and Sequential Monte Carlo Methods*, Doctoral Thesis, Faculty of Mathematics and Physics, Charles University in Prague, in preparation.

Acknowledgments: This work was partially supported by the Czech Science Foundation, grant P201-10-0472.

List of Participants

A. Abusaloua	Zawia University, Libya drabusaloua@gmail.com
Roka Ali	Tarbiat Modares University, Iran student.irann@yahoo.com
Š. Axman	Institute of Chemical Technolog Prague, Czech republic axmanns@vscht.cz
M. Biák	Institute of chemical technology Prague, Czech Republic biakm@vscht.cz
L. Borská	Institute of chemical technology Prague, Czech Republic borskal@vscht.cz
M. Branda	Charles University in Prague, MFF, Czech Republic branda@karlin.mff.cuni.cz
B. Cheddadi	University Hassan II, Morroco bcheddadi@hotmail.com
M. Dubcová	Institute of chemical technology Prague, Czech Republic dubcovam@vscht.cz
M. Feistauer	Charles University Prague, Czech Republic feist@karlin.mff.cuni.cz
K. Goncharuk	Lomonosov Moscow University of Fine, Russia kale007@gmail.com
S. A. Hashemi	Islamic Azad University , Lahijan, Iran sahashemi1980@yahoo.com
E. Hassabow	Norabia fir contracting, Sudan hassabow07@gmail.com
B. Hejna	Institute of chemical technology Prague, Czech Republic hejnab@vscht.cz
L. Heřmánek	Institute of chemical technology Prague, Czech Republic hermanel@vscht.cz
M. Isoz	Institute of chemical technology Prague, Czech Republic isozm@vscht.cz
D. Janovská	Institute of chemical technology Prague, Czech Republic janovskd@vscht.cz
V. Janovský	Charles University Prague, Czech Republic janovsky@karlin.mff.cuni.cz
F. Jaroš	Institute of chemical technology Prague, Czech Republic jarosf@vscht.cz
A. K. Kamara	Africhild Foundation For Peace and rebuilding, Sierra Leone officeuse33@gmail.com
L. Klíč	Institute of chemical technology Prague, Czech Republic kolokvium@vscht.cz
S. Kubeš	Institute of chemical technology Prague, Czech Republic stanislav.kubes@vscht.cz
Milan Kubíček	Institute of chemical technology Prague, Czech republic milan.kubicek@vscht.cz

M. Loučka	Institute of chemical technology Prague, Czech Republic louckam@vscht.cz
I. Marek	Czech Technical University Prague, Czech Republic marek@ms.mff.cuni.cz
J. Maxová	Institute of chemical technology Prague, Czech republic maxovaj@vscht.cz
M. Medved'	Department of Mathematical Analysis, Slovakia Milan.Medved@fmph.uniba.sk
S. Nandi	Narula Institute of Technology, India sumitnandi5@gmail.com
J. Němcová	Institute of chemical technology Prague, Czech republic Jana.Nemcova@vscht.cz
J. Nešetřil	Charles University in Prague, Czech Republic nesetril@iuuk.mff.cuni.cz
U. Okonye	Dam Technical College, South Africa trescaifeanyi@gmail.com
A. Oladipo	Cellulant Nigeria, Nigeria suspyo@yahoo.com
G. Opfer	Department of Mathematics, Universita of Hamburg, Germany gerhard.opfer@uni-hamburg.de
J. Pavlík	Institute of Chemical Technology Prague, Czech Republic pavlikj@vscht.cz
P. Pavlíková	Institute of Chemical Technology Prague, Czech Republic drabkovp@vscht.cz
P. Pokorný	Institute of Chemical Technology Prague, Czech Republic pavel.pokorny@vscht.cz
T. B. Rahimkay	Frida Abaka Foundation, South Africa fridaabakafoundation@yahoo.fr
P. K. Roy	Jadavpur University, India pritiju@gmail.com
I. Sankoh	Africhild Foundation For Peace and rebuilding, Sierra Leone officeuse33@gmail.com
P. Selyshchev	University of Pretoria, SA selyshchev@gmail.com
I. Schreiber	Institute of chemical technology Prague, Czech Republic igor.schreiber@vscht.cz
C. Simerská	Institute of chemical technology Prague, Czech Republic simerskc@vscht.cz
A. Spence	University of Bath, UK a.spence@bath.ac.uk
S. Sraman	Mahachulalongkornrajavidyalaya Univ, Thailand shimosraman@gmail.com
J. Šnupárková	Institute of chemical technology Prague, Czech Republic snupakoj@vscht.cz
K. Tanabe	Waseda University, Japan k.tanabe3@kurenai.waseda.jp

D. Turzík	Institute of Chemical Technogy Prague, Czech Republic turzikd@vscht.cz
E. Venturino	Dipartimento di Matematica "Giuseppe Peano", Italy ezio.venturino@unito.it
B. Werner	Department of Mathematics, Universita of Hamburg, Germany bodo_werner@t-online.de
Y. Zelenyuk	University of Witwatersrand, South Africa yuliya.zelenyuk@wits.ac.za
M. Zikmundová	Institute of Chemical Technogy Prague, Czech Republic zikmundm@vscht.cz